Summer 2022

Oxidized Graphitic Nano-Amendment of Cement Composites: Exploring Truly Low Concentrations and Novel Particle Morphologies

Shohana Iffat

OXIDIZED GRAPHITIC NANO-AMENDMENT OF CEMENT COMPOSITES: EXPLORING TRULY LOW CONCENTRATIONS AND NOVEL PARTICLE MORPHOLOGIES

by

Shohana Iffat

Bachelor of Science in Civil Engineering
Bangladesh University of Engineering and Technology, 2011

Master of Science in Civil Engineering
Bangladesh University of Engineering and Technology, 2014

Submitted in Partial Fulfillment of the Requirements

For the Degree of Doctor of Philosophy in

Civil Engineering

College of Engineering and Computing

University of South Carolina

2022

Accepted by:

Fabio Matta, Major Professor

Juan Caicedo, Committee Member

Yu Qian, Committee Member

Mohammed Baalousha, Committee Member

Jay Gaillard, Committee Member

Tracey Weldon, Vice Provost and Dean of the Graduate School

DEDICATION

To my parents, for their consistent support, and encouragement; and to my husband,

for his support and inspiration in every step of this journey.

ACKNOWLEDGEMENTS

I would like to express my sincere gratitude to my advisor, Dr. Fabio Matta, for his guidance, advice, and consistent support throughout these years to accomplish this research work with success.

I would like to thank Dr. Juan Caicedo, Dr. Yu Qian, Dr. Mohammed Baalousha and Dr. Jay Gaillard for their invaluable advice and time, and for being active part of my PhD Committee.

The research presented in this dissertation is based upon work supported by the U.S. Department of Energy, Office of Science, Office of Basic Energy Sciences, and Office of Biological and Environmental Research, under award number DE-SC0012530; Savannah River National Laboratory, Laboratory Directed Research & Development (LDRD), Project LDRD-2020-00122; the University of South Carolina (UofSC) Advanced Support for Innovative Research Excellence (ASPIRE) program; and a M. Bert Storey Endowed Graduate Fellowship. Special thanks are extended to Ms. Erika Rengifo (PhD), Ms. Laura Villegas (PhD student), and Ms. Sarah Riser (undergraduate research assistant), personnel of the Structures and Materials Laboratory at UofSC Department of Civil and Environmental Engineering, personnel of the Center for Environmental Nanoscience and Risk at the Arnold School of Public Health, and the Electron Microscopy Center, for their technical assistance.

ABSTRACT

Oxidized graphitic nanoparticles such as multiwalled carbon nanotubes (MWCNTs) and graphene nanoplatelets (GNPs), can produce enhancements in physico-mechanical properties of cement composites that are relevant to structural and durability performance, provided that said nanoparticles are well dispersed in the composite. Lower-bound MWCNT concentrations are reported in the literature in the range 0.01-0.05% in weight of cement (wt%). Such concentrations may not be cost-effective for practical applications and may also be excessive since they would result in a nanoparticle surface area at or above 10^5 m^2 for 1 m^3 of cement paste, or $10^{4.5}$ m^2 for 1 m^3 of concrete, which may be large enough to facilitate nanoparticle agglomeration in cement matrices. These agglomerates may contribute to the inhomogeneity of the cement matrix and introduce defect sites that negatively contribute to mechanical properties associated with strength, stiffness, and toughness.

In this research, low concentrations of MWCNTs in the range 0.001-0.05 wt% were explored as amendments in cement paste, thus one order of magnitude smaller than lower-bound concentrations reported in the literature. It was found that such decrease in MWCNT concentration continues to provide significant enhancement to compressive strength and stiffness compared to plain cement paste. In fact, neither significant enhancements in the 28-day compressive strength and stiffness, nor

noticeable changes in the nano- and micro-structure, were observed by increasing the MWCNT concentration by 50 times, from 0.001 wt% to 0.05 wt%. Instead, as originally hypothesized, MWCNT agglomerates were consistently observed in the cement matrix when using a 0.05 wt% MWCNT concentration.

The results above highlighted the merits of exploring more effective means of leveraging the specific surface area (SSA) of graphitic nanoparticles by considering alternative morphologies, in addition to truly low concentrations. To this end, partially unzipped carbon nanotubes (PUCNTs) are introduced in this research as nano-amendments for cement composites. Oxidized PUCNTs are of interest because they combine the aspect ratio and mechanical strength of MWCNTs, and the high graphene edge content and dispersibility of GNPs. In addition, PUCNTs offer a greater specific surface area compared to MWCNTs, which makes them suitable for exploring reduced concentrations. In this part of the research, truly low concentrations of PUCNTs in the range 0.001-0.05 wt% were utilized in cement paste. It was found that reducing the PUCNT concentration by one order of magnitude, from 0.05 wt% to 0.005 wt%, led to significantly enhanced nano- and micro-structure as well as compressive strength and elastic stiffness. These results were supported by SEM micrographs, which consistently showed PUCNT agglomerates for a concentration of 0.05 wt%; instead, for a concentration of 0.005 wt%, well dispersed PUCNTs were consistently observed, together with preferential and accelerated formation of C-S-H. This evidence agrees with dynamic light scattering test results on PUCNT suspensions where hydrodynamic

size and zeta potential values indicate less dispersibility of PUCNTs at concentrations equivalent to 0.05 wt% in the cement paste manufactured with these suspensions.

The research into more effective graphitic particle morphologies continued by investigating graphene oxide nanoribbons (GONRs), which are obtained by fully unzipping MWCNTs. GONRs combine the properties of carbon nanotubes and graphene, i.e., high surface area, graphene edge content, and aspect ratio. In fact, GONRs are easy to disperse in stable aqueous suspensions without compromising the sp^2 basal plane to defects. Due to their edge content resulting from oxidation, GONRs have higher contents –COOH edge groups compared to MWCNTs and GNPs, and to a lesser extent PUCNTs. A dispersibility study in aqueous solution was conducted using GONRs with different oxidation level (i.e., oxygen functional group content), and in different concentrations. Uniform GONR dispersions were quantitatively verified through DLS testing, based on hydrodynamic size and zeta potential measurements, for concentrations in the range 0.0125-1.25 g/L (equivalent to 0.0005 to 0.05 wt% of cement in concrete with water-to-cement ratio of 0.4), and for oxygen content in the range ~30-40 wt% for up to 7 days after initial sonication. These dispersed and stable aqueous suspensions of GONRs are suitable to explore novel graphitic-nanoamendment solutions for cement composites, including actual concrete, using more rational and practical concentrations.

TABLE OF CONTENTS

LIST OF TABLES

LIST OF FIGURES

LIST OF SYMBOLS

^{o}C	Degree Celsius
^{o}F	Degree Fahrenheit
g	Gram
Hrs	Hours
kHz	Kilohertz
L	Liter
ml	Milliliter
M	Moles per liter (mol/L)
nm	Nanometer
RH	Relative humidity
rpm	Revolutions per minute
w/c	Water-to-cement (mass) ratio
µm	Micrometer

LIST OF ABBREVIATIONS

C-S-H..... Calcium silicate hydrates

$Ca(OH)_2$..... Calcium hydroxide

DLS..... Dynamic light scattering

DI water..... Deionized water

FT-IR ..... Fourier-transform infrared spectroscopy

GO .....Graphene oxide

GNP ..... Graphene nanoplatelets

GONR..... Graphene oxide nanoribbons

HCl ..... Hydrochloric acid

HDS..... Hydrodynamic size

$KMnO_4$..... Potassium permanganate

OPC..... Ordinary Portland cement

MWCNT.....Multiwalled carbon nanotubes

PUCNT ..... Partially unzipped multiwalled carbon nanotubes

PTFE.....Polytetrafluoroethylene

SRNL ..... Savannah River National Laboratory

SEM ..... Scanning electron microscopy

SSA..... Specific surface area

XRD.....X-ray Diffraction

ZP.....Zeta potential

CHAPTER 1

BACKGROUND

1.1. GRAPHITIC NANOAMENDMENTS FOR CEMENT COMPOSITES

1.1.1 Multiwalled carbon nanotubes and graphene nanoplatelets

Different types of fibers are introduced to cement composites to control cracking and to provide post-cracking strength and deformability. Multiwalled carbon nanotubes (MWCNTs) are graphitic nanoparticles that are promising candidates as nanoamendments for cement composite materials. A MWCNT can be conceptualized by rolling up multiple sheets of graphene (i.e., two-dimensional sheets of carbon atoms) into a concentric cylinder. Researchers have found that multiwalled carbon nanotubes (MWCNTs) can serve as reinforcing agents for cement composites due to their high aspect ratio [Ayatollahia et al. 2011, Abu Al-Rub et al. 2012], stiffness [Konsta-Gdoutos et al. 2010], and high strength [Yu et al. 2000, Wei et al. 2008].

Notable mechanisms behind these mechanical property enhancements in cement composites amended with MWCNTs are found from the literature, originating from pore size refinement [Li et al. 2005, Sobolkina et al. 2012, Hu et al. 2014] and from MWCNTs acting as precipitation sites for cement hydrates [Li et al. 2005, Makar and Chan 2009]. Pore size refinement occurs by shifting the mean pore size in the cement

matrix towards a smaller diameter. In addition to pore refinement, reduction in total pore volume may occur if MWCNTs are added to cement paste [Sobolkina et al. 2012, Hu et al. 2014] and mortar [Li et al. 2005]. Addition of MWCNTs can improve the pore size distribution and reduce the total porosity of cement composites, especially lowering the volume of large pores (>50 nm) [Li et al. 2005]. As such, the incorporation of MWCNTs may result in a denser nano-and micro-structure than that of non-amended counterparts.

Accelerated and preferential formation of calcium silicate hydrates (C-S-H) on the surface of MWCNTs indicates that nanotubes nucleate the hydration reactions [Makar and Chan 2009]. When functionalized MWCNTs are well-dispersed in the cement matrix, these randomly oriented nanoparticles and the cement hydrates chemically combine through interaction between the functional groups present on the MWCNT edges and the C-S-H phase of the cement matrix, as verified by Li et al. [2005] through Fourier transform infrared spectroscopy (FTIR) analysis. Konsta-Gdoutos et al. [2010] found from nanoindentation tests that the incorporation of surfactant-coated MWCNTs led to a reduction in the volume of fine pores by filling up the areas between the C-S-H gel, and the amount of high-stiffness C-S-H increased. Through these mechanisms, different mechanical properties of cement composites are enhanced through the incorporation of MWCNTs. Most notably, it has been reported that amendment using functionalized MWCNTs resulted in enhancements in compressive strength [Li et al. 2005, Nasibulina et al. 2012, Collins et al. 2012, Zohhadi 2014, Kang et al. 2015, Parveen et al. 2015], tensile strength [Abu Al-Rub et al. 2012, Sobolkina et al.

2012, Kang et al. 2015, Konsta-Gdoutos et al. 2017], elastic stiffness [Tyson et al. 2011, Danoglidis et al. 2016, Rocha et al. 2019], and fracture toughness [Hu et al. 2014, Konsta-Gdoutos et al. 2017, Rocha et al. 2019].

Although most research on nano-amended cementitious composites has focused on MWCNTs, graphene have also been tested [Gong 2015]. Graphene is characterized by a two-dimensional sheet structure consisting of carbon atoms that are densely packed in a regular sp^2-bonded atomic-scale hexagonal pattern [Lee et al. 2008]. Graphene exhibits unique mechanical properties such as high Young's modulus (0.27 TPa to 1.47 TPa), tensile strength (3.6 to 63 GPa), and rupture strain up to 12% [Lee et al. 2008]. The results of molecular dynamics simulations showed that the attachment of carboxyl (–COOH) and hydroxyl (–OH) groups formed through oxidation produces an increase in the interfacial bond strength between graphene-particles and calcium silicate hydrate (C-S-H), and an increase in the elastic modulus and shear modulus of cement paste [Alkhateb et al. 2013]. The incorporation of graphene nanoplatelets (GNPs) [Alkhateb et al. 2013, Zohhadi 2014, Mokhtar et al. 2017, Du and Pang 2018], graphite nanofibers [Lee 2018], graphite flakes [Vega and Jr 2019], can enhance selected physico-mechanical properties of ordinary Portland cement (OPC) paste and mortar. GNPs, also referred to as nanosheets and nanoflakes, are ultra-thin forms of two-dimensional graphite materials having a thickness and/or lateral dimension less than 100 nm, unlike conventional graphite powders whose thickness is typically greater than 100 nm [Bianco et al. 2013]. The incorporation of GNPs in cement paste and mortar has been showed to result in enhanced mechanical properties, most notably compressive

strength [Alkhateb et al. 2013, Gong et al. 2015, Pan et al. 2015, Qureshi et al. 2019, Liu et al. 2019, Wang et al. 2019], and tensile strength [Alkhateb et al. 2013, Gong et al. 2015, Pan et al. 2015, Qureshi et al. 2019, Liu et al. 2019, Wang et al. 2019].

1.1.2 Functionalization and dispersibility assessments

MWCNTs and GNPs are typically introduced into cement mixtures through aqueous suspensions (e.g., [Zohhadi 2014]). Due to their high hydrophobicity and strong van der Waals interactions, it is difficult to achieve a stable and homogenous aqueous dispersion of the MWCNTs as well as GNPs.

To enhance the dispersibility of MWCNTs in aqueous solutions, and hypothetically enhance the interfacial bonding with cement hydrates, three common pretreatment methods have been reported in the literature on MWCNT-amended cement composites, namely: oxidation [Li et al. 2005, Manzur and Yazdani 2010, Nasibulina et al. 2012, Zohhadi 2014], surfactant-coating [Konsta-Gdoutos et al. 2010, Morsy et al. 2011, Collins et al. 2012, Sobolkina et al. 2012, Hu et al. 2014, Zohhadi 2014, Parveen et al. 2015, Danoglidis et al. 2016], and ultrasonication [Zohhadi 2014, Jeevanagoudar et al. 2017, Rocha et al. 2019]. Oxidation is intended to create oxygen-contained compounds, mainly carboxyl (–COOH) and hydroxyl (–OH) groups, on the surface of nanoparticles [Nasibulina et al. 2012]. These functional groups are water soluble and thus reduce the hydrophobicity of graphitic nanoparticles. In addition, functional groups attached on graphitic nanoparticle surfaces facilitate the precipitation of cement hydrates in cement matrices through chemical bonding with calcium silicate hydrates (C-S-H) [Makar and Chan 2009].

In the case of surfactant-coating, the graphitic nanopartcles are added to surfactant-aqueous solutions and sonicated to facilitate the absorption of surfactant molecules on the graphitic surfaces [Zohhadi 2014]. As a result, stable suspensions may be obtained as the steric or electrostatic repulsive forces between surfactant molecules counterbalance the van der Waals attractive forces between nanoparticles [Vaisman et al. 2006]. In many studies, polycarboxylate superplasticizers were used as surfactants. Polycarboxylates have active non-polar and polar groups, where the non-polar groups facilitate the dispersion of the graphitic nanoparticles, and the polar groups facilitate the dispersion of cement and water, thus leading to the formation of stable suspensions [Collins et al. 2012].

In the case of ultrasonication, the sonic energy is associated with high local shear forces that facilitate the separation of nanoparticle bundles [Zohhadi 2014]. As a result, a temporary dispersion of MWCNTs in water may be produced although these MWCNTs may re-agglomerate after halting the sonication process. However, higher contents of functionalized MWCNTs can more easily aggregate in aqueous solutions due to the limited inter-spaces between these particles, which result in physical restrictions to free Brownian motion [Baalousha 2009]. Once these suspensions are incorporated into a cement matrix, the MWCNT/graphene-agglomerates may form weak zones, reduce the homogeneity of the matrix, and negatively contribute to the mechanical properties of the resulting cement composite.

The stability of MWCNTs as well as GNPs in aqueous solutions indicates effective dispersion in water, which may be assessed through dynamic light scattering (DLS)

analysis and visual inspection. Achieving a stable aqueous suspension is a prerequisite to achieve uniform dispersion of graphitic nanoparticles in cement composite matrices. Li et al. [2005], Konsta-Gdoutos et al. [2010], Manzur and Yazdani [2010], Morsy et al. [2011], Nasibulina et al. [2012], Abu Al-Rub et al. [2012], Parveen et al. [2015], Kang et al. [2015], Danoglidis et al. [2016], Wang et al. [2017], Jeevanagoudar et al. [2017], Mohsen et al. [2017], Liu et al. [2019], Lee et al. [2019], Rocha et al. [2019], Lee et al. [2020], and Dalla et al. [2021] did not report an assessment of the dispersibility of MWCNTs in aqueous solutions. Similarly, Alkhateb et al. [2013], Gong et al. [2015], Pan et al. [2015], Mokhtar et al. [2017], and Qureshi et al. [2019] did not report an assessment of the dispersibility of GNPs in aqueous solutions. Tyson et al. [2011], Collins et al. [2012], Hu et al. [2014], Konsta-Gdoutos et al. [2017], and Alrekabi et al. [2017] utilized visual inspection to assess the dispersibility of MWCNTs in aqueous solutions. Du and Pang [2018], Liu et al. [2019], and Wang et al. [2019] utilized visual inspection to assess the dispersion of GNPs in aqueous solutions.

1.2. SIGNIFICANCE OF EXPLORING TRULY LOW CONCENTRATIONS OF GRAPHITIC NANOAMENDMENTS

As illustrated in Figure 1.1, in the archival literature found on MWCNT-amended cement paste and mortar in between 2005 and 2021, MWCNTs in a concentration range from 0.01% in weight of cement (wt%) to 1 wt%, the only exception being Morsy et al. [2011] where MWCNTs in concentrations as low as 0.005 wt% were incorporated in cement mortar. Thus, there is a research gap due to the lack of results from research on smaller concentrations of MWCNTs.

It is estimated that 0.01 wt% of MWCNTs cover approximately a 10^4 m^2 (Figure 1.2a) of surface area per cubic meter volume of cement paste. Only the external surfaces of MWCNT were considered to estimate the specific surface area (SSA) (Appendix A), as those surfaces participate in chemical reactions. The SSA of one side of a graphene sheet was assumed as 1315 m^2/g [Peigney et al. 2001], the length of C–C bonds in the curved graphene sheets was assumed as 0.1421 nm, and the inter-wall distance was assumed as 0.34 nm [Peigney et al. 2001]. The outer diameter of MWCNTs are considered in the range from 15 nm to 40 nm based on evidence from several research studies (e.g., [Li et al. 2005, Konsta-Gdoutos et al. 2010, Zohhadi 2014]) conducted on MWCNT-amended cement composites. From the average bulk density of cement paste, the weight of different MWCNT concentrations (e.g., 0.001 to 0.05% by weight of cement) in one cubic meter of cement paste was estimated. Next, the surface area covered by each concentration of MWCNT in one cubic meter of paste were estimated by multiplying the weight of particles per cubic meter of paste by the SSA. As a result, it appears that the range from 0.01 to 1 wt% covered in the literature results in a relatively large amount of MWCNTs, with a surface area between 10^4 and 10^6 m^2 per cubic meter volume of cement paste. In fact, MWCNTs in such amounts may agglomerate in cement matrices. When MWCNTs aggregate, the advantage of large surface area provided by these nanoparticles is hindered because of The presence of MWCNT agglomerates acting as defect sites. Between 0.001 to 0.01 wt% of MWCNT-contents, approximately 10^2 to 10^4 m^2 of surface area could be obtained in one cubic meter of cement concrete (Figure 1.2b). In addition, the incorporation of 0.01 to 1 wt%

of MWCNTs in OPC concrete is unlikely to be cost-effective. In fact, the incorporation of 0.05 wt% of MWCNTs would cost between $1500-2000 per cubic meter of concrete, assuming $10/g for the cost of MWCNTs. Hence, a radical reduction in the concentration of MWCNTs (e.g., 0.001 wt% and less) should be explored.

1.3. PARTIALLY UNZIPPED MULTIWALLED CARBON NANOTUBES

To take further advantage of the tailored morphology of graphitic nanoparticles, an idea was explored to longitudinal unzip the outer walls of MWCNTs [Song et al. 2014, Cheng et al. 2017], thus resulting in particles having a morphology similar to that of graphene. MWCNTs are characterized by a relatively high aspect ratio, which may be beneficial in cement composites [Abu Al-Rub et al. 2012]. Partial unzipping of the outer walls of MWCNTs (PUCNT) results in a radical increase in the open surface area [Jeong et al. 2016], and oxidation produces a larger number of functional groups [Song et al. 2014], thereby enhancing the chemical affinity with cement matrices. Through this process, a few outer layers of a given MWCNT are partially unzipped without affecting the inner core walls, resulting in a hybrid graphitic structure together with the intact inner carbon nanotubes [Shende et al. 2016]. Therefore, the resulting PUCNTs exhibit: (a) larger surface areas and greater functionality than the precursor MWCNTs, which may enhance the dispersibility in aqueous solutions and in cement matrices, and the chemical affinity with cement hydrates; and (b) a relatively high aspect ratio, which may facilitate the mechanical amendment of cement composites. As part of this collaborative research, PUCNTs were manufactured at Savannah River National Laboratory (SRNL) through an oxidative MWCNT unzipping process optimized from that

reported by Kosynkin et al. [2009]. To investigate the ideas of radically reducing the nano-amendment concentration and exploring more suitable nanoparticle, low concentrations of PUCNTs were used to study dispersibility (and stability thereof) in aqueous solutions, dispersion in cement paste, and enhancements (if any) to the uniaxial compressive strength of PUCNT-amended cement paste.

1.4. GRAPHENE OXIDE NANORIBBONS

Full instead of partial unzipping of the outer walls of MWCNTs would result in further increase in the open surface area, similar to GNPs, as shown in Figure 1.2. Also, functionalization by oxidation would produce a larger number of functional groups compared to the precursor MWCNTs or PUCNTs. The resulting nanoparticles, which are herein referred to as graphene oxide nanoribbons (GONR), consist of elongated strips of graphene. Therefore, the aspect ratio of GONRs is higher than that of GNPs. Through this process, a few outer layers of a given MWCNT will be fully unzipped, and the resulting GONR will exhibit: (a) larger surface area and greater functionality than the precursor MWCNT or PUCNT, thus further facilitating its dispersibility in aqueous solutions as well as in cement matrices; and (b) a higher aspect ratio compared to GNPs, which is expected to facilitate the mechanical amendment of cement composites. GONRs have exceptionally high graphene edge content that provides larger –COOH edge sites compared to GNP structures. Unlike GNPs, GONRs are expected to offer more suspension stability in aqueous solutions through edge functionalization without compromising the sp^2 basal plane due to defects resulting from oxidation. Due to their high functional edge content, GONRs are suitable for high-density crosslinking to

cement composite matrix. Therefore, a preliminary research was conducted in collaboration with SRNL to investigate the dispersibility of ultra-low concentrations of GONRs in aqueous solutions as a function of three different levels of oxidation.

1.5. RESEARCH GAPS

The examination of the state of the art presented in this introduction highlights the following research gaps:

- In most research, MWCNT (Figure 1.1) and graphene (Figure 1.3) concentrations in excess of 0.01 wt% were utilized, which would not be cost-effective if translated to actual concrete applications. In addition, high concentrations of MWCNTs result in large surface areas per unit volume of cement paste and concrete (Figure 1.2) that facilitate agglomeration, thus hindering dispersibility in cement matrices. To this end, the literature highlights a major gap given by the lack of research on smaller, and perhaps more suitable, concentrations of graphitic nano-amendments.
- Together with exploring truly low concentrations, there is a gap in exploring novel graphitic nanoparticle morphologies that may facilitate further reducing their concentrations and enhancing their chemical affinity with and amendment effects on cement matrices. To this end, PUCNTs and GONRs are investigated in this research.
- The dispersion of MWCNTs and GNPs was either not assessed or only visually examined. Dedicated measurements (e.g., DLS with zeta potential, average hydrodynamic size) should be enlisted to quantitatively describe the dispersibility of graphitic nanoamendments in aqueous suspensions, and the stability over time of said suspensions.

- Representative high-magnification scanning electron microscope (SEM) micrographs should be presented to document the distribution of MWCNTs and GNPs in cement matrices to illustrate dispersion.
- The influence of different levels of oxidation on nano- and micro-structural modifications and physico-mechanical properties of cement composites has not been documented in the literature.

1.6. OBJECTIVES

The objectives of this research are to investigate:

(1) Truly low concentrations of MWCNTs in the range of 0.001 – 0.05 wt% in cement paste, where 0.01 wt% was found as the typical lower-bound concentration in the literature.

(2) Oxidized partially unzipped carbon nanotubes (PUCNTs) as a nano-amendment option for cement composites that is more effective than precursor MWCNTs.

(3) Truly low concentrations of PUCNTs in the range of 0.001 – 0.05 wt%.

(4) Graphene oxide nanoribbons (GONRs) as a nano-amendment option for cement composites, producing stable aqueous suspensions that are suitable for advancing the research from cement paste to actual concrete.

(5) The dispersibility of ultra-low concentrations of GONRs in the range of 0.0005 – 0.05 wt% in aqueous suspensions as a function of the oxygen functional group contents.

1.7. RESEARCH QUESTIONS

In regard to the investigation into different graphitic nanoparticle morphologies, the scope is to unzip the outer walls of MWCNTs, resulting in PUCNTs or GONRs, to

enhance SSA and functionality, and introduce these nanoparticles in cement composites with concentration that are radically smaller than 0.01% in weight of cement (wt%). In fact, 0.01 wt% was found as the typical lower bound in the literature (Figure 1.1) to achieve uniform dispersion in cement composites and obtain enhanced mechanical properties. It is noted that 0.01 wt% of MWCNTs could cover 10^4 to $10^{4.5}$ m^2 of surface area per cubic meter of cement paste (Figure 1.2a), and 10^3 to 10^4 m^2 of surface area per cubic meter of concrete (Figure 1.2b), considering *w/c* ratio of 0.4. Partially unzipping the outer walls of MWCNTs enhances the SSA required for the introduction of functional groups that are chemically compatible with cement matrices. In addition, unzipping results in a comparable aspect ratio of PUCNTs to precursor MWCNTs, which may facilitate the mechanical amendment of cement composites. Fully unzipping the MWCNTs (GONRs) further increases the surface area between three to 30 times compared to similar concentrations of precursor MWCNTs. Furthermore, GONRs exhibit a relatively higher aspect ratio compared to GNPs. Therefore, reducing the concentration of PUCNTs or GONRs well below 0.01 wt% theoretically results in comparable SSA to 0.01 wt% of MWCNTs, with less likelihood of agglomeration. Due to the high edge content, GONRs are characterized by a relatively high amount of –COOH edge groups, making the material more attractive than their graphitic counterparts (MWCNTs and GNPs) as far as dispersibility and stability in aqueous suspensions, and chemical affinity with cement composite matrices. In this research, three different levels of oxidation were investigated while maintaining similar morphology and defects in the GONRs. More functionalities may lead to facilitating the precipitation of cement

hydrates, refinement of the pore structure, and associated enhancement of physico-mechanical properties that are important for both structural and durability performance.

1.8. METHODOLOGY

The research plan includes the following scope of work:

(1) Prepare the MWCNT-suspensions in DI water for concentrations in the range 0.02 – 1 g/L, which is equivalent to 0.001 – 0.05 wt% for cement paste with a *w/c* ratio of 0.5 and verify their dispersibility in water. To this end, dynamic light scattering (DLS) testing is conducted to measure zeta potential (ZP) and hydrodynamic size (HDS). Values of ZP less than -30 mV indicate stable dispersion [Freitas and Muller 1998] while decreasing values of HDS indicate less agglomeration.

(2) Prepare 25 × 25 × 76 mm prismatic cement paste specimens with Type I OPC and MWCNT suspensions. Control cement paste specimens are manufactured to serve as benchmark. With these samples, uniaxial compression tests and SEM micrograph analysis are conducted after 7, 14 and 28 days of curing.

(3) Prepare and oxidize PUCNTs through SRNL, and quantify their functionality level (e.g., based on Raman spectra, FT-IR spectra, and XPS data).

(4) Prepare PUCNT suspensions in DI water for concentrations in the range 0.02 – 1 g/L, which is equivalent to 0.001 – 0.05 wt% for cement paste with a *w/c* ratio of 0.5 and verify dispersibility based on ZP and HDS measurements.

(5) Prepare 25 × 25 × 76 mm prismatic cement paste specimens with Type I OPC and PUCNT aqueous suspensions. Control cement paste specimens are manufactured to

serve as benchmark. With these samples, uniaxial compression tests and SEM micrograph analysis are conducted after 7, 14 and 28 days of curing.

(6) Prepare GONR samples with three different oxidation levels through SRNL, and experimentally characterize their functionality level.

(7) Prepare GONR-suspensions in DI water for concentrations in the range 0.0125 – 1.25 g/L, which is equivalent to 0.0005 – 0.05 wt% for cement concrete with a *w/c* ratio of 0.4, with three different oxygen contents at ~40 wt%, 30 – 35 wt%, and 20 – 25 wt%, and verify their dispersibility in water. DLS testing is performed to measure ZP and HDS values.

(8) Prepare 50 × 100 mm cylindrical cement concrete specimens with Type I OPC, silica sand, crushed stone with nominal maximum aggregate size of 9.5 mm, and GONR aqueous suspensions. Control cement concrete specimens are manufactured to serve as benchmark. With these samples, uniaxial compression tests and SEM micrograph analysis are conducted after 7 days of curing.

1.9. RESEARCH NOVELTY

The novel aspects of this research are:

(1) Exploring truly low concentrations of oxidized MWCNTs in the range 0.001 – 0.05 wt% as a means to taking better advantage of the functionalized SSA for the purpose of amending cement paste, where 0.01 wt% emerged as the lower-bound concentration in the literature (Figure 1.1). In this research, this lower-bound concentration is reduced by one order of magnitude.

(2) Exploring oxidized PUCNTs as amendment for cement composites through partially unzipping the outer walls of precursor MWCNTs, as a means to leverage the increased functionalized SSA compared to precursor MWCNTs.

(3) Low contents of PUCNTs are considered in the range 0.001 – 0.05 wt% in cement paste. Here, the lower-bound concentration for MWCNTs (Figure 1.1) as amendment in cement paste is reduced by one order of magnitude.

(4) Exploring ultra-low concentrations of GONRs as amendment for cement concrete through fully unzipping the outer walls of MWCNTs, as a means to further leverage the increased functionalized SSA compared to precursor MWCNTs and PUCNTs.

(5) Ultra-low-contents of GONRs are investigated in the range 0.0005 – 0.05 wt% when used for cement concrete with *w/c* ratio of 0.4. Here, the lower-bound 0.01 wt% concentration of MWCNTs (Figure 1.1) is reduced by two orders of magnitude.

(6) Three different levels of oxygen functionalities for GONRs, i.e., oxygen contents of ~40 wt%, 30 – 35 wt%, and 20 – 25 wt% will be evaluated for similar GONR morphology and defects resulting from the oxidative process. Effect of level of oxidation and GONR concentration on the dispersion and stability in aqueous solutions is evaluated through DLS testing.

1.10. OUTLINE OF DISSERTATION

The incorporation of truly low concentrations of oxidized MWCNTs on the nano- and micro-structure and salient physico-mechanical properties of cement paste is presented in Chapter 2. The incorporation of truly low concentrations of oxidized PUCNTs in cement paste is presented in Chapter 3. The dispersion of ultra-low

concentrations of oxidized GONRs with different oxidation levels in aqueous solution and their application on Portland cement concrete is presented in Chapter 4. Finally, Chapter 5 summarizes conclusions and recommendations for further research. A flow chart of the research plan is shown in Figure 1.4.

1.11. REFERENCES

ASTM International. Standard Practice for Mechanical Mixing of Hydraulic Cement Pastes and Mortars of Plastic Consistency. ASTM C305-14. West Conshohocken, PA: ASTM International, 2014.

Abu Al-Rub RK, Ashour AI, Tyson B M. On the Aspect Ratio Effect of Multi-Walled Carbon Nanotube Reinforcements on the Mechanical Properties of Cementitious Nanocomposites. Construction and Building Materials 2012; 35, 647–655.

Alkhateb H, Al-Ostaz A, Cheng AHD, Li X. Materials genome for graphene-cement nanocomposites. Journal of Nanomechanics and Micromechanics 2013; 3, 67-77.

Alrekabi S, Cundy AB, Lampropoulos A, Whitby RLD, Savina I. Effect of High-Intensity Sonication on the Dispersion of Carbon-Based Nanofilaments in Cementitious Composites, and Its Impact on Mechanical Performance. Materials and Design 2017; 136, 223–237.

An J, McInnis M, Chung W, Nam B. Feasibility of Using Graphene Oxide Nanoflake (GONF) as Additive of Cement Composite. Applied Sciences 2018; 8, 419.

Ayatollahia MR, Shadloua S, Shokriehb MM, Chitsazzadehc M. Effect of Multi-Walled Carbon Nanotube Aspect Ratio on Mechanical and Electrical Properties of Epoxy-Based Nanocomposites. Polymer Testing 2011; 30(5), 548–556.

Baalousha M. Aggregation and disaggregation of iron oxide nanoparticles: Influence of particle concentration, pH and natural organic matter. Science of the Total Environment 2009; 407, 2093-2101.

Bai S, Jiang L, Xu N, Jin M, Jiang S. Enhancement of Mechanical and Electrical Properties of Graphene/Cement Composite Due to Improved Dispersion of Graphene by Addition of Silica Fume. Construction and Building Materials 2018; 164, 433–44.

Bianco A, Cheng HM, Enoki T, Gogotsi Y, Hurt RH, Koratkar N, Kyotani T, Monthioux M, Park CR, Tascon JMD, Zhang J. All in the graphene family – A recommended nomenclature for two-dimensional carbon materials. Carbon 2013; 65, 1-6.

Chen Z, Zhou X, Wang X, Guo P. Mechanical Behavior of Multilayer GO Carbon-Fiber Cement Composites. Construction and Building Materials 2018; 159, 205–212.

Cheng Y, Zhang S, Li J, Sun J, Wang J, Qin C, Dai L. Preparation of Functionalized Partially Unzipped Carbon Nanotube/Polyimide Composite Fibers with Increased Mechanical and Thermal Properties. Royal Society of Chemistry Advances 2017; 7, 21953–21961.

Chuah S, Li W, Chen SJ, Sanjayan JG, Duan WH. Investigation on Dispersion of Graphene Oxide in Cement Composite Using Different Surfactant Treatments. Construction and Building Materials 2018; 161, 519–527.

Collins F, Lambert J, Duan WH. The Influences of Admixtures on the Dispersion, Workability, and Strength of Carbon Nanotube–OPC paste mixtures. Cement and Concrete Composites 2012; 34, 201-207.

Cwirzen A, Cwirzen KH, Nasibulin AG, Kaupinen EI, Mudimel PR, Penttala V. SEM/AFM Studies of Cementitious Binder Modified by MWCNT and Nano-Sized Fe Needles. Materials Characterization 2009; 60, 735-740.

Dalla PT, Tragazikis IK, Trakakis G, Galiotis C, Dassios KG, Matikas TE. Multifunctional Cement Mortars Enhanced with Graphene Nanoplatelets and Carbon Nanotubes. Sensors 2021; 21, 933.

Danoglidis PA, Konsta-Gdoutos MS, Gdoutos EE, Shah SP. Strength, Energy Absorption Capability and Self-Sensing Properties of Multifunctional Carbon Nanotube Amended Mortars. Construction and Building Materials 2016; 120, 265–274.

Du H, Pang SD. Dispersion and stability of graphene nanoplatelet in water and its influence on cement composites. Construction and Building Materials 2018; 167, 403–413.

Freitas C and Muller RH. Effect of Light and Temperature on Zeta Potential and Physical Stability in Solid Lipid Nanoparticle (SLN™) Dispersions. International Journal of Pharmaceutics 1998; 168, 221–229.

Gong K, Pan Z, Korayem AH, Qiu L, Li D, Collins F, Wang CM, Duan WH. Reinforcing effects of graphene oxide on Portland cement paste. Journal of Materials in Civil Engineering 2015; 27(2), A4014010.

Gholampour A, Kiamahalleh MV, Tran DNH, Ozbakkaloglu T, Losic D. Revealing the Dependence of the Physiochemical and Mechanical Properties of Cement Composites on Graphene Oxide Concentration. Royal Society of Chemistry Advances 2017; 7, 55148–55156.

Hu Y, Luo D, Li P, Li Q, Sun G, Key S. Fracture Toughness Enhancement of Cement Paste with Multi-Walled Carbon Nanotubes. Construction and Building Materials 2014; 70, 0332–338.

Jeevanagoudar YV, Krishna RH, Gowda R, Preetham R, Prabhakara R. Improved Mechanical Properties and Piezoresistive Sensitivity Evaluation of MWCNTs Amended Cement Mortars. Construction and Building Materials 2017; 144, 188–194.

Jeong YC, Lee K, Kim T, Kim JH, Park J, Cho YS, Yang SJ, Park CR. Partially Unzipped Carbon Nanotubes for High-Rate and Stable Lithium–Sulfur Batteries. Journal of Materials Chemistry A 2016; 4, 819–826.

Kang ST, Seo JY, Park SH. The Characteristics of CNT/Cement Composites with Acid-Treated MWCNTs. Advances in Materials Science and Engineering 2015; Article ID 308725.

Kaur R, Kothiyal NC. Comparative Effects of Sterically Stabilized Functionalized Carbon Nanotubes and Graphene Oxide as Reinforcing Agent on Physico-mechanical Properties and Electrical Resistivity of Cement Nanocomposites. Construction and Building Materials 2019; 202, 121–138.

Konsta-Gdoutos MS, Metaxa ZS, Shah SP. Multi-Scale Mechanical and Fracture Characteristics and Early-Age Strain Capacity of High Performance Carbon Nanotubes/Cement Nanocomposites. Cement and Concrete Composites 2010; 32 (2), 110-115.

Konsta-Gdoutos MS, Batis G, Danoglidis PA, Zacharopoulou AK, Zacharopoulou EK, Falara MG, Shah SP. Effect of CNT And CNF Loading and Count on The Corrosion Resistance, Conductivity and Mechanical Properties of Nanomodified OPC Mortars. Construction and Building Materials 2017; 147, 48–57.

Kosynkin DV, Higginbotham AL, Sinitskii A, Lomeda JR, Ayrat Dimiev A, Price BK, Tour JM. Longitudinal Unzipping of Carbon Nanotubes to form Graphene Nanoribbons. Nature 2009; 458, 872–877.

Kudzma A, Samat J, Stonys R, Krasnikovs A, Kuznetsov D, Girskas G, Antonovi V. Study on the Effect of Graphene Oxide with Low Oxygen Content on Portland Cement Based Composites. Materials 2019; 12, 802.

Lee C, Wei X, Kysar JW, Hone J. Measurement of the Elastic Properties and Intrinsic Strength of Monolayer Graphene. Science 2008; 321.

Lee S, Kawashima S, Kimb K, Woo S, Won J. Shrinkage characteristics and strength recovery of nanomaterials-cement composites. Composite Structures 2018; 202, 559–565.

Lee H, Jeong S, Park S, Chung W. Enhanced Mechanical and Heating Performance of Multi-Walled Carbon Nanotube-Cement Composites Fabricated Using Different Mixing Methods. Composite Structures 2019; 225, 111072.

Lee H, Jeong S, Cho S, Chung W. Enhanced Bonding Behavior of Multi-Walled Carbon Nanotube Cement Composites and Reinforcing Bars. Composite Structures 2020; 243, 112201.

Li GY, Wang PM, Zhao X. Mechanical Behavior and Microstructure of Cement Composites Incorporating Surface-Treated Multi-Walled Carbon Nanotubes, Carbon 2005; 43, 1239–1245.

Li X, Wang L, Liu Y, Li W, Dong B, Duan WH. Dispersion of Graphene Oxide Agglomerates in Cement Paste and Its Effects on Electrical Resistivity and Flexural Strength. Cement and Concrete Composites 2018; 92, 145–154.

Liew KM, Kai MF, Zhang LW. Mechanical and Damping Properties of CNT-Amended Cementitious Composites. Composite Structures 2017; 160, 81–88.

Liu J, Fu J, Ni T, Yang Y. Fracture toughness improvement of multi-wall carbon nanotubes/graphene sheets reinforced cement paste. Construction and Building Materials 2019; 200, 530–538.

Lu Z, Chen B, Leung CKY, Li Z, Sun G. Aggregation Size Effect of Graphene Oxide on Its Reinforcing Efficiency to Cement-Based Materials. Cement and Concrete Composites 2019; 100, 85–91.

Lv SH, Deng LJ, Yang WQ, Zhou QF, Cui YY. Fabrication of Polycarboxylate/Graphene Oxide Nanosheet Composites by Copolymerization for Reinforcing and Toughening Cement Composites. Cement and Concrete Composites 2016; 66, 1-9.

Makar JM and Chan GW. Growth of Cement Hydration Products on Single-Walled Carbon Nanotubes. Journal of the American Ceramic Society 2009; 92 (6), 1303–1310.

Manzur T, Yazdani N. Strength Enhancement of Cement Mortar with Carbon Nanotubes: Early Results and Potential. Transportation Research Record: Journal of the Transportation Research Board 2010; 2142, 102–108.

Mohsen MO, Taha R, Taqa AA, Shaat A. Optimum Carbon Nanotubes' Content for Improving Flexural and Compressive Strength of Cement Paste. Construction and Building Materials 2017; 150, 395–403.

Mokhtar MM, Abo-El-Enein SA, Hassaan MY, Morsy MS, Khalil MH. Mechanical performance, pore structure and micro-structural characteristics of graphene oxide nano platelets reinforced cement. Construction and Building Materials 2017; 138, 333–339.

Morsy MS, Alsayed SH, Aqel M. Hybrid Effect of Carbon Nanotube and Nano-Clay on Physico-Mechanical Properties of Cement Mortar. Construction and Building Materials 2011; 25, 145–149.

Nasibulina LI, Anoshkin IV, Nasibulin AG, Cwirzen A, Penttala V, Kauppinen EI. Effect of Carbon Nanotube Aqueous Dispersion Quality on Mechanical Properties of Cement Composite. Journal of Nanomaterials 2012; Article ID 169262.

Pan Z, He L, Qiu L, Korayem AH, Li G, Zhu ZW, Collins F, Li D, Duan WH, Wang MC. Mechanical properties and microstructure of a graphene oxide–cement composite. Cement and Concrete Composites 2015; 58, 140–147.

Parveen S, Rana S, Fangueiro R, Paiva MC. Microstructure and Mechanical Properties of Carbon Nanotube Amended Cementitious Composites Developed Using A Novel Dispersion Technique. Cement and Concrete Research 2015; 73, 215–227.

Peigney A, Laurent Ch, Flahaut E, Bacsa RR, Rousset A. Specific Surface Area of Carbon Nanotubes and Bundles of Carbon Nanotubes. Carbon 2001; 39 (4), 507-514.

Peng H, Ge Y, Cai CS, Zhang Y, Liu Z. Mechanical Properties and Microstructure of Graphene Oxide Cement-Based Composites. Construction and Building Materials 2019; 194, 102–109.

Qureshi T, Panesar DK, Sidhureddy B, Chen A, Wood PC. Nano-Cement Composite with Graphene Oxide Produced from Epigenetic Graphite Deposit. Composites Part B 2019; 159, 248–258.

Rocha VV, Ludvig P, Trindade ACC, Silva FA. The Influence of Carbon Nanotubes on the Fracture Energy, Flexural and Tensile Behavior of Cement Based Composites. Construction and Building Materials 2019; 209, 1–8.

Sabziparvar AM, Hosseini E, Chiniforush V, Korayem AH. Barriers to Achieving Highly Dispersed Graphene Oxide in Cementitious Composites: An Experimental and Computational Study. Construction and Building Materials 2019; 199, 269–278.

Sobolkina A, Mechtcherine V, Khavrus V, Maier D, Mende M, Ritschel M, Leonhardt A. Dispersion of Carbon Nanotubes and Its Influence on the Mechanical Properties of the Cement Matrix. Cement and Concrete Composites 2012; 34 (2012), 1104–1113.

Shende RS, Ramaprabhu S. Thermo-Optical Properties of Partially Unzipped Multiwalled Carbon Nanotubes Dispersed Nanofluids for Direct Absorption Solar Thermal Energy Systems. Solar Energy Materials & Solar Cell, 2016; 157, 117–125.

Song Y, Feng M, Zhan H. Electrochemistry of Partially Unzipped Carbon Nanotubes. Electrochemistry Communications 2014; 45, 95–98.

Tyson BM, Abu Al-Rub RK, Yazdanbakhsh A, Grasley Z. Carbon Nanotubes and Carbon Nanofibers for Enhancing the Mechanical Properties of Nanocomposite Cementitious Materials. Journal of Materials in Civil Engineering 2011; 23(7), 1028-1035.

Vaisman L, Wagner HD, and Marom G. The Role of Surfactants in Dispersion of Carbon MWCNTs. Advances in Colloid and Interface 2006; 128, 37-46.

Vega MSDCD, Jr MRV. Plasma-functionalized exfoliated multilayered graphene as cement reinforcement. Composites Part B 2019; 160, 573–585.

Wang Y, Hu H, Rong C. The Effect of the Diameter of Carbon Nanotube on the Mechanical and Electrical Properties of Cement Mortar. Key Engineering Materials 2017; 730, 479-485.

Wang B, Pang B. Mechanical property and toughening mechanism of water reducing agents modified graphene nanoplatelets reinforced cement composites. Construction and Building Materials 2019; 226, 699–711.

Wei T, Fan Z, Luo G, Wei F. A New Structure for Multi-Walled Carbon Nanotubes Amended Alumina Nanocomposite with High Strength and Toughness. Materials Letters 2008; 62(4–5), 641–644.

Xu S, Liu J, Li Q. Mechanical Properties and Microstructure of Multi-Walled Carbon Nanotube-Amended Cement Paste. Construction and Building Materials 2015; 76, 16–23.

Yu MF, Lourie O, Dyer MJ, Moloni K. Strength and Breaking Mechanism of Multiwalled Carbon Nanotubes under Tensile Load. Science 2000; 287, 637-640.

Zhao L, Guo X, Ge C, Li Q, Guo L, Shu X, Liu J. Mechanical Behavior and Toughening Mechanism of Polycarboxylate Superplasticizer Modified Graphene Oxide Reinforced Cement Composites. Composites Part B 2017; 113, 308-316.

Zohhadi N. Functionalized Graphitic Nanoreinforcement for Cement Composites. PhD Dissertation 2014; University of South Carolina, Columbia.

1.12. FIGURES

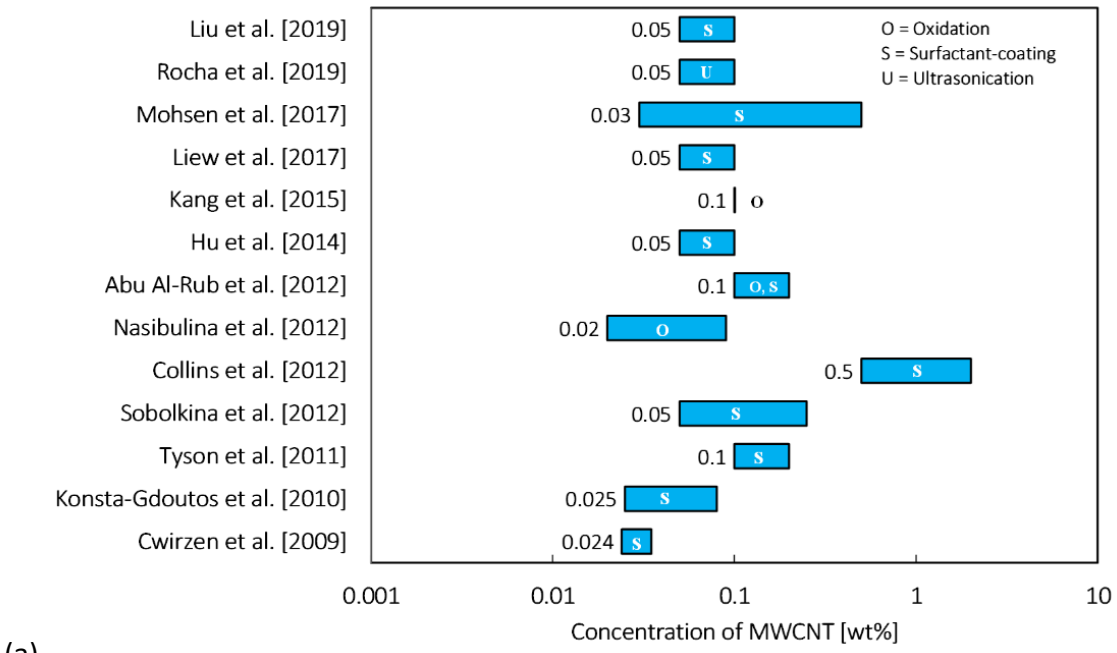

(a)

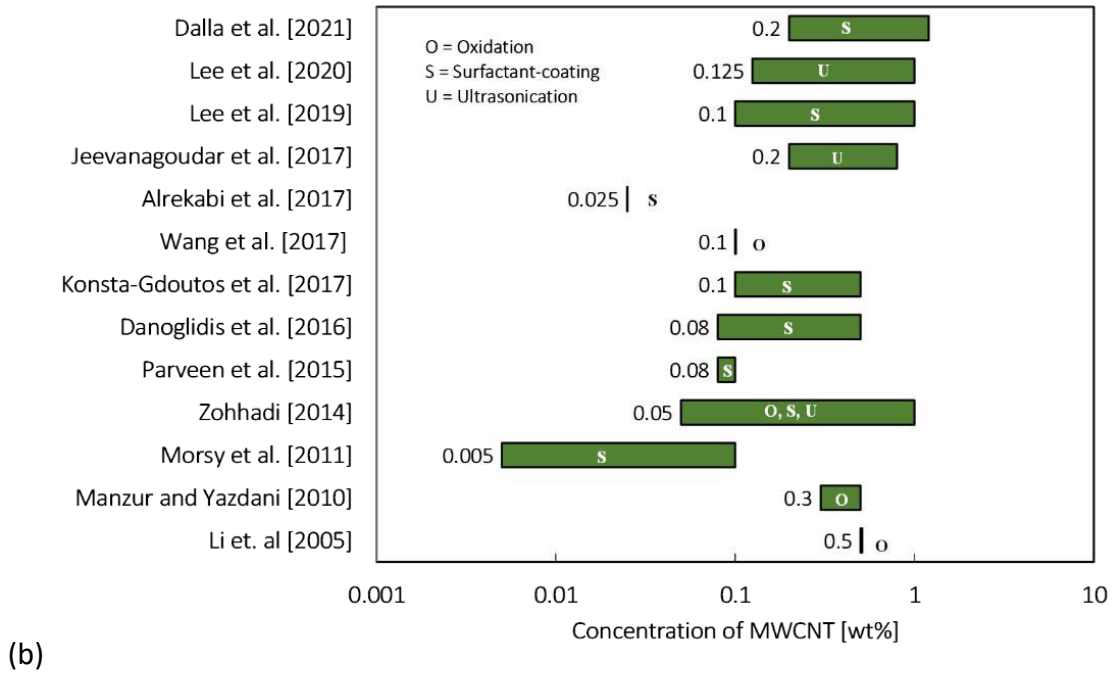

(b)

Figure 1.1 Researchers utilized different range of MWCNT-contents in cement composites (a) cement paste (b) cement mortar

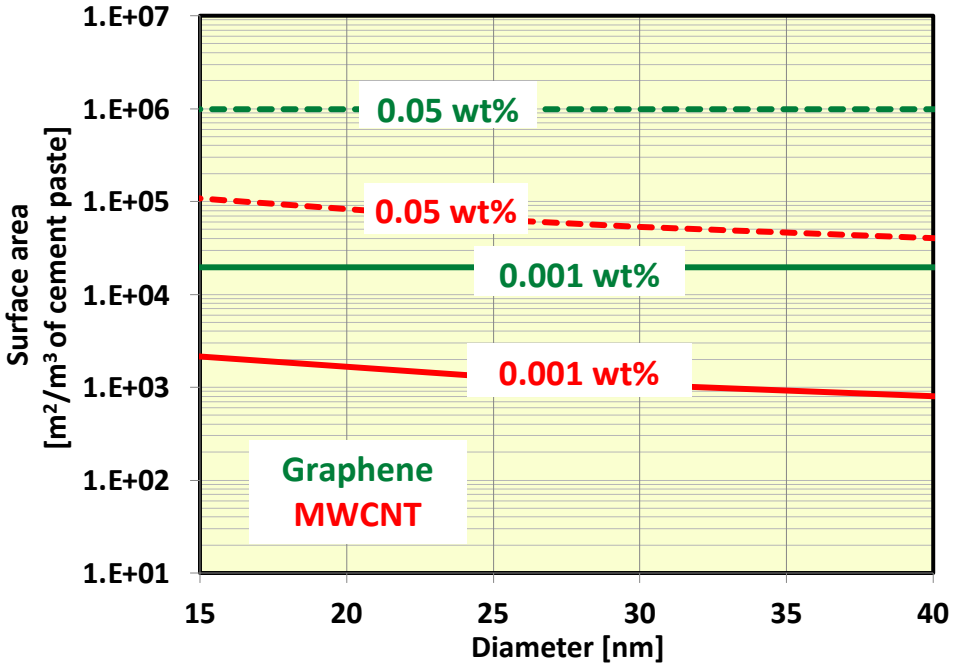

(a)

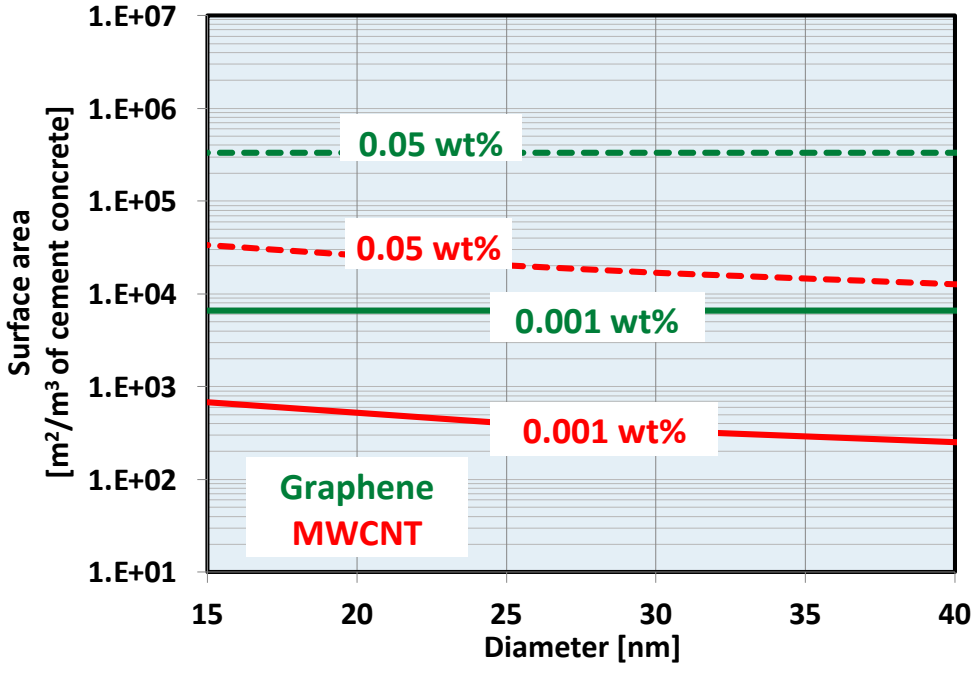

(b)

Figure 1.2 Surface area of different concentrations of MWCNTs and graphene in (a) 1m^3 of cement paste (b) 1 m^3 of cement concrete

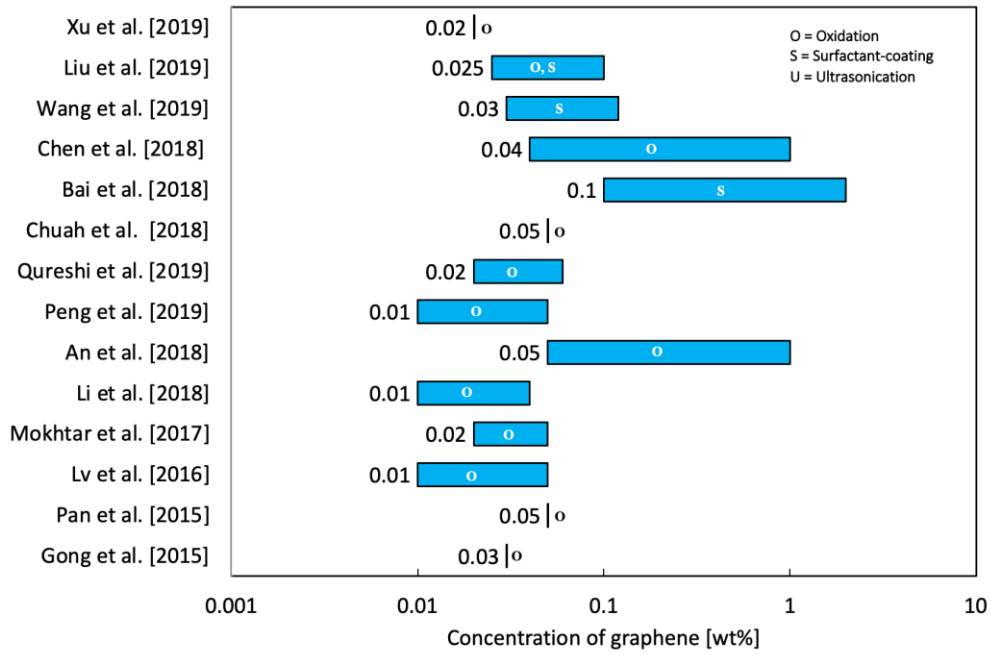

(a)

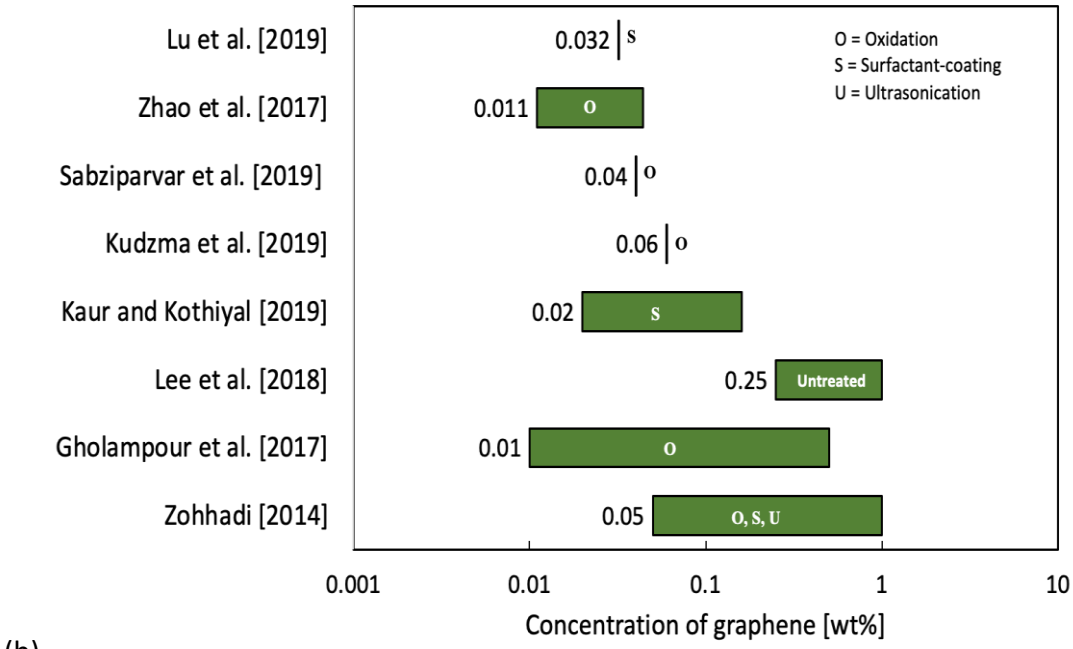

(b)

Figure 1.3 Researchers utilized different range of graphene-contents in cement composites (a) cement paste (b) cement mortar

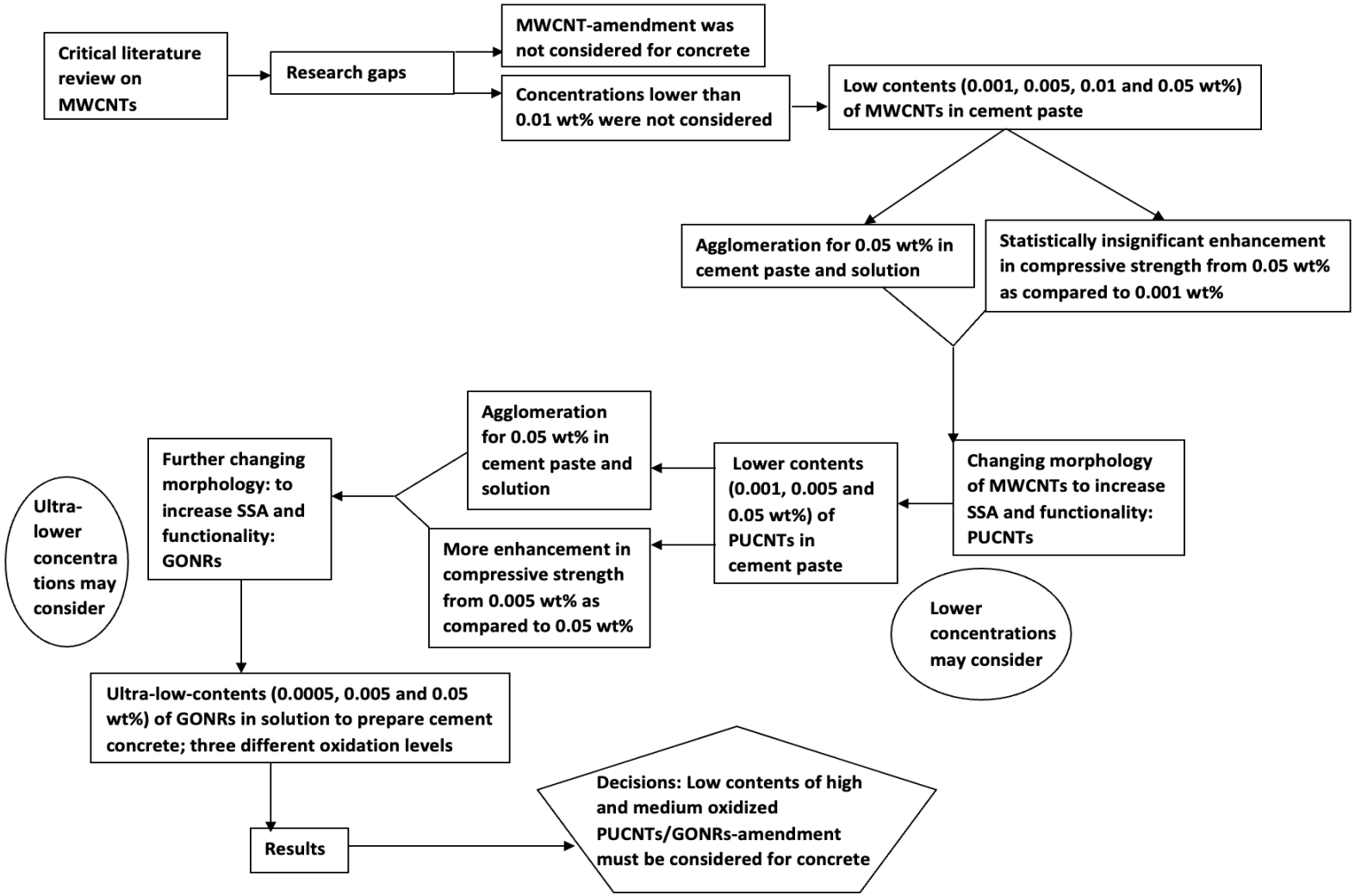

Figure 1.4 Flowchart of the research methodology

CHAPTER 2

INFLUENCE OF MULTIWALLED CARBON NANOTUBE CONCENTRATION ON PHYSICO-MECHANICAL PROPERTIES OF NANO-AMENDED CEMENT PASTE

2.1. INTRODUCTION

This chapter discusses the influence of incorporating different concentrations of oxidized MWCNTs on the compressive strength and the nano- and micro-structure of ordinary Portland cement paste. In particular, low concentrations of MWCNTs in the range from 0.001 to 0.05 wt% range are considered, thus deviating from the literature where decidedly higher concentrations are reported. MWCNTs were oxidized and then dispersed in water through sonication. Dispersion in aqueous solutions is experimentally assessed through DLS analysis. The resulting suspensions are used to manufacture cement paste specimens for follow-on physico-mechanical characterization.

2.2. EXPERIMENTAL PROGRAM

2.2.1 Materials

The research was conducted on cement paste consisting of Type I OPC and deionized (DI) water, with a *w/c* ratio of 0.5. The MWCNTs were added to the cement mixtures in the form of aqueous suspensions. MWCNTs with a nominal maximum diameter of 8 nm (Cheap Tubes Inc., cat# SKU-030101, Brattleboro, VT) were utilized as-

received. Oxidation was performed following the procedure reported by Aich et al. [2012] and Zohhadi [2014]. The MWCNTs were introduced in an aqueous solution containing 187.5 g of 98% ammonium persulfate (Sigma Aldrich, cat#215589) and 13.6 mL of 95-98% sulfuric acid (Sigma Aldrich, cat#339741). The resulting suspension was stirred for 24 hours using a magnetic stirrer (VWR stirrer, Henry Troemner LLC., Thorofare, NJ). To facilitate the penetration of oxidants along the inner nanotubes, the suspensions were sonicated for 10 minutes using an ultrasonic dismembrator S-4000 (Misonix, Inc., Farmingdale, NY) and then stirred at 1200 rpm for 24 hours. Then, the MWCNTs were washed with DI water and filtered through 0.45 µm PVDF membrane filter (Millipore, Billerica, MA) to raise the pH level to 7, and then dried and stored as dry powder. The dry powder of oxidized MWCNTs was added to DI water and bath sonicated for 35 minutes at a frequency of 40 kHz before incorporating it into the cement mixtures. The effectiveness of this method with respect to the formation of active carbon atoms was verified by Zohhadi [2014] through Raman spectroscopy analysis. In addition, the attachment of –OH and –COOH functional groups to the oxidized MWCNTs was previously verified through FT-IR (Fourier transform infrared) spectroscopy analysis with C-O stretches of functional groups [Zohhadi 2014].

2.2.2 Preparation of MWCNT-suspensions

The concentrations of MWCNTs ranged from 0.001 wt% (% by weight of cement) to 0.01 wt%, 0.005 wt% and 0.05 wt% (in weight of cement), in addition to control (0 wt%) mixtures. The *w/c* ratio for the cement paste was 0.5. To prepare a 0.001 wt% suspension, 8 mg of MWCNTs were weighted and added to 400 ml of DI water. Similarly,

to make the 0.005, 0.01 and 0.05 wt% MWCNT suspensions, 40 mg, 80 mg and 400 mg of MWCNTs were added to 400 ml of DI water, respectively. The initial pH of the solutions was measured using a pH meter (Mettler Toledo, pH electrode LE 438). Then, 5 mol/L NaOH solution in DI water was added to each suspension to reach the desired pH of ~12 (Table 2.1). At an acidic pH, functional groups tend to have a relatively low surface charge as they are deprotonated. Therefore, increasing the pH leads to protonating the functional groups, resulting in better dispersion and, thus, a lower zeta potential. Ultrasonication was performed for 35 minutes at a frequency of 40 kHz to disperse the oxidized MWCNTs uniformly in the suspensions using an ultrasonic bath sonicator (Branson 2800 CPX). Samples of the resulting MWCNT suspensions after sonication are shown in Figure 2.1.

2.2.3 Dispersibility assessment in solutions

Hydrodynamic size (HDS) was measured via dynamic light scattering (DLS) tests using a particle and molecular size analyzer (model Zetasizer nano ZS, Malvern Panalytical Ltd.). For each suspension, a 1 mL sample of solution was used for the measurement, which was performed five times for each sample to assess the variability of the results. Zeta potential was also measured using the same equipment (model Zetasizer nano ZS, Malvern Panalytical Ltd.). For each suspension, a 1 mL sample of solution was used for the measurement, which was performed 10 times to assess the variability of the results.

2.2.4 Cement paste preparation

Cement paste prisms with dimensions of 25 × 25 × 76 mm were manufactured using the MWCNT solutions and Type I OPC, with a *w/c* ratio of 0.5 (Figure 2.2). Plain cement paste prisms were also manufactured with Type I OPC and DI water for use as control specimens (0 wt%). Uniaxial compression tests and SEM micrograph analysis were conducted on these specimens. The cement paste prisms were manufactured according to ASTM C305 [2014]. The mixes were cast in acrylic molds and after 24 hours, the specimens were demolded, and then cured under saturated lime water for up to 28 days. Four samples per type were utilized for compression testing and SEM imaging. The test matrix is presented in Table 2.2.

2.2.5 Uniaxial compression test

Uniaxial compression tests were performed on the cement paste prisms after 7, 14, and 28 days of curing, using a servo-hydraulic loading frame. The load was applied in displacement-control mode at a rate of 0.3 mm/minute and was measured using a 20-kip load cell. Here, prisms with an aspect ratio of 3.0 were used to minimize the confining effects due to friction between the loading platens and the specimen surfaces and assess behavior under uniaxial loading. To this end, 0.4-mm polytetrafluoroethylene (PTFE) inserts were also placed between the specimen surfaces and the loading platens. The test setup is shown in Figure 2.3.

2.2.6 Scanning electron microscopy imaging

The dispersion of MWCNTs in cement paste and the nano- and -micro-structure of the amended cement matrix were examined through SEM imaging. After 5, 12 and 26

days of curing, the prism specimens were removed from the lime-saturated water, and then broken into pieces. These pieces were air-dried in a controlled-temperature (68 to 85°F) and humidity (42 to 68 RH%) chamber for 48 hours. Air drying was preferred to oven-drying over concerns on the possibility of affecting the formation of cement hydrates. After air drying, pieces lesser than 5 mm in size in any direction were selected for SEM imaging based on the capacity of the microscope. Prior to testing, the selected samples were placed in a vacuum-suction chamber for one hour to remove the excess moisture. Then, these samples were gold sputtered.

A field-emission scanning electron microscope (Ultraplus Thermal Field Emission Scanning Electron Microscope, Zeiss) was utilized to observe the distribution of MWCNTs in the fractured cement paste samples and observe the nano- and micro-structure of the composite matrix, thus making it possible to obtain high-magnification SEM micrographs while minimizing electrostatic distortions. A different microscope (Tescan Vega3 SEM) was utilized to obtain lower-magnification and detailed images of the free curing surfaces (i.e., surfaces that cured in direct contact with the lime-saturated water) of the MWCNT-amended and control cement paste samples.

2.3. RESULTS AND DISCUSSIONS

2.3.1 Dispersibility assessment in solution

With the increase in MWCNT content, a tendency to agglomerate was observed visually after sonication (Figure 2.1). In fact, while the 0.001 wt% (0.02 g/L) suspension was nearly transparent, relatively darker solutions were observed for 0.005 to 0.01 wt% (0.1 to 0.2 g/L) concentrations, the darkest being observed for the 0.05 wt% (1 g/L)

concentration in which MWCNT agglomerates were visible. Increasing MWCNT concentrations from 0.001 to 0.05 wt% led to increasing values of HDS (Figure 2.4). As the MWCNT concentration increases, aggregation is facilitated also because the free Brownian motion of the particles is restrained due to the limited space between these particles, a concept illustrated previously (e.g., [Baalousha 2009]).

Therefore, better dispersion was achieved at decreasing MWCNT concentrations. In addition, for suspensions with MWCNT concentration from 0.001 to 0.01 wt% (0.02 to 0.2 g/L), suspensions were found stable as highlighted by the zeta potential values below the -30 mV threshold). Instead, samples having 0.05 wt% (1 g/L) concentration of MWCNTs (Figure 2.5) were found unstable as highlighted by the zeta potential consistently well above the -30 mV threshold [Freitas and Muller 1998].

2.3.2 Compressive strength assessment

Figure 2.6 presents the compressive strength mean and standard deviation for the cement paste specimens as a function of MWCNT concentration and curing time (e.g., "0.001-7" includes specimens with 0.001 wt% MWCNT concentration tested after 7 days of curing). The incorporation of oxidized MWCNTs did not produce consistent enhancements in compressive strength up to 14 days of curing, Instead, the average compressive strength after 28 days of curing was consistently higher for the MWCNT-amended cement paste specimens compared to the plain cement paste specimens. The average increase in strength was in the range 18-25% for concentrations in the range 0.001-0.05 wt%.

It is important to notice that a statistically insignificant enhancement in

compressive strength was attained after 28 days of curing using 0.05 wt% MWCNT concentrations compared to 0.01 wt% as well as 0.001 wt%. In fact, it is reasonable to expect that the visible MWCNT agglomerates in unstable aqueous suspensions contribute to reducing the homogeneity of the cement paste, thereby negatively contributing to enhancements produce through other means. To better understand the dispersibility and embedment of MWCNTs in the cement paste, SEM micrographs were acquired from fractured surfaces.

2.3.3 Scanning electron microscopy analysis

SEM imaging was enlisted to gain visual evidence on the physical structure of the plain and MWCNT-amended cement paste. Figure 2.7 through Figure 2.9 show representative SEM micrographs of the free surface (i.e., in direct contact with the curing water) after 5, 12 and 26 days of curing for plain and MWCNT-amended cement paste. The MWCNT-amended cement paste clearly exhibited a less porous surface micro-structure. This evidence suggests that surface modification resulting from the incorporation of oxidized MWCNTs may be an important factor to enhance durability, for example by curtailing the ingress of aggressive ions in air or water (e.g., deicing salts).

The nano- and micro-structures of the control and MWCNT-amended (0.001 and 0.05 wt%) cement paste after 5 days of curing are shown in the representative SEM micrographs in Figure 2.10. Well-dispersed and non-agglomerated MWCNTs were consistently noted for the 0.001 wt% concentration (Figure 2.10b) in the cement paste matrix were observed whereas agglomerated MWCNTs were consistently observed for

the 0.05 wt% concentration (Figure 2.10c). However, accelerated formation of amorphous C-S-H was consistently observed in cement paste amended with 0.001 and 0.05 wt% of MWCNTs, as highlighted by the yellow dashed lines in Figure 2.10b and Figure 2.10c, respectively.

The nano- and micro-structures of the control and MWCNT-amended cement paste after 12 days of curing are shown in the representative SEM micrographs in Figure 2.11. Ettringite was consistently found in the control samples (orange arrows in Figure 2.11a). Plate-like calcium monosulfate hydrates [Mehta and Monteiro 2006] were also found in the control samples (green circles); it is noted that these hydrates may contribute to making cement composites more susceptible to undesired sulfate attack [Mehta and Monteiro 2006]. Again, a uniform distribution of the oxidized MWCNTs was consistently observed for the 0.001 wt% concentration (Figure 2.11b) whereas agglomerated MWCNTs were consistently observed for the 0.05 wt% concentration (Figure 2.11c). Again, preferential (i.e., in the vicinity of MWCNTs) formation of amorphous C-S-H was noticed for 0.001 and 0.05 wt% MWCNT concentrations (Figure 2.11b and Figure 2.11c).

The nano- and micro-structures of the control and MWCNT-amended cement paste after 26 days of curing are shown in the representative SEM micrographs in Figure 2.12. Plate-like calcium monosulfate hydrates [Mehta 2006] were consistently found in the control samples (Figure 2.12a). Uniform distribution of MWCNTs was observed at a 0.001 wt% concentration (Figure 2.12b) whereas, again, agglomerated MWCNTs were consistently observed at a 0.05 wt% concentration (Figure 2.12c). Preferential formation

of amorphous C-S-H was confirmed for both MWCNT concentrations of 0.001 and 0.05 wt% (Figure 2.12b and Figure 2.12c).

Larger pores (>50 nm) were more frequently observed in the matrix of control samples after 26 days of curing (red arrows in Figure 2.12a) compared to MWCNT-amended samples, where smaller pores (<50 nm) were more frequently observed after 12 days of curing (red arrows in Figure 2.11b and Figure 2.11c) as well as 26 days of curing (red arrows in Figure 2.12b and Figure 2.12c), which indicates pore size refinement as a structural modification resulting from the incorporation of oxidized MWCNTs.

It is concluded that the nano- and micro-structure of cement paste was significantly modified through the incorporation of oxidized MWCNTs, in concentrations as low as 0.001 wt%. The intrusion of MWCNTs in voids and possibly the preferential formation of cement hydrates in the vicinity of the embedded MWCNTs appear to result in pore-size refinement, together with less porous and more homogeneous curing surfaces.

2.4. CONCLUSIONS

The evidence presented in this chapter shows that:

- Good dispersion of oxidized MWCNTs in aqueous solutions was observed visually for concentrations from 0.02 to 0.2 g/L (0.001 to 0.01 wt%).
- Visible MWCNT agglomerates were observed at a concentration of 1 g/L (0.05 wt%) in aqueous suspensions.

- Good dispersion in aqueous solutions was achieved with 0.001-0.01 wt% of MWCNT concentrations in terms of hydrodynamic size, unlike the 0.05 wt% concentration.
- An absolute value of zeta potential consistently above 30 mV for MWCNT concentrations in the range 0.001-0.01 wt% confirmed the stability of the aqueous suspensions.
- An absolute value of zeta potential consistently below 30 mV for an upper-bound MWCNT concentration of 0.05 wt% (typically portrayed as a low concentration in the archival literature) of MWCNTs confirmed the instability of aqueous suspensions, and a tendency of the MWCNTs to agglomerate.
- Insignificant enhancements in compressive strength were observed in MWCNT-amended cement paste specimens with 0.05 wt% concentration compared to 0.01 wt% and 0.001 wt% concentrations after 28 days of curing.
- A less porous surface micro-structure of cement paste was observed as a result of MWCNT-amendment.
- Well-dispersed MWCNTs were consistently observed in cement paste for a MWCNT concentration of 0.001 wt%. Instead, MWCNTs consistently aggregated at a concentration of 0.05 wt%.
- No ettringite and calcium monosulfate hydrates and a greater amount of C-S-H were identified in MWCNT-amended paste samples, which resulted in enhanced nano- and micro-structures.

- Pore-size refinement was observed in MWCNT-amended cement paste, irrespective of the MWCNT concentration.

- Based on SEM analysis, it appears that possible mechanisms of strength enhancement due to MWCNT amendment include the preferential and well-distributed formation of C-S-H, and pore-size refinement, irrespective of the MWCNT concentration. However, the consistent tendency of MWCNTs to aggregate at a 0.05 wt% concentration seems to contribute to reducing homogeneity and introducing defect sites, resulting in less strength enhancement.

- At a MWCNT concentration of 0.05 wt% (and above, one may reasonably hypothesize), the aggregation of MWCNTs reduces the specific surface area, thus hindering the nucleation effect leading to the preferential formation of C-S-H. Therefore, lower MWCNT concentrations may be preferable compared to 0.05 wt% or higher, which are predominant in the literature.

- By reducing the concentration of MWCNTs by 50 times compared to the lower-bound value of 0.05 wt% in the literature for cement paste, similar strength enhancements were achieved. This contribution to the current state of the art is important also because it highlights the potential of exploring lower concentrations, thereby more rationally taking advantage of the surface area of oxidized MWCNTs.

- Partially or fully unzipping the outermost layers of MWCNTs increases the open surface area and functionality, thus facilitating the use of smaller concentrations of graphitic nanoparticles. These novel concepts related to particle morphology and concentration are explored for the first time in Chapters 3 and 4.

2.5. REFERENCES

ASTM International. Standard Practice for Mechanical Mixing of Hydraulic Cement Pastes and Mortars of Plastic Consistency. ASTM C305-14. West Conshohocken, PA: ASTM International, 2014.

Aich N, Zohhadi N, Khan IA, Matta F, Ziehl P, and Saleh NB. Applied TEM approach for micro/nanostructural characterization of carbon nanotube reinforced cementitious composites. Journal of Research Updates in Polymer Science 2012; 1, 14-23.

Baalousha M. Aggregation and Disaggregation of Iron Oxide Nanoparticles: Influence of Particle Concentration, PH and Natural Organic Matter. Science of the Total Environment 2009; 407, 2093-2101.

Freitas C, Muller RH. Effect of Light and Temperature on Zeta Potential and Physical Stability in Solid Lipid Nanoparticle (SLN™) Dispersions. International Journal of Pharmaceutics 1998; 168, 221–229.

Li GY, Wang PM, Zhao X. Mechanical Behavior and Microstructure of Cement Composites Incorporating Surface-Treated Multi-Walled Carbon Nanotubes. Carbon 2005; 43(2005), 1239–1245.

Matta F, Cuellar-Azcarate MC, Wylie EM, Mejia Y, Iffat S, Sikder M, Powell B, Serkiz S, Baalousha M, Caicedo J. Nano-Amended Cement Waste Forms for Nuclear Waste Storage. 6th International Symposium on Nanotechnology in Construction (NICOM6), 2018; Hong Kong, China.

Makar JM and Chan GW. Growth of Cement Hydration Products on Single-Walled Carbon Nanotubes. Journal of the American Ceramic Society 2009; 92 (6), 1303–1310.

Mehta PK, Monteiro PJM. Concrete microstructure, properties, and materials. McGraw-Hill Education; 4th Edition, 2006.

Nochaiya T and Chaipanich A. Behavior of Multi-Walled Carbon Nanotubes on the Porosity and Microstructure of Cement-Based Materials. Applied Surface Science 2011; 257, 1941–1945.

Zohhadi N. Functionalized Graphitic Nanoreinforcement for Cement Composites. PhD Dissertation 2014; University of South Carolina, Columbia.

2.6. TABLES

Table 2.1 Controlling pH of the oxidized MWCNT-suspensions

MWCNT-content [wt%]	Initial pH	Amount of added NaOH [µL]	Adjusted pH	Final Volume [mL]	Final Concentration of NaOH [Mol/L]
0.001	5.30	10	12.03	10	0.005
0.01	4.61	40	12.08	10	0.02
0.05	3.98	60	12.20	10	0.025

Table 2.2 Test matrix for physico-mechanical tests on cement paste with MWCNTs

MWCNT concentration [wt%]	Tests	Number of specimens	Specimens to be cast
Control (0)	Compressive strength	4*	5
	SEM imaging	Crushed from failed prisms	
0.001	Compressive strength	4*	5
	SEM imaging	Crushed from failed prisms	
0.005	Compressive strength	4*	5
	SEM imaging	Crushed from failed prisms	
0.01	Compressive strength	4*	5
	SEM imaging	Crushed from failed prisms	
0.05	Compressive strength	4*	5
	SEM imaging	Crushed from failed prisms	

* While a minimum number of 4 specimens are considered to ensure statistical meaningfulness, up to 5 specimens were cast

2.7. FIGURES

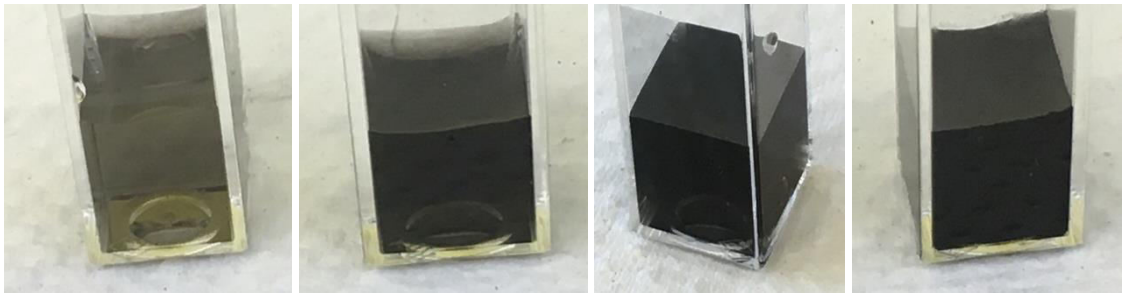

Figure 2.1 MWCNT-suspensions in DI water

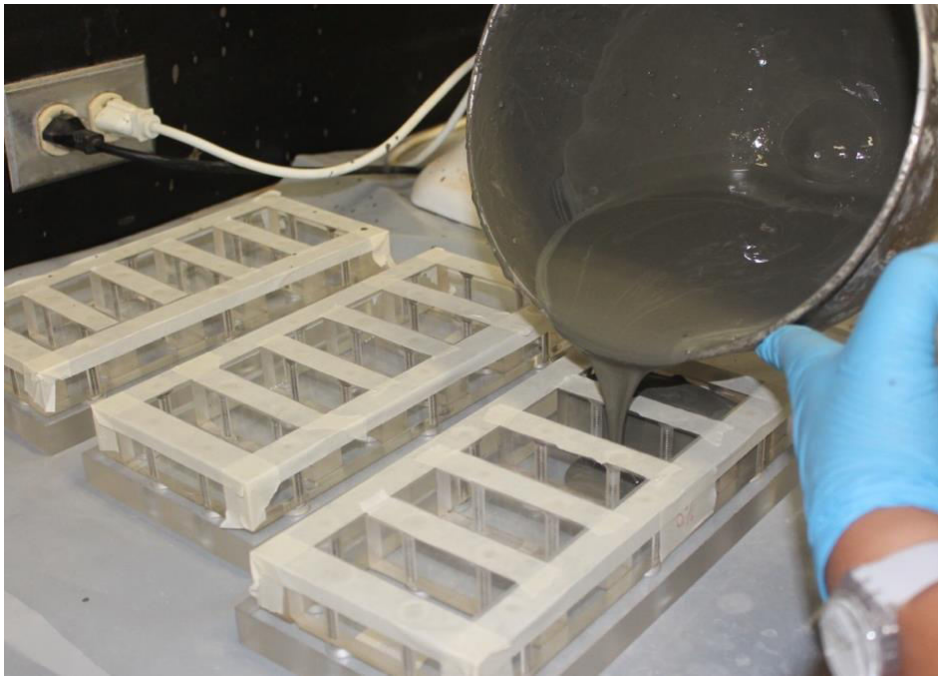

Figure 2.2 Casting cement paste prisms

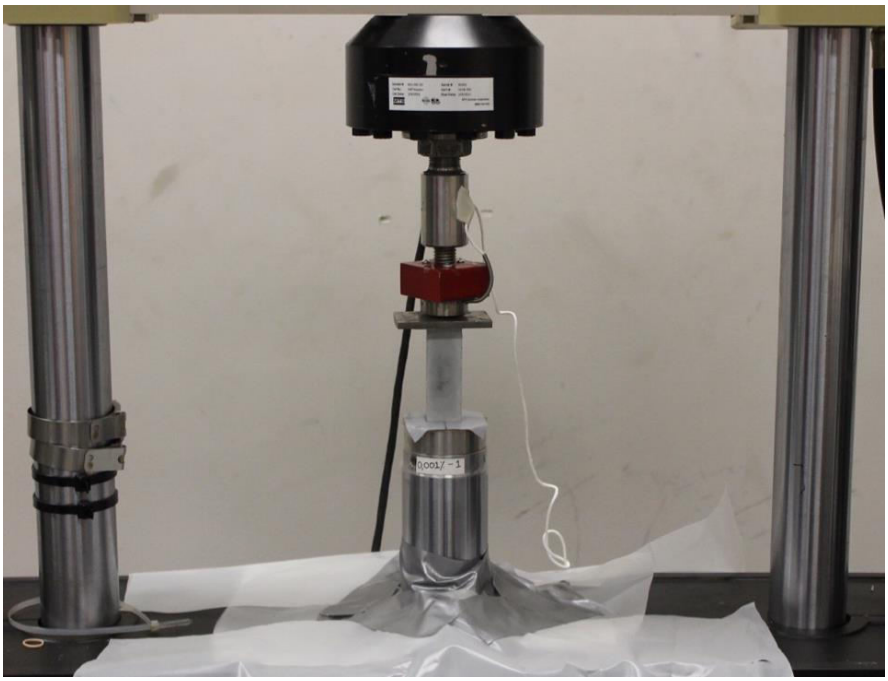

Figure 2.3 Uniaxial compression test

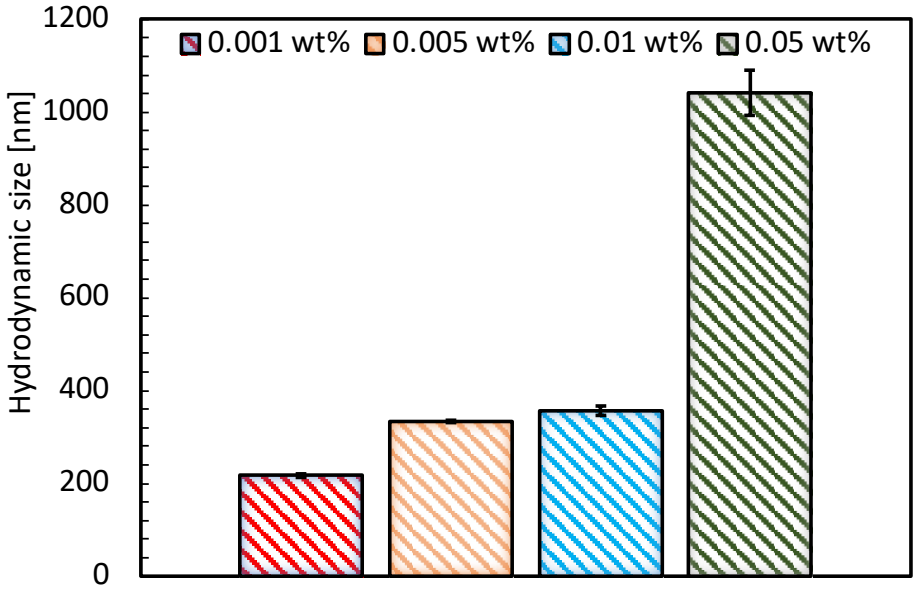

Figure 2.4 Hydrodynamic size for different MWCNT concentrations (0.02 g/L, 0.1 g/L, 0.2 g/L and 1 g/L)

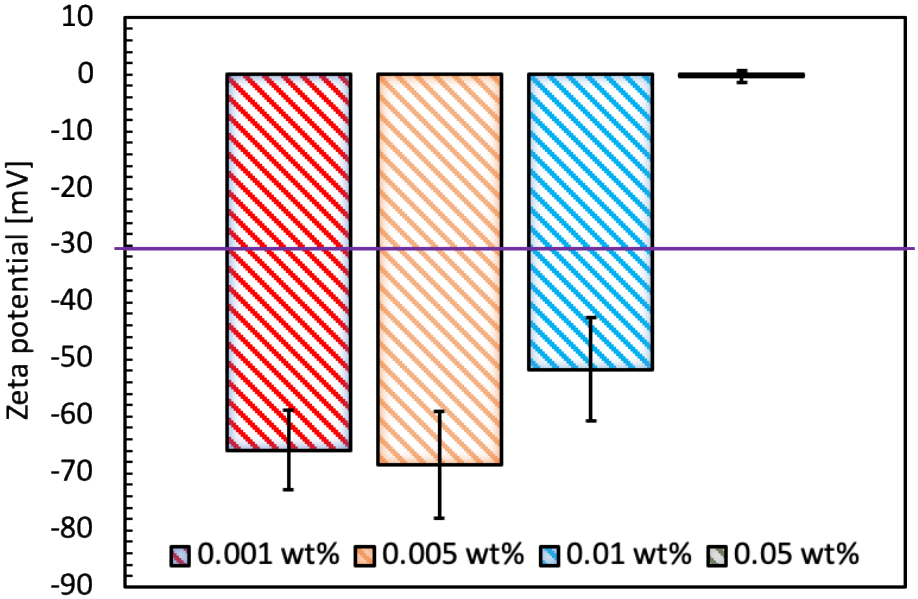

Figure 2.5 Zeta potential for different MWCNT concentrations (0.02 g/L, 0.1 g/L, 0.2 g/L and 1 g/L)

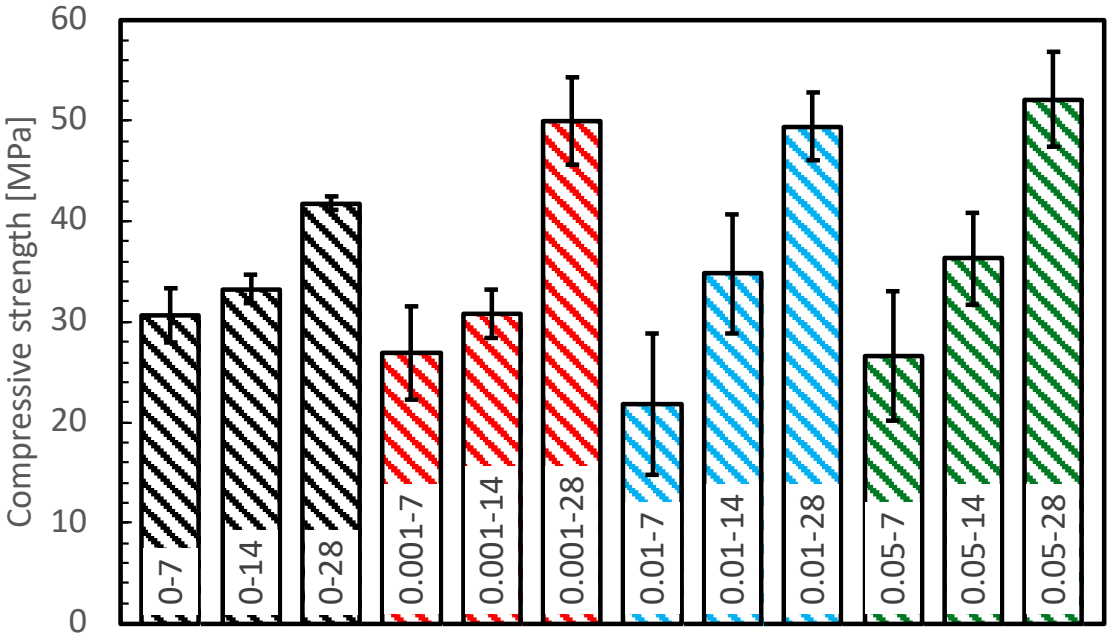

Figure 2.6 Uniaxial compressive strength results for cement paste prisms

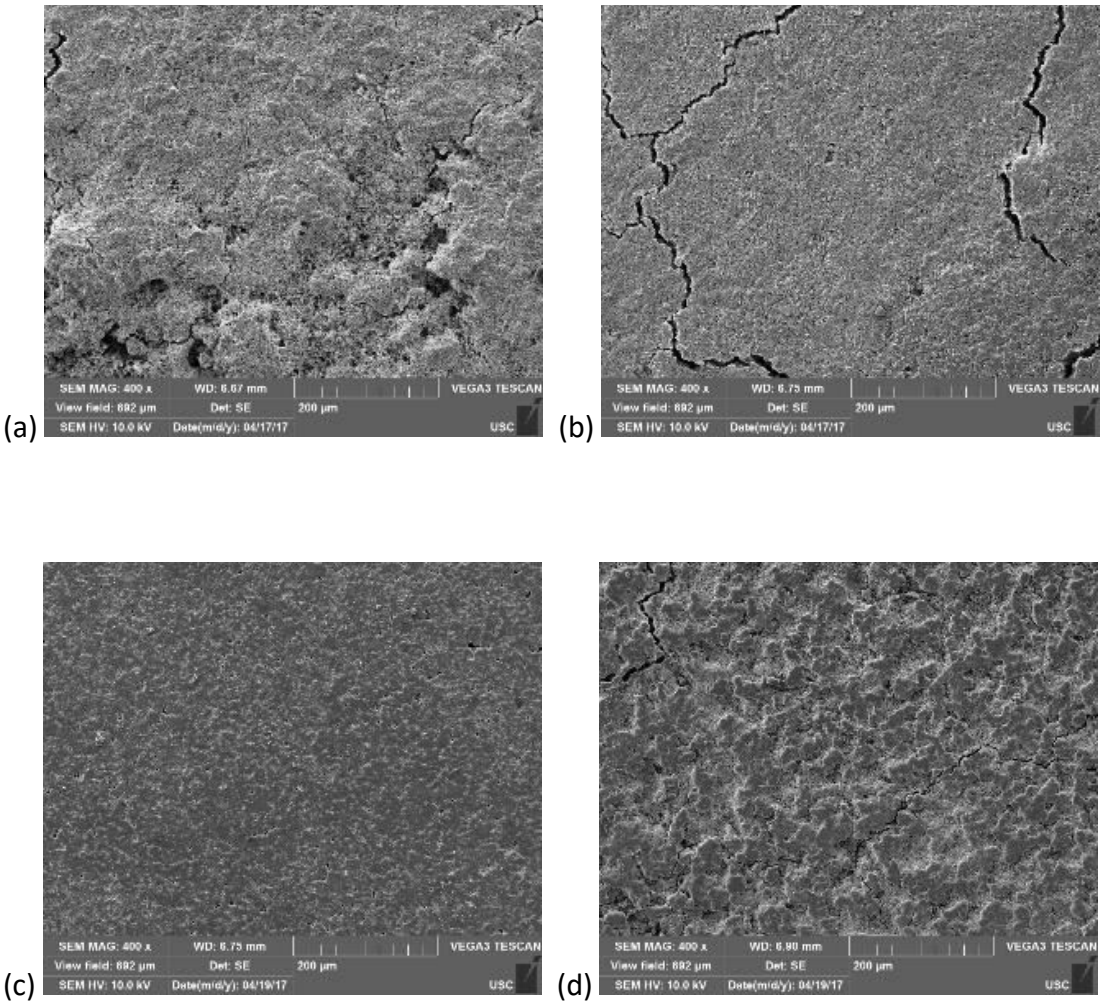

Figure 2.7 Free curing surfaces of cement paste amended with (a) 0 wt% (b) 0.001 wt% (c) 0.005 wt% (d) 0.05 wt% of MWCNTs, after 5 days of curing

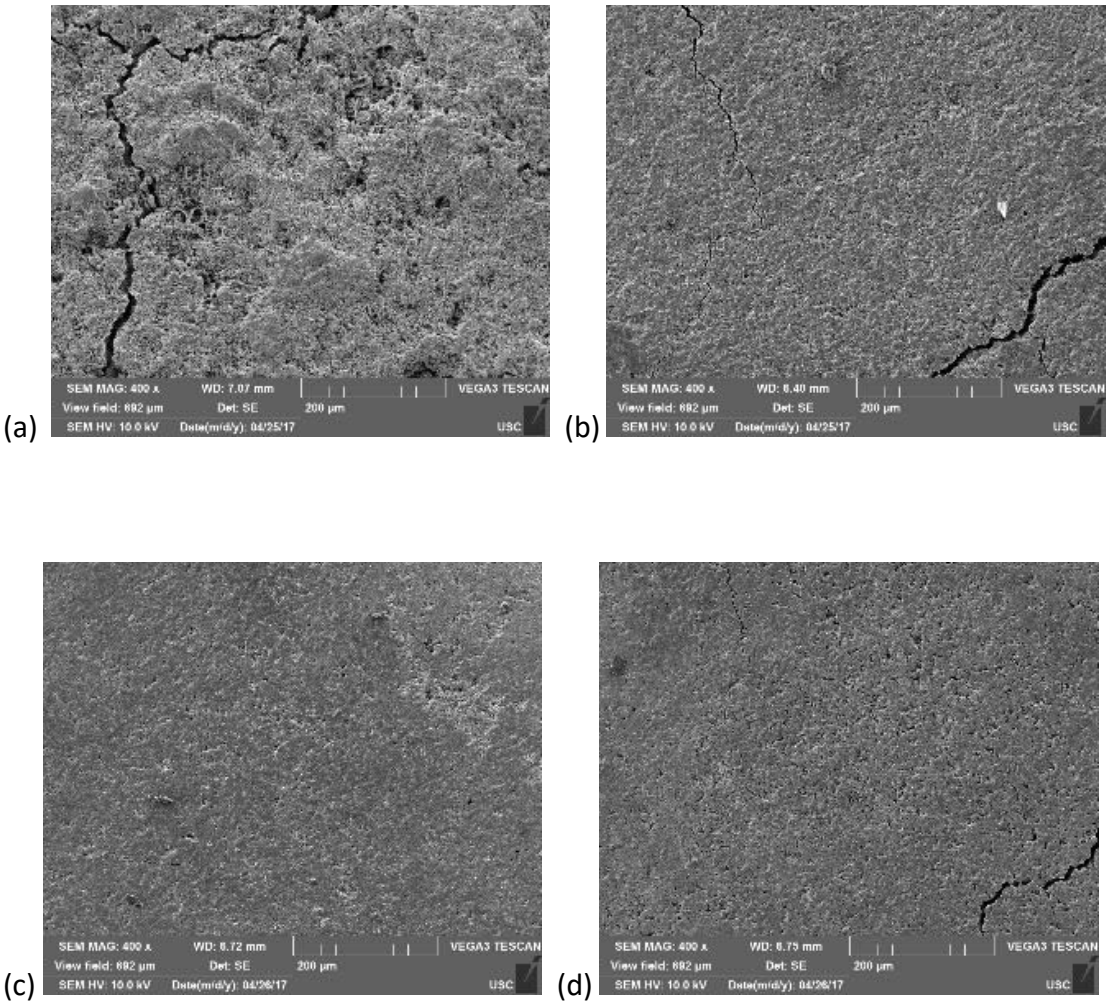

Figure 2.8 Free curing surfaces of cement paste amended with (a) 0 wt% (b) 0.001 wt% (c) 0.005 wt% (d) 0.05 wt% of MWCNTs, after 12 days of curing

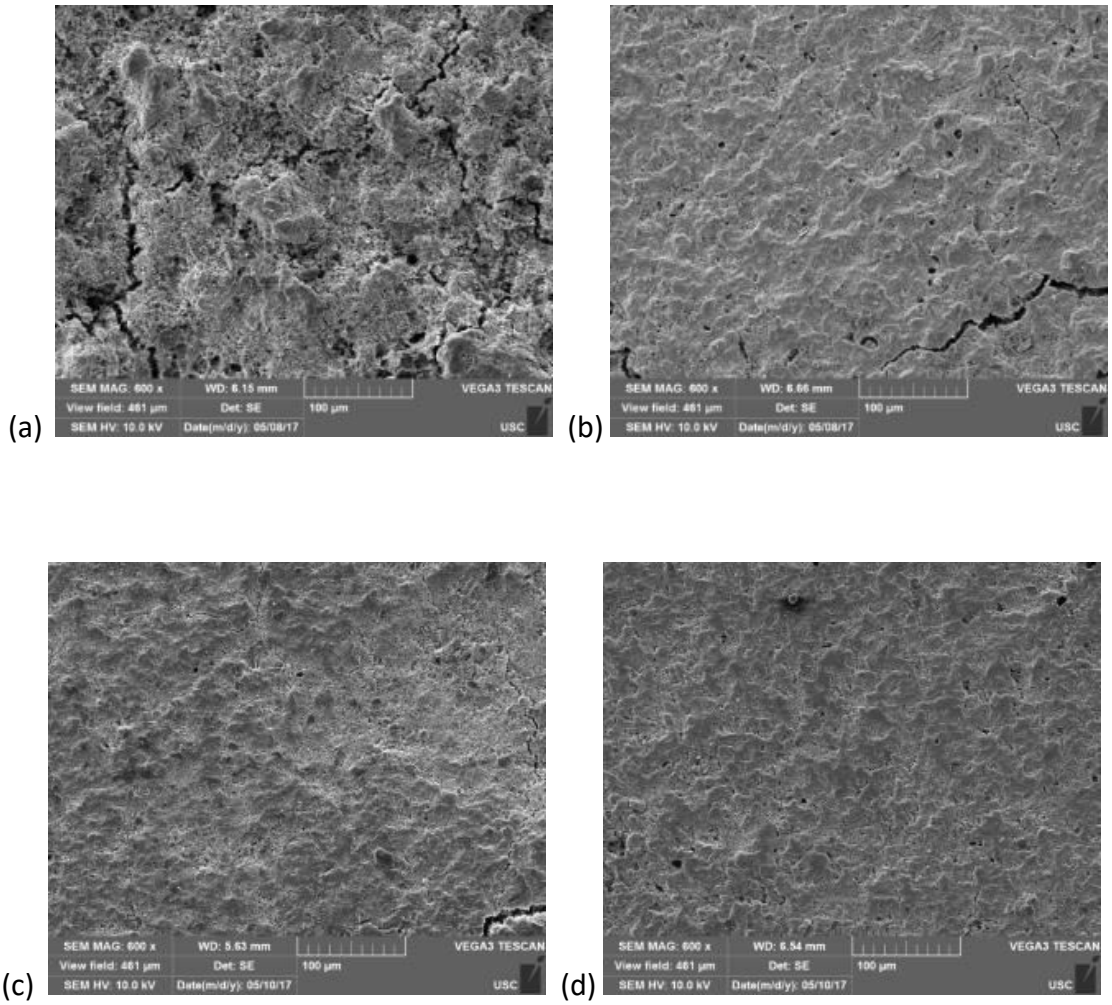

Figure 2.9 Free curing surfaces of cement paste amended with (a) 0 wt% (b) 0.001 wt% (c) 0.005 wt% (d) 0.05 wt% of MWCNTs, after 26 days of curing

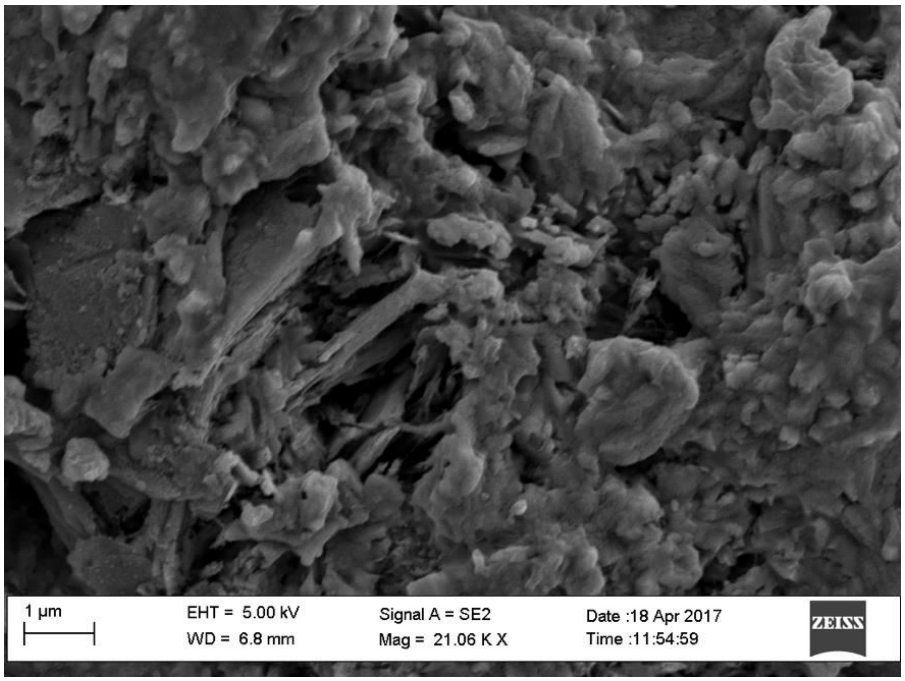
1 µm
EHT = 5.00 kV
WD = 6.8 mm
Signal A = SE2
Mag = 21.06 K X
Date :18 Apr 2017
Time :11:54:59
ZEISS

(a)

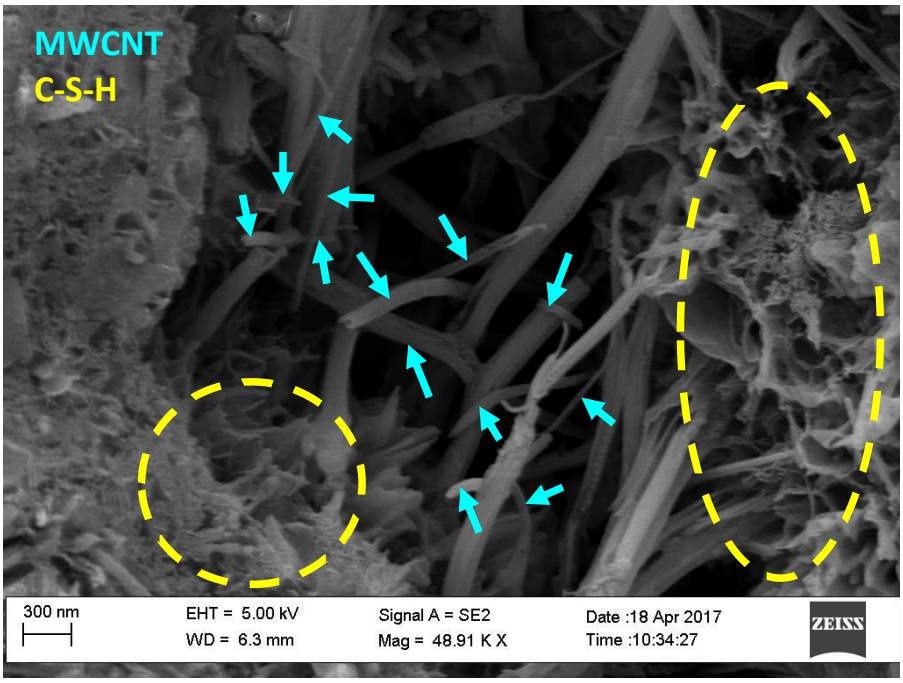
MWCNT
C-S-H
300 nm
EHT = 5.00 kV
WD = 6.3 mm
Signal A = SE2
Mag = 48.91 K X
Date :18 Apr 2017
Time :10:34:27
ZEISS

(b)

(c)

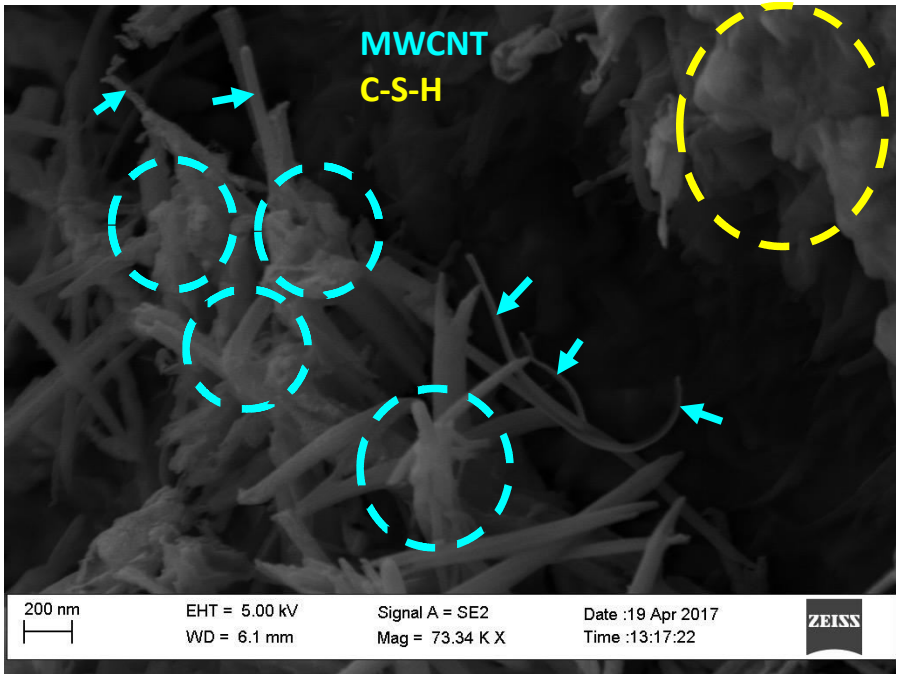

Figure 2.10 Nano- and micro-structure of cement paste for (a) 0 wt% (b) 0.001 wt% (c) 0.05 wt% MWCNT concentration after 5 days of curing

(a)

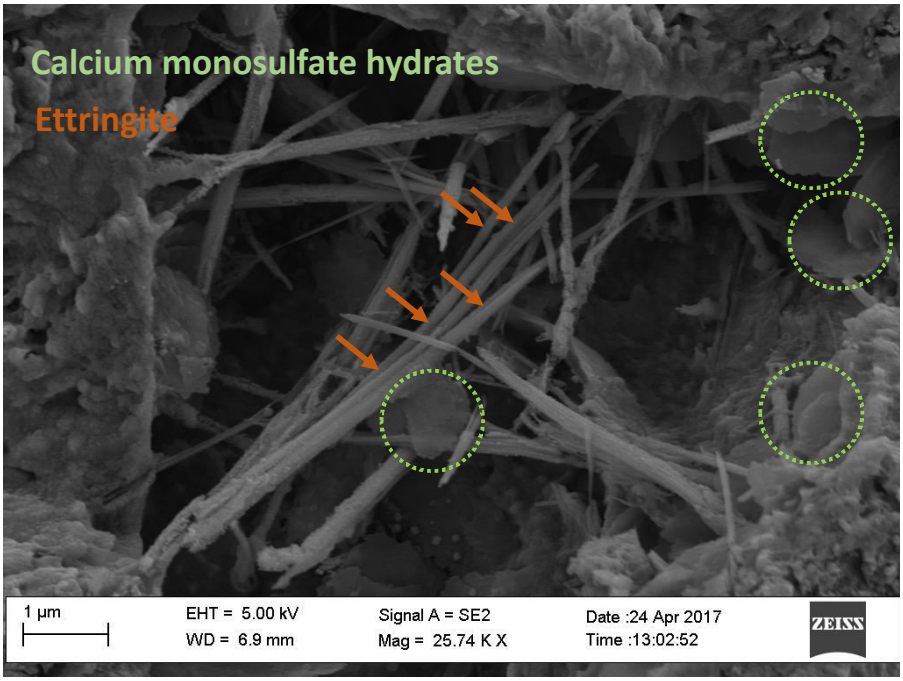

(b)

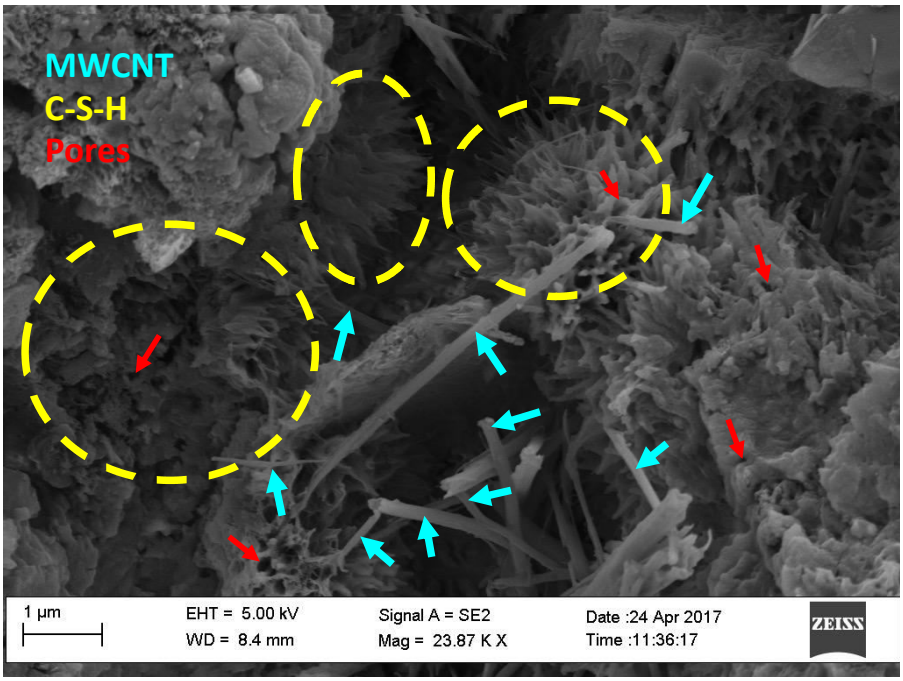

(c)

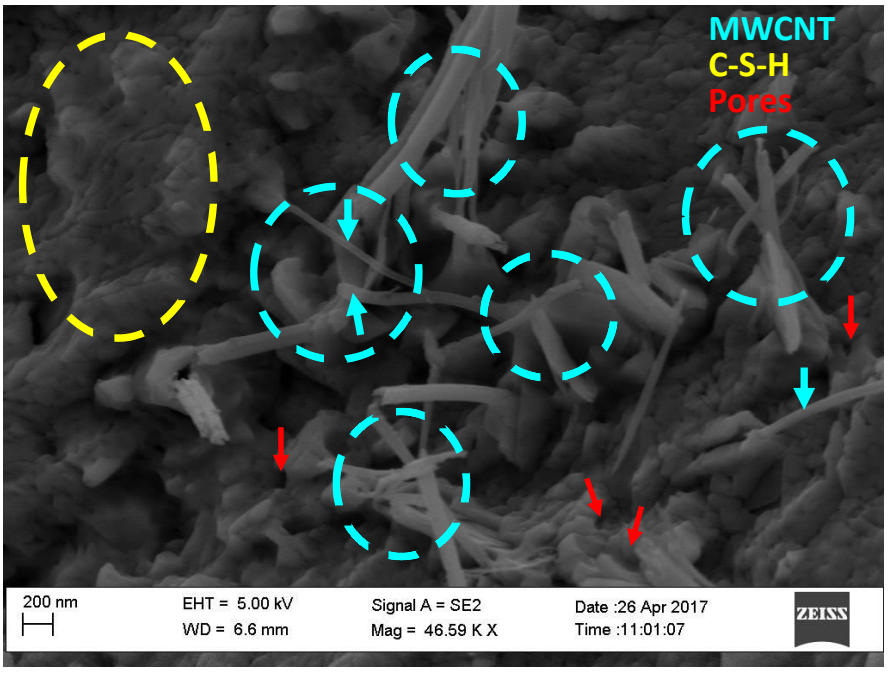

Figure 2.11 Nano- and micro-structure of cement paste for (a) 0 wt% (b) 0.001 wt% (c) 0.05 wt% MWCNT concentration after 12 days of curing

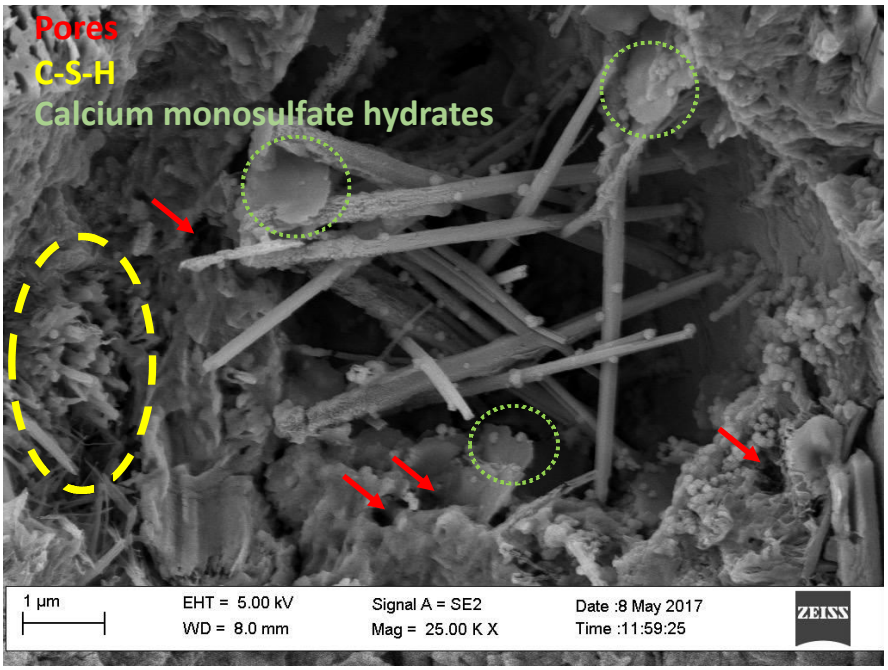
Pores
C-S-H
Calcium monosulfate hydrates
1 µm
EHT = 5.00 kV
WD = 8.0 mm
Signal A = SE2
Mag = 25.00 K X
Date :8 May 2017
Time :11:59:25
ZEISS

(a)

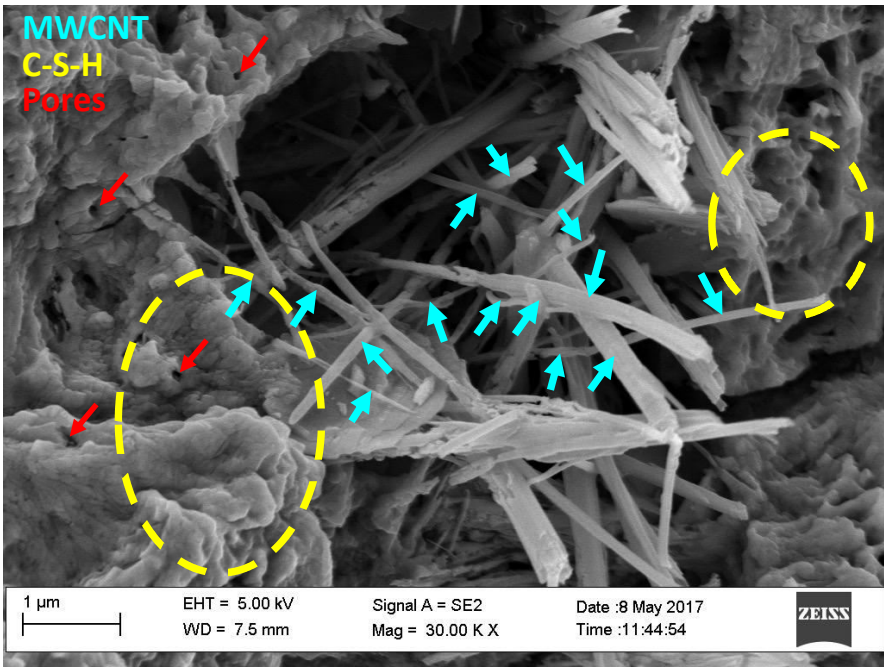
MWCNT
C-S-H
Pores
1 µm
EHT = 5.00 kV
WD = 7.5 mm
Signal A = SE2
Mag = 30.00 K X
Date :8 May 2017
Time :11:44:54
ZEISS

(b)

(c)

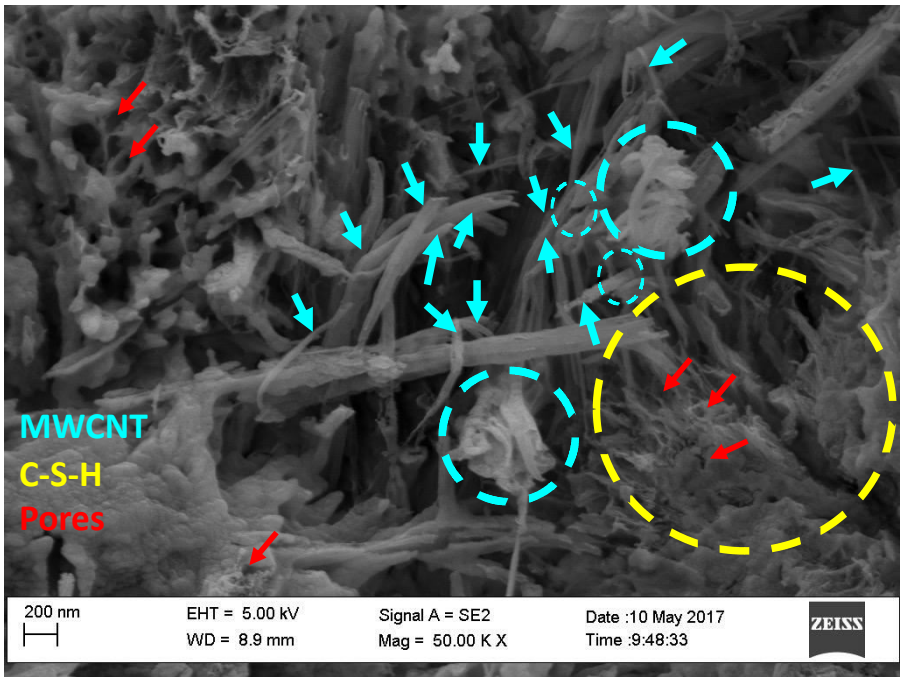

Figure 2.12 Nano- and micro-structure of cement paste for (a) 0 wt% (b) 0.001 wt% (c) 0.05 wt% MWCNT concentration after 26 days of curing

CHAPTER 3

AMENDMENT OF CEMENT PASTE WITH PARTIALLY-UNZIPPED CARBON NANOTUBES

3.1. INTRODUCTION

This chapter discusses the effect of embedding different concentrations of oxidized partially unzipped carbon nanotubes (PUCNTs) on salient mechanical properties and the nano- and micro-structure of cement paste. Partial unzipping of the outer walls of MWCNTs results in a radical increase in the open surface area [Jeong et al. 2016] while oxidation produces functional groups on said areas [Song et al. 2014], thereby hypothetically enhancing the chemical affinity with cement matrices.

3.2. EXPERIMENTAL PROGRAM

3.2.1 Preparation of PUCNTs and functionalization

In this research, oxidation was utilized as a functionalization method to create water-soluble oxygen-contained compounds on the surfaces of PUCNTs, to reduce their hydrophobicity. The MWCNTs (C-grade) used in this experiment were sourced from NanoTechLabs (Yadkinville, NC) and used as received. Sulfuric acid (ACS reagent,95.0-98.0%), hydrogen peroxide (30 wt%), and potassium permanganate (>99.0% purity)

were obtained from Sigma Aldrich. O-phosphoric acid (85% solution) and hydrochloric acid (32-38% solution) were obtained from Fisher Scientific Co.

MWCNTs were added to a beaker containing sulfuric acid. This mixture was stirred for 1 hour and 10 minutes before adding O-phosphoric acid. After 15 minutes elapsed, potassium permanganate ($KMnO_4$) was added to the mixture slowly with continued stirring. Immediately after this addition, the beaker was heated such that it maintained 65 °C ± 1.5 °C. The heat-treatment time interval was 1 hour and 30 minutes. When cooled, ice and hydrogen peroxide were poured into two beakers. Half of the reaction product was poured slowly into each beaker containing ice and peroxide, ensuring boiling did not occur. Once fully quenched, the solution was diluted with an additional deionized (DI) water and allowed to coagulate overnight (15 hours). The reaction product was decanted from the separatory funnel, and any remaining liquid was filtered through a vacuum filtration apparatus. The filter cake was then rinsed with HCl twice while stirring to prevent the filter cake from condensing. The agitated material was then washed several times with DI water until neutralized from the acid. The filter cake was then resuspended in DI water.

PUCNTs were unzipped from MWCNTs via an oxidative heating process [Kosynkin et al. 2009]. Defects in the pristine MWCNTs were created by soaking them in concentrated acid with the oxidant. By controlling the amount of oxidant, heating time, and soaking time, the oxidized PUCNTs were obtained (Figure 3.1).

3.2.2 X-ray Diffraction

XRD analysis was performed to monitor the degree of oxidative unzipping. The unzipping procedure was optimized by varying the oxidizer ($KMnO_4$) content and reaction time. $KMnO_4$ content was varied between 300 and 800 wt% with oxidation times ranging from 1 to 2 hrs. The key signature is the graphite reflection observed at ~26° for 0.335 nm carbon layer spacing, which is present in CNTs. As the graphitic content decreases there is a corresponding decrease in magnitude of the 26° diffraction signal. As shown in Figure 3.2, where at 1.5 hrs. oxidation time, a trend of increasing oxidizer content and decreasing peak intensity can be observed. This indicates loss of 0.335 nm carbon layer spacing corresponding with increased unzipping. Full unzipping can be observed at 500 wt% $KMnO_4$ (1.5 hrs.) when the peak at 26° disappears completely. Optimal conditions to produce a PUCNT with high oxygen content (>20%) while still maintaining high aspect ratio was determined to be 400 wt% $KMnO_4$ for 1.5 hrs.

3.2.3 FTIR Spectroscopy

An FTIR analysis of CNTs, PUCNTs, and fully unzipped nanoribbons (GONRs) was performed to characterize the type and degree of functionalization. The PUCNTs and GONRs samples show a pattern of vibrations consistent with that of oxidatively unzipped CNTs. The absorbance peak observed at 2911 cm^{-1} is assigned to the C-H stretching frequency which decrease in intensity with increased nanoribbon oxidation (Figure 3.3). The broad absorptions from ~3200 cm^{-1} to ~3600 cm^{-1} correlate with O-H stretching corresponding with surface adsorbed water as well as water trapped

between stacked ribbon layers and carboxylic acid groups both of which increase in magnitude with increased oxidation and indicate increased hydrophilicity (Figure 3.3). The adsorption peak at 1737 cm^{-1} is assigned to the unconjugated C=O stretch of carboxylic acid while the peaks at 1613 cm^{-1}, 1416 cm^{-1}, 1219 cm^{-1}, 1037 cm^{-1} and 970 cm^{-1} correspond to various C-O stretching frequencies such as carboxylic acids, and esters. The C=O and C-O based oxygen functionalities were most prevalent in the fully unzipped nanoribbons which is indicative of edge site population. There was an apparent shift in the stretching frequency of the C=O bond from the partially unzipped (1715 cm^{-1}; red line) to the fully unzipped (1737 cm^{-1}; blue line) nanoribbon. This was consistent with the findings from Kosynkin et al. [2009] and was attributed to decreasing conjugation in the nanoribbon plane which occur when significant in-plane functionalization takes place. The FTIR spectroscopy qualitatively shows an increase in oxygen functional groups for the PUCNTs with a larger increase to oxygen content including additional in-plane, edge site functionalization for the GONRs.

3.2.4 Raman Spectroscopy

The Raman spectrum, Figure 3.4, shows three Raman scattering bands of interest at approximately 1360 cm^{-1}, 1590 cm^{-1}, and 2710 cm^{-1}, corresponding to the D1 band, G band, and the second order 2D1 band respectively. An intense, narrow G-band peak at 1590 cm^{-1} is associated with ordered sp^2 structures (i.e., the hexagonal planar structure), which can be observed in the pristine CNT spectrum and decreases in magnitude with greater oxidation as does the 2D1 band which is nearly absent in the GONRs. In contrast, the D1 band corresponds to the degree of disorder/defects in the

sp^2 single atomic layer planes. The Raman spectra shows an increasing D1 band (i.e., increasing disorder) for the partially unzipped and fully unzipped CNTs with an accompanying increase in the full width at half maximum for both the G and D1 bands. Finally, a small positive frequency shift is observed in the G band which can be attributed to increasing in-plane oxygen content. Raman spectral analysis of the MWCNTs, PUCNTs, and GONRs shows decreasing sp^2 hybridization and increasing disorder and defects with increasing oxidation and unzipping, as originally hypothesized.

3.2.5 Preparation of PUCNT-suspensions in DI water

Stock solution of prepared oxidized PUCNTs was diluted with DI water to prepare 0.02g/L (0.001wt%), 0.1 g/L (0.005 wt%) and 1g/L (0.05 wt%) solutions (Figure 3.5). The initial pH values of the suspensions were recorded with a pH meter (Mettler Toledo, pH electrode LE 438) and are presented in Table 3.1. As the supplied PUCNTs were acid treated, the initial pH of the suspensions was in the acidic range 2-4. To raise the pH to ~12, a negligible amount of (<0.01 mol/L) NaOH solution in DI water was added to the suspensions. The resultant molar concentrations of the added NaOH solutions in 0.001, 0.005 and 0.05 wt% of PUCNT suspensions were estimated as 0.002, 0.003 and 0.012 mol/L, respectively (Table 3.1). Ultrasonication was performed using a bath sonicator (Branson, 2800 CPX) only on the initial day for 15 minutes at a frequency of 40 kHz to confirm good dispersion of the PUCNTs in the suspensions.

3.2.6 Dispersibility assessment in aqueous solutions

The dispersed suspensions should be stable over time to avoid re-agglomeration. Stability of suspensions indicates effective dispersion of the nanoparticles in water,

which can be quantitatively assessed through DLS analysis. The zeta potential (ZP) indicates the stability of the dispersion of colloidal particles, which is evaluated through DLS. Absolute values of ZP above 30 mV indicate standard stability, 40-60 mV indicate good stability, and above 60 mV indicate excellent stability [Freitas and Muller 1998]. The dispersion of PUCNTs in aqueous solutions may also be assessed based on average hydrodynamic size (HDS) (e.g., [Gigault et al. 2012] and [Zohhadi 2014]). In particular, if the HDS value is consistent over time, then PUCNTs are likely not aggregating.

In this research, visual inspection of the suspensions, ZP and HDS measurements were performed at 0, 3, 7 and 10 days after the preparation of the suspensions to verify stability over time. HDS and ZP were measured through DLS testing using a particle and molecular size analyzer (model Zetasizer nano ZS, Malvern Panalytical Ltd.). A 1 mL sample of solution was used in each case; to assess the variability of the results, for ZP measurement each measurement was performed 10 times, and for HDS measurement each measurement was performed five times.

3.2.7 Uniaxial compression testing

After confirming good dispersion in water through DLS, 25×25×76 mm cement paste prisms were made with the prepared solutions and Type I ordinary Portland cement (OPC), with a water-to-cement mass ratio of 0.5. Plain cement paste prisms were also manufactured with DI water and used as control specimens (0 wt%). The cement paste prisms were manufactured according to ASTM C305 [2014]. The mixes were cast in acrylic molds and, after 24 hours, the specimens were demolded and placed in saturated lime water for up to 28 days. Four samples per type were utilized for

compression testing and imaging, to confirm statistical meaningfulness. The test matrix is presented in Table 3.2.

Uniaxial compression tests were performed using a servo-hydraulic loading frame. A representative test setup is shown in Figure 3.6. Four specimens were tested for each PUCNT concentration (0, 0.001, 0.005 and 0.05 wt%) under displacement-control mode, with a displacement rate of 0.3 mm/minute (Figure 3.6). Polytetrafluoroethylene (PTFE) inserts with a thickness of 0.4 mm were placed between the specimen surfaces and the loading platens to minimize friction.

3.2.8 Dispersibility assessment in cement paste

The dispersion of PUCNTs in cement paste was observed through scanning electron microscopy (SEM) imaging. SEM micrographs were taken from fracture surfaces and were used to investigate the distribution of PUCNTs throughout the cement matrix. SEM images of free curing surfaces were also acquired.

After 7, 14 and 28 days of curing, dedicated cement paste samples were removed from the lime-saturated water. To observe the structure of free curing surfaces, approximately 2 mm thick slices were cut from each sample surface with a tile saw, then broken into pieces, and air-dried for 24 hours. To assess the distribution of PUCNTs in the cement paste, samples were sourced from the failed prism specimens previously used for the compression tests. These samples were also air-dried for 24 hours, after the compression tests.

Samples of less than 5 mm in length in any direction were selected for SEM imaging of the free-curing surface structure. Thinner (flaky) samples were selected to

assess the distribution of PUCNTs in the cement paste using the high-magnification microscope. All samples were placed in a vacuum-suction chamber for one hour to remove the excess moisture and were then gold-sputtered before acquiring the SEM micrographs.

A field-emission scanning electron microscope (Ultraplus Thermal Field Emission Scanning Electron Microscope, Zeiss) was utilized to observe the distribution of MWCNTs in the fractured cement paste samples and observe the nano- and micro-structure of the composite matrix, thus making it possible to obtain high-magnification SEM micrographs while minimizing electrostatic distortions. A different microscope (Tescan Vega3 SEM) was utilized to obtain lower-magnification and detailed images of the free curing surfaces (i.e., surfaces that cured in direct contact with the lime-saturated water) of the MWCNT-amended and control cement paste samples.

3.3. RESULTS AND DISCUSSIONS

3.3.1 Dispersibility assessment in solution

With an increase in PUCNT concentration, a tendency to agglomerate (Figure 3.5) was not observed visually for up to 10 days. In fact, relatively opaque solutions were observed for a concentration of 0.1 g/L (0.005 wt%) compared to 0.02 g/L (0.001 wt%), and more opaque solutions were observed for a concentration of 1 g/L (0.05 wt%). All suspensions appeared well dispersed, without visible PUCNT clusters.

DLS testing was conducted for up to 10 days on the original suspensions, without further sonication. Similar HDS values were observed for PUCNT concentrations of 0.02 and 0.1 g/L (0.001 and 0.005 wt%), and consistently higher HDS values were observed

for a concentration of 1 g/L (0.05 wt%) (Figure 3.7). This evidence suggests that PUCNTs tend to agglomerate for the upper-bound concentration considered herein. However, a decreasing trend in average HDS was observed over time for similar concentrations (Figure 3.7), which may be explained by possible partial sedimentation of the suspended PUCNTs over time [Keller et al. 2010]. Therefore, the HDS values suggest that the suspensions with PUCNT concentrations of 0.02 and 0.1 g/L (0.001 and 0.005 wt%) were similarly dispersed whereas less dispersibility was observed at a concentration of 1 g/L (0.05 wt%).

To quantitively assess dispersibility and the stability thereof, ZP was measured through DLS testing using the same PUCNT suspensions up to 10 days. Stable suspensions were obtained for PUCNT concentrations of 0.02 and 0.1 g/L (0.001 and 0.005 wt%) since zeta potential < –30 mV (Figure 3.8), and unstable suspensions were obtained for a concentration of 1 g/L (0.05 wt%) since zeta potential > –30 mV. With an increase in PUCNT concentration, free Brownian motion was also likely hindered [Baalousha 2009], which may have facilitated agglomeration. At higher particle concentrations, the likelihood of agglomeration increases [Phenrat et al. 2009 and 2010], and the mobility of the particles may also decrease [Evers 1998] due to the reduced spacing. Higher particle concentration facilitate aggregation as noted through a decrease in electrostatic repulsion between particles (zeta potential) [Evers et al. 1998]. Thus, the higher zeta potential values for 0.05 wt% of PUCNTs indicate agglomeration.

3.3.2 Compressive strength and elastic stiffness

Enhancements in compressive strength were observed in PUCNT-amended cement paste. In fact, compared to plain cement paste, the incorporation of 0.001, 0.005 and 0.05 wt% concentrations of PUCNTs resulted in +15, +0.05 and +25% increase in average 7-day compressive strength; +23, +34 and +21% increase in average 14-day compressive strength; and +10, +29 and +14% increase in average 28-day compressive strength (Figure 3.9). Samples with a 0.05 wt% concentration of PUCNTs also showed largest standard deviation in compressive strength results after 28 days of curing, which suggests that the agglomeration of PUCNTs negatively affected the homogeneity of the cement matrix.

Enhancements in elastic stiffness were also observed in PUCNT-amended cement paste. In fact, compared to plain cement paste, the incorporation of 0.001, 0.005 and 0.05 wt% concentrations of PUCNTs resulted in +4, -4 and +46% increase in average 7-day elastic stiffness; +28, +27 and +26% increase in average 14-day elastic stiffness; and -4, +26 and +10% increase in average 28-day elastic stiffness (Figure 3.10). Samples with 0.05 wt% concentration of PUCNTs showed the largest standard deviation in elastic stiffness results after 7 and 28 days of curing whereas 0.001 and 0.005 wt% concentrations resulted in more consistent elastic stiffness values. This evidence corroborates that from the compressive strength results, suggesting that PUCNT agglomerates negatively affected the homogeneity of the cement matrix when using a 0.05 wt% concentration of PUCNTs.

It is concluded that significant enhancements in compressive strength and elastic stiffness were observed for a PUCNT concentration of 0.005 wt% in cement paste after 28 days of curing, and less significant strength and stiffness enhancements were obtained in the case of a 0.05 wt% concentration, with greater variability in the results.

3.3.3 Dispersibility assessment in cement paste

To evaluate the reasons behind less significant strength and stiffness enhancements from 0.05 wt% of PUCNT concentration compared to 0.005 wt%, representative SEM micrographs were taken from the curing surfaces and fracture surfaces of the failed specimens after compression testing, allowing one to observe the nano- and micro-structure of the cement matrix. Well dispersed PUCNTs were observed for 0.001 wt% (Figure 3.11a) and 0.005 wt% concentrations (Figure 3.11b) after 7 days of curing. Instead, PUCNT agglomerates were consistently observed for the 0.05 wt% concentration (blue circles in Figure 3.11c).

Similarly, well dispersed PUCNTs were observed for 0.001 and 0.005 wt% concentrations (Figure 3.12a, and Figure 3.12b) after 14 days of curing. Consistent agglomeration of PUCNTs was observed for the 0.05 wt% concentration (Figure 3.12c). These observations were confirmed from the cement paste samples that cured for 28 days (Figure 3.13).

For higher contents, it is difficult to achieve uniform dispersion of PUCNTs as the nanoparticles tend to form aggregates in aqueous solutions due to strong van der Waals forces [Lu et al. 2019]. These aggregates may cause defects in the cement matrix, which negatively contribute to mechanical properties (e.g., strength, stiffness).

Ettringite was found in the samples without PUCNTs after 7 days of curing (green circles in Figure 3.14a). Accelerated and preferential formation of amorphous calcium silicate hydrate (C-S-H) [Mehta and Monteiro 2006] was observed after 7 days of curing in cement paste amended with PUCNTs in concentrations of 0.001 wt% (Figure 3.14b), 0.005 wt% (Figure 3.14c) and 0.05 wt% (Figure 3.14d), as marked by yellow circles. In the PUCNT-amended samples, well distributed C-S-H was consistently identified (Figure 3.14b-d). Pore refinement was also observed after 7 days of curing in samples with PUCNTs (Figure 3.14b, Figure 3.14c and Figure 3.14d where smaller pores with size <50 nm are marked by magenta arrows).

Ettringite was consistently found in the samples without PUCNTs (Figure 3.15a) after 14 days of curing. Preferential formation of C-S-H [Mehta and Monteiro 2006] was facilitated when incorporating with PUCNTs, located near PUCNTs in the case of 0.001 wt% (Figure 3.15b) and 0.005 wt% (Figure 3.15c) concentrations, as clearly noted also in the case of 0.05 wt% concentration (Figure 3.15d). These micrographs confirm the likelihood that –OH and –COOH functional groups on the PUCNT edges act as nucleating sites for cement hydrates [Makar and Chan 2009]. Therefore, the incorporation of oxidized PUCNTs appears to facilitate the hydration reaction of calcium silicates [Makar 2009], resulting in the preferential formation of C-S-H whereas plain cement paste consistently featured more aluminum hydration products (ettringite). It is noted that the formation of ettringite may contribute to the weakness of the cement matrix [Sharma et al. 2016] whereas C-S-H contributes to strengthening the nano-micro-structure. In addition to C-S-H formation, pore refinement was observed with addition

of PUCNTs after 14 days of curing. Samples with PUCNTs (Figure 3.15b, Figure 3.15c and Figure 3.15d) feature numerous smaller pores (<50 nm in size). Hence, a comparatively denser microstructure was visible in PUCNT-amended cement paste compared to plain cement paste (Figure 3.15a).

Plate-like calcium monosulfate hydrates (Figure 3.16a) formed in the plain cement samples after 28 days of curing, which originate from the previously observed ettringite [Mehta and Monteiro 2006] and may make cement composites more susceptible to sulfate attack [Mehta and Monteiro 2006]. Instead, preferential formation of C-S-H was located near the PUCNTs for all concentrations (Figure 3.16b, Figure 3.16c and Figure 3.16d). Similar to previous observations after 14 days of curing, cement paste with PUCNTs (Figure 3.16b, Figure 3.16c and Figure 3.16d) featured numerous smaller pores (<50 nm in size) after 28 days of curing. Thus, a comparatively less porous microstructure was consistently observed with the incorporation of PUCNTs compared to plain cement (Figure 3.16a). Also, compared to the evidence collected after 14 days of curing (Figure 3.15b, Figure 3.15c and Figure 3.15d), more C-S-H formation was observed after 28 days of curing as a result of PUCNT-amendment (Figure 3.16b, Figure 3.16c and Figure 3.16d).

The preferential formation of C-S-H formation and pore refinement led to compressive strength and elastic stiffness enhancements for cement paste with 0.005 and 0.05 wt% concentrations of PUCNTs after 28 days of curing. However, agglomeration of PUCNTs in the case of 0.05 wt% concentration negatively contributed to such enhancements, resulting in inferior strength and stiffness compared to the

cement paste amended with a 0.005 wt% concentration (i.e., one order of magnitude less) of PUCNTs.

As hydration progresses from 7 to 28 days of curing, smoother free curing surfaces were observed (Figure 3.17 to Figure 3.19). In fact, less porous surface structures were observed (Figure 3.17 to Figure 3.19) for PUCNT-amended cement paste compared to the control samples without PUCNTs, which also suggests accelerated and preferential cement hydration.

Accelerated and preferential formation of C-S-H and significant amounts of smaller (<50 nm) pores were observed with the addition of PUCNTs after 7 days (Figure 3.14), 14 days (Figure 3.15) and 28 days (Figure 3.16) of curing. Thus, it is concluded that the precipitation of hydrates, and the pore-size refinement observed in the nano- and micro-structure, led to the strengthening and stiffening of the cement matrix. In fact, the functional groups on the well dispersed PUCNT walls act as nucleation sites [Makar and Chan 2009] for hydration products, facilitating the development of strong covalent interactions between oxidized PUCNTs and hydration products [Sharma et al. 2016].

The PUCNT-amended cement paste displayed less porous surface micro-structure with a well-distributed formation of hydrates. This visual evidence suggests that the surface modification resulted from the incorporation of oxidized PUCNTs may contribute to enhancing the durability of cement composites, in addition to enhancing compressive strength and elastic stiffness as also observed for MWCNTs in Chapter 2.

3.4. CONCLUSIONS

Based on the results presented in this chapter, the following conclusions are drawn.

- It is feasible to incorporate well-dispersed and chemically-affine PUCNTs to enhance the physico-mechanical properties of cement paste.
- Due to the morphology and the high graphene-edge content of PUCNTs, dispersibility in aqueous solutions was easily attained with 0.001-0.005 wt% concentrations. Unstable aqueous solutions were obtained with a 0.05 wt% concentration.
- Significant enhancements in compressive strength and elastic stiffness of cement paste were obtained with a PUCNT concentration of 0.005 wt%, which is one order of magnitude smaller than lower-bound concentrations reported in the literature for MWCNTs and other graphitic nanoparticles. Less significant strength enhancements were observed from 0.05 wt% of PUCNTs.
- SEM imaging of the cement paste structure suggests that plausible contributing mechanisms for strength enhancement include the preferential and well-distributed formation of cement hydrates in presence of PUCNTs for concentrations up to 0.05 wt%, also resulting in a less porous structure, compared to plain cement paste. Aggregation of PUCNTs in cement paste with 0.05 wt% PUCNT concentration resulted in less significant strength and stiffness enhancements.
- Smoother, less porous free (curing) surfaces were observed for PUCNT concentrations in the range 0.001 to 0.05 wt% compared to plain cement paste.

- At higher concentrations, the aggregation of PUCNTs negatively impact their advantage of having high specific surface area and hinders their functioning as nucleation sites for the preferential and accelerated formation of cement hydrates. As such, a PUCNT concentration of 0.05 wt% resulted in PUCNT agglomeration in aqueous solution as well as in cement paste, and less significant enhancements in compressive strength and elastic stiffness compared to a concentration of 0.005 wt%.
- In the literature, 0.01-0.05 wt% have been reported as lower-bound concentrations for MWCNTs and GNPs. PUCNTs have higher specific surface area and functionality as compared to MWCNTs, and higher aspect ratio as compared to GNPs. Thus, radically smaller concentrations (e.g., 0.005 wt%) may be used for successful amendment of cement paste.

3.5. REFERENCES

ASTM International. Standard Practice for Mechanical Mixing of Hydraulic Cement Pastes and Mortars of Plastic Consistency. ASTM C305-14. West Conshohocken, PA: ASTM International, 2014.

Baalousha M. Aggregation and disaggregation of iron oxide nanoparticles: Influence of Particle Concentration, PH and Natural Organic Matter. Science of the Total Environment 2009; 407, 2093-2101.

Evers M, Garbow N, Hessinger D, Palberg T. Electrophoretic Mobility of Interacting Colloidal Spheres. Physical Review E 1998; 57 (6), 6774.

Freitas C, Muller RH. Effect of Light and Temperature on Zeta Potential and Physical Stability in Solid Lipid Nanoparticle (SLN™) Dispersions. International Journal of

Pharmaceutics 1998; 168, 221–229.

Gigault J, Grassl B, Lespes G. A New Analytical Approach Based on Asymmetrical Flow Field-Flow Fractionation Coupled to Ultraviolet Spectrometry and Light Scattering Detection for SWCNT Aqueous Dispersion Studies. Analyst 2012; 137, 917.

Jeong YC, Lee K, Kim T, Kim JH, Park J, Cho YS, Yang SJ, Park CR. Partially Unzipped Carbon Nanotubes for High-Rate and Stable Lithium–Sulfur Batteries. Journal of Materials Chemistry A 2016; 4, 819–826.

Keller AA, Wang H, Zhou D, Lenihan HS, Cherr G, Cardinale BJ, Miller R, Ji Z. Stability and Aggregation of Metal Oxide Nanoparticles in Natural Aqueous Matrices. Environmental Science and Technology 2010; 44 (6), 962–1967.

Kosynkin DV, Higginbotham AL, Sinitskii A, Lomeda JR, Ayrat Dimiev A, Price BK, Tour JM. Longitudinal Unzipping of Carbon Nanotubes to form Graphene Nanoribbons. Nature 2009; 458, 872-877.

Krystek M, Pakulski D, Patroniak V, Gorski M, Szojda L. Ciesielski A, Samori P. High-Performance Graphene-Based Cementitious Composites. Advanced Science 2019; 1801195.

Lu Z, Chen B, Leung CKY, Li Z, Sun G. Aggregation Size Effect of Graphene Oxide on Its Reinforcing Efficiency to Cement-Based Materials. Cement and Concrete Composites 2019; 100, 85–91.

Makar JM, Chan GW. Growth of Cement Hydration Products on Single-Walled Carbon Nanotubes. Journal of the American Ceramic Society 2009; 92 (6), 1303–1310.

Mehta PK and Monteiro PJM. Concrete Microstructure, Properties, and Materials. McGraw-Hill Education; 4th Edition, 2006.

Phenrat T, Kim H, Fagerlund F, Illangasekare T, Tilton RD, Lowry GV. Particle Size Distribution, Concentration, and Magnetic Attraction Affect Transport of Polymer-Modified Fe^0 Nanoparticles in Sand Columns. Environmental Science and Technology 2009; 43(13), 5079–5085.

Phenrat T, Cihan A, Kim H, Mital M, Illangasekare T, Lowry GV. Transport and Deposition of Polymer-Modified Fe^0 Nanoparticles in 2-D Heterogeneous Porous Media: Effects of Particle Concentration, Fe^0 Content, and Coatings. Environmental Science and Technology 2010; 44(23), 9086–9093.

Sharma S, Kothiyal NC. Facile Growth of Carbon Nanotubes Coated with Carbon Nanoparticles: A Potential Low-Cost Hybrid Nano-Additive for Improved Mechanical, Electrical, Microstructural and Crystalline Properties of Cement Mortar Matrix. Construction and Building Materials 2016; 123, 829–846.

Song Y, Feng M, Zhan H. Electrochemistry of Partially Unzipped Carbon Nanotubes. Electrochemistry Communications 2014; 45, 95–98.

Zohhadi N. Functionalized Graphitic Nanoreinforcement for Cement Composites. PhD Dissertation 2014; University of South Carolina, Columbia.

3.6. TABLES

Table 3.1 Controlling pH of oxidized PUCNT suspensions

Concentration [wt%]	Initial pH	Amount of added 5M NaOH [µL]	Adjusted pH	Final concentration of NaOH [mol/L]
0.001	3.84	300	11.18	0.002
0.005	3.34	400	11.21	0.003
0.05	2.24	1700	11.3	0.012

Table 3.2 Test matrix for physico-mechanical tests on cement paste with PUCNTs

PUCNT concentration [wt%]	Tests	Number of specimens	Specimens to be cast
Control (0)	Compressive strength	4*	5
	SEM imaging	Crushed from failed prisms	
0.001	Compressive strength	4*	5
	SEM imaging	Crushed from failed prisms	
0.005	Compressive strength	4*	5
	SEM imaging	Crushed from failed prisms	
0.05	Compressive strength	4*	5
	SEM imaging	Crushed from failed prisms	

* While a minimum number of 4 specimens are considered to ensure statistical meaningfulness, up to 5 specimens were cast

3.7. FIGURES

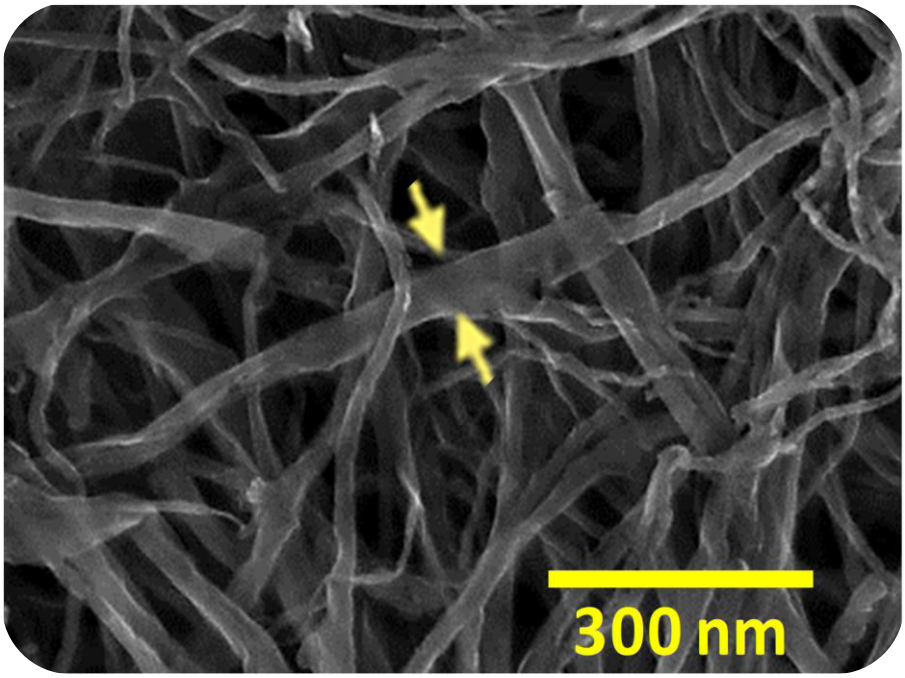

Figure 3.1 SEM images of PUCNTs

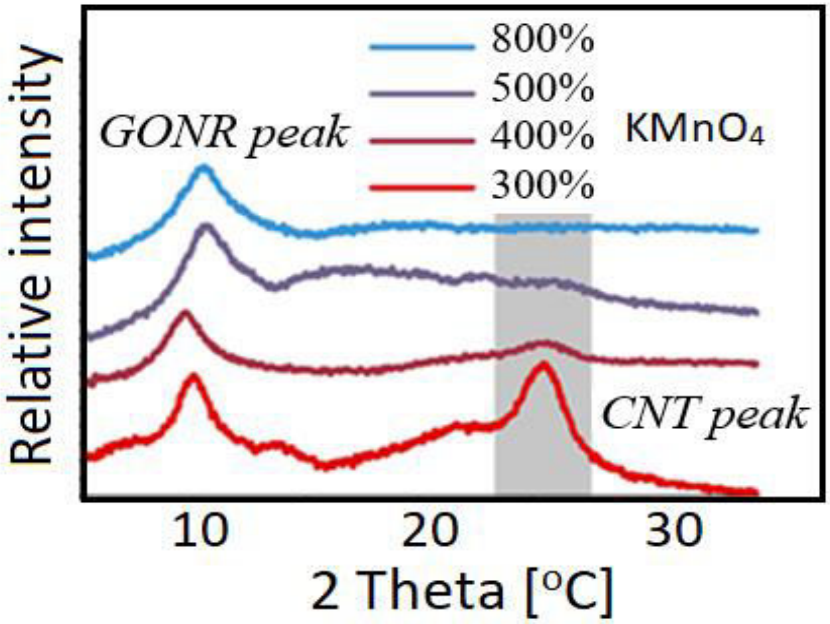

Figure 3.2 XRD for different oxidation levels

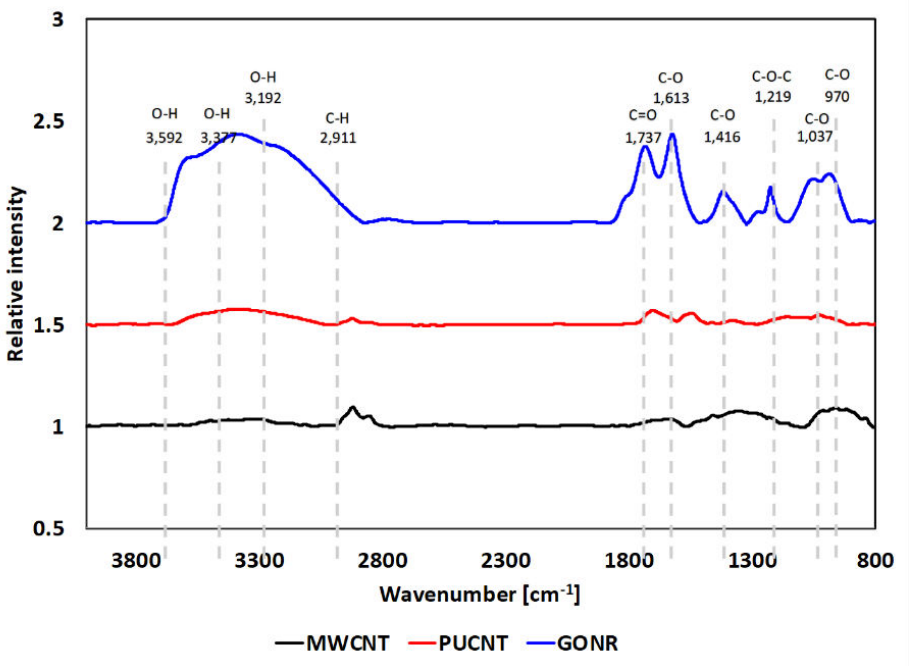

Figure 3.3 FT-IR spectra of MWCNT, PUCNT and GONR

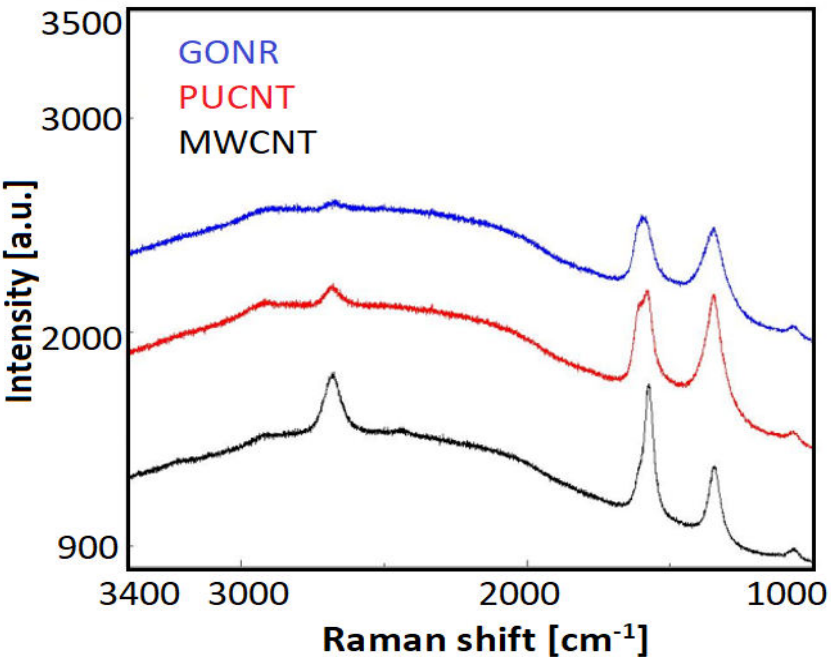

Figure 3.4 Raman spectra of MWCNT, PUCNT and GONR

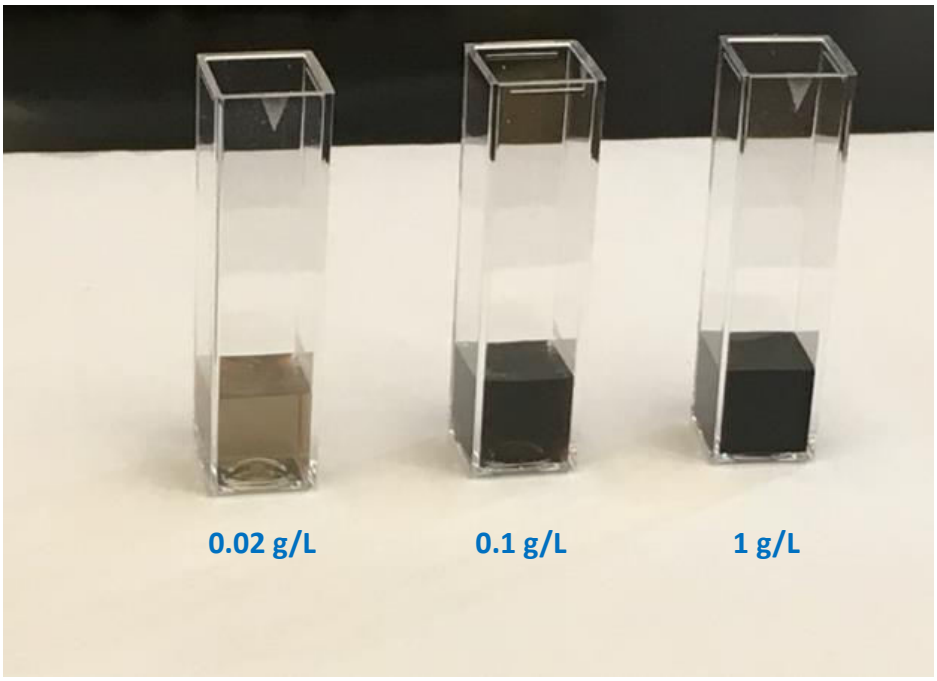

Figure 3.5 PUCNT suspensions in DI water 0 days after sonication

Figure 3.6 Uniaxial compression testing of cement paste prism specimen

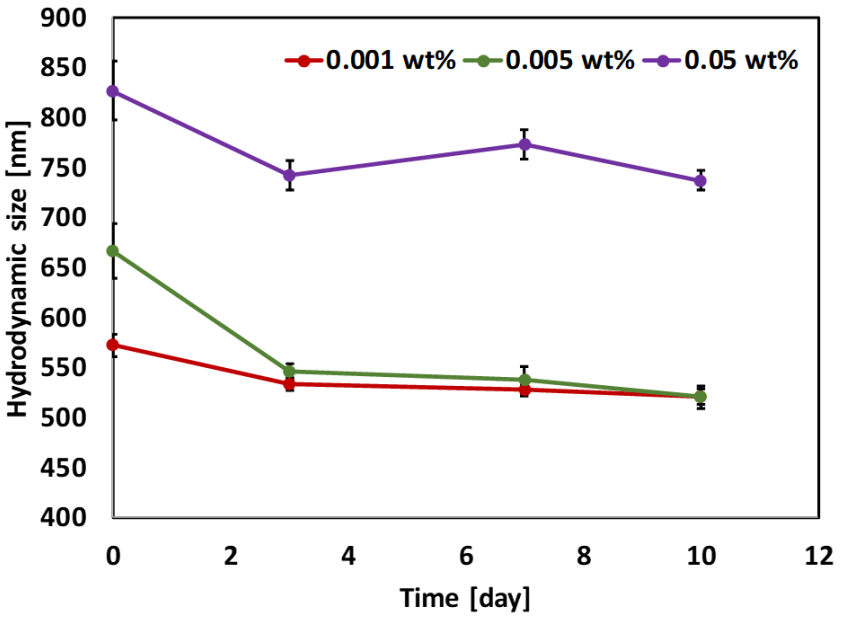

Figure 3.7 Hydrodynamic size for different concentrations of PUCNTs up to 10 days of sonication

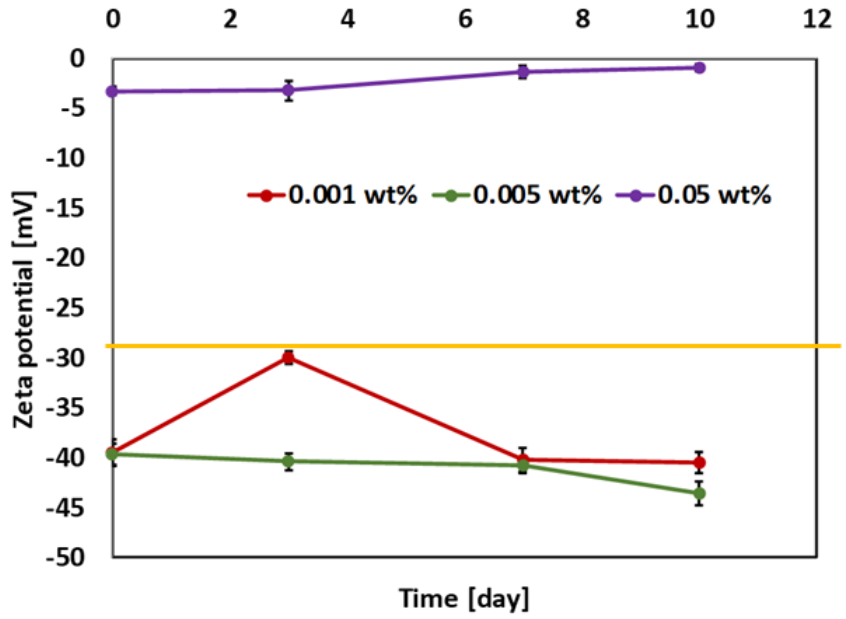

Figure 3.8 Zeta potential for different concentrations of PUCNTs up to 10 days of sonication

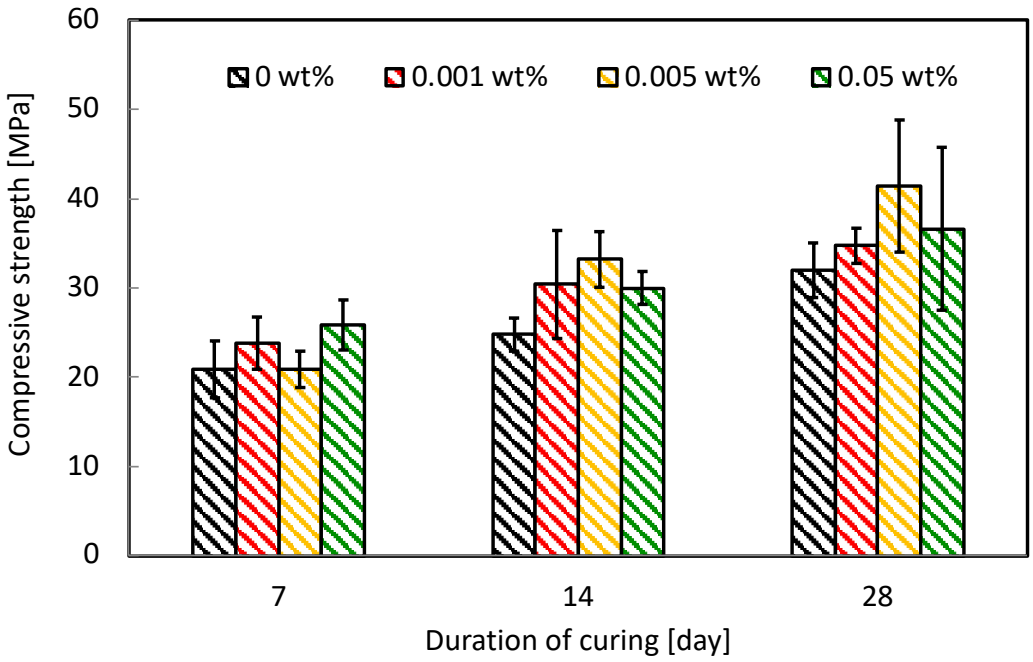

Figure 3.9 Uniaxial compressive strength of control and PUCNT-amended cement paste specimens after 7, 14 and 28 days of curing

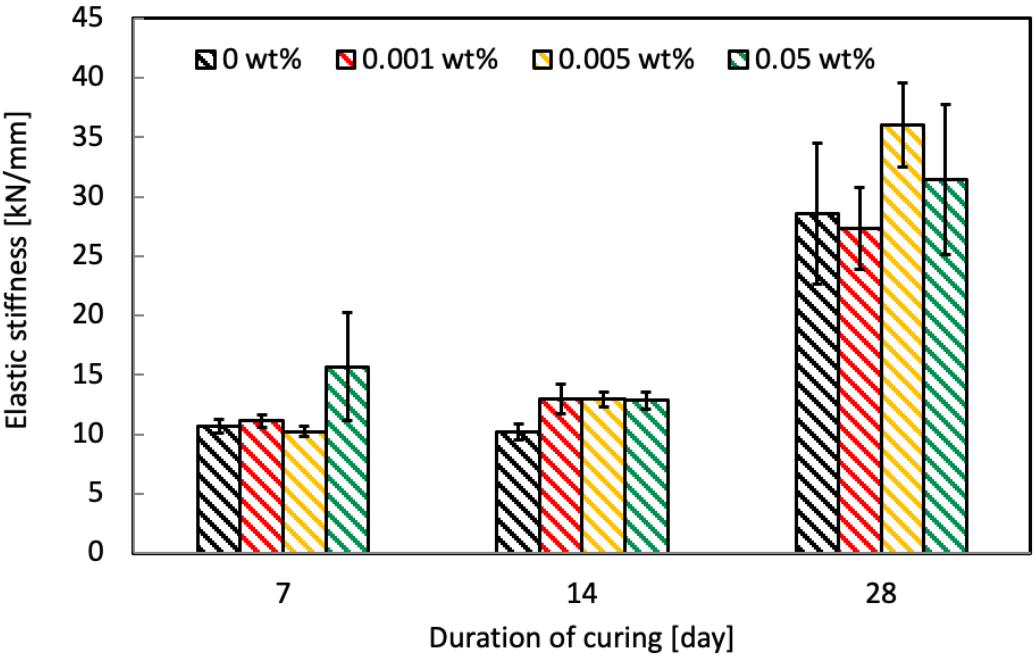

Figure 3.10 Elastic stiffness of control and PUCNT-amended cement paste specimens after 7, 14 and 28 days of curing

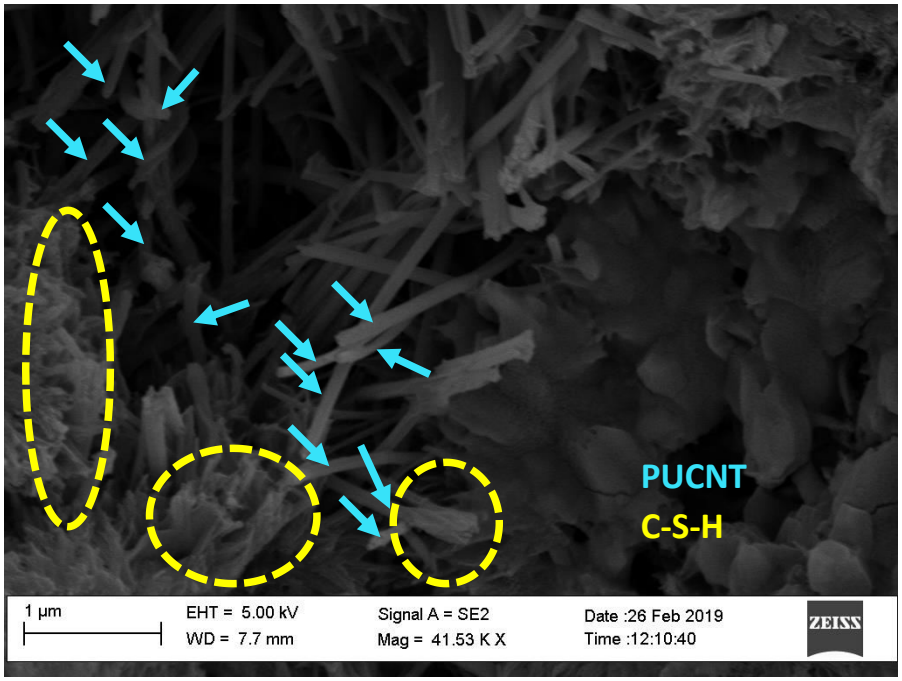
PUCNT
C-S-H
1 µm
EHT = 5.00 kV
WD = 7.7 mm
Signal A = SE2
Mag = 41.53 K X
Date :26 Feb 2019
Time :12:10:40
ZEISS

(a)

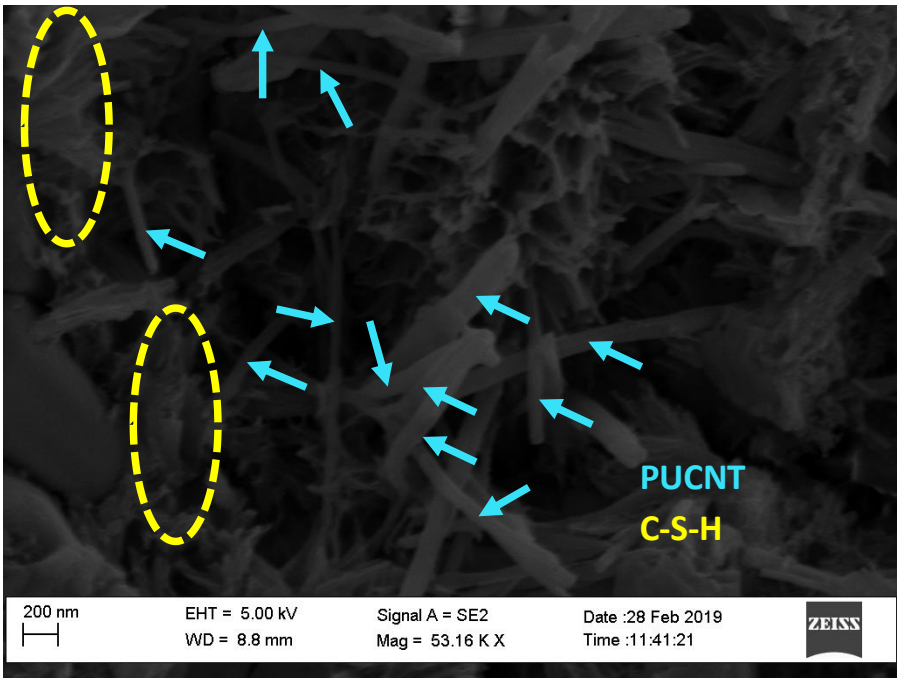
PUCNT
C-S-H
200 nm
EHT = 5.00 kV
WD = 8.8 mm
Signal A = SE2
Mag = 53.16 K X
Date :28 Feb 2019
Time :11:41:21
ZEISS

(b)

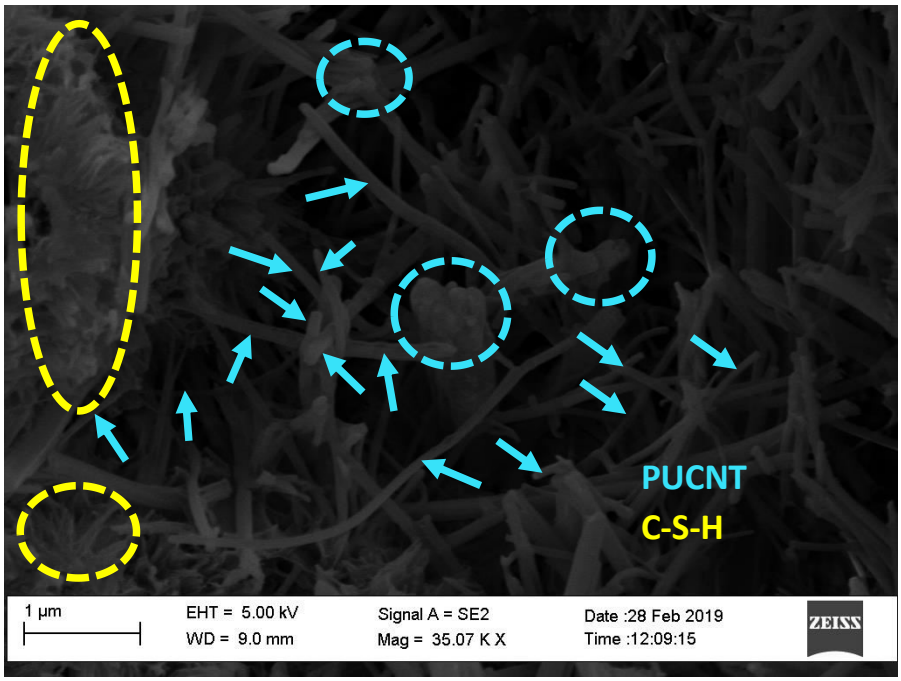

(c)

Figure 3.11 Distribution of PUCNTs in cement paste (a) 0.001 wt% (b) 0.005 wt% (c) 0.05 wt% of PUCNT concentration, after 7 days of curing

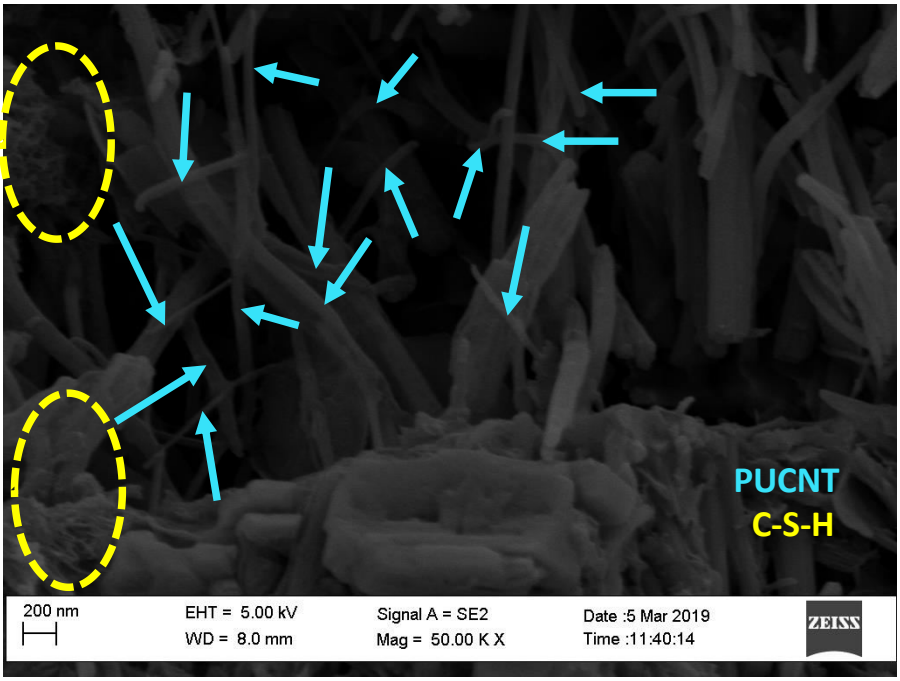

(a)

(b)

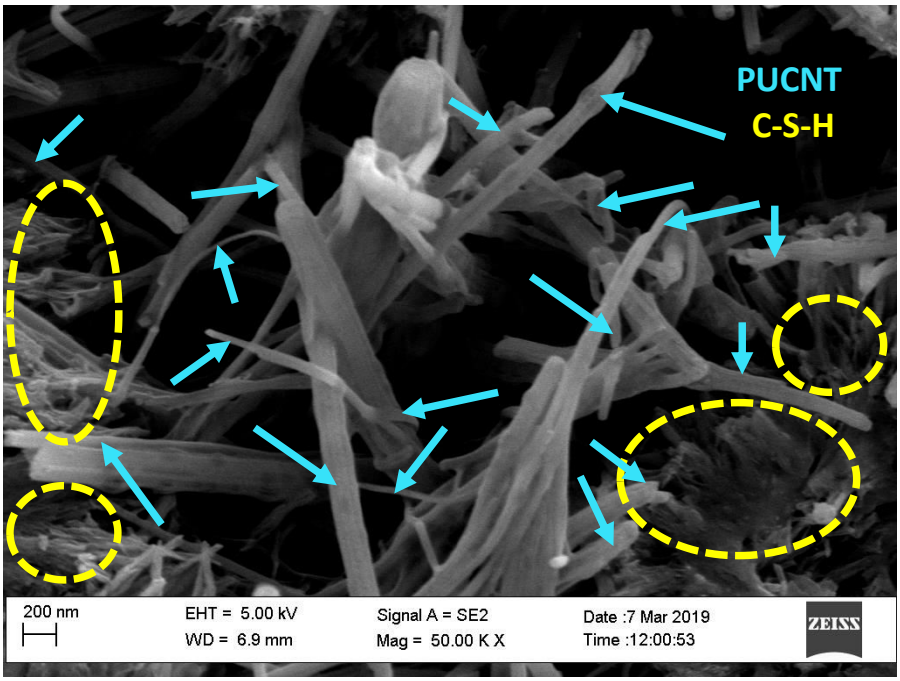

(c)

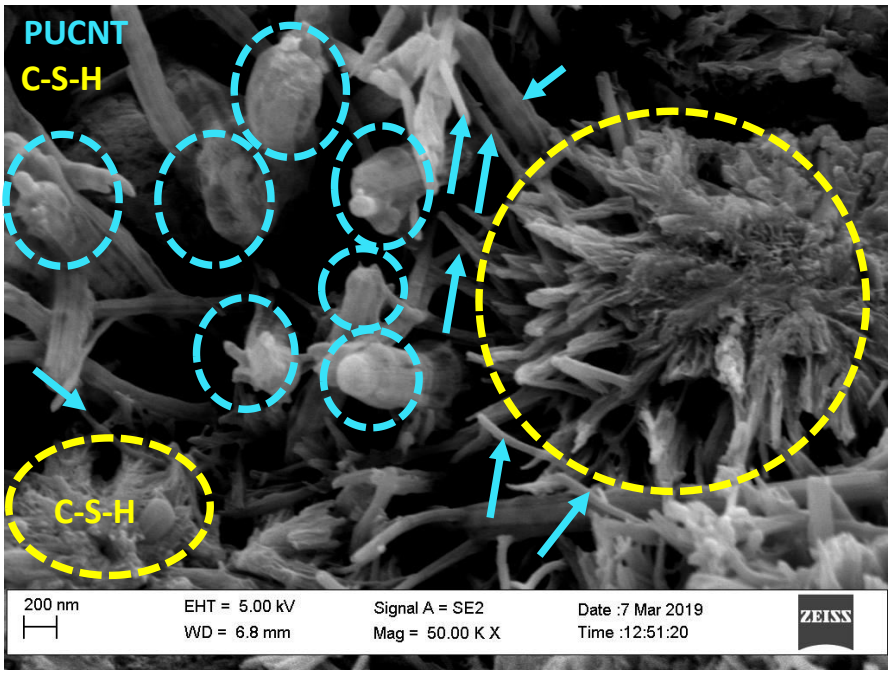

Figure 3.12 Distribution of PUCNTs in cement paste (a) 0.001 wt% (b) 0.005 wt% (c) 0.05 wt% of PUCNT concentration after 14 days of curing

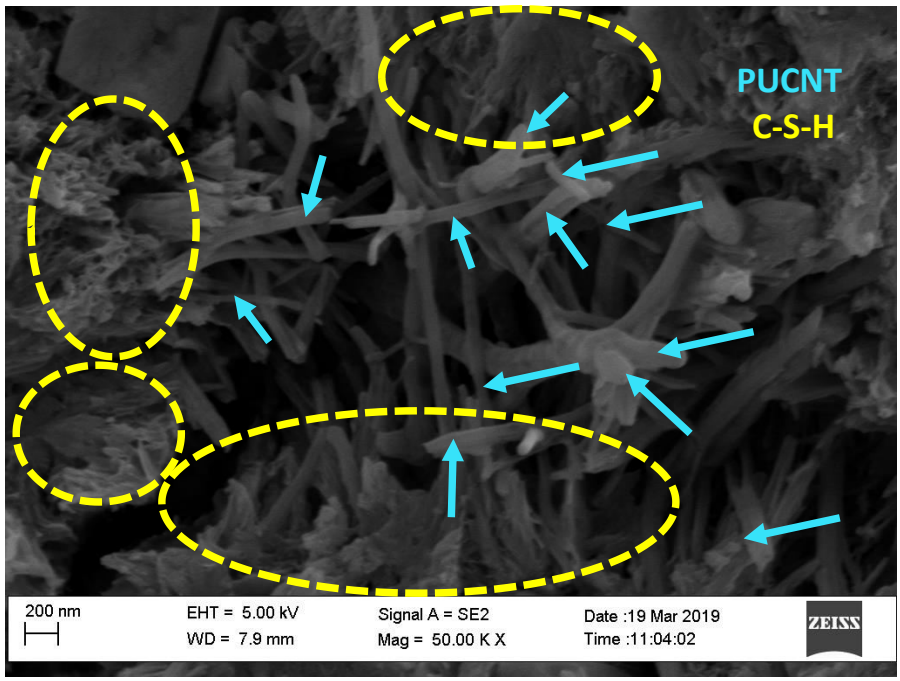
PUCNT
C-S-H
200 nm
EHT = 5.00 kV
WD = 7.9 mm
Signal A = SE2
Mag = 50.00 K X
Date :19 Mar 2019
Time :11:04:02
ZEISS

(a)

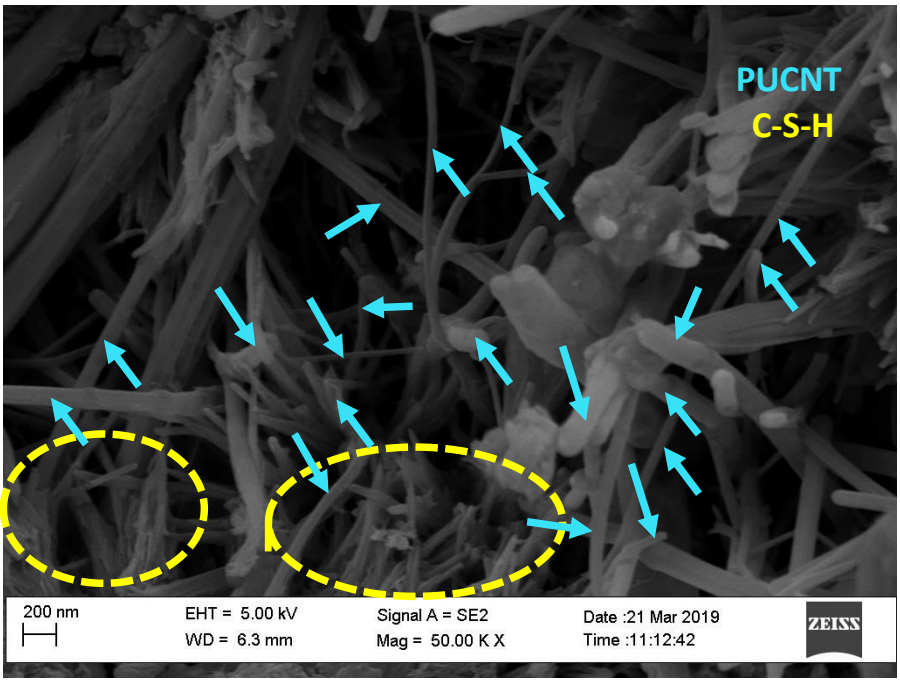
PUCNT
C-S-H
200 nm
EHT = 5.00 kV
WD = 6.3 mm
Signal A = SE2
Mag = 50.00 K X
Date :21 Mar 2019
Time :11:12:42
ZEISS

(b)

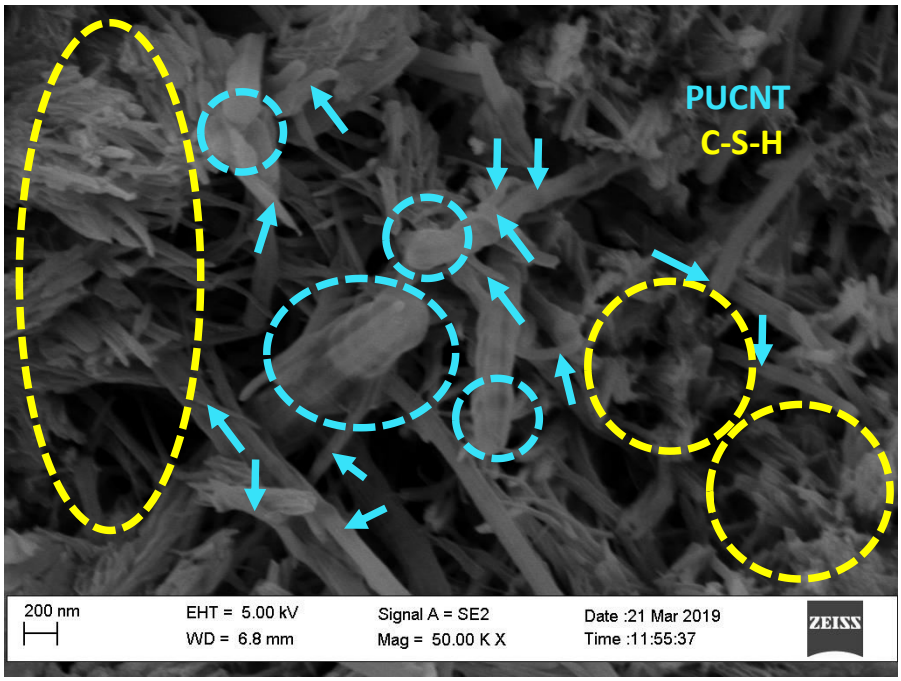

(c)

Figure 3.13 Distribution of PUCNTs in cement paste (a) 0.001 wt% (b) 0.005 wt% (c) 0.05 wt% of PUCNT concentration after 28 days of curing

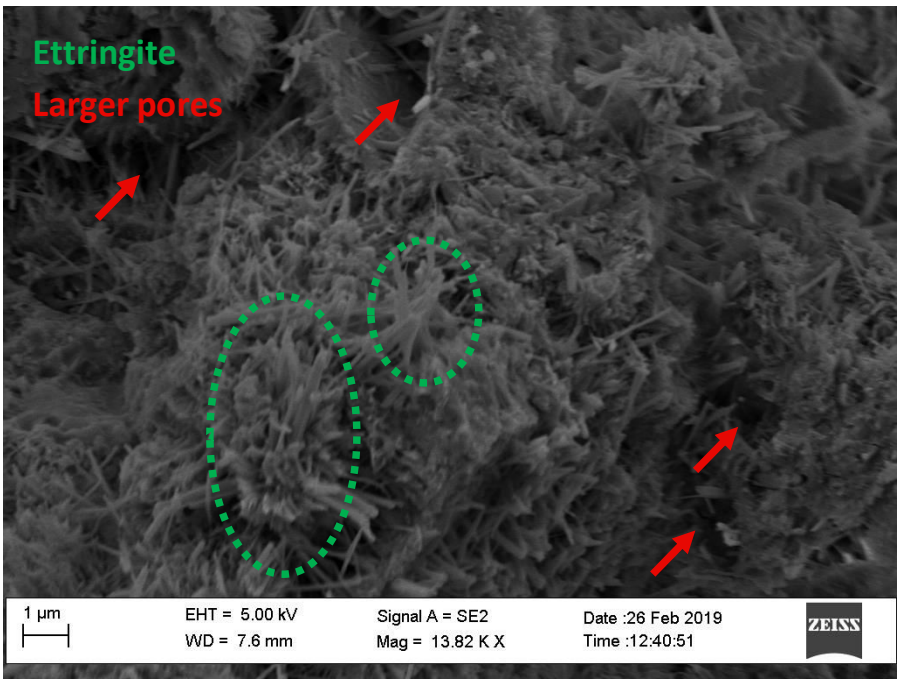

(a)

(b)

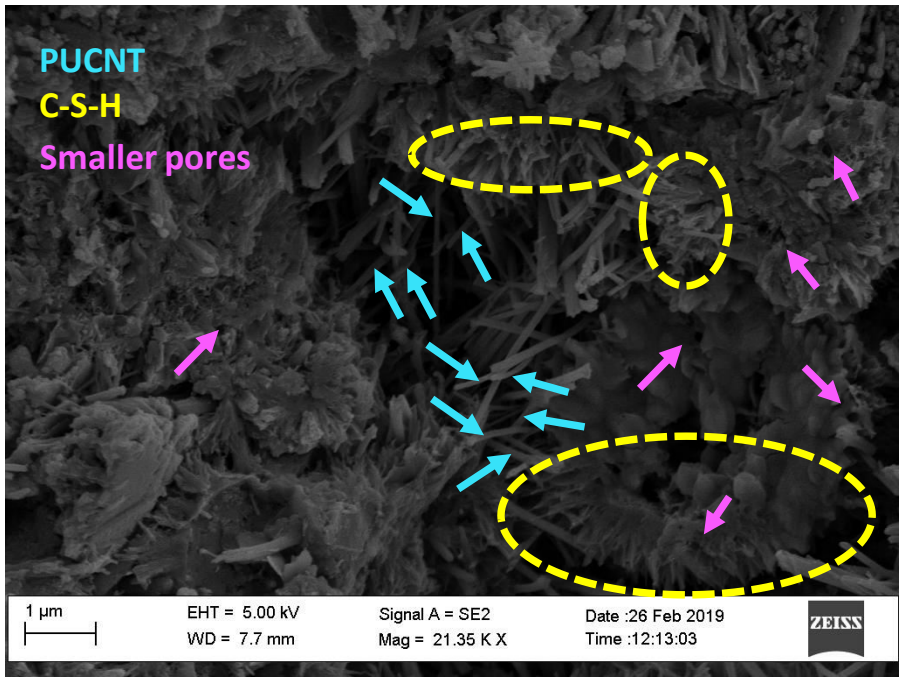
PUCNT
C-S-H
Smaller pores
1 µm
EHT = 5.00 kV
WD = 7.7 mm
Signal A = SE2
Mag = 21.35 K X
Date :26 Feb 2019
Time :12:13:03
ZEISS

(c)

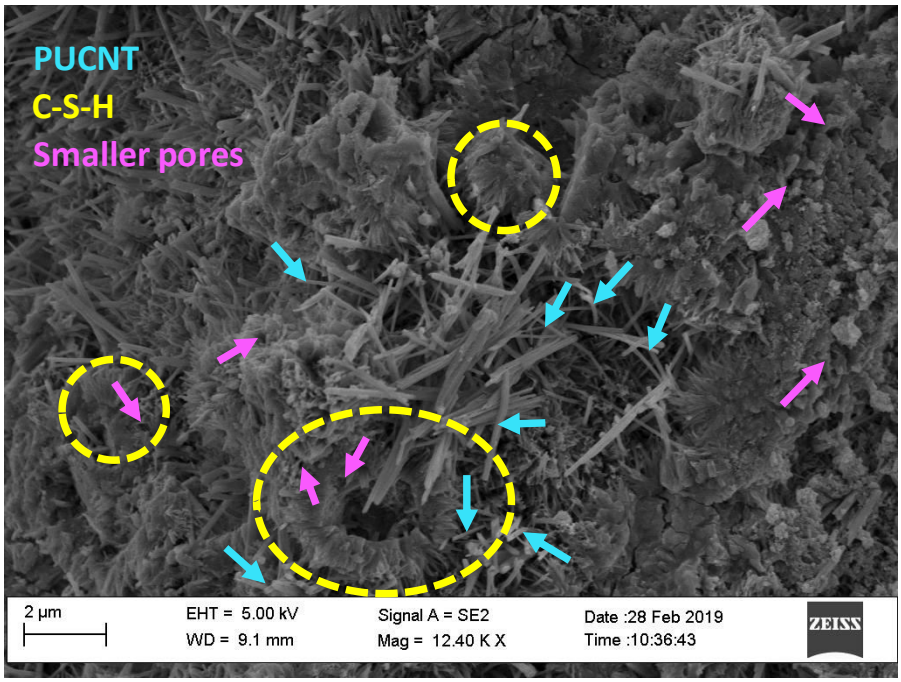
PUCNT
C-S-H
Smaller pores
2 µm
EHT = 5.00 kV
WD = 9.1 mm
Signal A = SE2
Mag = 12.40 K X
Date :28 Feb 2019
Time :10:36:43
ZEISS

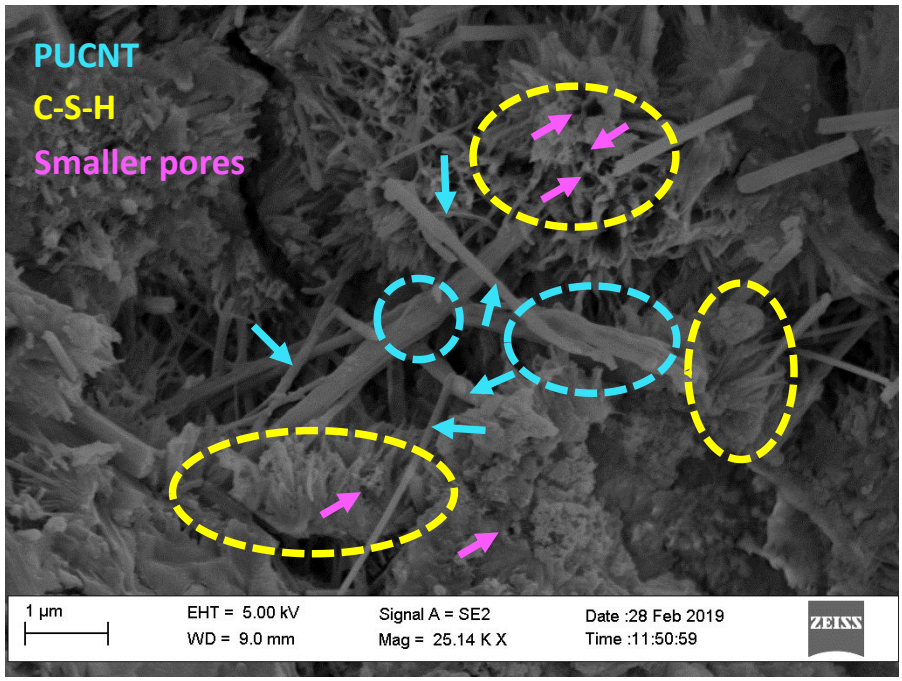

(d)

Figure 3.14 Formation of hydrates after 7 days of curing (a) 0 wt% (b) 0.001 wt% (c) 0.005 wt% (d) 0.05 wt% of PUCNT concentrations

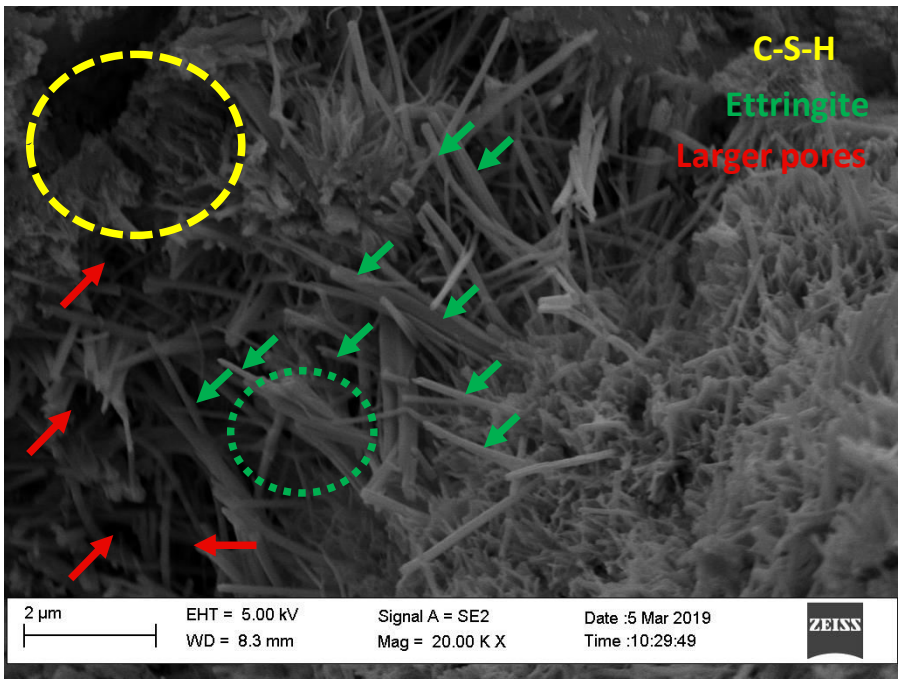

(a)

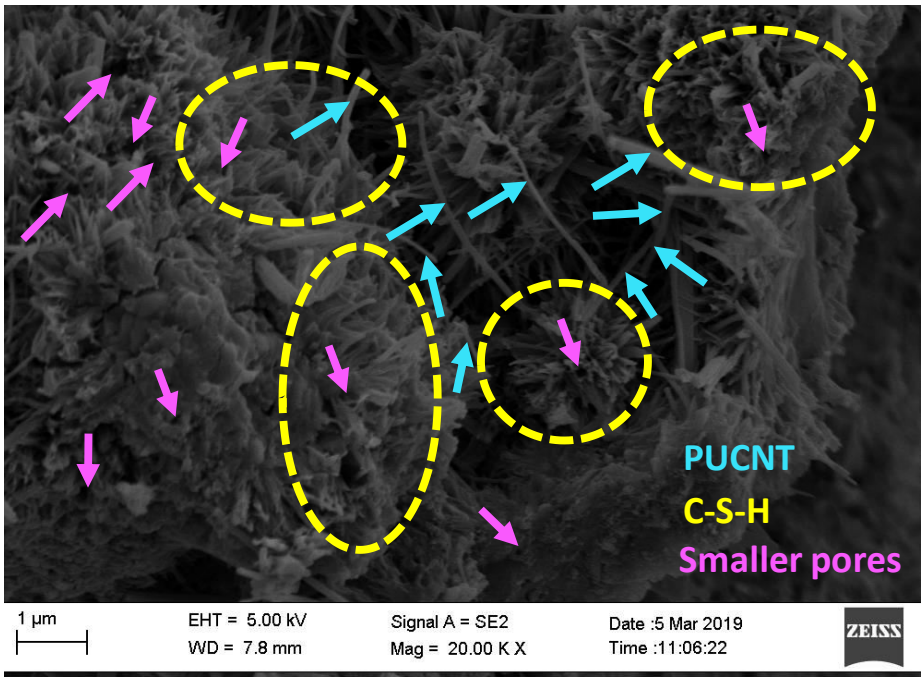
PUCNT
C-S-H
Smaller pores
1 µm
EHT = 5.00 kV
WD = 7.8 mm
Signal A = SE2
Mag = 20.00 K X
Date :5 Mar 2019
Time :11:06:22
ZEISS

(b)

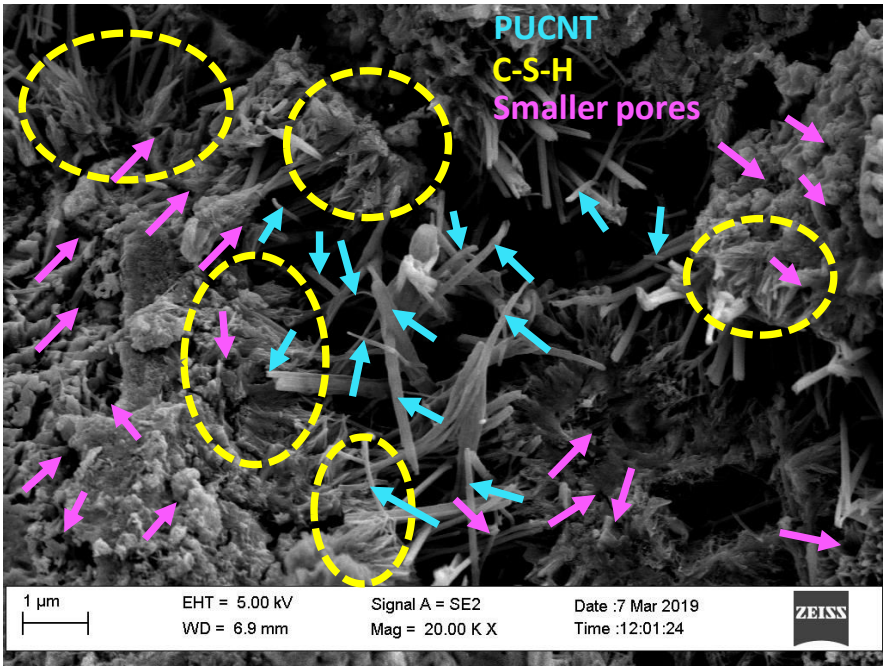
PUCNT
C-S-H
Smaller pores
1 µm
EHT = 5.00 kV
WD = 6.9 mm
Signal A = SE2
Mag = 20.00 K X
Date :7 Mar 2019
Time :12:01:24
ZEISS

(c)

(d)

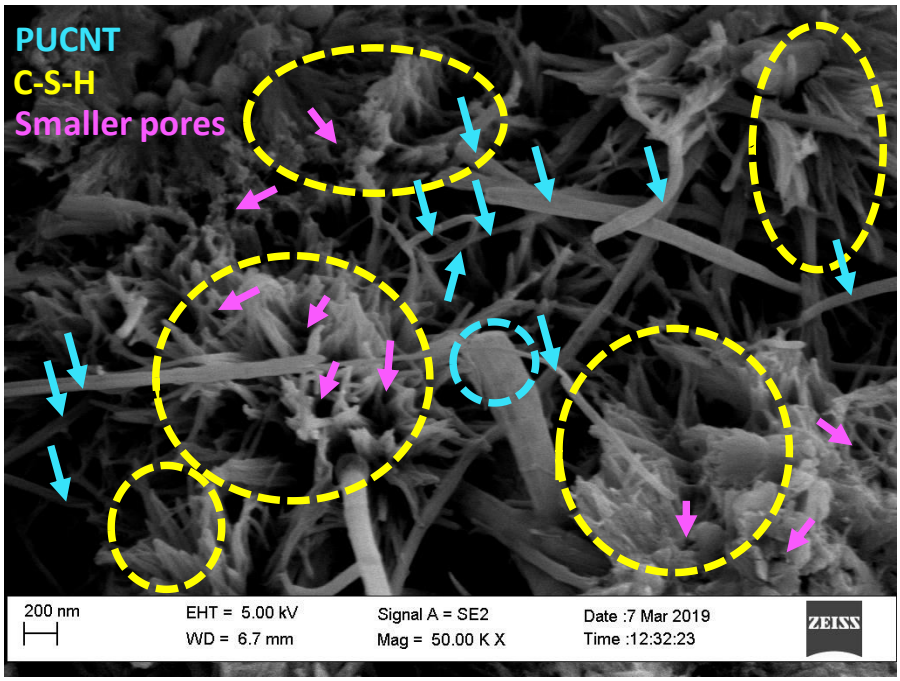

Figure 3.15 Formation of hydrates after 14 days of curing (a) 0 wt% (b) 0.001 wt% (c) 0.005 wt% (d) 0.05 wt% of PUCNT concentrations

(a)

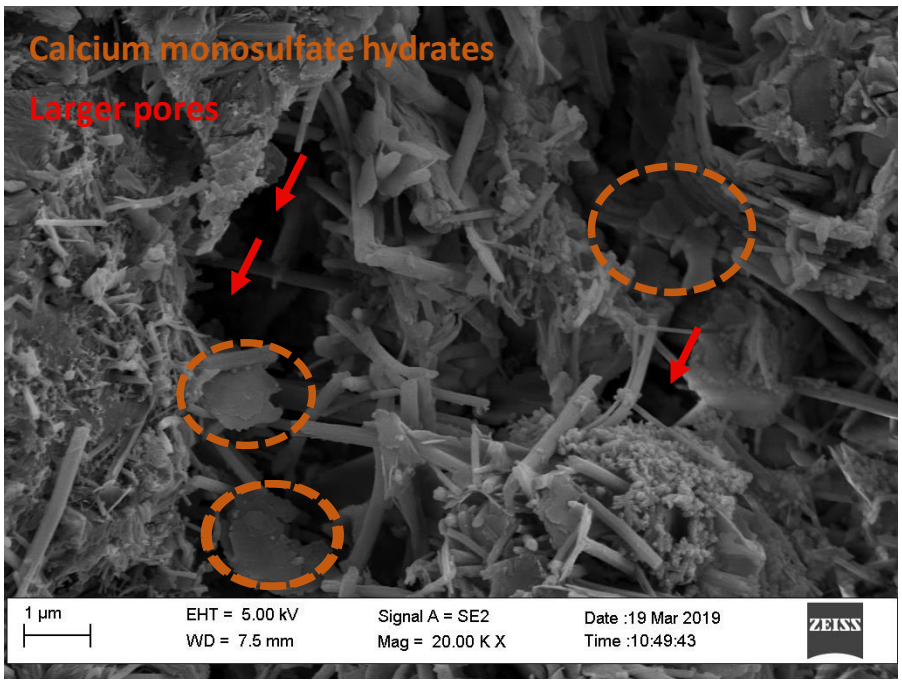

(b)

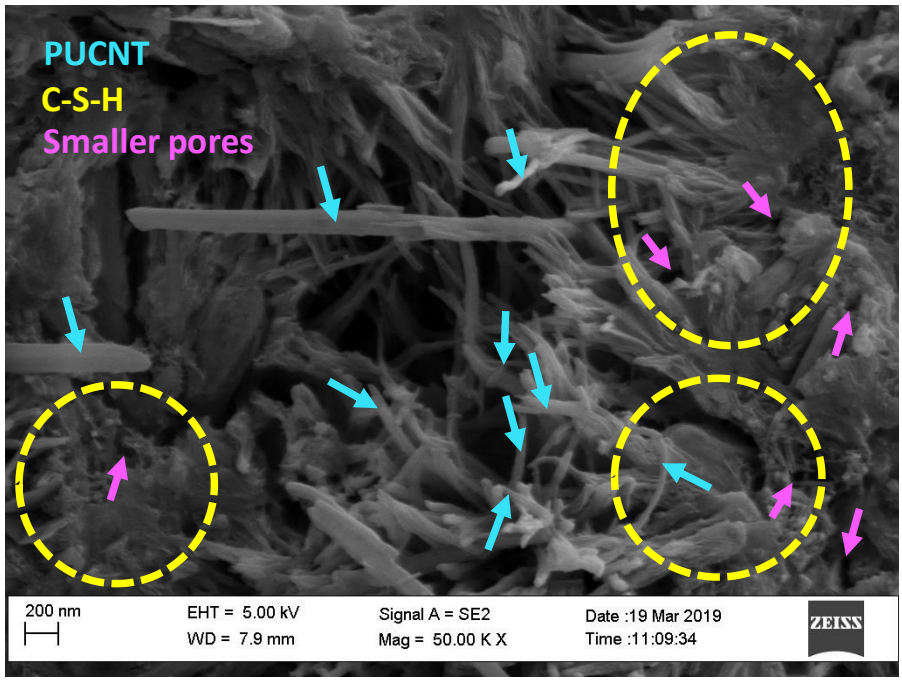
PUCNT
C-S-H
Smaller pores
200 nm
EHT = 5.00 kV
WD = 7.9 mm
Signal A = SE2
Mag = 50.00 K X
Date :19 Mar 2019
Time :11:09:34
ZEISS

(c)

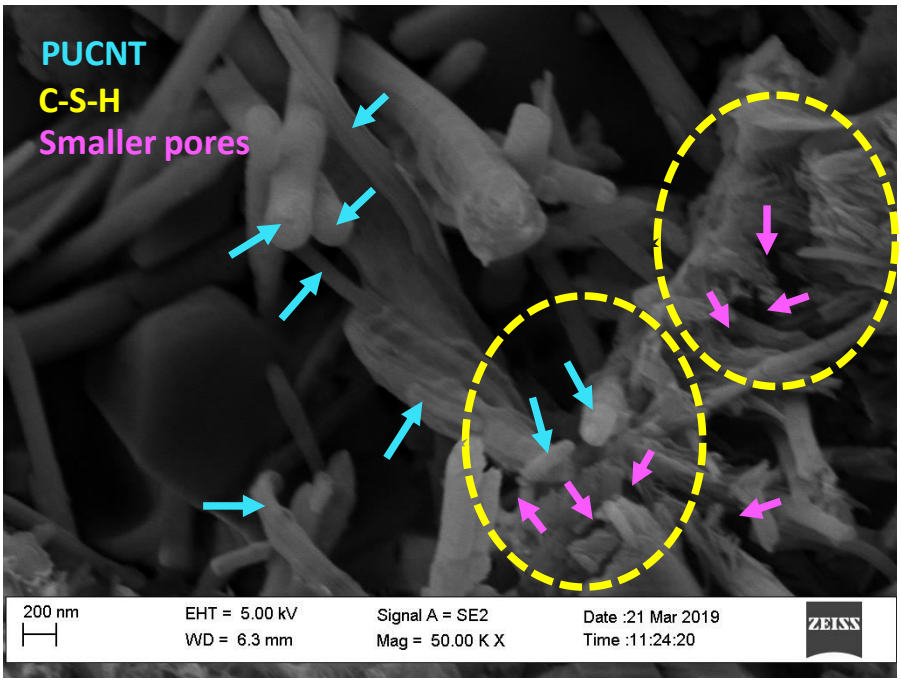
PUCNT
C-S-H
Smaller pores
200 nm
EHT = 5.00 kV
WD = 6.3 mm
Signal A = SE2
Mag = 50.00 K X
Date :21 Mar 2019
Time :11:24:20
ZEISS

(d)

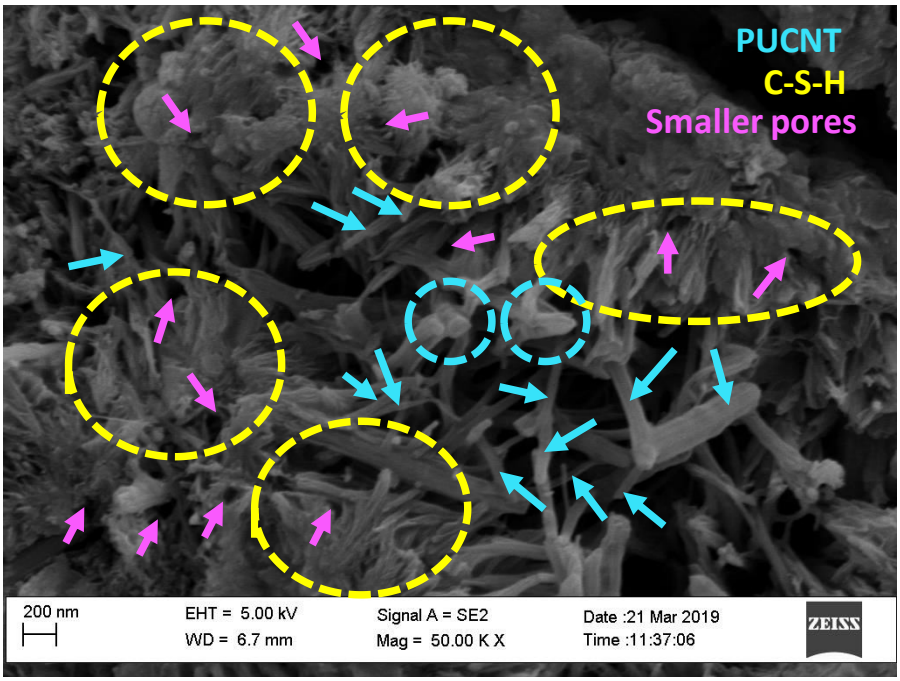

Figure 3.16 Formation of hydrates after 28 days of curing (a) 0 wt% (b) 0.001 wt% (c) 0.005 wt% (d) 0.05 wt% of PUCNT concentrations

(a)

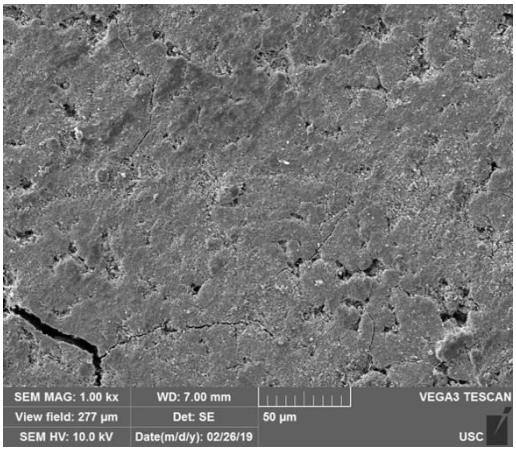

(b)

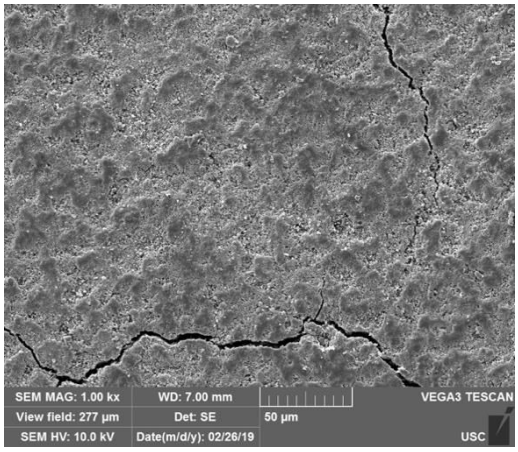

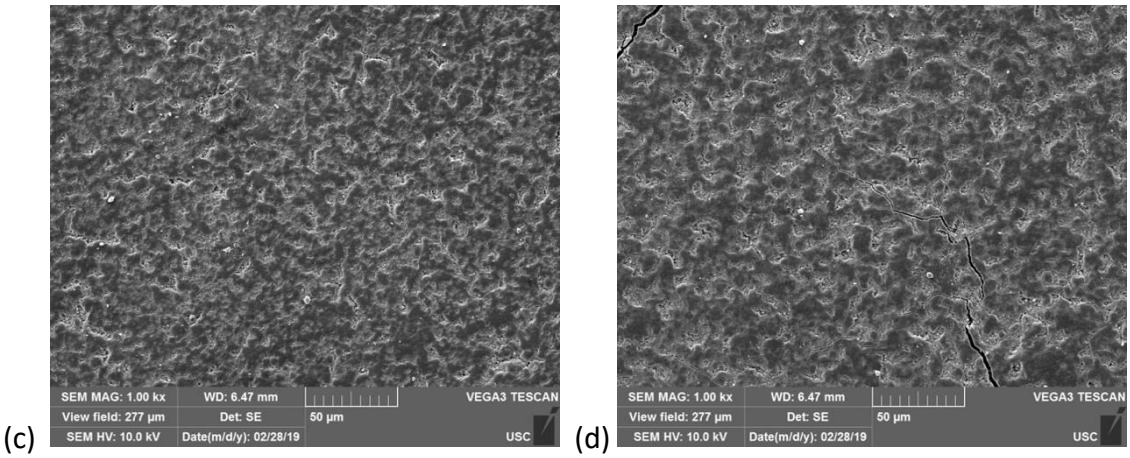

Figure 3.17 Free curing surfaces of control and PUCNT-amended cement paste with (a) 0 wt% (b) 0.001 wt% (c) 0.005 wt% (d) 0.05 wt% of PUCNTs, after 7 days of curing

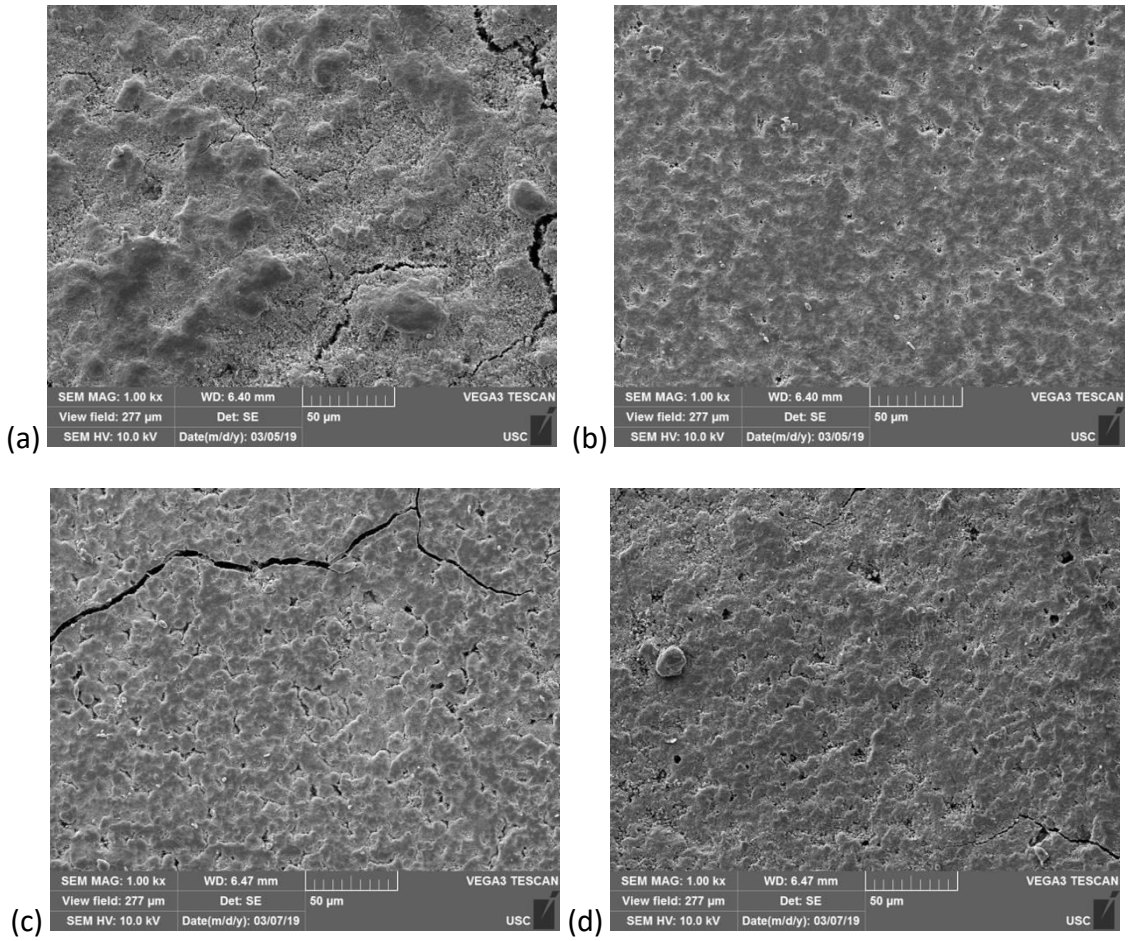

Figure 3.18 Free curing surfaces of control and PUCNT-amended cement paste with (a) 0 wt% (b) 0.001 wt% (c) 0.005 wt% (d) 0.05 wt% of PUCNTs, after 14 days of curing

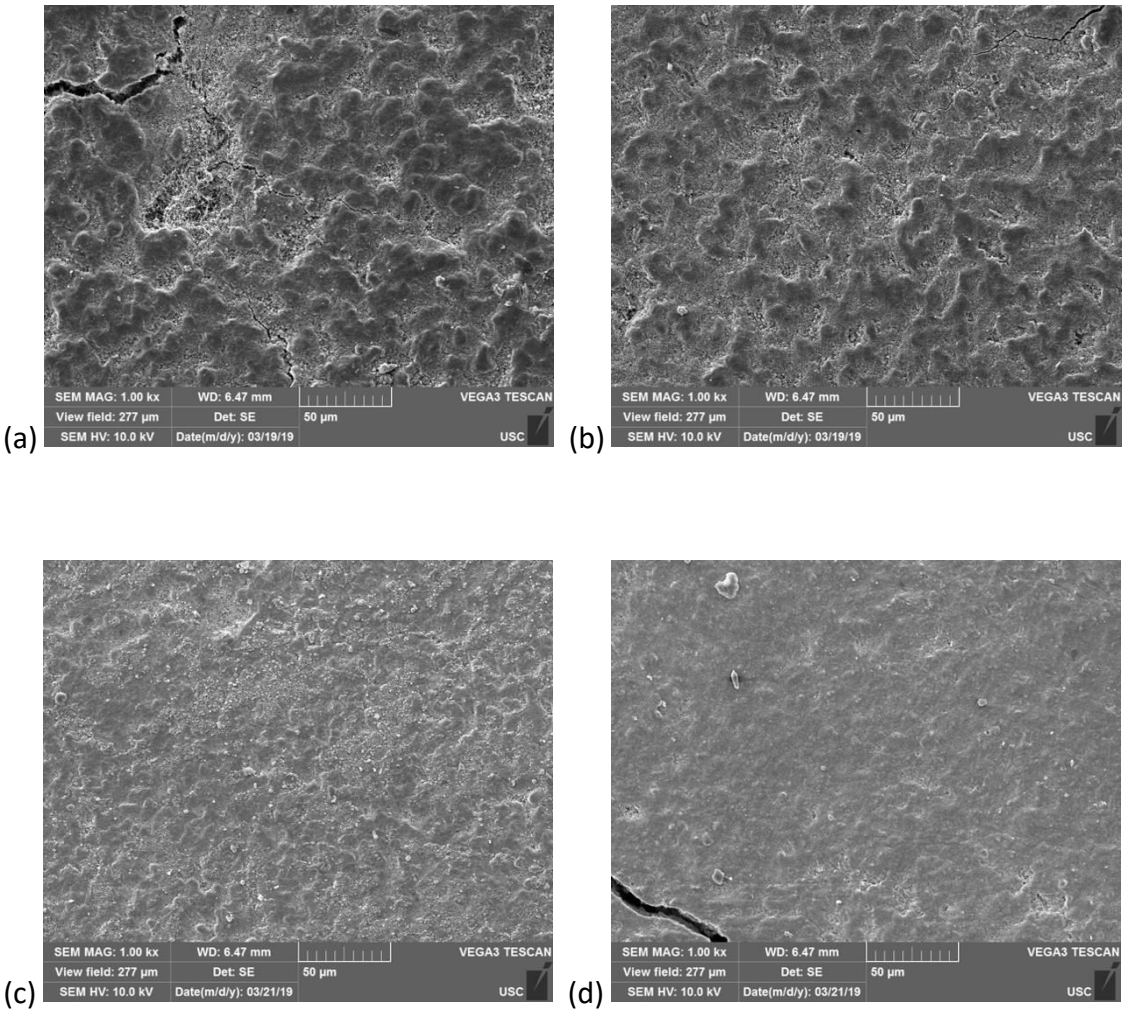

Figure 3.19 Free curing surfaces of control and PUCNT-amended cement paste with (a) 0 wt% (b) 0.001 wt% (c) 0.005 wt% (d) 0.05 wt% of PUCNTs, after 28 days of curing

CHAPTER 4

DISPERSION OF GRAPHENE NANORIBBONS IN AQUEOUS SOLUTIONS AND APPLICATION ON PORTLAND CEMENT CONCRETE

4.1. INTRODUCTION

This chapter reports on the dispersibility and dispersion stability of different concentrations of graphene oxide nanoribbons (GONRs) in aqueous solutions, which may be used in nano-amended cement composite mix designs. GONRs are elongated strips of graphene [Kosynkin et al. 2009] having thickness smaller than graphene nanoplatelets (GNP), higher aspect ratio, and higher specific surface area compared to MWCNTs and PUCNTs. In addition, GONRs have an exceptionally high graphene edge content due to much higher –COOH edge sites compared to standard graphene structures [Kosynkin et al. 2009]. Due to their high functional edge content, GONRs are suitable for chemical crosslinking with cement hydrates. Therefore, in this research, very low concentrations of GONRs will be considered, in the range 0.0125-1.25 g/L (equivalent to 0.0005 – 0.05 wt% of cement in concrete with *w/c* = 0.4). Three different levels of oxygen functionality, ~40 wt%, ~30 wt%, and ~20 wt%, will be evaluated without changing the morphology and oxidation defects of GONRs.

4.2. EXPERIMENTAL PROGRAM FOR PHASE I

4.2.1 Preparation of GONR-suspensions in DI water

The GONRs (length in range 10 to 100 µm, and width approximately 40 nm) were prepared at Savannah River National Laboratory (SRNL) through a similar procedure described in Chapter 3, Section 3.2.1 for PUCNTs, and incorporated into DI water suspensions. The GONR concentrations were selected as 0.0125 g/L (0.0005 wt% for cement in concrete), 0.025 g/L (0.001 wt% for cement in concrete), 0.125 g/L (0.005 wt% for cement in concrete), 0.5 g/L (0.02 wt% for cement in concrete), and 1.25 g/L (0.05 wt% for cement in concrete) as summarized in Table 4.1. The initial pH values of the suspensions were measured with a pH meter (Mettler Toledo, pH electrode LE 438) and are presented in Table 4.1. Ultrasonication was performed only on the initial day (day 0) for 15 minutes at a frequency of 40 kHz to confirm good dispersion of the GONRs in the suspensions with an ultrasonic bath sonicator (Branson, 2800 CPX). Three different levels of oxygen functionality, namely 40.7 wt%, 32.5 wt%, and 22.7 wt%, were considered.

4.2.2 Dispersibility assessment in aqueous solutions

Stability of the suspensions, which indicates effective dispersion of the nanoparticles, can be quantitatively assessed through DLS analysis based on HDS and ZP measurements, as reported in Chapter 2 and Chapter 3 for MWCNTs and PUCNTs, respectively.

In this preliminary study, visual inspection of the suspensions, ZP and HDS measurements were performed at 0, 7, 14, 21, and 28 days after initial sonication to

assess the stability of the suspensions over time (Figure 4.1). HDS and ZP were measured through DLS using a particle and molecular size analyzer (Zetasizer nano ZS, Malvern Panalytical Ltd.). A 1 mL sample of solution was used for each concentration, oxygen level, and testing time, for ZP measurement, which was repeated 10 times. Similar samples were used also for HDS measurement, which was repeated five times, to assess the variability of the results.

4.3. RESULTS AND DISCUSSIONS OF PHASE I

4.3.1 Visual inspection

4.3.1.1 After sonication

With an increase in GONR concentration for each oxidation level, the color of the suspensions became darker (Figure 4.1) due to an increase in amount of GONRs. Good dispersion was observed visually for 40.7 wt% and 33.5 wt% oxidized GONRs for all concentrations. Poor dispersion was observed, with numerous visible agglomerates, for 0.02 and 0.05 wt% of 22.7 wt% oxidized GONRs.

4.3.1.2 After 7-day of sonication

Good dispersion was observed visually for 40.7 wt% and 33.5 wt% oxidized GONRs for all concentrations. Poor dispersion with some agglomerates was observed for 0.005 wt% of 22.7 wt% oxidized GONRs. Suspensions with 0.02 and 0.05 wt% of 22.7 wt% oxidized GONRs were dark and showed many visible agglomerates. Changes in the color of the suspensions was observed with time, especially from 0.005 to 0.05 wt% of GONR-suspensions. For all three oxidation levels, 0.005 to 0.05 wt% of GONR suspensions appeared darker 7 days after sonication compared to the initial day.

4.3.1.3 After 14 to 28-day of sonication

Good dispersion was observed visually for 40.7 wt% oxidized GONRs for all concentrations. Poor dispersion with some agglomerates was observed for 0.05 wt% of 33.5 wt% oxidized GONRs, and 0.005 wt% of 22.7 wt% oxidized GONRs. The suspensions with 0.02 and 0.05 wt% of 22.7 wt% oxidized GONRs showed many visible agglomerates, suggesting that the lower oxidation level is unsuitable for further consideration. No noticeable changes in the color of the suspensions were observed 14, 21, and 28 days after sonication compared to the suspensions 7 days after sonication.

4.3.2 Zeta potential

All GONR suspensions were considered as physically stable immediately after sonication (day 0) as the absolute value of zeta potential was consistently above 30 for all samples (Figure 4.2). After 7 days from sonication, only the 0.05 wt% suspension of 22.7 wt% oxidized GONRs was unstable whereas the other suspensions were considered stable (Figure 4.3). After 14, 21, and 28 days from sonication, the 0.05 wt% suspensions of 22.7 wt% and 33.5 wt% oxidized GONR were considered unstable (Figure 4.4 through Figure 4.6). Other suspensions were physically stable. Good stability was observed for the suspensions with 0.0005 and 0.001 wt% concentrations of GONRs for all three oxidation levels up to 21 days after sonication, and for 33.5 and 40.7 wt% oxidation levels up to 28 days after sonication. Good stability was also observed for the suspensions with 0.005 wt% of GONRs for the 40.7% oxidation level up to 28 days after sonication. Marginal stability (~-30 mV) was observed for suspensions with 0.02 wt%

concentration of GONRs for all three oxidation levels up to 28 days after sonication (Figure 4.6).

An increase in absolute value for the zeta potential was observed with an increase in oxidation level, especially at 7, 14, 21, and 28 days after sonication, indicating that more stable suspensions tend to be attained as the oxygen content increases as a result of functionalization. These results indicate that, to achieve stable suspensions (<-30 mV of zeta potential) with a 0.05 wt% of GONR concentration 7 days after sonication, more than 30 wt% of oxygen content is essential.

4.3.3 Hydrodynamic size

The hydrodynamic size (HDS) values show relatively small differences for all concentrations of 40.7 wt% and 33.5 wt% oxidized GONRs immediately after sonication (Figure 4.7) and at 7 days after sonication (Figure 4.8). However, the 22.7 wt% oxidized GONRs were relatively less well dispersed as suggested by the larger variability in HDS. At 14 days after sonication, the suspensions with 33.5 wt% and 22.7 wt% oxidized GONRs in concentration of 0.05 wt% showed larger variability in HDS, suggesting subpar dispersion (Figure 4.9). All suspensions with 40.7 wt% oxidized GONRs, and those with 33.5 wt% oxidized GONRs in concentrations from 0.0005 to 0.02 wt% showed statistically significant results after 14-day of sonication. All suspensions having 22.7 wt% oxidized GONRs yielded more inconsistent results over time, and up to 28 days from sonication, compared to the higher oxidation levels (Figure 4.7 to Figure 4.11).

4.4. SUMMARY OF PHASE I

- No visible changes in the suspensions were observed at 14 and 28 days after sonication, compared to 7 days after sonication.
- An increase in zeta potential (absolute value) was observed at increasing oxidation levels, especially at 7, 14, 21, and 28 days after sonication, indicating that suspension stability decreases over time at decreasing oxidation levels.
- A decrease in hydrodynamic size was observed at increasing oxidation levels, indicating better dispersibility resulting from higher functionalization levels.
- The visible agglomerates for 22.7 wt% oxidized GONRs may hinder chemical bonding with cement hydrates due to the comparatively smaller amount of functionalized surface area that is available for the precipitation of cement hydrates. Therefore, similar to MWCNT and PUCNT agglomerates, these agglomerates may result in GONR aggregation in cement matrices, thus acting as defect sites.
- For a final (Phase II) analysis to verify the repeatability of the preparation of GONRs as well as GONR suspensions, based on the outcomes of Phase I, two levels of oxidation in the range ~30-40 wt% were selected to produce stable aqueous suspensions. Three different contents of GONRs i.e., 0.0005 wt% (ultra-low), 0.005 wt% (low), and 0.05 wt% were also considered in the final step. The stability of the suspensions was observed up to 7 days.

4.5. EXPERIMENTAL PROGRAM FOR PHASE II

4.5.1 Preparation of GONR-suspensions in DI water

GONR suspensions in DI water were prepared using concentrations of 0.0125 g/L (0.0005 wt%), 0.125 g/L (0.005 wt%) and 1.25 g/L (0.05 wt%) as summarized in Table 4.2. The initial pH of the suspensions was measured with a pH meter (Mettler Toledo, pH electrode LE 438) and is presented in Table 4.2. Ultrasonication was performed only on the initial day for 15 minutes at a frequency of 40 kHz using an ultrasonic bath sonicator (Branson, 2800 CPX).

4.5.2 Dispersibility assessment in solutions

Visual inspection of the suspensions, ZP and HDS measurements were performed at 0 and 7 days after sonication to verify the stability of the suspensions over time. HDS and ZP were measured using the same equipment and method presented in Section 4.2.

4.5.3 Uniaxial compression testing

After confirming stable dispersion in DI water through DLS testing, 50×100 mm cement concrete cylinders were fabricated with 0.0005 wt% GONR suspensions with 32.3 wt% oxygen content, 0.005 wt% GONR suspensions with 41.3 wt% oxygen content, and 0.05 wt% GONR suspensions with 41.3 wt% oxygen content. Type I OPC, silica sand with specific gravity of 2.60, and crushed stone with nominal maximum size of 9.5 mm were utilized in all cases (Figure 4.12). The Portland cement concrete mix design and properties of crushed stone are reported in Appendix E. Plain cement concrete cylinders were also manufactured with DI water and used as control specimens (0 wt%). A constant water-to-cement mass ratio of 0.4 was considered for all cases. The mixes

were cast in cylindrical plastic molds with lids and then left to cure at room temperature. Four specimens per mix design were utilized for compression testing after 7 days of curing. The test matrix is presented in Table 4.3.

Uniaxial compression tests were performed on the concrete cylinders using a servo-hydraulic loading frame. The specimens were capped with sulfur mortar according to ASTM C617 [2012]. The load was applied in displacement-control mode at a rate of 0.3 mm/minute. To minimize the confining effects due to friction between the loading platens and the specimen surfaces, 0.4-mm polytetrafluoroethylene (PTFE) inserts were also placed between the specimen surfaces and the loading platens. The test setup is shown in Figure 4.13.

4.5.4 Scanning electron microscopy imaging

The dispersion of GONRs in cement concrete, and the nano- and -micro-structure of the amended cement concrete, were examined through SEM imaging. After 7 days of curing, the cylindrical specimens were broken into fragments. These fragments were air-dried at room temperature for 48 hours. Air drying was preferred to oven-drying over concerns on the possibility of affecting the formation of cement hydrates. After air drying, fragments lesser than 5 mm in size in any direction were selected for SEM imaging. Prior to testing, the selected samples were placed in a vacuum-suction chamber for one hour to remove the excess moisture. Then, these samples were gold sputtered.

A field-emission scanning electron microscope (Ultraplus Thermal Field Emission Scanning Electron Microscope, Zeiss) was utilized to observe the nano- and micro-

structure of the composite matrix, thus making it possible to obtain high-magnification SEM micrographs while minimizing electrostatic distortions.

4.6. RESULTS AND DISCUSSIONS FOR PHASE II

4.6.1 Visual inspection

With the increase in GONR concentration for each oxidation level (Figure 4.14), the color of the suspensions became darker due to an increase in number of nanoparticles. Good dispersion was observed visually for all suspensions. No GONR agglomerates were visible immediately after sonication and up to 7 days after sonication.

4.6.2 Zeta potential

All GONR suspensions were physically stable immediately after sonication (Figure 4.15) as well as 7 days after sonication (Figure 4.16) because the zeta potential was below -30 mV for each sample. In particular, good stability was obtained with 0.0005 and 0.005 wt% of GONRs for both oxidation levels immediately and up to 7 days after sonication as the zeta potential was below -40 mV [Freitas and Muller 1998].

4.6.3 Hydrodynamic size

For the 15-minute measurement time, the HDS values for 0.0005 and 0.005 wt% of GONRs were statistically similar (for 5 replicates) after sonication (Figure 4.17), and after 7-day of sonication (Figure 4.18) for both oxidation levels with low variability in hydrodynamic size. The 0.05 wt% of GONRs were relatively less well dispersed as they showed larger variability in hydrodynamic size.

Decrease in hydrodynamic size was observed with oxidation level after sonication (Figure 4.17) for all GONR-contents, and for 0.005 and 0.05 wt% of GONRs at 7 days after sonication (Figure 4.18). No trend was observed with decrease in the hydrodynamic size with oxidation level for 0.0005 wt% of GONRs at 7 days after sonication. However, the results are not inconsistent from statistical point of view.

4.6.4 Compressive strength

Figure 4.19 presents the compressive strength mean and standard deviation for the cement concrete specimens as a function of GONR concentration. The incorporation of oxidized GONRs produced enhancements in compressive strength after 7 days of curing. In fact, compared to plain cement concrete, the incorporation of 0.0005 wt% (32.3 wt% oxygen content), 0.005 wt% (41.3% oxygen content) and 0.05 wt% (41.3 wt% oxygen content) concentrations of GONRs resulted in +22, +25, and +32% increase in average 7-day compressive strength, with less variability compared to the control samples without GONRs. It is important to notice that a minor enhancement in compressive strength was attained after 7 days of curing using 0.05 wt% GONR concentrations compared to a GONR concentration of 0.0005 wt%, which is 100 times smaller. To better understand the dispersibility and embedment of GONRs in the cement concrete, SEM micrographs were acquired from fractured surfaces.

4.6.5 Scanning electron microscopy analysis

The nano- and micro-structures of the control and GONR-amended cement concrete after 7 days of curing are shown in the representative SEM micrographs in Figure 4.20 to Figure 4.23. Improved interfacial transition zones (ITZs) were observed in

GONR-amended concrete (e.g., Figure 4.22a, and Figure 4.23a) compared to plain concrete (e.g., Figure 4.20). Accelerated and preferential formation of amorphous calcium silicate hydrate (C-S-H) [Mehta and Monteiro 2006] was observed after 7 days of curing in cement concrete amended with GONRs in concentrations of 0.0005 wt% (Figure 4.21), 0.005 wt% (Figure 4.22), and 0.05 wt% (Figure 4.23), in the vicinity of embedded GONRs (marked by dashed yellow circles in the SEM micrographs), which may be acting as precipitation sites. No GONR agglomerates were observed for 0.0005 wt%, 0.005 wt% or 0.05 wt% GONR concentrations.

4.7. CONCLUSIONS

- Uniform GONR dispersions were observed visually for concentrations of 0.0005 wt%, 0.005 wt% and 0.05 wt% of GONRs with 32.3 wt% and 41.3 wt% of oxygen content immediately and up to 7 days after sonication.
- All suspensions were found stable up to 7 days in terms of zeta potential results.
- Larger variability in hydrodynamic size was obtained for 0.05 wt% of GONRs for both oxidation levels after sonication.
- pH values of all suspensions were found in the acidic range. However, stable dispersions were obtained based on zeta potential results. With low pH, stable dispersion of GONRs may still be easily attained through sonication. GONRs have high-functionality edges and a relatively large number of functional groups compared to MWCNTs and PUCNTs. Therefore, some functional groups may have been deprotonated at low pH values although not enough to hinder dispersibility and stability thereof in aqueous suspensions.

- Compressive strength of cement concrete was similarly enhanced for a concentration range of 0.0005-0.05 wt% of GONRs with oxygen content of 32.3 wt% and 41.3 wt%, after 7 days of curing.
- The nano- and micro-structure of cement concrete was significantly modified by the incorporation of GONRs, as reflected in visual evidence of enhanced ITZs and accelerated and preferential formation of C-S-H in the vicinity of embedded GONRs.

4.8. REFERENCES

ASTM International. Standard Practice for Capping Cylindrical Concrete Specimens. ASTM C617-12. West Conshohocken, PA: ASTM International, 2012.

Freitas C, Muller RH. Effect of light and temperature on zeta potential and physical stability in solid lipid nanoparticle (SLN™) dispersions. Int J Pharm 1998; 168, 221–229.

Gigault J, Grassl B, Lespes G. A new analytical approach based on asymmetrical flow field-flow fractionation coupled to ultraviolet spectrometry and light scattering detection for SWCNT aqueous dispersion studies. Analyst 2012; 137, 917.

Kosynkin DV, Higginbotham AL, Sinitskii A, Lomeda JR, Ayrat Dimiev A, Price BK, Tour JM. Longitudinal Unzipping of Carbon Nanotubes to form Graphene Nanoribbons. Nature 2009; 458, 872-877.

Mehta PK, Monteiro PJM. Concrete microstructure, properties, and materials. McGraw-Hill Education; 4th Edition, 2006.

Zohhadi N. Functionalized Graphitic Nanoreinforcement for Cement Composites. PhD Dissertation 2014; University of South Carolina, Columbia.

4.9. TABLES

Table 4.1 Description of Phase I GONR suspensions

GONR content [wt% cement in concrete]	*w/c* ratio	GONR-content [g/L]	Oxidation level	% Oxygen	pH
0.0005	0.4	0.0125	High	40.7	4.93
0.001		0.025			4.72
0.005		0.125			3.93
0.02		0.5			3.83
0.05		1.25			2.79
0.0005		0.0125	Medium	33.5	4.72
0.001		0.025			4.68
0.005		0.125			4.36
0.02		0.5			3.89
0.05		1.25			3.09
0.0005		0.0125	Low	22.7	4.72
0.001		0.025			4.45
0.005		0.125			4.29
0.02		0.5			4.17
0.05		1.25			3.21

Table 4.2 Description of Phase II GONR-suspensions

GONR-content [wt% of cement in concrete]	*w/c* ratio	GONR-content [g/L]	Oxidation level	% Oxygen	pH
0.0005	0.4	0.0125	High	41.3	3.57
0.005		0.125			2.49
0.05		1.25			2.18
0.0005		0.0125	Medium	32.3	6.76
0.005		0.125			4.58
0.05		1.25			3.53

Table 4.3 Test matrix for physico-mechanical tests on plain and GONR-amended cement concrete

GONR concentration [wt%]	% Oxygen (in weight)	Tests	Number of specimens	Specimens to be cast
Control (0)	-	Compressive strength	4*	5
		SEM imaging	Crushed from failed cylinders	
0.0005	32.3	Compressive strength	4*	5
		SEM imaging	Crushed from failed cylinders	
0.005	41.3	Compressive strength	4*	5
		SEM imaging	Crushed from failed cylinders	
0.05	41.3	Compressive strength	4*	5
		SEM imaging	Crushed from failed cylinders	

* While a minimum number of 4 specimens are considered to ensure statistical meaningfulness, up to 5 specimens were cast

4.10. FIGURES

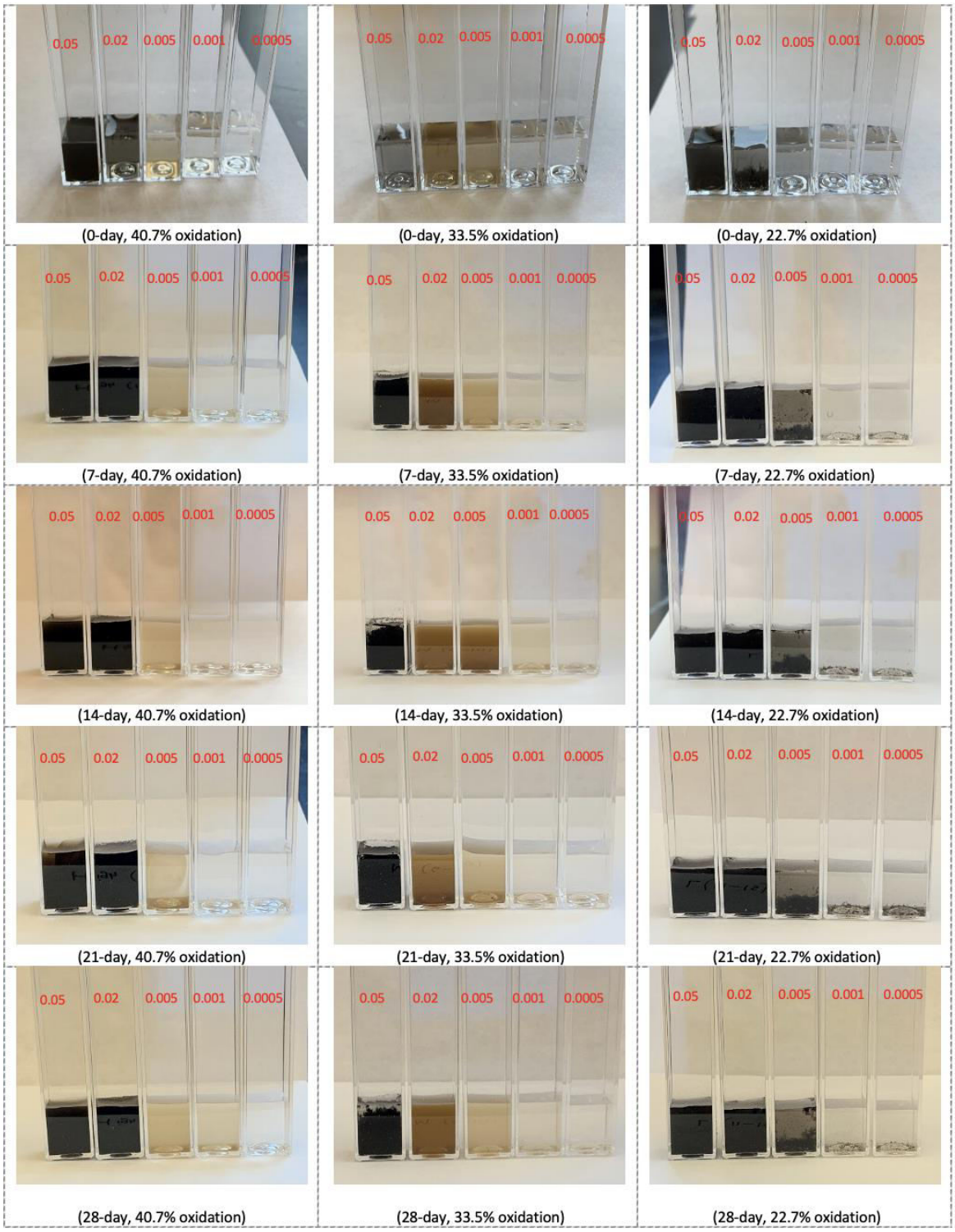

Figure 4.1 Visual inspection of suspensions with 0.0005 to 0.05 wt% of GONRs with three different oxygen contents at 7, 14, 21, and 28 days after sonication

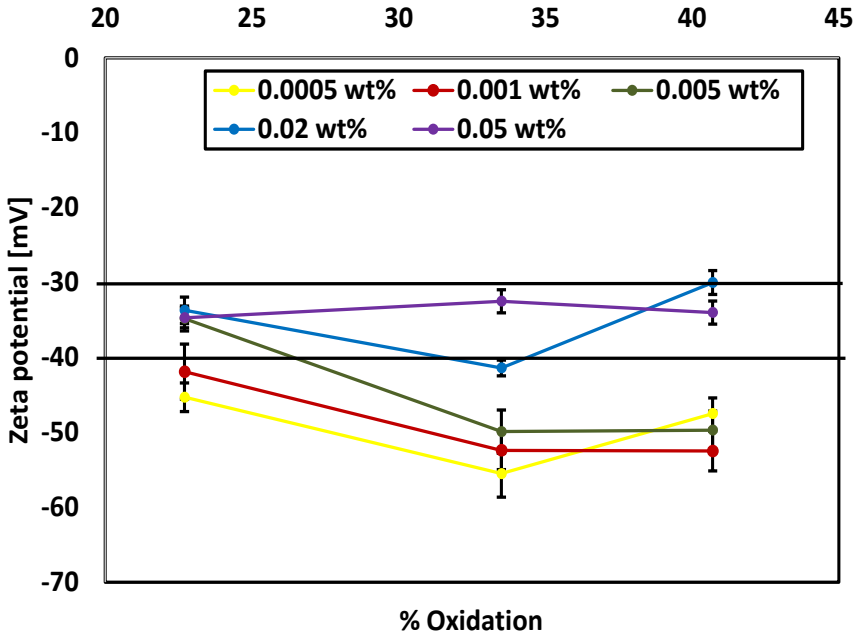

Figure 4.2 Zeta potential (average and standard deviation) immediately after sonication

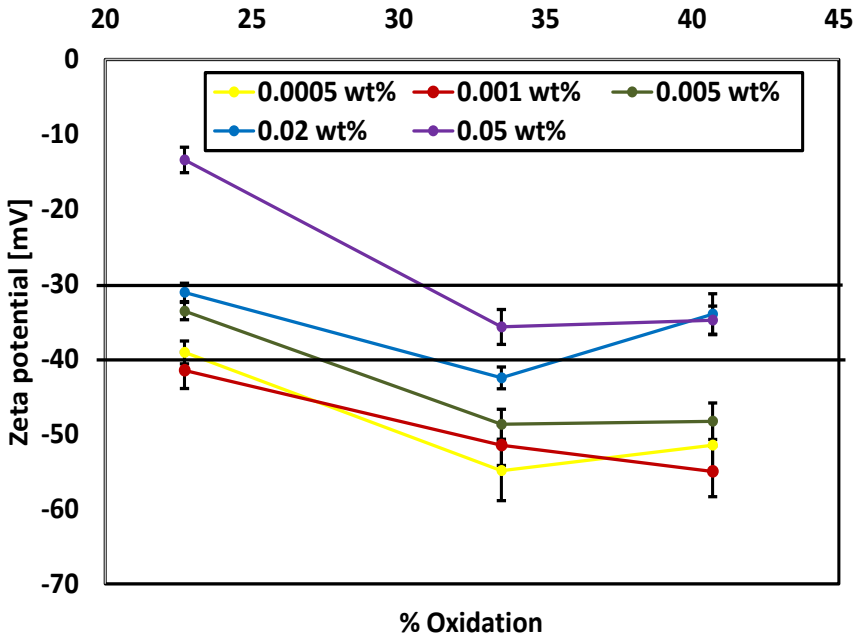

Figure 4.3 Zeta potential (average and standard deviation) 7 days after sonication

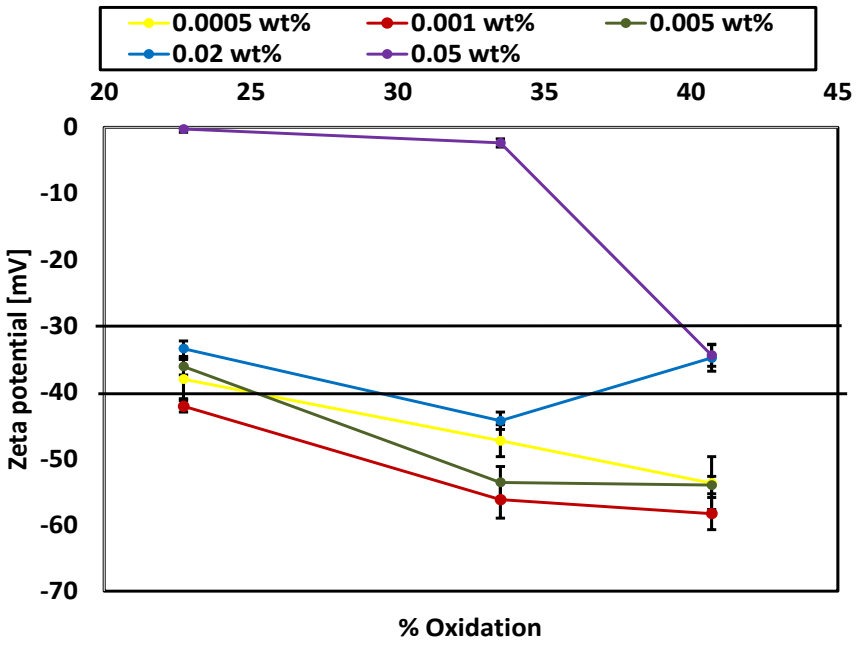

Figure 4.4 Zeta potential (average and standard deviation) 14 days after sonication

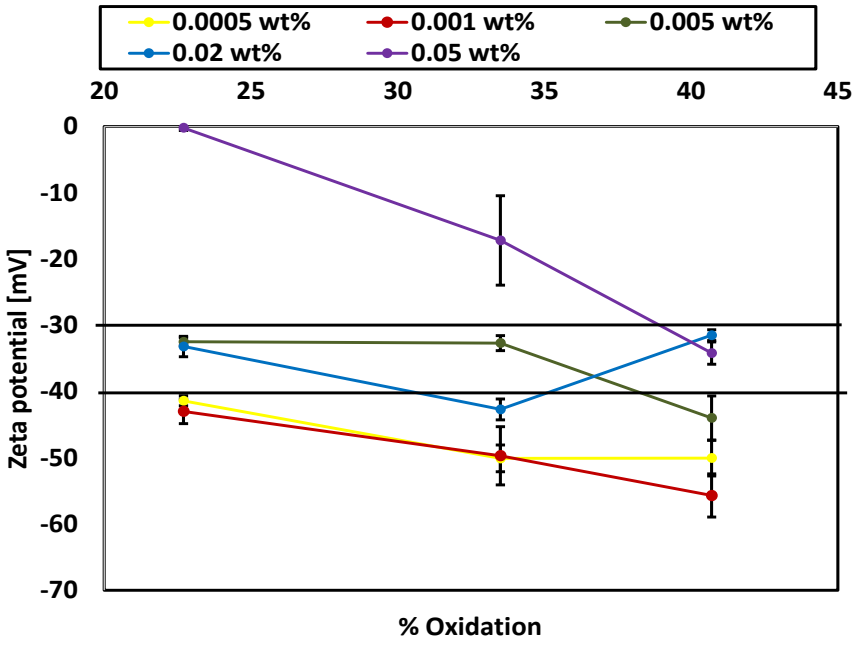

Figure 4.5 Zeta potential (average and standard deviation) 21 days after sonication

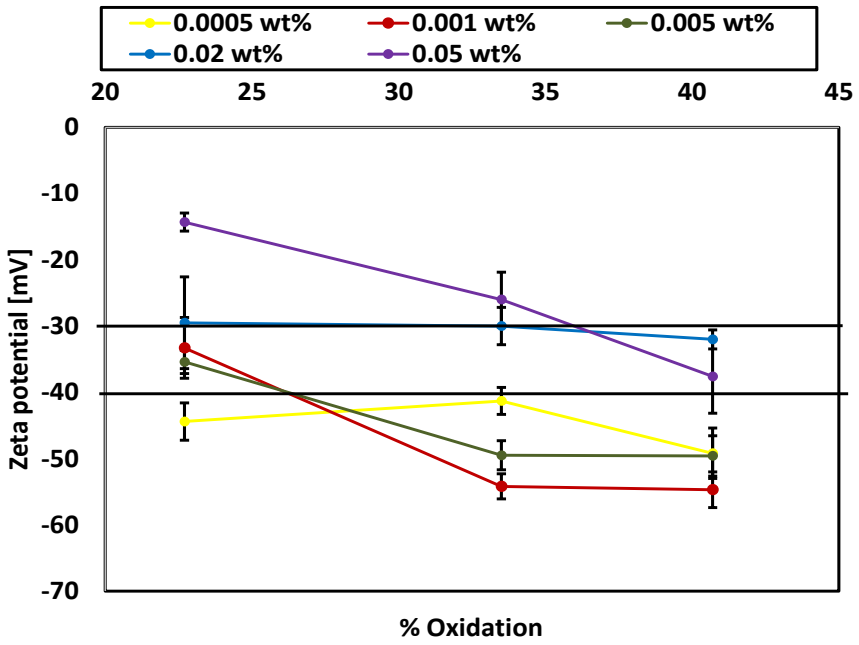

Figure 4.6 Zeta potential (average and standard deviation) 28 days after sonication

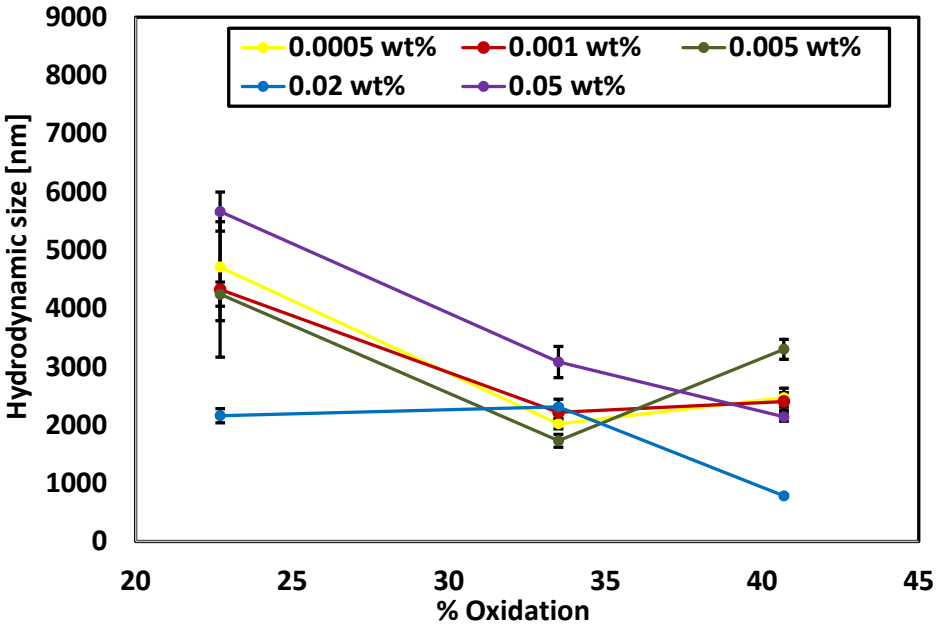

Figure 4.7 Hydrodynamic size (average and standard deviation) immediately after sonication

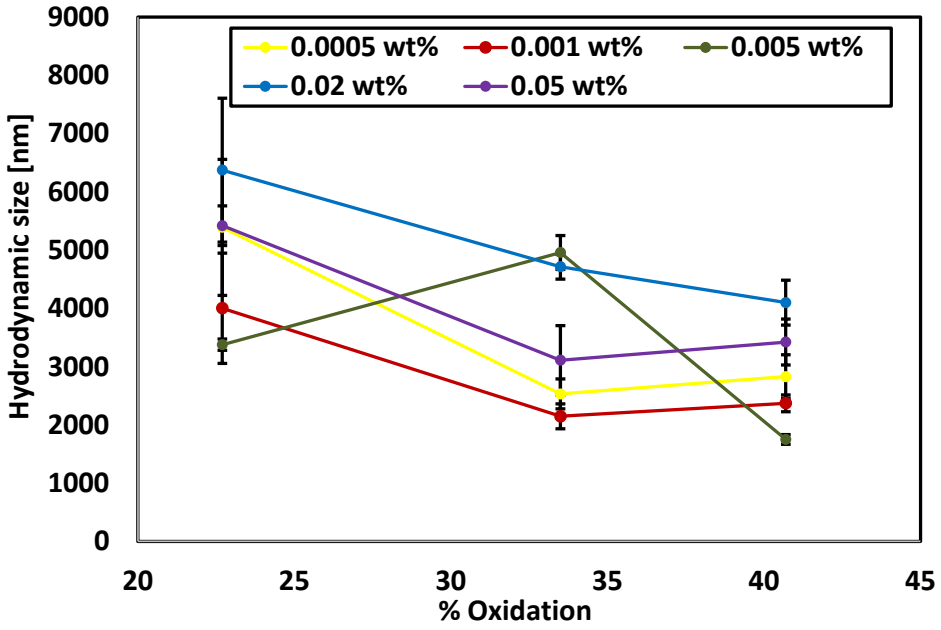

Figure 4.8 Hydrodynamic size (average and standard deviation) 7 days after sonication

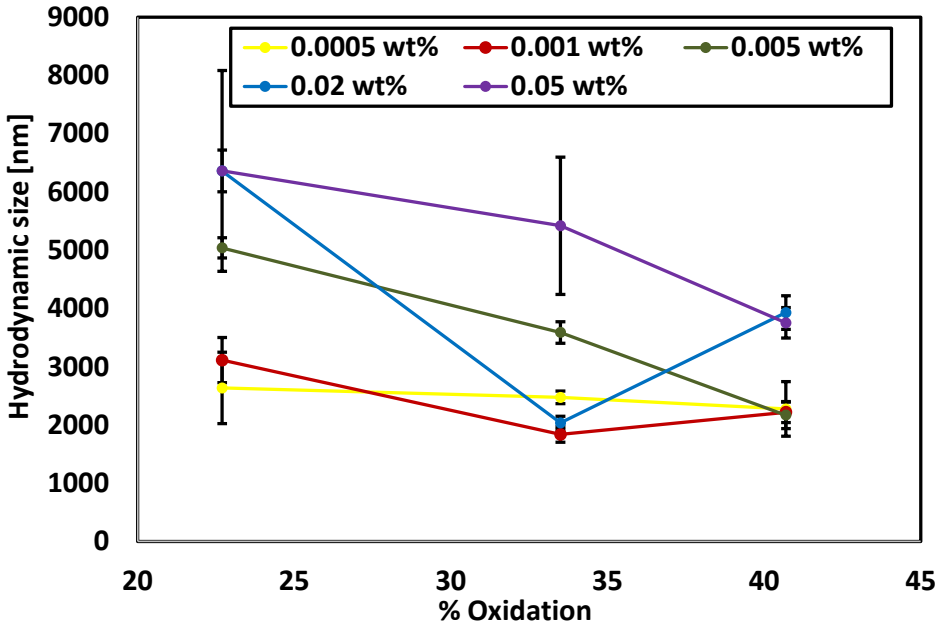

Figure 4.9 Hydrodynamic size (average and standard deviation) 14 days after sonication

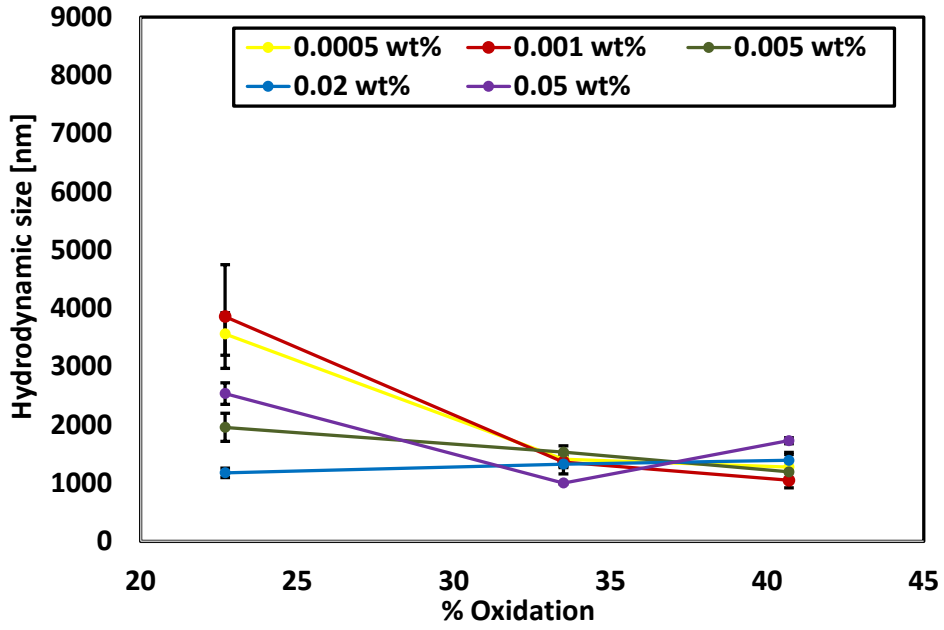

Figure 4.10 Hydrodynamic size (average and standard deviation) 21 days after sonication

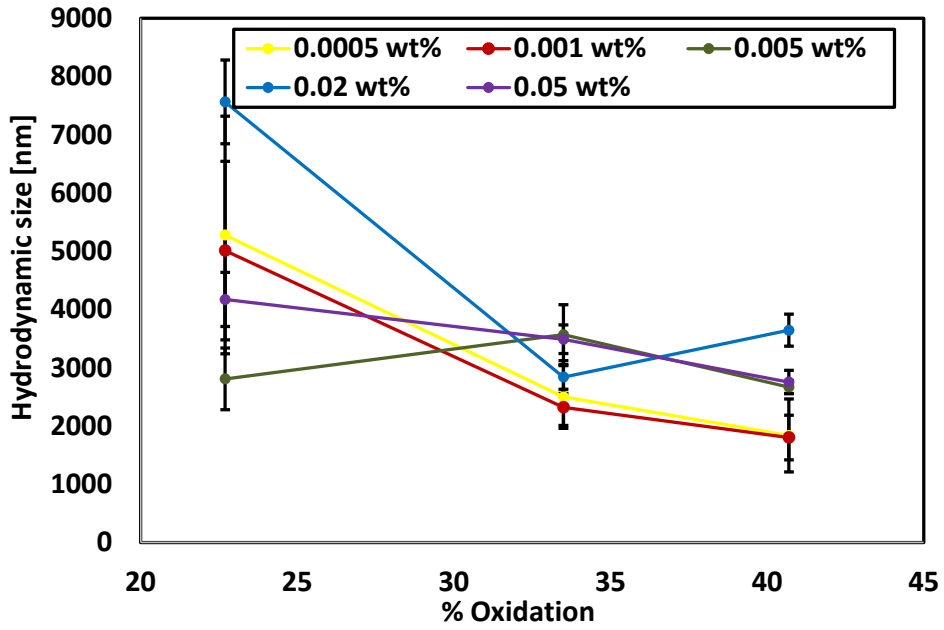

Figure 4.11 Hydrodynamic size (average and standard deviation) 28 days after sonication

Figure 4.12 From left to right: GONR suspension (1.25 g/L, equivalent to 0.05 wt%), OPC, sand, and crushed stone, used to fabricate GONR-amended concrete cylinder specimens

Figure 4.13 Photograph of concrete cylinder uniaxial compression test setup

(a)

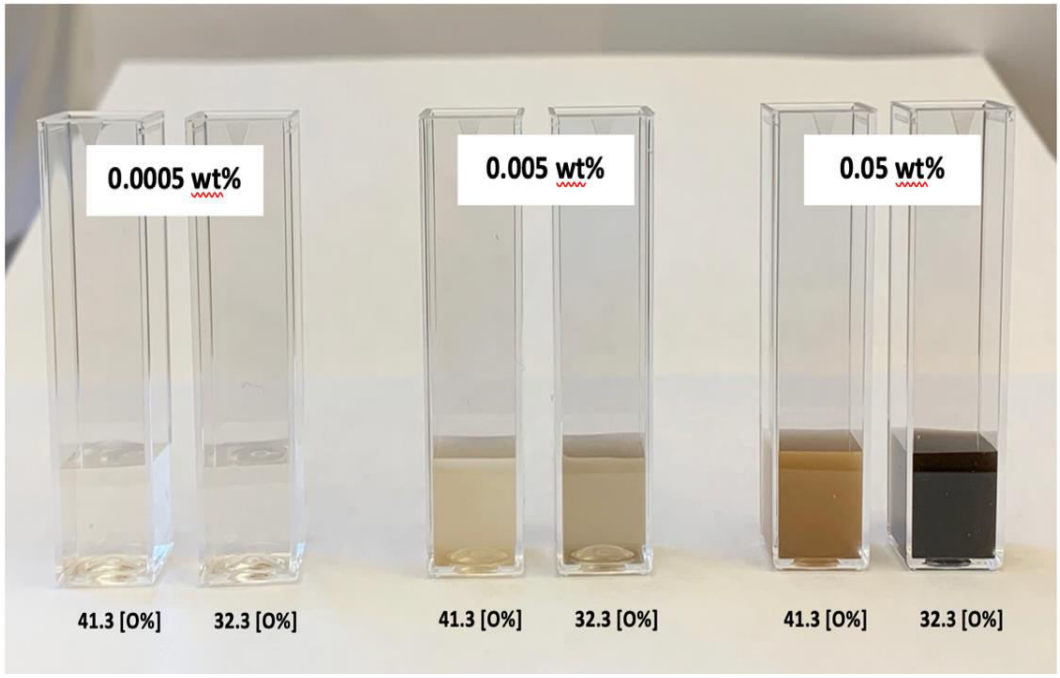

(b)

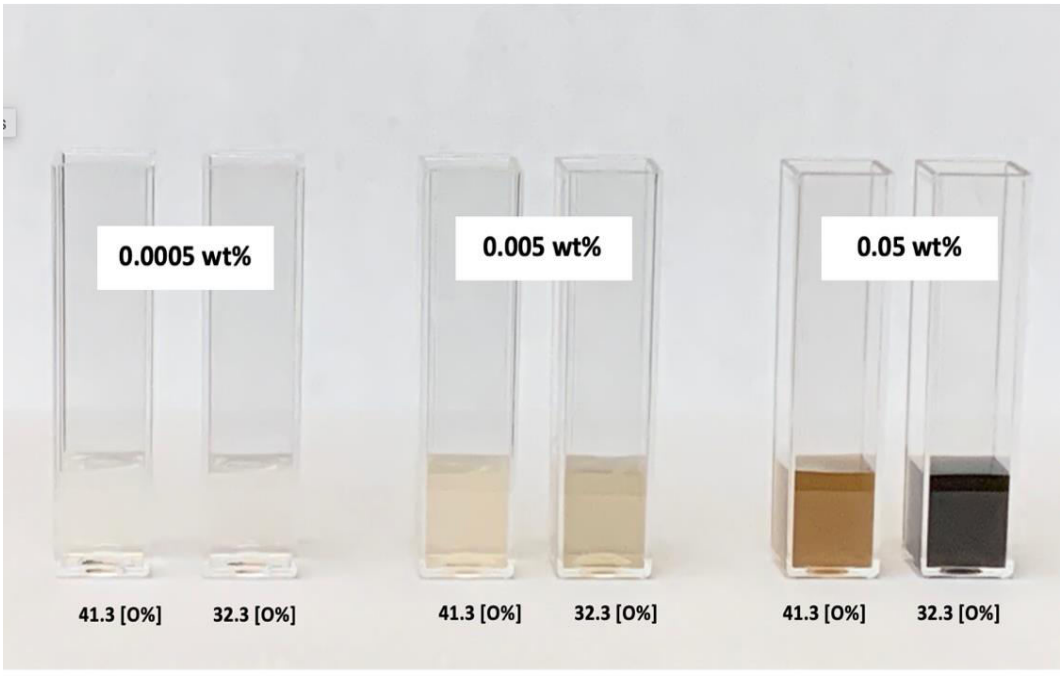

Figure 4.14 Visual inspection of aqueous suspensions with 0.0005 to 0.05 wt% of GONRs with two different levels of oxygen content: (a) immediately after sonication (b) 7 days after of sonication

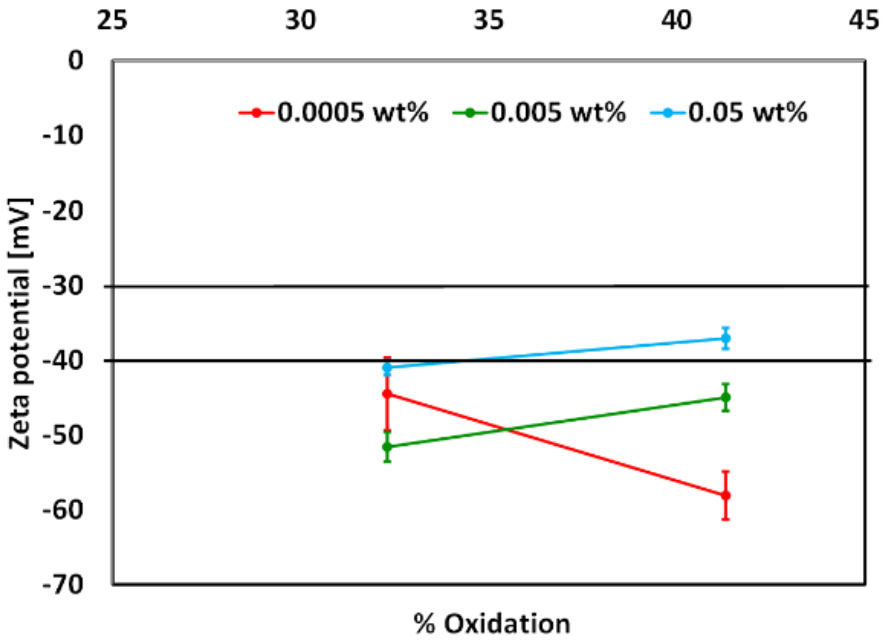

Figure 4.15 Zeta potential (average and standard deviation) immediately after sonication

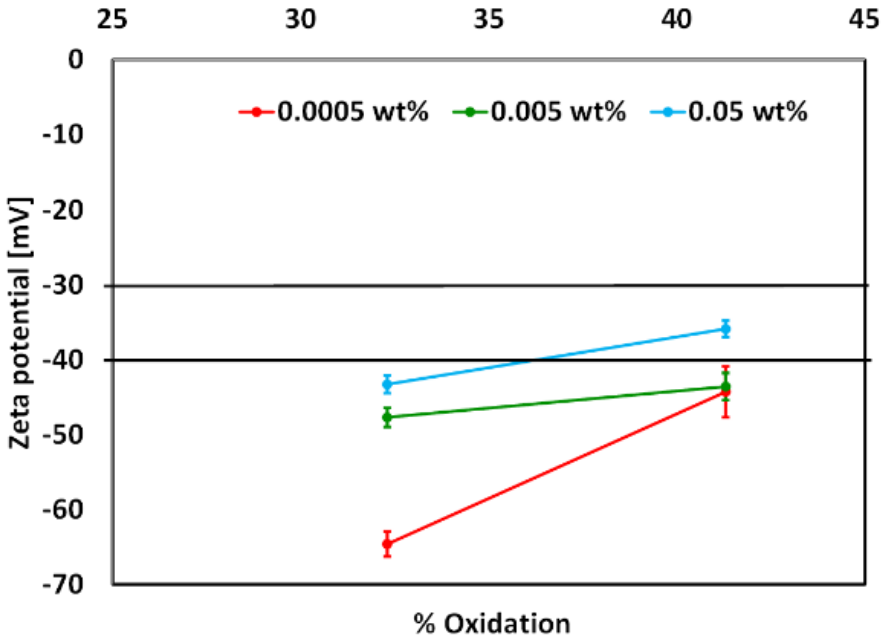

Figure 4.16 Zeta potential (average and standard deviation) 7 days after sonication

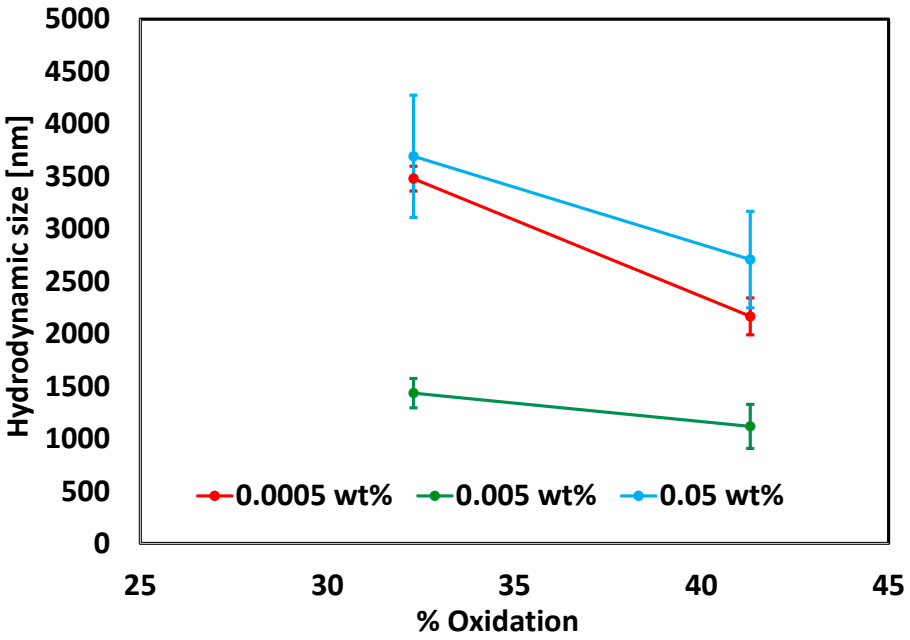

Figure 4.17 Hydrodynamic size (average and standard deviation) immediately after sonication

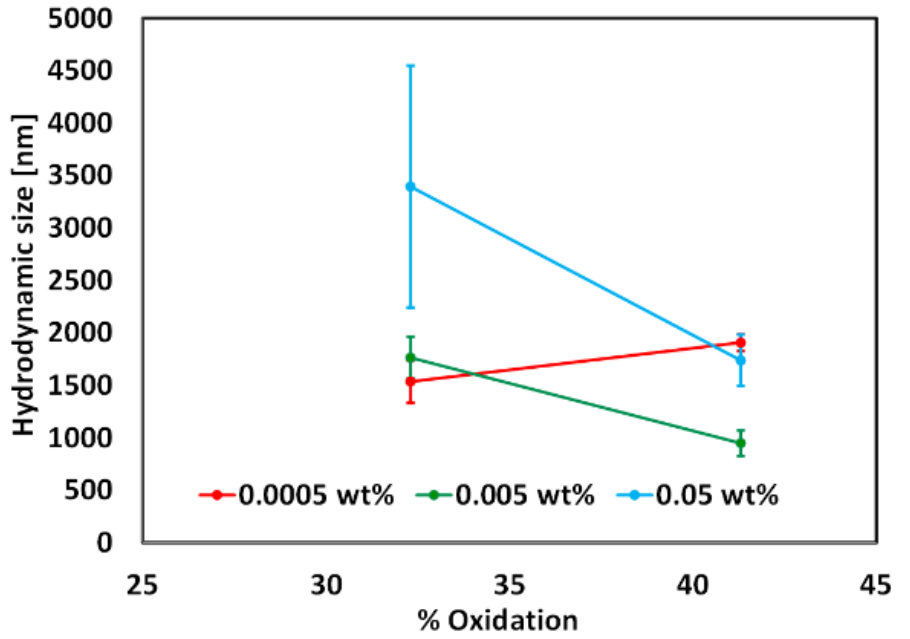

Figure 4.18 Hydrodynamic size (average and standard deviation) 7 days after initial sonication

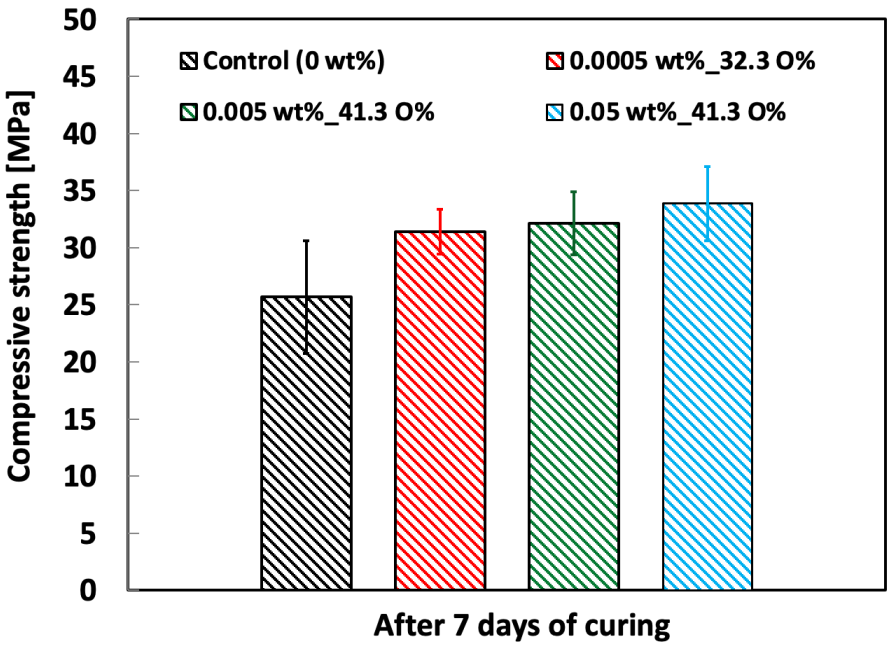

Figure 4.19 Preliminary uniaxial compressive strength results for plain and GONR-amended cement concrete

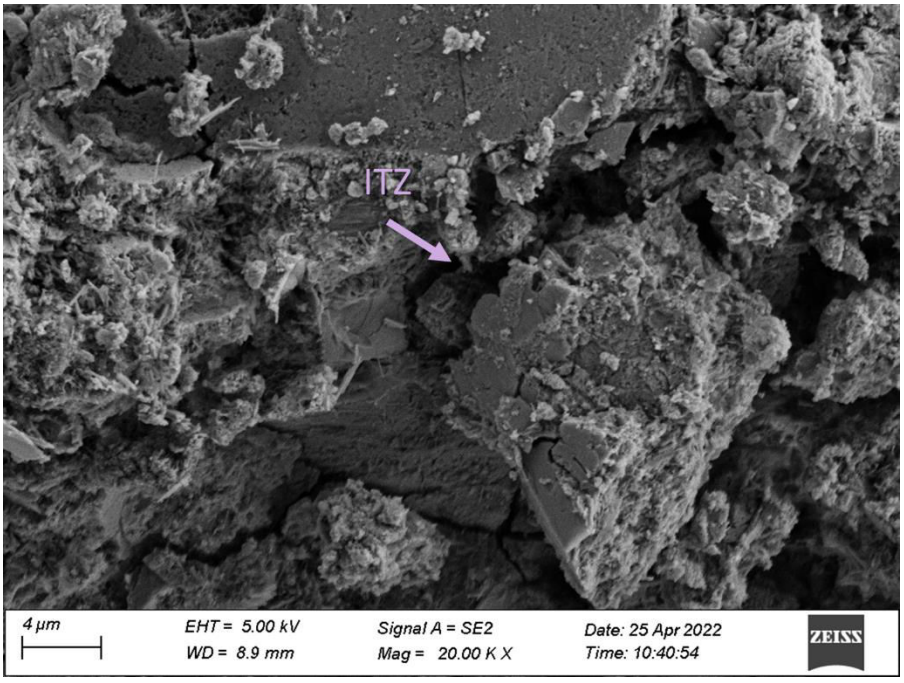

Figure 4.20 Nano- and micro-structure of control (0 wt%) cement concrete after 7 days of curing

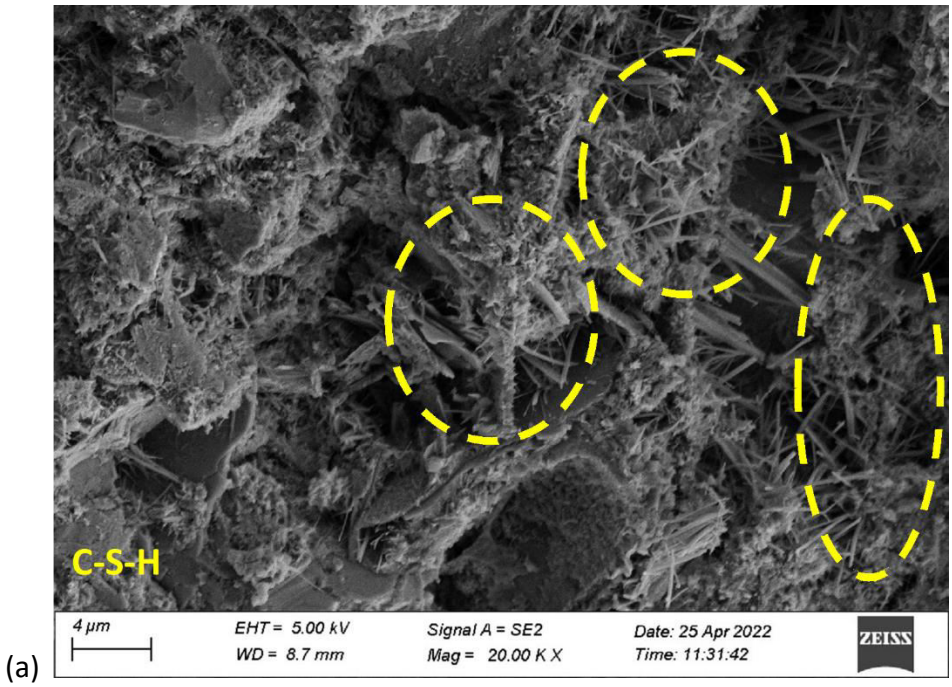

(a)

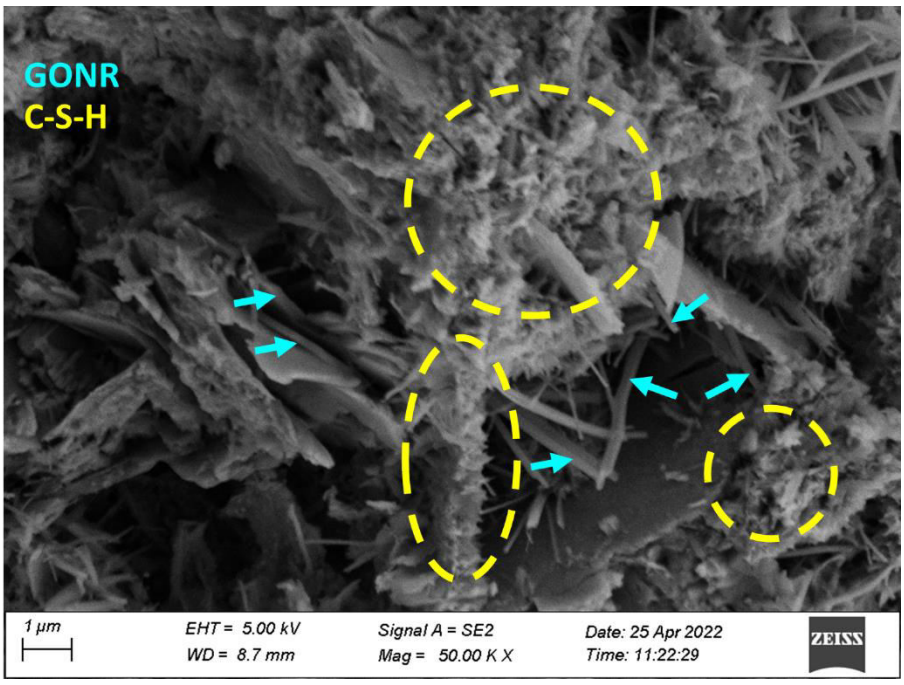

(b)

Figure 4.21 Nano- and micro-structure of cement concrete for 0.0005 wt% GONR (32.3 wt% oxygen content) concentration after 7 days of curing

(a)

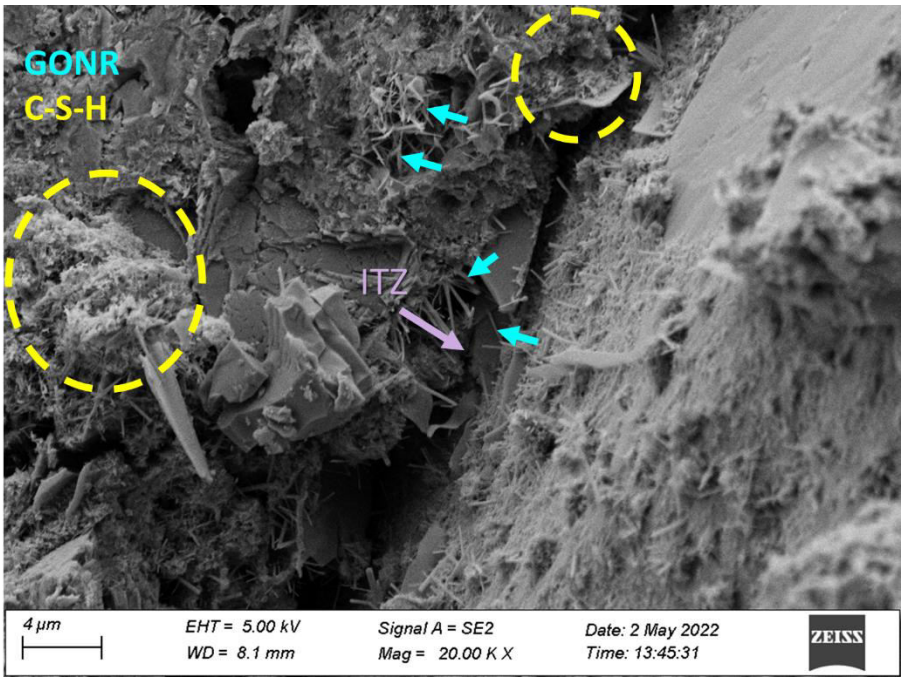

(b)

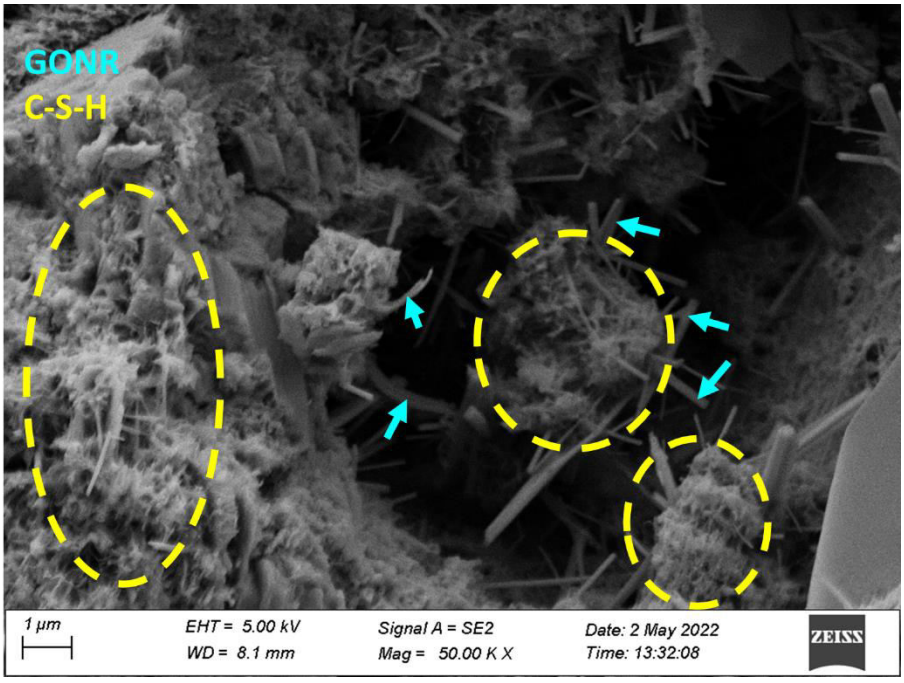

Figure 4.22 Nano- and micro-structure of cement concrete for 0.005 wt% GONR (41.3 wt% oxygen content) concentration after 7 days of curing

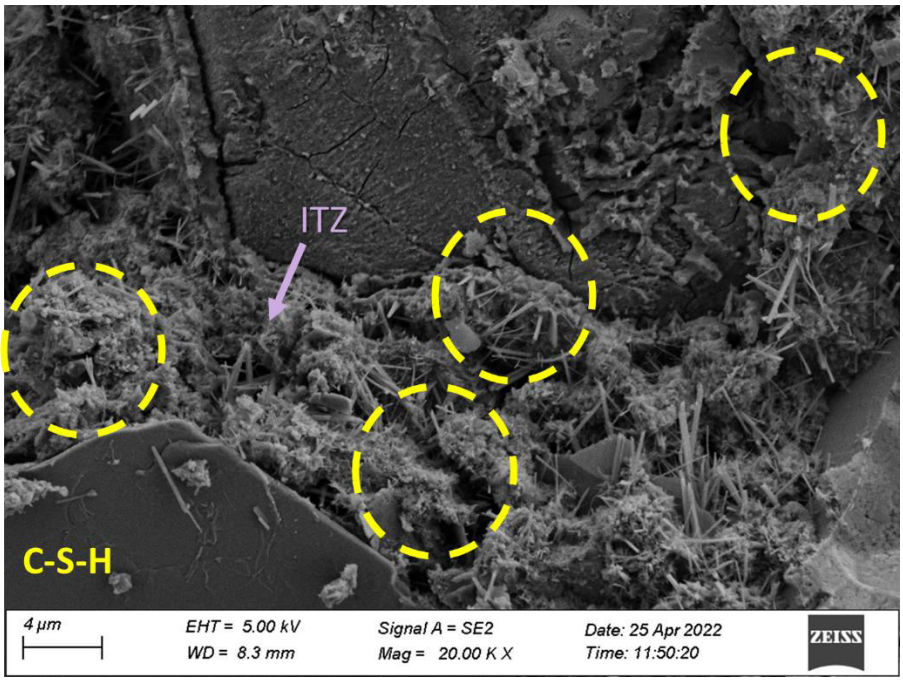

(a)

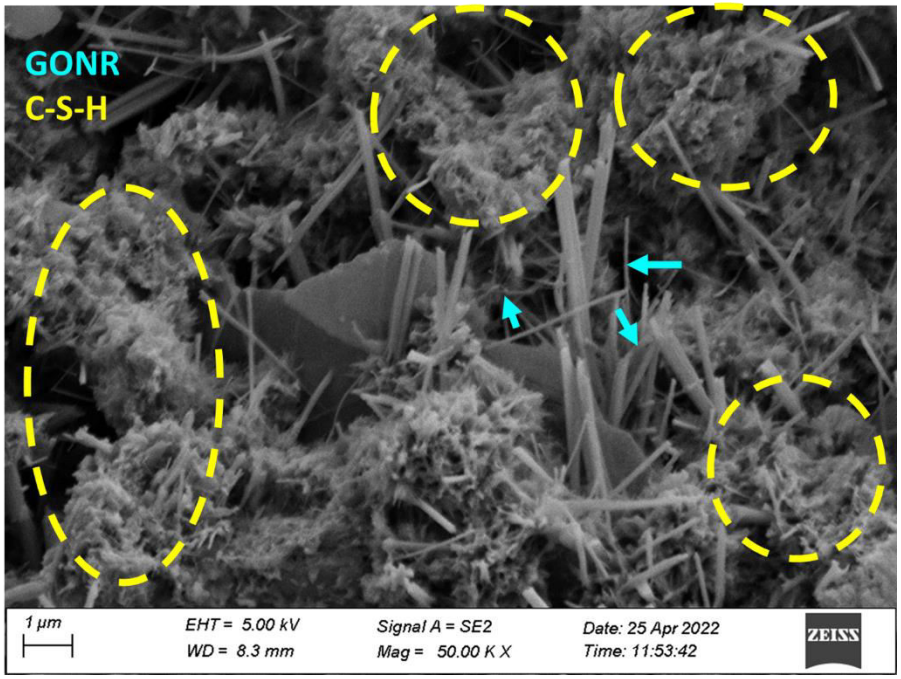

(b)

Figure 4.23 Nano- and micro-structure of cement concrete for 0.05 wt% GONR (41.3 wt% oxygen content) concentration after 7 days of curing

CHAPTER 5

CONCLUSIONS

5.1. CONCLUSIONS

The experimental results presented in this research show that:

- Good dispersion of oxidized MWCNTs in aqueous solutions was observed visually for concentrations from 0.02 to 0.2 g/L (0.001 to 0.01 wt%).
- Visible MWCNT agglomerates were observed at a concentration of 1 g/L (0.05 wt%) in aqueous suspensions.
- Good dispersion in aqueous solutions was achieved with 0.001-0.01 wt% of MWCNT concentrations in terms of hydrodynamic size, unlike the 0.05 wt% concentration.
- An absolute value of zeta potential consistently above 30 mV for MWCNT concentrations in the range 0.001-0.01 wt% confirmed the stability of the aqueous suspensions.
- An absolute value of zeta potential consistently below 30 mV for an upper-bound MWCNT concentration of 0.05 wt% (typically portrayed as a low concentration in the archival literature) of MWCNTs confirmed the instability of aqueous suspensions, and a tendency of the MWCNTs to agglomerate.

- Insignificant enhancements in compressive strength were observed in MWCNT-amended cement paste specimens with 0.05 wt% concentration compared to 0.01 wt% and 0.001 wt% concentrations after 28 days of curing.
- A less porous surface micro-structure of cement paste was observed as a result of MWCNT-amendment.
- Well-dispersed MWCNTs were consistently observed in cement paste for a MWCNT concentration of 0.001 wt%. Instead, MWCNTs consistently aggregated at a concentration of 0.05 wt%.
- No ettringite and calcium monosulfate hydrates and a greater amount of C-S-H were identified in MWCNT-amended paste samples, which resulted in enhanced nano- and micro-structures.
- Pore-size refinement was observed in MWCNT-amended cement paste, irrespective of the MWCNT concentration.
- Based on SEM analysis, it appears that possible mechanisms of strength enhancement due to MWCNT amendment include the preferential and well-distributed formation of C-S-H, and pore-size refinement, irrespective of the MWCNT concentration. However, the consistent tendency of MWCNTs to aggregate at a 0.05 wt% concentration seems to contribute to reducing homogeneity and introducing defect sites, resulting in less strength enhancement.
- At a MWCNT concentration of 0.05 wt% (and above, one may reasonably hypothesize), the aggregation of MWCNTs reduces the specific surface area, thus hindering the nucleation effect leading to the preferential formation of C-S-H.

Therefore, lower MWCNT concentrations may be preferable compared to 0.05 wt% or higher, which are predominant in the literature.

- It is feasible to incorporate well-dispersed and chemically-affine PUCNTs to enhance the physico-mechanical properties of cement paste.
- Due to the morphology and the high graphene-edge content of PUCNTs, dispersibility in aqueous solutions was easily attained with 0.001-0.005 wt% concentrations. Unstable aqueous solutions were obtained with a 0.05 wt% concentration.
- Significant enhancements in compressive strength and elastic stiffness of cement paste were obtained with a PUCNT concentration of 0.005 wt%, which is one order of magnitude smaller than lower-bound concentrations reported in the literature for MWCNTs and other graphitic nanoparticles. Less significant strength enhancements were observed from 0.05 wt% of PUCNTs.
- SEM imaging of the cement paste structure suggests that plausible contributing mechanisms for strength enhancement include the preferential and well-distributed formation of cement hydrates in presence of PUCNTs for concentrations up to 0.05 wt%, also resulting in a less porous structure, compared to plain cement paste. Aggregation of PUCNTs in cement paste with 0.05 wt% PUCNT concentration resulted in less significant strength and stiffness enhancements.
- Smoother, less porous free (curing) surfaces were observed for PUCNT concentrations in the range 0.001 to 0.05 wt% compared to plain cement paste.

- At higher concentrations, the aggregation of PUCNTs negatively impact their advantage of having high specific surface area and hinders their functioning as nucleation sites for the preferential and accelerated formation of cement hydrates. As such, a PUCNT concentration of 0.05 wt% resulted in PUCNT agglomeration in aqueous solution as well as in cement paste, and less significant enhancements in compressive strength and elastic stiffness compared to a concentration of 0.005 wt%.
- In the literature, 0.01-0.05 wt% have been reported as lower-bound concentrations for MWCNTs and GNPs. PUCNTs have higher specific surface area and functionality as compared to MWCNTs, and higher aspect ratio as compared to GNPs. Thus, radically smaller concentrations (e.g., 0.005 wt%) may be used for successful amendment of cement paste.
- Uniform GONR dispersions were observed visually for concentrations of 0.0005 wt%, 0.005 wt% and 0.05 wt% of GONRs with 32.3 wt% and 41.3 wt% of oxygen content immediately and up to 7 days after sonication.
- All suspensions were found stable up to 7 days in terms of zeta potential results.
- Larger variability in hydrodynamic size was obtained for 0.05 wt% of GONRs for both oxidation levels after sonication.
- pH values of all suspensions were found in the acidic range. However, stable dispersions were obtained based on zeta potential results. With low pH, stable dispersion of GONRs may still be easily attained through sonication. GONRs have high-functionality edges and a relatively large number of functional groups compared to MWCNTs and PUCNTs. Therefore, some functional groups may have been deprotonated

at low pH values although not enough to hinder dispersibility and stability thereof in aqueous suspensions.

- Compressive strength of cement concrete was similarly enhanced for a concentration range of 0.0005-0.05 wt% of GONRs with oxygen content of 32.3 wt% and 41.3 wt%, after 7 days of curing.
- The nano- and micro-structure of cement concrete was significantly modified by the incorporation of GONRs, as reflected in visual evidence of enhanced ITZs and accelerated and preferential formation of C-S-H in the vicinity of embedded GONRs.
- These ultra-low concentrations of GONRs may serve as an amendment that offers sustainability as well as cost effectiveness; for example, by enhancing durability, and reducing the amount of concrete needed for a given application, thus contributing to controlling CO_2 emissions.
- Given the potential of GONRs as well as other graphitic nanoparticles (such as MWCNTs and PUCNTs) to enhance durability by modifying the nano- and micro-structure of cement paste and concrete, such amendment may also be explored in the context of low-level nuclear waste containment using cement composites.

5.2. RECOMMENDATIONS

- In literature, 0.01 wt% was reported as a very low concentration in cases of MWCNTs and GNPs. As, PUCNTs have higher specific surface area and functionality as compared to MWCNTs, and higher aspect ratio as compared to GNPs, 0.01 to 0.05 wt% of PUCNTs could not be considered as a low concentration. As a result, agglomeration occurred for 0.05 wt% of PUCNTs and less significant and more variable mechanical

strength enhancement resulted. Lower concentrations of PUCNTs could be evaluated in cement mortar and concrete specimens.

- GONRs have more SSA, and functionality as compared to MWCNTs or PUCNTs. 30 to 40 wt% of oxidized GONRs in range of 0.0005 to 0.005 wt% can provide stable aqueous suspensions and hypothetically uniform dispersion is expected in cement composites with these solutions. Therefore, ultra-low concentration of GONRs could be considered in cement concrete where the presence of coarse aggregate and localized higher-porosity regions (e.g., the interfacial transition zone) may affect the nano- and micro-structural, mechanical and durability properties.

APPENDIX A - ESTIMATION OF SPECIFIC SURFACE AREA OF GRAPHITIC NANOPARTICLES

A.1. INTRODUCTION

This section illustrates the estimation of the specific surface area (SSA) of multiwalled carbon nanotubes (MWCNTs), graphene nanoplatelets (GNPs) and graphene oxide nanoribbons (GONRs) for a unit volume of cement composite (paste, mortar, concrete), as a function of nanoparticle concentration in weight of cement.

A.2. ASSUMPTIONS

Commonly used graphitic nanoparticles in cement composites such as, multiwalled carbon nanotubes (MWCNTs) and graphene (GNPs and GONRs) are considered herein. Only the exterior surfaces of MWCNTs are considered to estimate the SSA as they are those where chemical interactions are expected to occur with the surrounding cement matrix. Instead, to estimate the specific weight, areas of both inner and outer walls are considered. Therefore, the SSA of single walled carbon nanotubes (SWCNTs) and graphene are considered constant whereas, for MWCNTs, the specific weight depends on the diameter of the inner and outer walls and, thus, it varies as a function of the diameter. To estimate the SSA of MWCNTs, the SSA of one side of a graphene sheet is assumed as 1315 m^2/g [Peigney et al. 2001], the length of C–C bonds

in the curved graphene sheets is assumed as 0.1421 nm, and the inter-wall distance is assumed as 0.34 nm [Peigney et al. 2001]. The outer diameter of MWCNTs is considered in the range from 5 to 50 nm and containing between 4 and 49 walls [Chiodarelli et al. 2012], which reflects the range of MWCNT morphologies reported in the literature on cement composites (e.g., Li et al. [2005], Konsta-Gdoutos et al. [2010], Zohhadi [2014]).

A.3. PROCEDURE

The SSA of MWCNTs is estimated by dividing the outer cylindrical surface area by the total weight of the nanotube walls.

One cubic meter of cement composite (including paste, mortar, and concrete) was considered to estimate the total surface area of the embedded nanoparticles. From the average bulk density of cement paste, mortar and concrete, weight of different concentrations (e.g., 0.001 to 0.05% by weight of cement) of MWCNTs and GNPs in 1 m^3 of cement composite was estimated. The *w/c* ratio was considered as 0.4 for cement paste, mortar and concrete. Next, the SSA was estimated for different MWCNT diameters (e.g., the SSA of a MWCNT with a 20 nm diameter and 19 walls is ~100 m^2/g). In the case of GNPs, the SSA of SWCNTs (1315 m^2/g, that is, one side of graphene sheet) was considered. Finally, the surface areas covered by different concentrations of MWCNTs and GNPs in 1 m^3 of paste, mortar and concrete were estimated by multiplying the weight of the nanoparticles per unit volume of composite by the SSA.

A.4. RESULTS

A.4.1 Ordinary Portland cement paste

For a MWCNT diameter range of 5-50 nm, a surface area in the range 600-300000 m^2 is estimated for MWCNT concentrations in the range 0.001-0.05 wt% in 1 m^3 of cement paste (Figure A.1). In the case of GNPs, a surface area in the range 20000-1000000 m^2 is estimated for GNP concentrations in the range 0.001-0.05 wt% in 1 m^3 of cement paste (Figure A.1).

A.4.2 Ordinary Portland cement mortar

For a MWCNT diameter range of 5-50 nm, a surface area in the range 210-110000 m^2 is estimated for MWCNT concentrations in the range 0.001-0.05 wt% in 1 m^3 of mortar (Figure A.2). In the case of GNPs, a surface area in the range 7000-350000 m^2 is estimated for GNP concentrations in the range 0.001-0.05 wt% in 1 m^3 of mortar (Figure A.2). The volume occupied by fine aggregate was assumed to be 60% of the total volume of mortar.

A.4.3 Ordinary Portland cement concrete

For a MWCNT diameter range 5-50 nm, a surface area in the range 200-100000 m^2 is estimated for MWCNT concentrations in the range 0.001-0.05 wt% in 1 m^3 of concrete (Figure A.3). In the case of GNPs, a surface area in the range 6500-330000 m^2 is estimated for GNP concentrations in the range 0.001-0.05 wt% in 1 m^3 of concrete (Figure A.3). The volume occupied by fine and coarse aggregate was assumed to be 62% of the total volume of concrete.

A.5. OBSERVATIONS

- The commonly used range of 15-35 nm for the diameter of MWCNTs in concentrations of 0.001 to 0.05 wt% is associated with surface areas in the range 10^3 to 10^5 m^2, and $10^{2.5}$ to $10^{4.5}$ m^2 in 1 m^3 of cement paste, and mortar or concrete, respectively. The *w/c* ratio was assumed as 0.4.

- Approximately $10^{4.5}$ m^2 to 10^6 m^2, and 10^4 m^2 to $10^{5.5}$ m^2 of surface area is estimated for GNP concentrations from 0.001 to 0.05 wt% in 1 m^3 of cement paste, and mortar or concrete, respectively. The *w/c* ratio was assumed as 0.4.

- Surface area covered by GNPs per unit volume of cement paste, mortar and concrete is independent of particle size.

A.6. REFERENCES

Chiodarelli N, Richard O, Bender H, Heyns M, Gendt DS, Groeseneken G, Vereecken PM. Correlation between Number of Walls and Diameter in Multiwall Carbon Nanotubes Grown by Chemical Vapor Deposition. Carbon 2012; 50 (2012), 1748-1752, 2012.

Konsta-Gdoutos MS, Metaxa ZS, Shah SP. Multi-Scale Mechanical and Fracture Characteristics and Early-Age Strain Capacity of High-Performance Carbon Nanotube/Cement Nanocomposites. Cement and Concrete Composites 2010; 32(2010), 110–115.

Konsta-Gdoutos MS, Metaxa ZS, Shah SP. Highly Dispersed Carbon Nanotube Amended Cement Based Materials. Cement and Concrete Research 2010; 40(2010), 1052–1059.

Li GY, Wang PM, Zhao X. Mechanical Behavior and Microstructure of Cement Composites Incorporating Surface-Treated Multi-Walled Carbon Nanotubes. Carbon 2005; 43(2005), 1239–1245.

Peigney A, Laurent Ch, Flahaut E, Bacsa RR, Rousset A. Specific Surface Area of Carbon Nanotubes and Bundles of Carbon Nanotubes. Carbon 2001; 39(4), 507-514.

Zohhadi N. Functionalized Graphitic Nanoreinforcement for Cement Composites. PhD Dissertation 2014; University of South Carolina, Columbia.

A.7. TABLES

Table A.1 Surface area of MWCNTs in 1m^3 of cement paste, mortar, and concrete

Volume of composite [m^3]	Diameter [nm]	No. of wall	Specific surface area [m^2/g]	Particle Concentration [wt%]	Surface area in paste [m^2/m^3]	Surface area in mortar [m^2/m^3]	Surface area in concrete [m^2/m^3]
1	5	4	413	0.001	6638	2239	2091
	10	9	201		3226	1088	1016
	15	14	133		2140	722	674
	25	24	80		1281	432	404
	30	29	66		1068	360	336
	40	39	50		800	270	252
	50	49	40		640	216	202
	5	4	413	0.005	33188	11196	10454
	10	9	201		16128	5441	5080
	15	14	133		10701	3610	3371
	25	24	80		6407	2161	2018
	30	29	66		5338	1801	1681
	40	39	50		4002	1350	1261
	50	49	40		3201	1080	1008
	5	4	413	0.05	331877	111959	104541
	10	9	201		161278	54407	50803
	15	14	133		107011	36100	33708
	25	24	80		64070	21614	20182
	30	29	66		53376	18006	16813
	40	39	50		40022	13501	12607
	50	49	40		32015	10800	10085

Table A.2 Surface area of GNPs in 1m^3 of cement paste, mortar, and concrete

Volume of composite [m^3]	**Specific surface area [m^2/g]**	**Particle Concentration [wt%]**	**Surface area in paste [m^2/m^3]**	**Surface area in mortar [m^2/m^3]**	**Surface area in concrete [m^2/m^3]**
1	1315	0.001	21134	7130	6657
		0.005	105670	35648	33286
		0.05	1056696	356476	332859

A.8. FIGURES

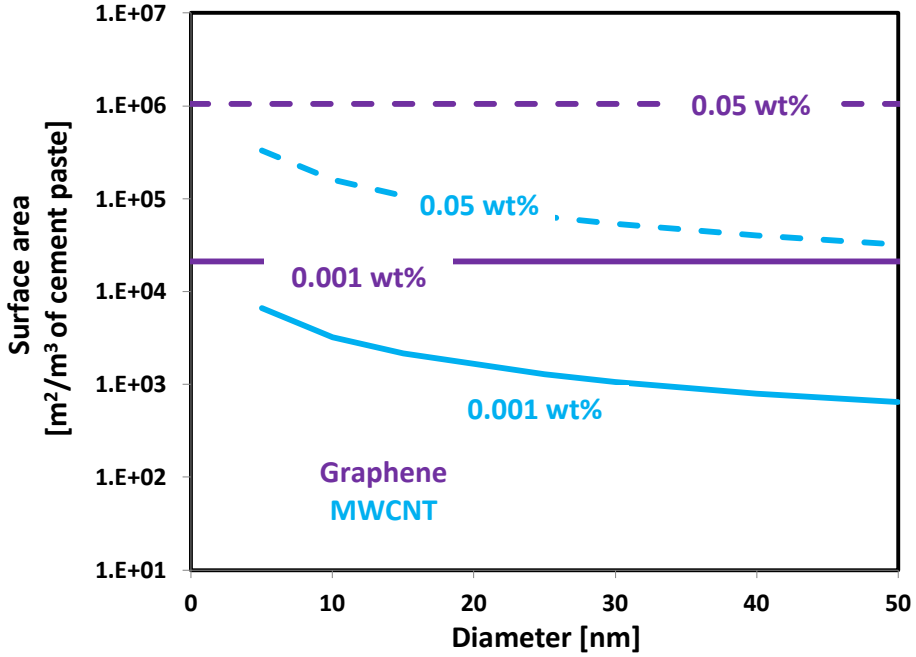

Figure A.1 Surface area as function of MWCNT and GNP concentration in 1 m^3 of cement paste

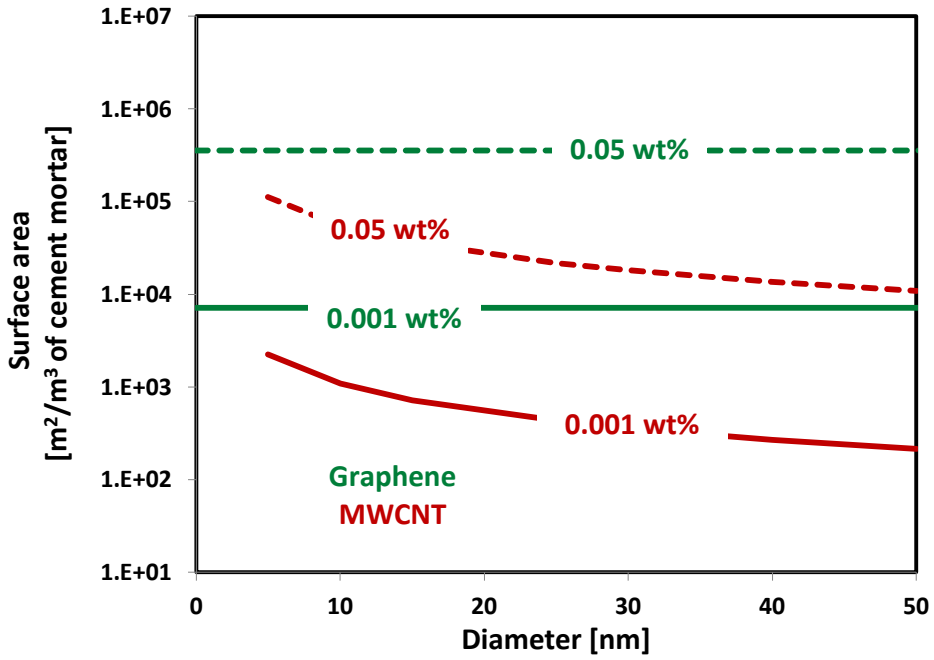

Figure A.2 Surface area as function of MWCNT and GNP concentration in 1 m^3 of cement mortar

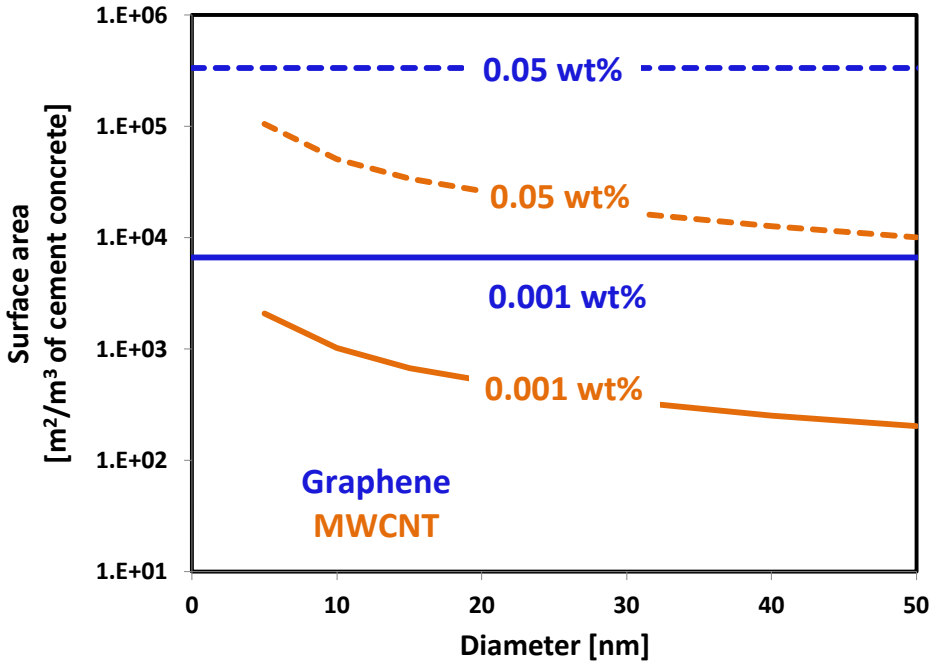

Figure A.3 Surface area as function of MWCNT and GNP concentration in 1 m^3 of cement concrete

APPENDIX B - INFLUENCE OF DECREASING MULTIWALLED CARBON NANOTUBE CONCENTRATIONS ON PHYSICO-MECHANICAL PROPERTIES OF CEMENT PASTE

B.1. TABLES

Table B.1 Zeta potential for different concentrations of MWCNTs

Concentration [wt%]	**0.001**	**0.003**	**0.005**	**0.01**	**0.05**
	Zeta potential [mV]	**Zeta potential [mV]**	**Zeta potential [mV]**	**Zeta potential [mV]**	**Zeta potential [mV]**
Replicate 1	-53.2	-40.6	-50.8	-47.6	-0.764
Replicate 2	-59.4	-43.8	-59.1	-53.8	0.107
Replicate 3	-60.6	-44.5	-62.4	-56.3	1.43
Replicate 4	-63	-40.8	-65.1	-61.3	-1.28
Replicate 5	-65.2	-44	-67.7	-62.9	-0.114
Replicate 6	-67.9	-46	-71	-62.2	-0.333
Replicate 7	-69.4	-47	-74.6	-49.7	-1.7
Replicate 8	-72	-44.5	-76	-46.9	1.11
Replicate 9	-74.5	-47	-78.3	-38.4	-0.0778
Replicate 10	-74	-45.4	-80.4	-38.8	-1.75
Average	-65.9	-44.4	-68.5	-51.8	-0.337
Standard deviation	6.94	2.24	9.36	9.07	1.08

Table B.2 Hydrodynamic size for different concentrations of MWCNTs

Concentration [wt%]	**0.001**	**0.003**	**0.005**	**0.01**	**0.05**
	Hydrodynamic size [nm]	**Hydrodynamic size [nm]**	**Hydrodynamic size [nm]**	**Hydrodynamic size [nm]**	**Hydrodynamic size [nm]**
Replicate 1	221.6	271.8	332.2	365	1057
Replicate 2	217.9	286	335	355	988.9
Replicate 3	219.1	282.7	329.9	350.3	1109
Replicate 4	213.3	277.8	334.2	369.9	1000
Replicate 5	214.7	275.8	335.1	346.2	1048
Average	**217.3**	**278.8**	**333.3**	**357.3**	**1041**
Standard deviation	**3.348**	**5.614**	**2.22**	**9.944**	**48.28**

Table B.3 Density and bulk volume of cement paste amended with MWCNTs

No	Content of MWCNT [wt%]	Weight [g]	Bulk Density [g/cc]	Bulk Volume [cc]	Duration of curing [days]
1	0	0.3696	2.3306	0.1586	5
2		0.0815	2.4900	0.0327	
3		0.1644	2.3934	0.0687	
4		0.1302	2.4101	0.0540	
5		0.0860	2.4214	0.0355	
6	0.001	0.1116	2.3820	0.0469	
7		0.3223	2.3034	0.1399	
8		0.2050	2.3838	0.0860	
9	0.005	0.4135	2.3067	0.1793	
10		0.3171	2.3687	0.1339	
11		0.2315	2.3773	0.0974	
12	0.05	0.2305	2.3372	0.0986	
13		0.2459	2.3114	0.1064	
14		0.3726	2.3161	0.1609	
15	0	0.2823	2.3363	0.1208	12
16		0.1310	2.2309	0.0587	
17		0.2422	2.1992	0.1101	
18		0.1965	2.1822	0.0900	
19		0.3233	2.1473	0.1506	
20	0.001	0.2298	2.1546	0.1067	
21		0.2661	2.1962	0.1212	
22		0.1667	2.1732	0.0767	
23		0.1983	2.3747	0.0835	
24	0.005	0.4280	2.0338	0.2104	
25		0.2418	2.0332	0.1189	
26		0.2113	2.2309	0.0947	
27		0.1627	2.1250	0.0766	
28	0.05	0.4070	2.0521	0.1983	
29		0.2408	2.1712	0.1109	
30		0.4588	2.1083	0.2176	
31		0.4601	2.1416	0.2148	
32	0	0.3209	2.1576	0.1487	26
33		0.2855	2.1413	0.1333	
34		0.1881	2.1022	0.0895	
35		0.3668	2.1671	0.1693	
36		0.1818	2.1545	0.0844	
37	0.001	0.2035	2.2435	0.0907	
38		0.1847	2.2347	0.0827	
39		0.2381	2.3128	0.1029	
40		0.4391	2.2513	0.1950	
41	0.005	0.3909	2.2136	0.1766	
42		0.5663	2.1726	0.2607	
43		0.6052	2.1619	0.2799	
44		0.3957	2.1569	0.1835	
45		0.3976	2.1641	0.1837	
46	0.05	0.3093	2.1739	0.1423	
47		0.4240	2.1383	0.1983	
48		0.4121	2.1608	0.1907	
49		0.3798	2.1673	0.1752	
50		0.1432	2.1681	0.0660	

Table B.4 Average compressive strength of cement paste amended with MWCNTs

	CNT-content [wt%]	Compressive strength [MPa]		
		Average	Standard deviation	% Enhancement
7-day	0	30.66	2.73	0%
	0.001	26.95	4.66	-12%
	0.002	24.85	5.34	-19%
	0.005	25.95	4.27	-15%
	0.01	21.80	7.02	-29%
	0.05	26.56	6.45	-13%
14-day	0	33.24	1.41	0%
	0.001	30.79	2.38	-7%
	0.002	32.25	1.60	-3%
	0.005	35.77	3.92	8%
	0.01	34.77	5.90	5%
	0.05	36.27	4.57	9%
28-day	0	41.80	0.64	0%
	0.001	50.03	4.34	20%
	0.002	45.21	3.70	8%
	0.005	42.78	4.60	2%
	0.01	49.41	3.39	18%
	0.05	52.11	4.75	25%

B.2. FIGURES

(a)

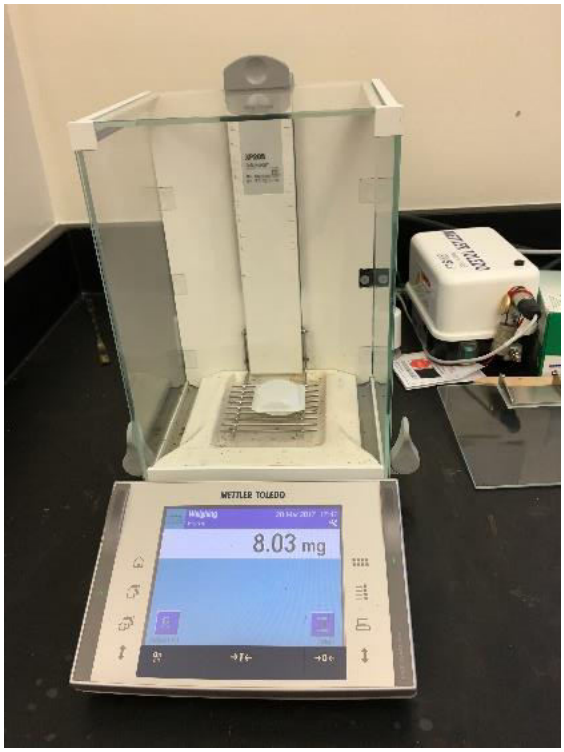

(b)

Figure B.1 Taking mass of (a) powdered CNT-sample (b) CNT-suspension

(a)

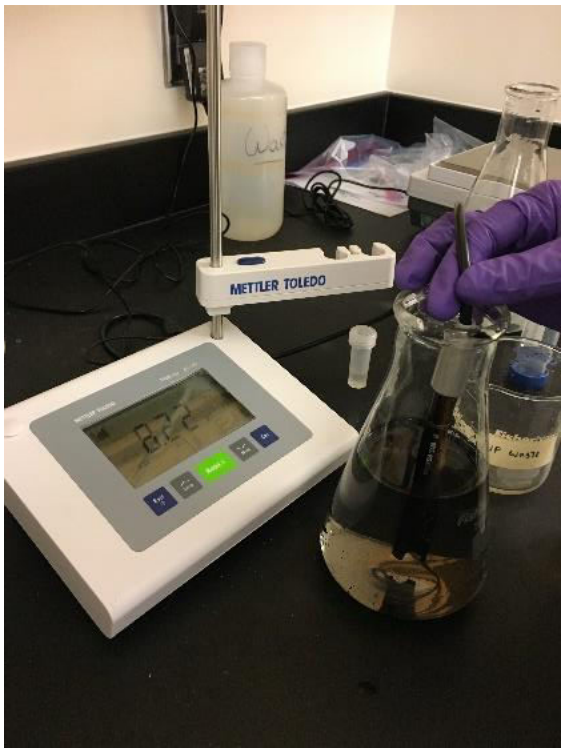

(b)

Figure B.2 Adjusting pH (a) measuring pH with pH meter (b) adding 5 mol/L NaOH solution

(a)

(b)

Figure B.3 (a) Ultrasonication (b) final suspensions after sonication; 2: 0.02 g/L, 3: 0.1 g/L, 4: 1 g/L of MWCNTs in DI water

(a) 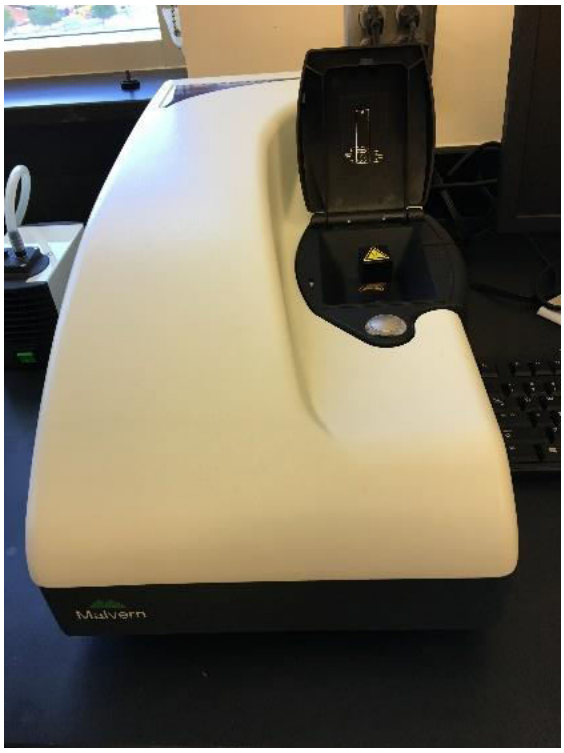

(b) 

Figure B.4 DLS experiment (a) Zetasizer Nano-ZS (b) sample placed in the chamber

(a)

(b)

Figure B.5 Casting cement paste prisms (a) CNT-suspension and cement powder (b) DI water and cement powder

(a)

(b)

Figure B.6 Casting cement paste prisms (a) mixing (b) placing in the mold

(a)

(b)

Figure B.7 Casting cement paste prisms (a) surface preparation (b) covering with wet burlaps

(a)

(b)

Figure B.8 Casting cement paste prisms (a) covering with plastic sheets (b) curing chamber with saturated lime water

(a)

(b)

Figure B.9 Sample preparation for SEM imaging (a) breaking the prisms (b) air drying process

Figure B.10 Samples placed for air drying

(a) 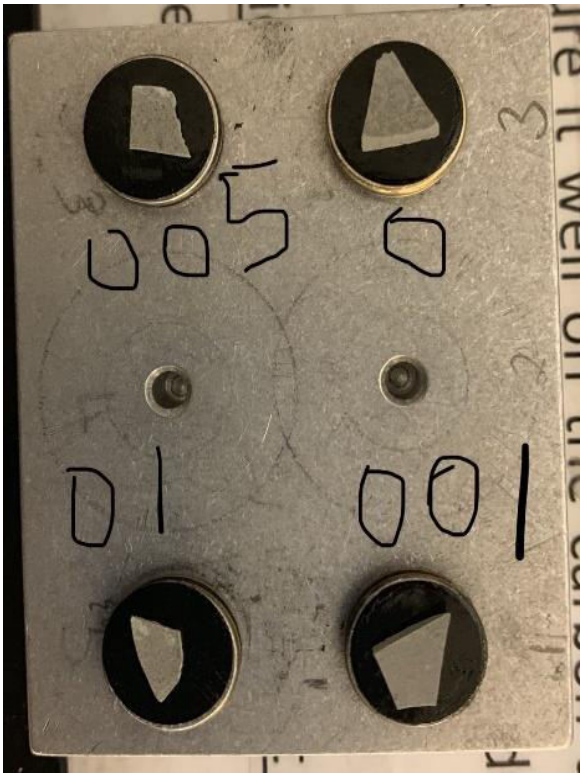

(b) 

Figure B.11 SEM imaging (a) samples in stubs (c) gold sputtering

(a) 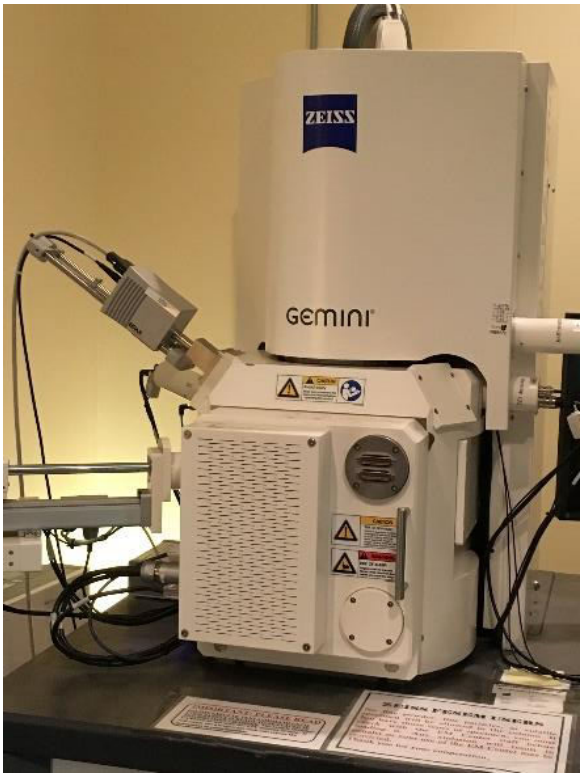

(b)

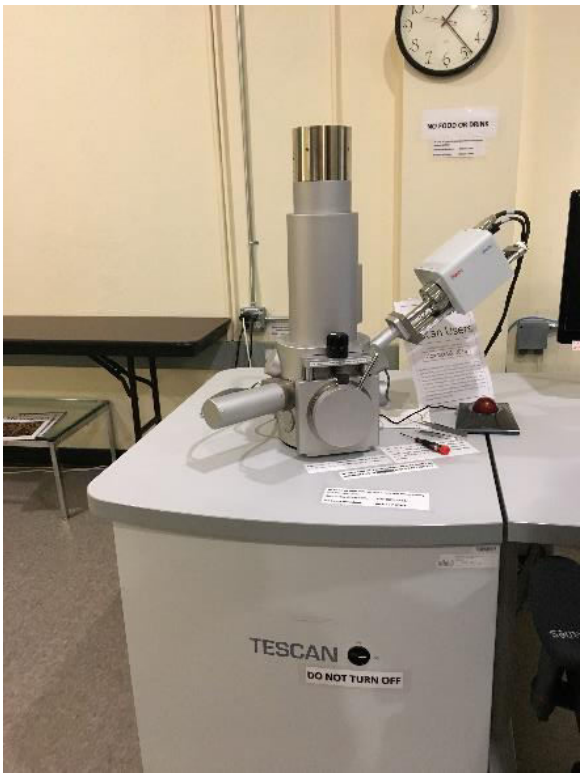

Figure B.12 SEM imaging (a) Zeiss Ultra Plus Field Emission Scanning Electron Microscope (FESEM) (b) Tescan Vega3 SEM

(a)

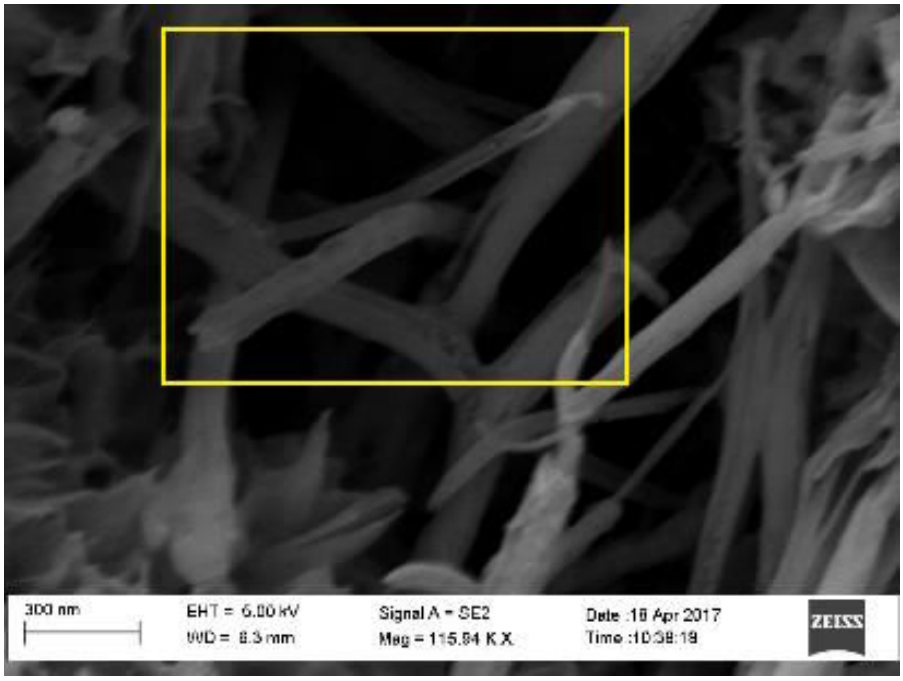

(b)

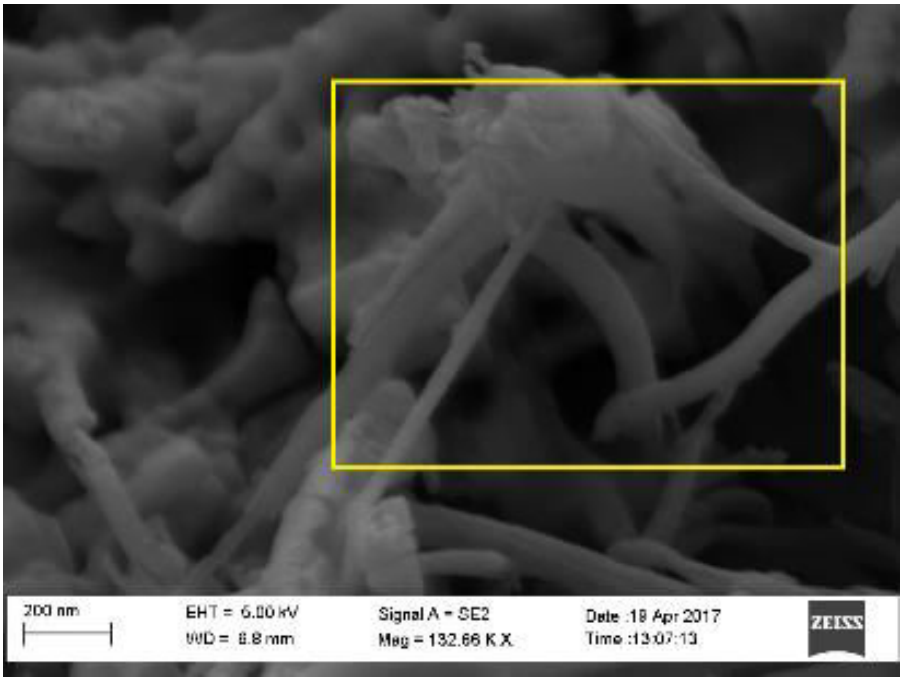

(c)

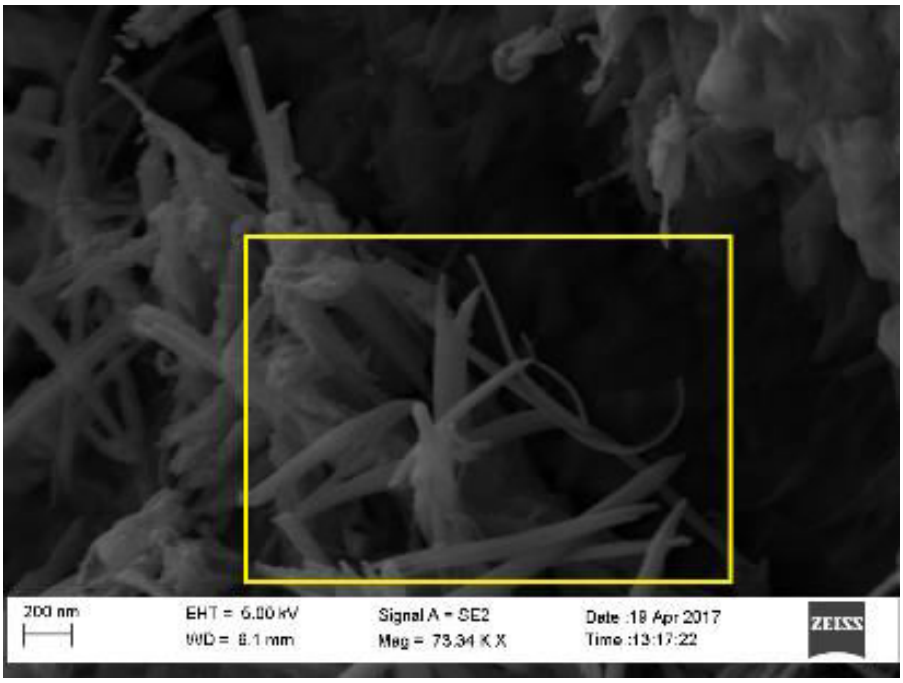

Figure B.13 Distribution of MWCNTs inside the cement paste (a) 0.001 wt% (b) 0.005 wt% (c) 0.05 wt% of MWCNTs, after 5 days of curing

(a)

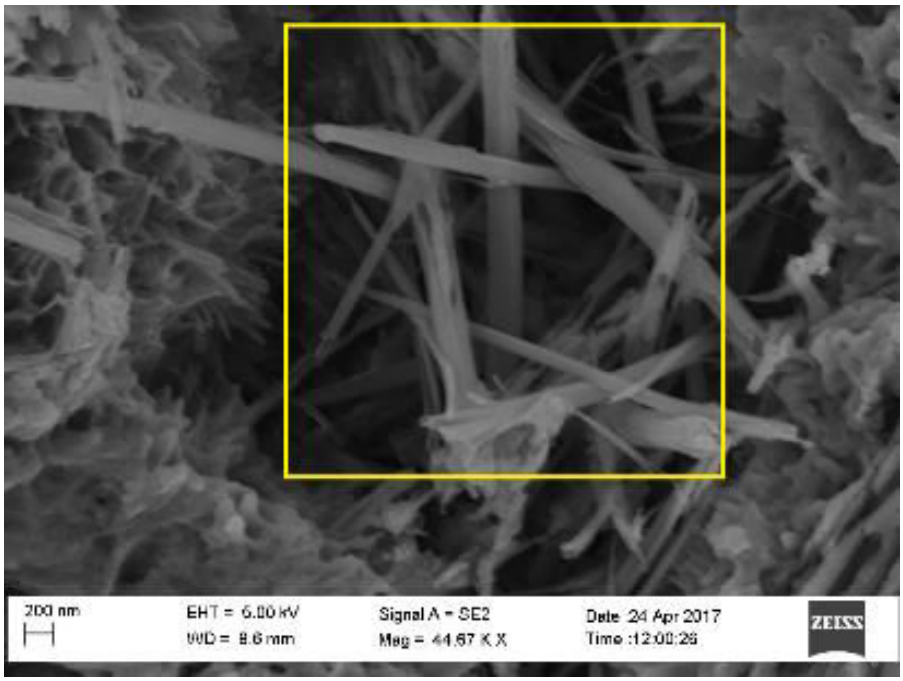
200 nm
EHT = 5.00 kV
WD = 8.6 mm
Signal A = SE2
Mag = 44.67 K X
Date :24 Apr 2017
Time :12:00:26
ZEISS

(b)


100 nm
EHT = 5.00 kV
WD = 8.4 mm
Signal A = SE2
Mag = 148.60 K X
Date :28 Apr 2017
Time :10:09:46
ZEISS

(c)

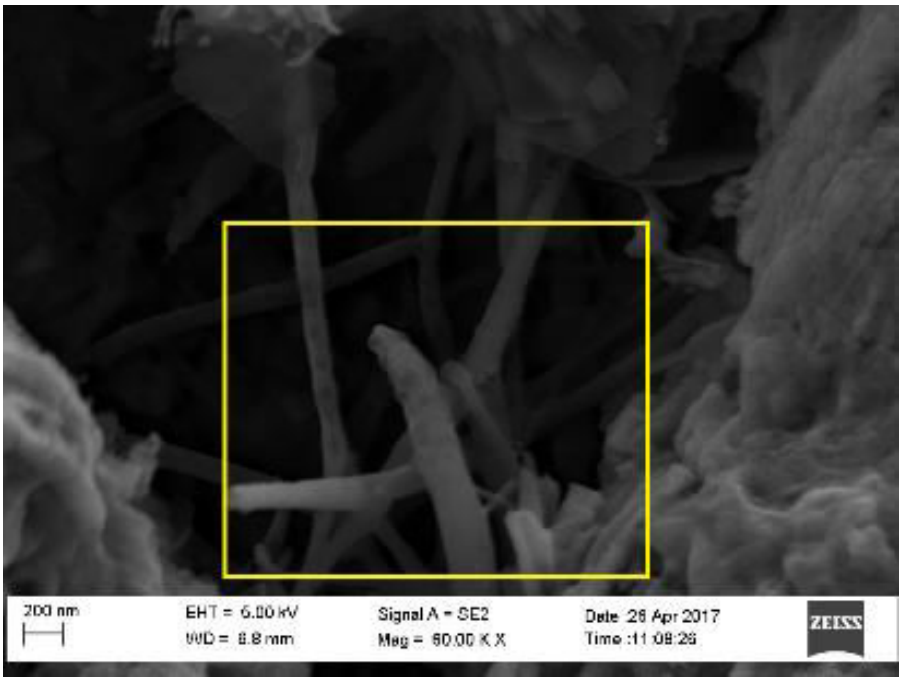

Figure B.14 Distribution of MWCNTs inside the cement paste (a) 0.001 wt% (b) 0.005 wt% (c) 0.05 wt% of MWCNTs, after 12 days of curing

(a)

(b)

(c)

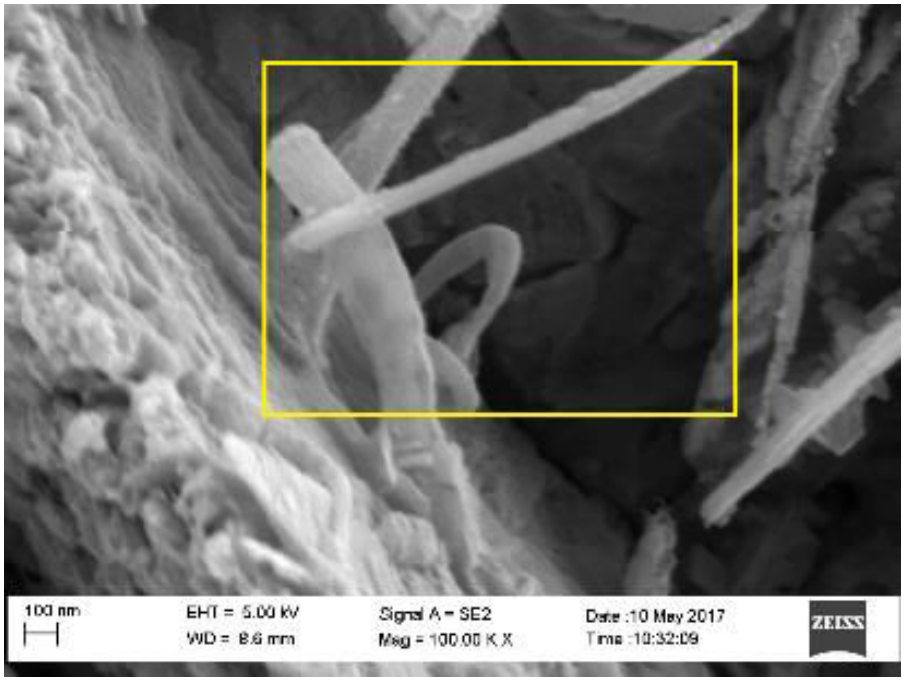

Figure B.15 Distribution of MWCNTs inside the cement paste (a) 0.001 wt% (b) 0.005 wt% (c) 0.05 wt% of MWCNTs, after 26 days of curing

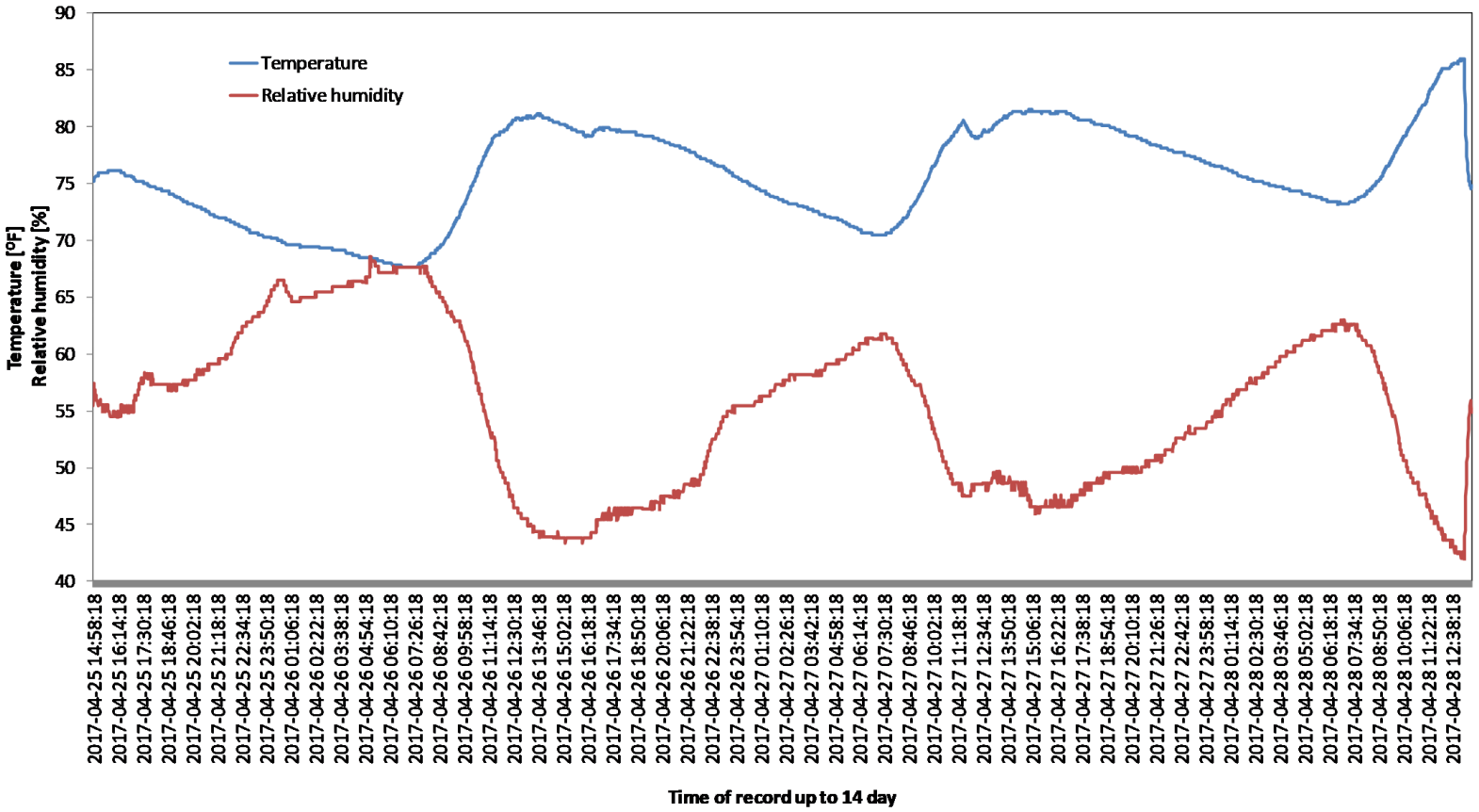

Figure B.16 Temperature and relative humidity data of air-drying chamber (corridor) up to 14-day

APPENDIX C - AMENDMENT OF CEMENT PASTE WITH PARTIALLY-UNZIPPED CARBON NANOTUBES

C.1. TABLES

Table C.1 Hydrodynamic size for 0.001 wt% of PUCNTs up to 10 days of sonication

Replicate number	Day 0	Day 3	Day 7	Day 10
	Hydrodynamic size [nm]	Hydrodynamic size [nm]	Hydrodynamic size [nm]	Hydrodynamic size [nm]
1	586.9	533.7	527	518
2	572.9	530.3	524.1	523.8
3	575.6	528.4	529.2	509.3
4	569.7	530.8	536.4	528.6
5	555.7	541.6	521.6	524.4
Average	**572.2**	**533**	**527.7**	**520.8**
Standard deviation	**11.25**	**5.19**	**5.67**	**7.465**

Table C.2 Hydrodynamic size for 0.005 wt% of PUCNTs up to 10 days of sonication

Replicate number	Day 0	Day 3	Day 7	Day 10
	Hydrodynamic size [nm]	Hydrodynamic size [nm]	Hydrodynamic size [nm]	Hydrodynamic size [nm]
1	705.6	553.1	555.3	539.2
2	652.8	549.2	547.5	517
3	686.3	548.6	530.3	521
4	645.2	535.3	534	517
5	643.6	547	522.7	507.8
Average	**666.7**	**546.6**	**538**	**520.4**
Standard deviation	**27.78**	**6.724**	**13.22**	**11.57**

Table C.3 Hydrodynamic size for 0.05 wt% of PUCNTs up to 10 days of sonication

Replicate number	Day 0	Day 3	Day 7	Day 10
	Hydrodynamic size [nm]	Hydrodynamic size [nm]	Hydrodynamic size [nm]	Hydrodynamic size [nm]
1	837.9	761.7	778.8	740.9
2	871.8	749.1	778.3	721.2
3	824.3	741.7	784.4	743.7
4	798.8	732.5	779.4	747
5	801.9	724.4	747.6	733.2
Average	**826.9**	**741.9**	**773.7**	**737.2**
Standard deviation	**29.83**	**14.48**	**14.79**	**10.3**

Table C.4 Zeta potential for 0.001 wt% of PUCNTs up to 10 days of sonication

Replicate number	Day 0	Day 3	Day 7	Day 10
	Zeta potential [mV]	Zeta potential [mV]	Zeta potential [mV]	Zeta potential [mV]
1	-37.8	-28.6	-38.7	-38.4
2	-37.4	-30.2	-41	-40
3	-39.8	-29.7	-39.9	-40.9
4	-38.3	-29.9	-39.2	-40.5
5	-40.9	-30.5	-40.8	-40.4
6	-40.8	-30.4	-38.4	-41.3
7	-40.5	-30.7	-42.1	-41.9
8	-39.8	-30.2	-40.6	-39.8
9	-40.8	-29.5	-39.5	-41.9
10	-39.4	-29.8	-41.7	-40.1
Average	**-39.5**	**-30**	**-40.2**	**-40.5**
Standard deviation	**1.3**	**0.606**	**1.25**	**1.06**

Table C.5 Zeta potential for 0.005 wt% of PUCNTs up to 10 days of sonication

Replicate number	Day 0	Day 3	Day 7	Day 10
	Zeta potential [mV]	Zeta potential [mV]	Zeta potential [mV]	Zeta potential [mV]
1	-37.9	-40.1	-40	-44.1
2	-38.2	-40.1	-41.1	-42.7
3	-38.1	-39.2	-40.1	-43.6
4	-40.2	-40.1	-40.4	-43.9
5	-39.8	-40.4	-42.1	-41.9
6	-40.3	-40.5	-40.1	-42.6
7	-40.6	-40.6	-41.1	-44.9
8	-40.3	-39.5	-40.8	-44.2
9	-39.9	-41.9	-41.1	-42.7
10	-40.5	-41.8	-41.7	-45.7
Average	**-39.6**	**-40.4**	**-40.8**	**-43.6**
Standard deviation	**1.07**	**0.868**	**0.709**	**1.17**

Table C.6 Zeta potential for 0.05 wt% of PUCNTs up to 10 days of sonication

Replicate number	Day 0	Day 3	Day 7	Day 10
	Zeta potential [mV]	Zeta potential [mV]	Zeta potential [mV]	Zeta potential [mV]
1	-3.64	-1.3	-0.547	-1.03
2	-3.82	-2.18	-1.18	-0.918
3	-3.5	-3.08	-1.66	-0.995
4	-3.18	-2.72	-0.853	-1.13
5	-3.3	-4.34	-0.877	-1.43
6	-2.68	-3.73	-1.67	-0.295
7	-3.48	-4.1	-2.27	-1.04
8	-3.74	-4.29	-2.37	-1.49
9	-2.87	-4.22	-1.59	-0.648
10	-2.93	-2.83	-0.969	-0.758
Average	**-3.31**	**-3.28**	**-1.4**	**-0.973**
Standard deviation	**0.39**	**1.03**	**0.615**	**0.353**

Table C.7 Compressive strength results with control and PUCNTs-added cement paste samples

Compressive strength [MPa]												
Concentration	**0 wt%**			**0.001 wt%**			**0.005 wt%**			**0.05 wt%**		
Sample ID	**7-day**	**14-day**	**28-day**	**7-day**	**14-day**	**28-day**	**7-day**	**14-day**	**28-day**	**7-day**	**14-day**	**28-day**
1	25.12	26.38	35.33	27.72	29.31	32.33	20.32	31.80	32.67	29.03	N/A	30.51
2	19.58	23.70	33.80	21.52	34.55	33.99	20.28	36.52	48.76	23.66	31.09	27.08
3	17.71	22.77	30.05	24.46	35.47	36.26	23.74	29.55	38.10	23.33	27.79	43.71
4	21.00	26.19	28.74	21.54	22.20	36.30	19.08	34.97	46.01	27.41	30.89	45.02
Average [MPa]	20.85	24.76	31.98	23.81	30.38	34.72	20.86	33.21	41.39	25.86	29.93	36.58
Standard deviation [MPa]	3.14	1.80	3.10	2.95	6.09	1.93	2.01	3.13	7.36	2.81	1.85	9.11

N/A = Not available

Table C.8 Elastic stiffness results with control and PUCNTs-added cement paste samples

Elastic stiffness [N/mm]												
Concentration	**0 wt%**			**0.001 wt%**			**0.005 wt%**			**0.05 wt%**		
Sample ID	**7-day**	**14-day**	**28-day**	**7-day**	**14-day**	**28-day**	**7-day**	**14-day**	**28-day**	**7-day**	**14-day**	**28-day**
1	10977	10994	30645	11635	13426	26452	9708	12168	37654	10599	N/A	38386
2	10551	10468	32471	11190	13954	24436	10415	13069	33001	17005	13654	35201
3	11306	9526	19765	10336	13414	31159	N/A	12754	40236	19406	12283	25951
4	9978	9698	31473	11289	11183	N/A	10602	13710	33141	N/A	12650	26145
Average [kN/mm]	10.70	10.17	28.59	11.11	12.99	27.35	10.24	12.93	36.01	15.67	12.86	31.42
Standard deviation [kN/mm]	0.57	0.68	5.93	0.55	1.23	3.45	0.47	0.64	3.55	4.55	0.71	6.34

N/A = Not available

C.2. FIGURES

(a)

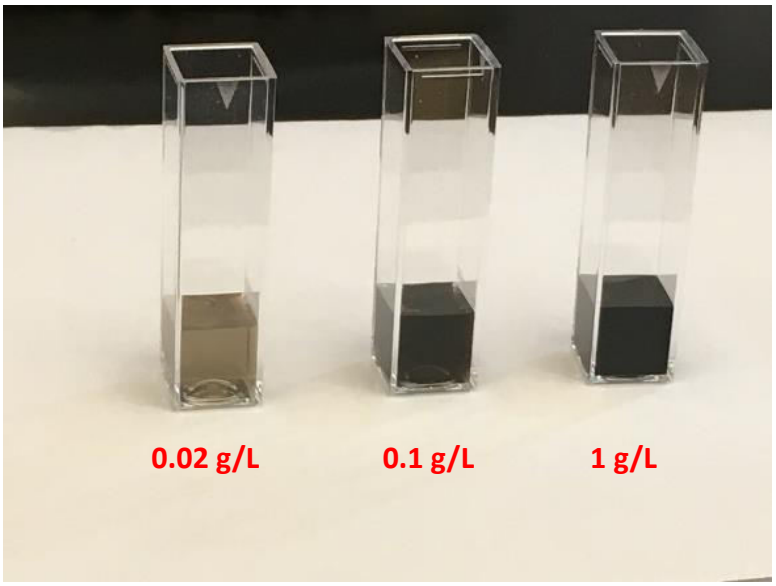

(b)

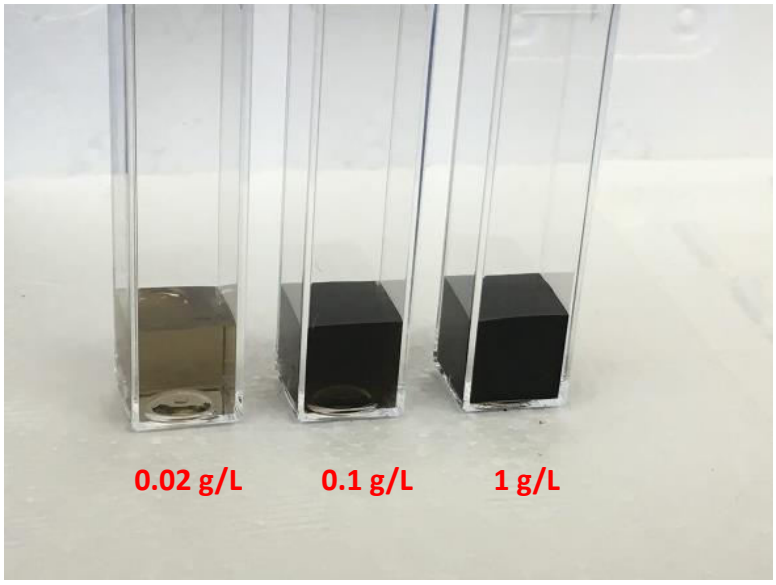

(c)

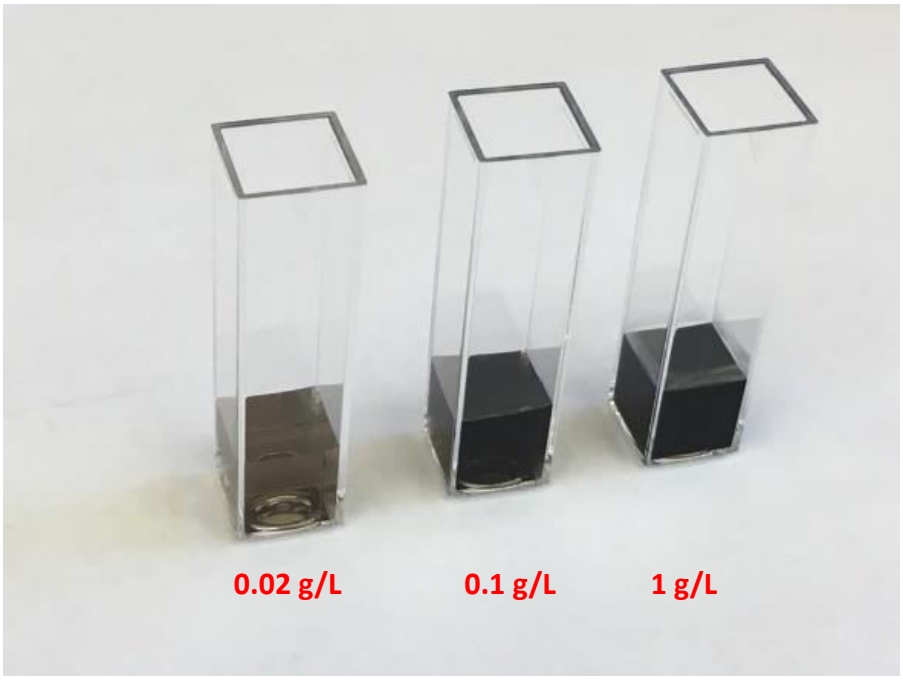

(d)

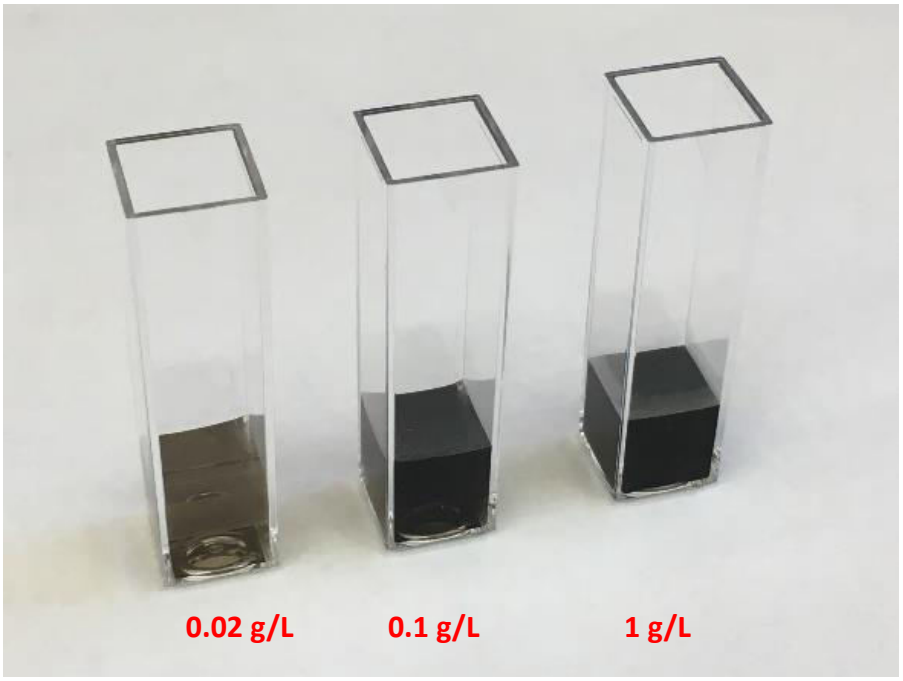

Figure C.1 PUCNT suspensions after sonication: (a) 0 days (b) 3 days (c) 7 days (d) 10 days

(a)

(b)

Figure C.2 Casting cement paste prisms (a) PUCNT-suspension and cement powder (b) DI water and cement powder

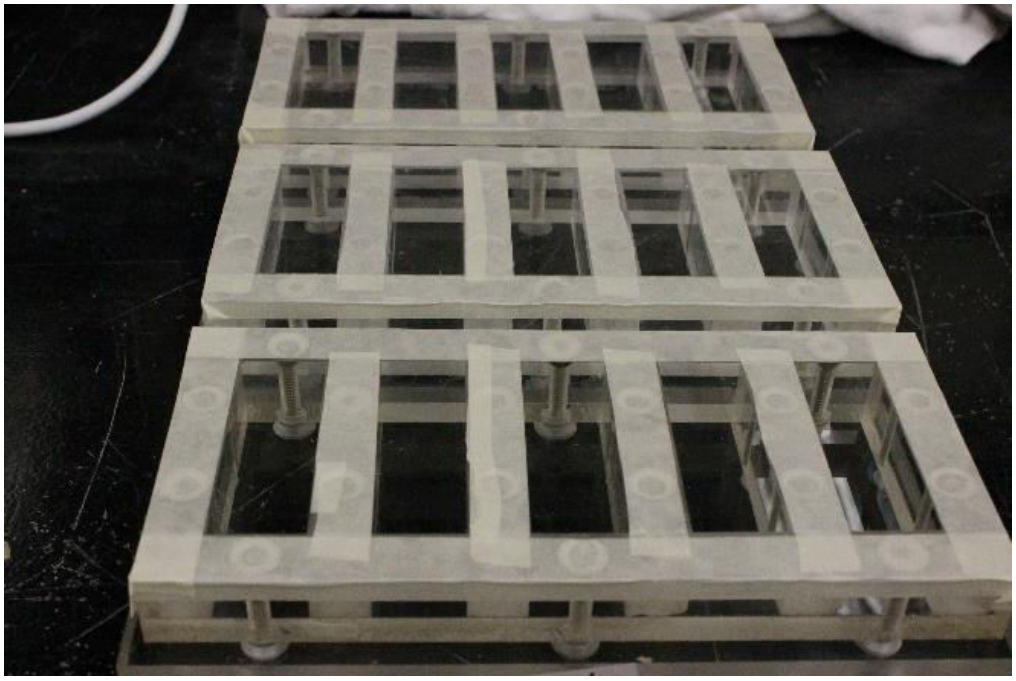

Figure C.3 Molds of prisms

(a) 

(b)

Figure C.4 Casting cement paste prisms (a) mixing (b) placing in the mold

(a)

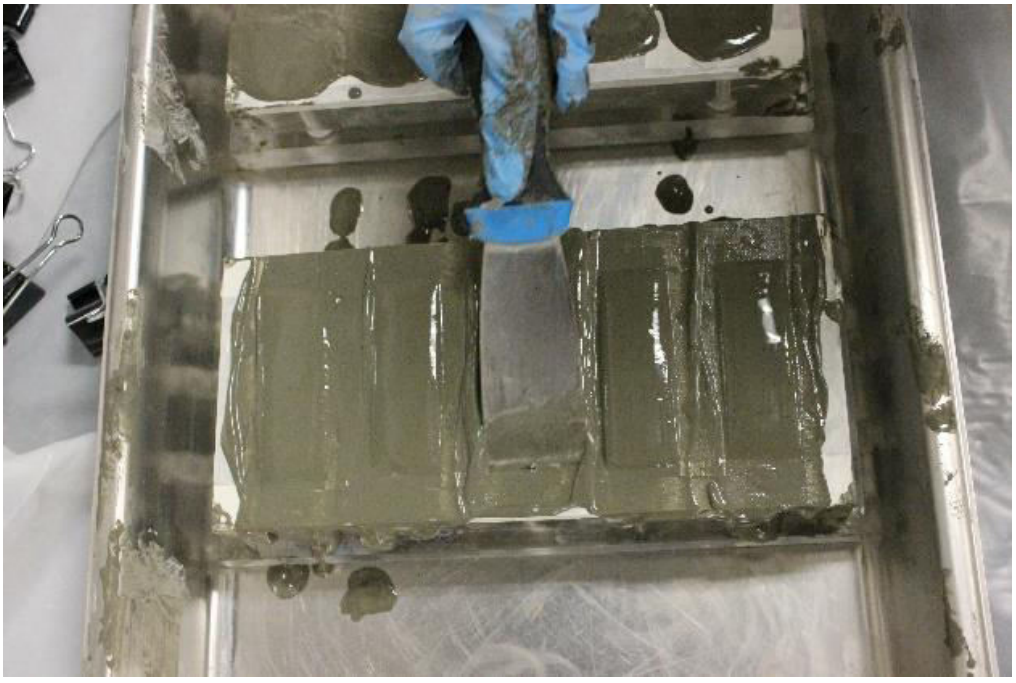

(b)

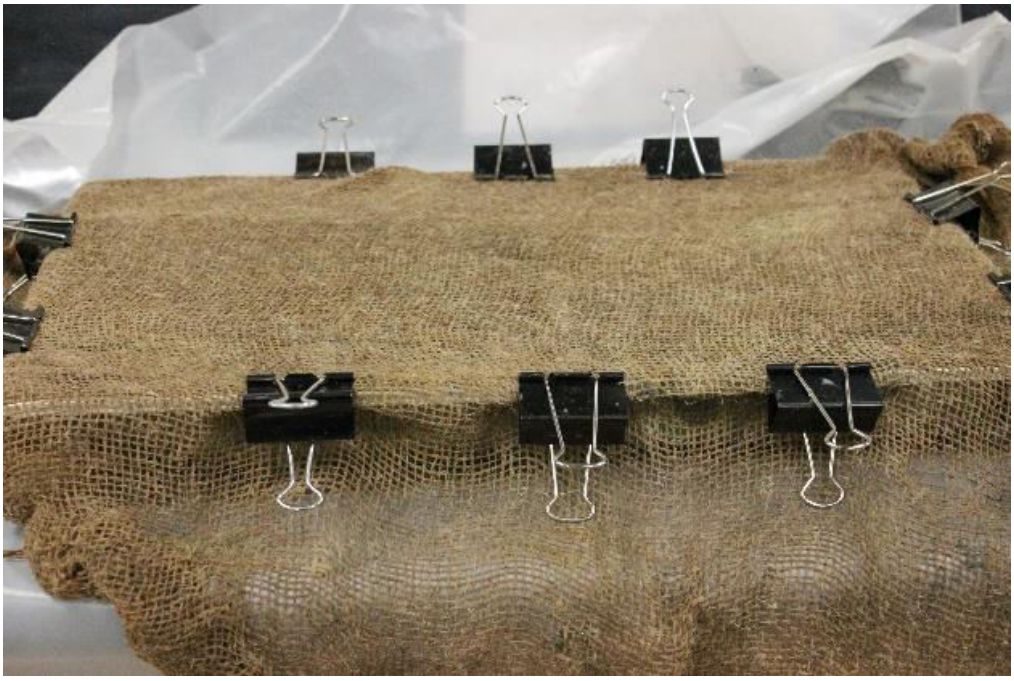

Figure C.5 Casting cement paste prisms (a) surface preparation (b) covering with wet burlaps

(a)

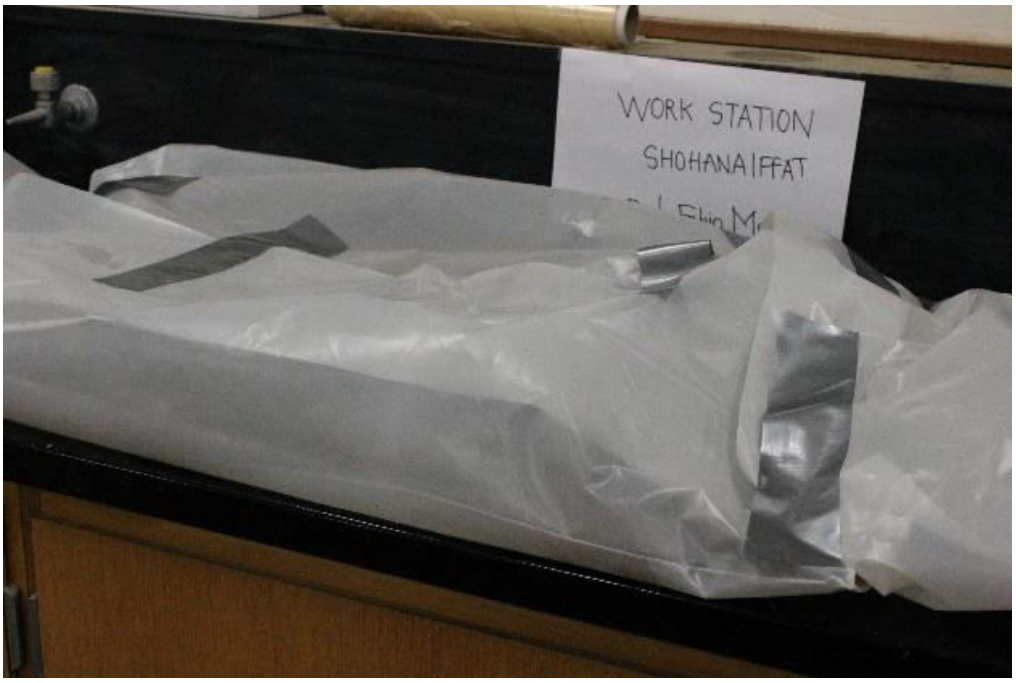

(b)

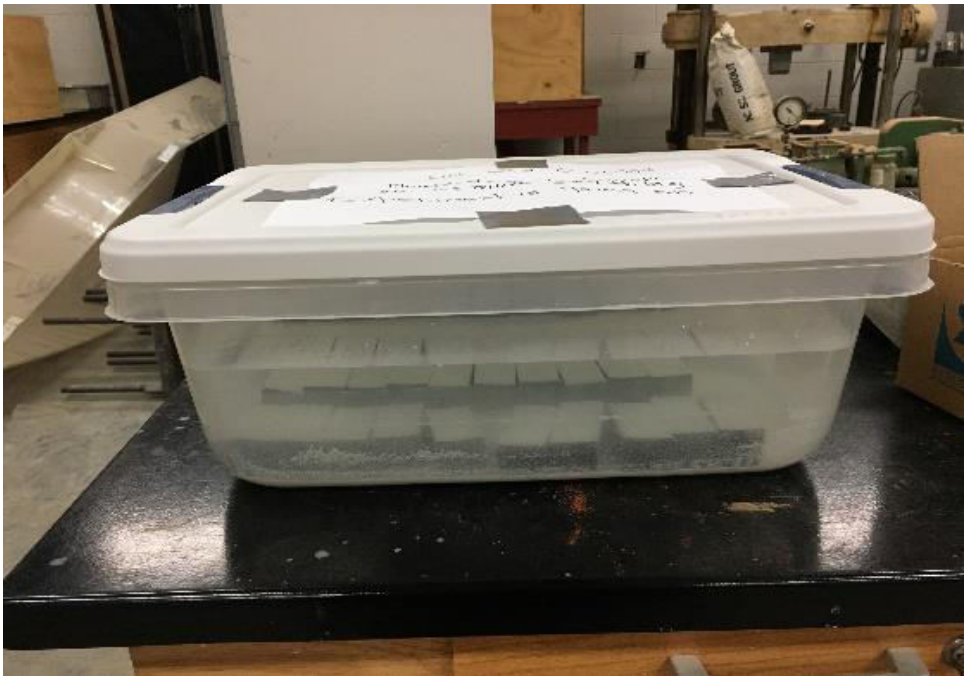

Figure C.6 Casting cement paste prisms (a) covering with plastic sheet (b) curing chamber with saturated lime water

(a)

(b)

Figure C.7 Uni-axial compression test (a) centering and leveling (b) compression (splitting) failure

Figure C.8 Representative cement paste sample for SEM imaging

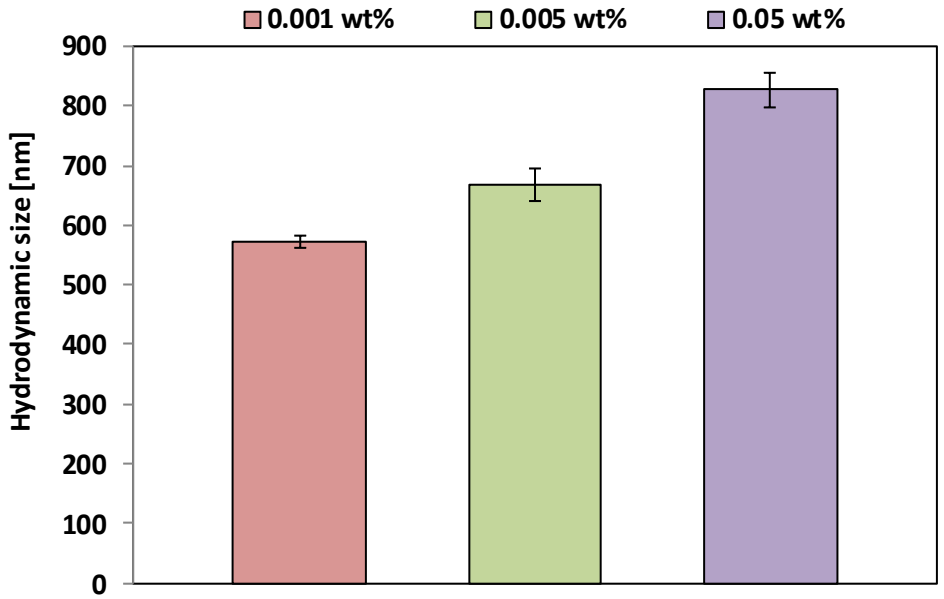

(a)

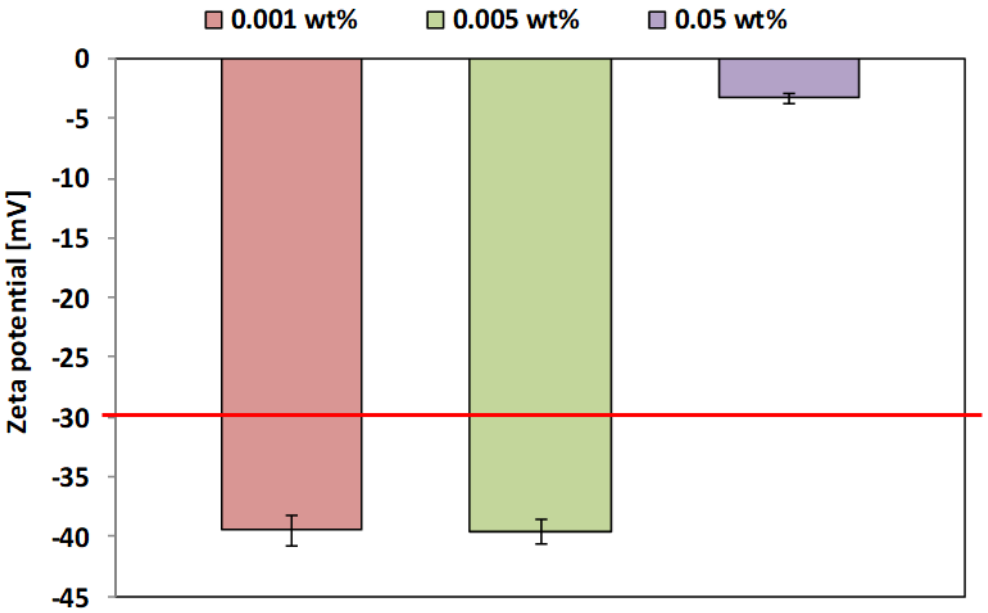

(b)

Figure C.9 DLS test results: (b) hydrodynamic size (b) zeta potential for different concentrations of PUCNTs at 0 days after sonication

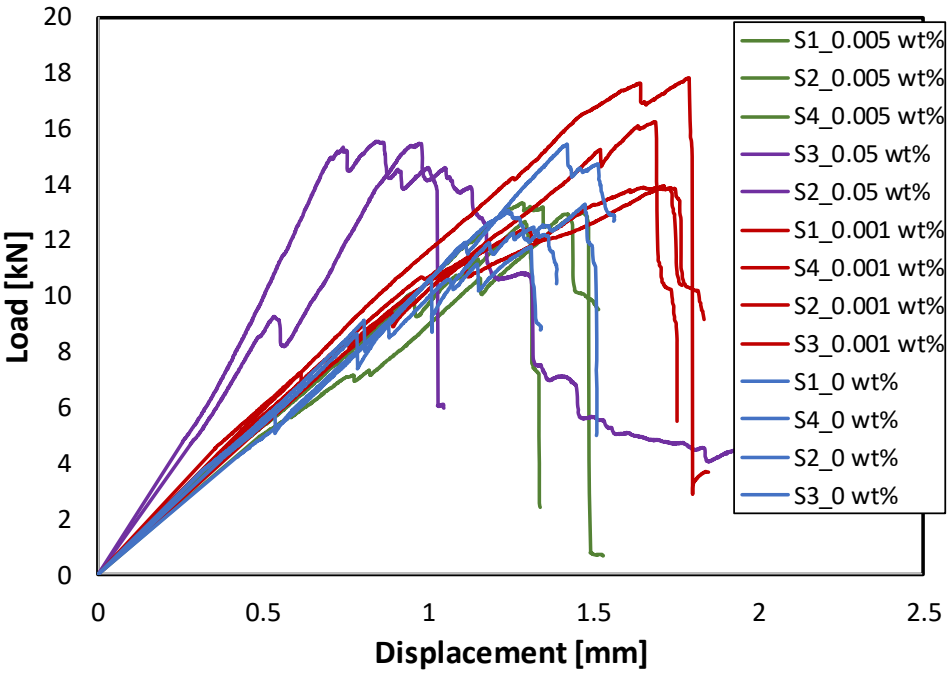

Figure C.10 Load-deflection curves of control and PUCNT-added cement paste samples after 7 days of curing

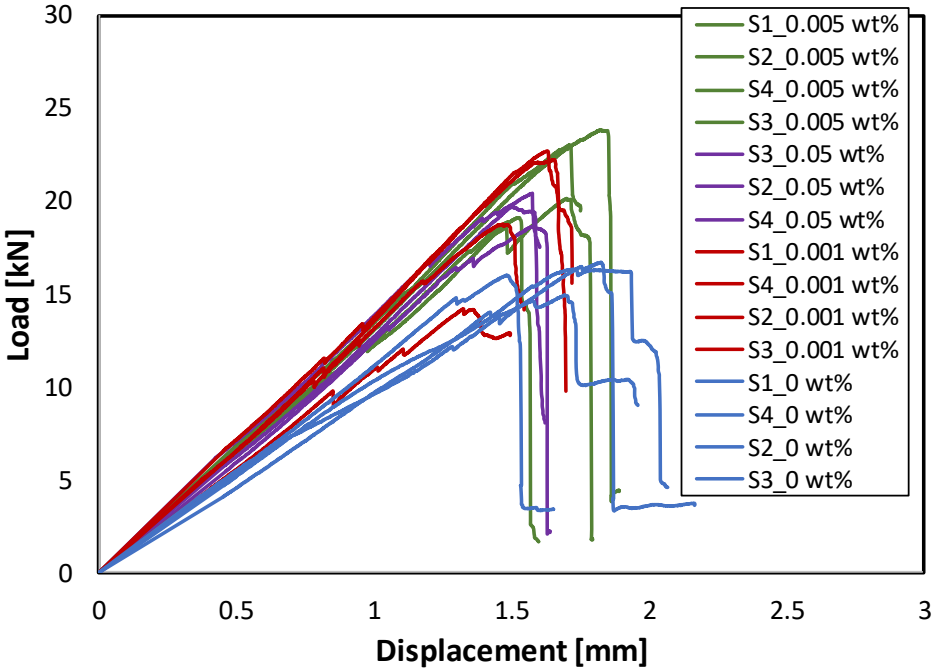

Figure C.11 Load-deflection curves of control and PUCNT-added cement paste samples after 14 days of curing

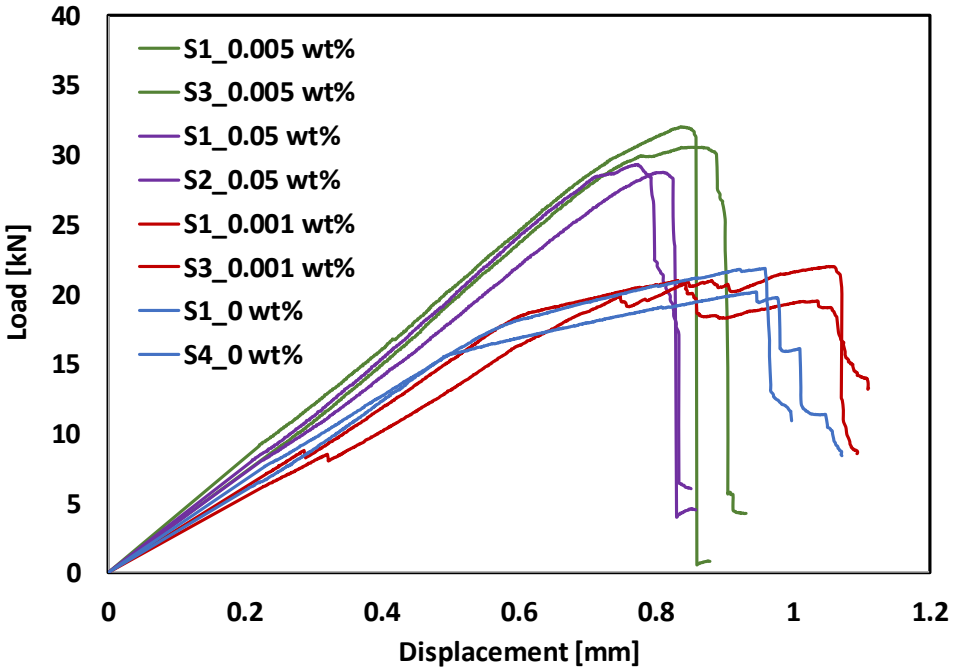

Figure C.12 Load-deflection curves of control and PUCNT-added cement paste samples after 28 days of curing

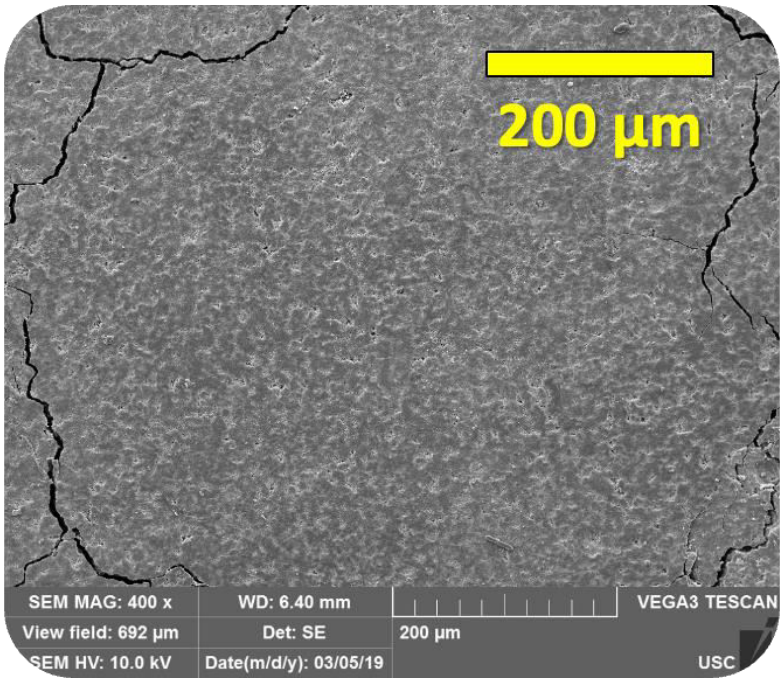

Figure C.13 Free curing surface of 0.005 wt% of PUCNT-amended cement paste after 14 days of curing

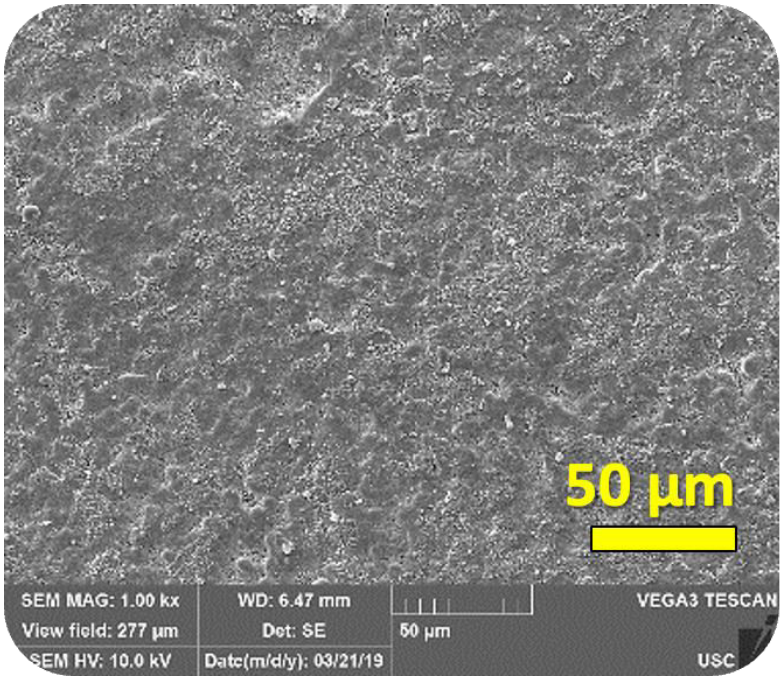

Figure C.14 Free curing surface of 0.005 wt% of PUCNT-amended cement paste after 28 days of curing

APPENDIX D - EFFECT OF ADDING SODIUM HYDROXIDE ON PHYSICO-MECHANICAL PROPERTIES OF CEMENT PASTE

D.1. OBJECTIVES

The objectives are to verify the effect of adding NaOH-solution on cement paste through evaluating

- enhancement in mechanical properties in terms of compressive strength.
- nano- and micro-structural modifications in terms of SEM micrograph-analysis.

D.2. HYPOTHESIS

As the supplied MWCNTs and PUCNTs were acid treated, the initial pH of the suspensions was found in the acidic range (Table 2.1, Table 3.1). To raise the pH to 12, thereby enhancing the stability of acid-treated nanoparticles in water, a negligible amount of NaOH solutions were added to the suspensions. At an acidic pH, functional groups tend to have a relatively low surface charge as they are deprotonated. Therefore, increasing the pH aims to protonate the –OH and –COOH groups, resulting in a lower zeta potential and a more stable dispersion in water.

D.3. MATERIALS AND EQUIPMENTS

The molar concentrations of added NaOH solution in 0.001, 0.005 and 0.05 wt% of PUCNTs-suspensions were estimated as 0.002, 0.003 and 0.012 mol/L, respectively.

The pH of the suspensions was measured with a pH meter, manufactured by Mettler Toledo (pH electrode LE 438). The resultant pH of each suspension with NaOH was found ≈12. The resultant molar concentrations and pH values are reported in Table D.1.

Stock solution of 5 mol/L NaOH and DI water were utilized to prepare the NaOH-suspensions. Cement paste prisms were prepared with ordinary Portland cement Type I and the prepared suspensions.

D.4. EXPERIMENTAL PROGRAM

To verify the effect of adding NaOH itself on compressive strength and nano-micro-structure of the cement paste, prisms with 25 mm x 25 mm x 76 mm dimensions were made with 0.001, 0.005 and 0.01 mol/L of NaOH solutions and ordinary Portland cement Type I. The prisms were cast according to ASTM C305 [2014]. Uniaxial compression tests (Figure D.1) and SEM micrograph analysis were conducted on those specimens. Three number of samples per type were tested after 28 days of curing under saturated lime water, to verify the statistical meaningfulness.

D.5. RESULTS AND DISCUSSIONS

- Average 28-day compressive strength of control and NaOH-added cement paste samples were observed as similar (Figure D.2, Table D.2).
- Average 28-day elastic stiffness of control and NaOH added cement paste samples, observed from the slope of load-deflection curves in linear elastic range, were as similar (Figure D.3, Table D.3).
- Similar free curing surface-structures and inside-structures were observed with or without NaOH addition (Figure D.4).

D.6. CONCLUSIONS

The addition of NaOH to increase the pH of MWCNT-solutions and PUCNT-solutions appears to have a negligible effect on the nano-structure, micro-structure, and compressive strength of cement paste.

D.7. REFERENCES

ASTM International. Standard Practice for Mechanical Mixing of Hydraulic Cement Pastes and Mortars of Plastic Consistency. ASTM C305-14. West Conshohocken, PA: ASTM International, 2014.

D.8. TABLES

Table D.1 Molar concentrations and pH for different content of PUCNT-solutions

Concentration of PUCNTs [wt%]	Initial pH	Total PUCNT-solution [mL]	Amount of added 5 mol/L NaOH [µL]	Adjusted pH	Final concentration of NaOH [mol/L]
0.001	3.84	700	300	11.18	0.002
0.005	3.34	700	400	11.21	0.003
0.05	2.24	700	1700	11.3	0.012

Table D.2 Results on compressive strength of cement paste with or without NaOH

Concentration [mol/L]	0	0.001	0.005	0.01
Average [MPa]	33.77	30.77	32.79	34.96
Standard deviation [MPa]	4.33	3.46	5.02	2.03

Table D.3 Results on elastic stiffness of cement paste with or without NaOH

Concentration [mol/L]	0	0.001	0.005	0.01
Average stiffness [kN/mm]	13	12	12	12
Standard deviation [kN/mm]	1.13	0.82	1.12	2.06

D.9. FIGURES

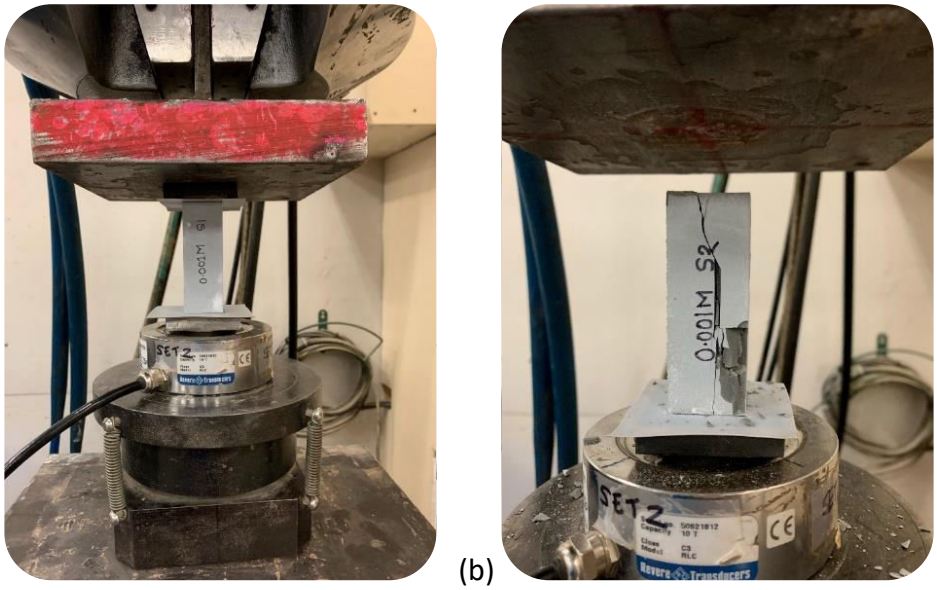

Figure D.1 Uniaxial compression test on NaOH-added samples after 28 days of curing (a) test set up (b) failed sample

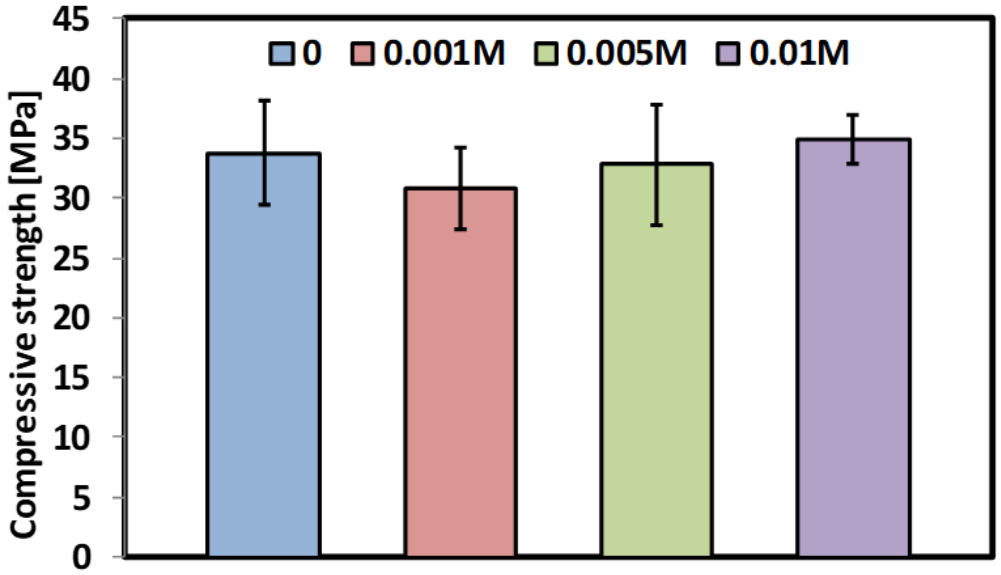

Figure D.2 Results on average compressive strength after 28 days of curing, of control and NaOH-added cement paste

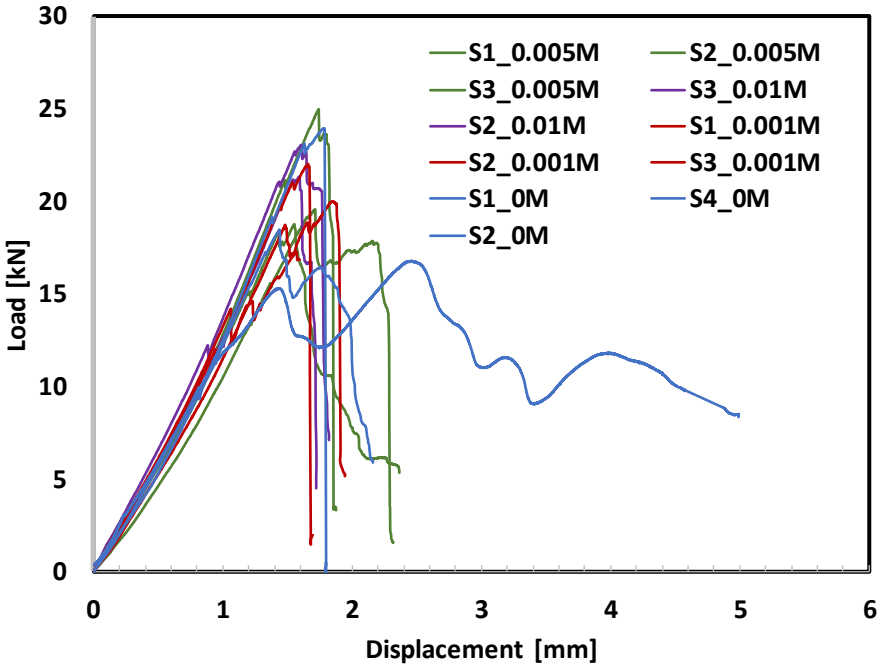

Figure D.3 Representative load-deflection curves after 28 days of curing, of control and NaOH-added cement paste

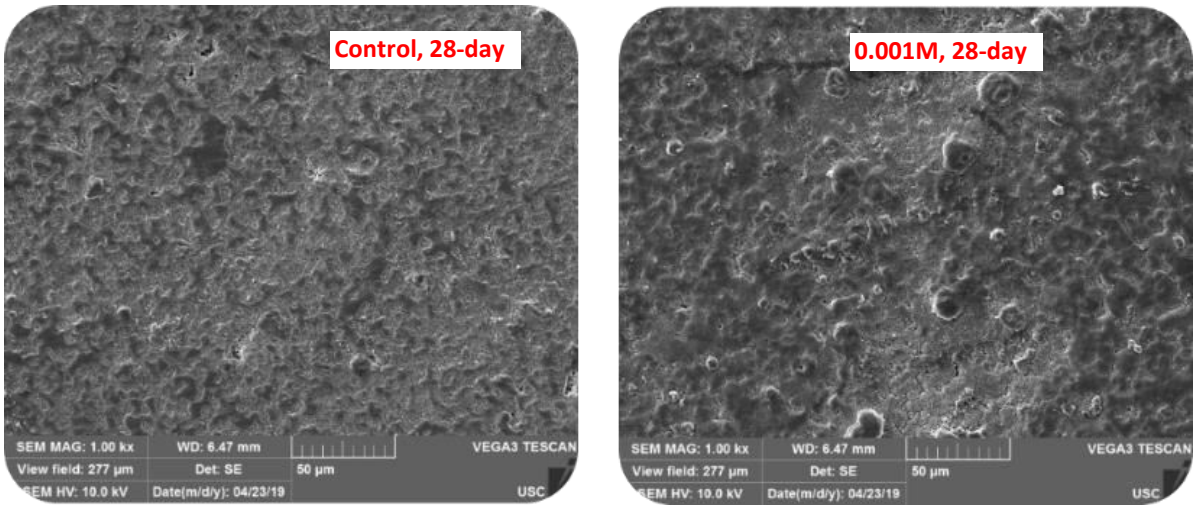

(a)

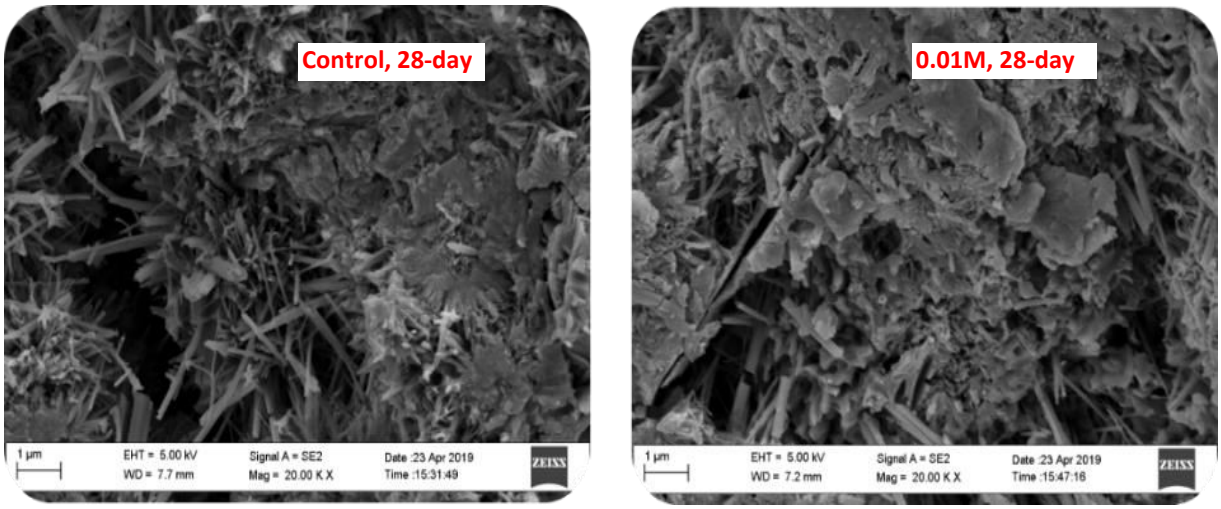

(b)

Figure D.4 Nano- and micro-structure analysis of control and NaOH-added cement paste after 28 days of curing (a) free curing surfaces (b) inside the failed specimens

APPENDIX E - DISPERSION OF GRAPHENE NANORIBBONS IN AQUEOUS SOLUTIONS AND APPLICATION ON PORTLAND CEMENT CONCRETE

E.1.TABLES

Table E.1 Results on zeta potential at 0 days after sonication (phase I)

Concentration [wt%]	0.0005	0.001	0.005	0.02	0.05
Oxidation [%]	**Average zeta potential [mV]**				
40.7	-47.5	-52.50	-49.70	-30.00	-34.00
33.5	-55.5	-52.40	-49.90	-41.40	-32.50
22.7	-45.3	-41.90	-34.80	-33.70	-34.70
Oxidation [%]	**Standard deviation [mV]**				
40.7	2.08	2.64	2.56	1.60	1.55
33.5	3.14	2.58	2.90	1.06	1.53
22.7	1.91	3.68	1.68	1.77	1.35

Table E.2 Results on zeta potential at 7 days after sonication (phase I)

Concentration [wt%]	0.0005	0.001	0.005	0.02	0.05
Oxidation [%]	**Average zeta potential [mV]**				
40.7	-51.5	-55.00	-48.30	-34.00	-34.80
33.5	-54.9	-51.50	-48.70	-42.50	-35.70
22.7	-39.1	-41.50	-33.60	-31.10	-13.40
Oxidation [%]	**Standard deviation [mV]**				
40.7	3.34	3.39	2.43	2.73	1.86
33.5	4	2.71	2.00	1.45	2.33
22.7	1.52	2.44	1.16	1.24	1.70

Table E.3 Results on zeta potential at 14 days after sonication (phase I)

14-day results					
Concentration [wt%]	0.0005	0.001	0.005	0.02	0.05
Oxidation [%]	**Average zeta potential [mV]**				
40.7	-53.7	-58.30	-54.00	-34.80	-34.40
33.5	-47.3	-56.20	-53.60	-44.30	-2.34
22.7	-38	-42.10	-36.10	-33.40	-0.26
Oxidation [%]	**Standard deviation [mV]**				
40.7	3.99	2.42	1.32	2.01	1.66
33.5	2.42	2.79	2.40	1.31	0.62
22.7	2.95	0.88	1.29	1.17	0.50

Table E.4 Results on zeta potential at 21 days after sonication (phase I)

Concentration [wt%]	0.0005	0.001	0.005	0.02	0.05
Oxidation [%]	**Average zeta potential [mV]**				
40.7	-50.06	-55.70	-44.00	-31.50	-34.20
33.5	-50.1	-49.70	-32.70	-42.70	-17.20
22.7	-41.4	-43.00	-32.50	-33.20	-0.20
Oxidation [%]	**Standard deviation [mV]**				
40.7	2.70	3.25	3.32	0.82	1.69
33.5	2.01	4.40	1.14	1.57	6.75
22.7	0.75	1.87	0.60	1.54	0.41

Table E.5 Results on zeta potential at 28 days after sonication (phase I)

Concentration [wt%]	0.0005	0.001	0.005	0.02	0.05
Oxidation [%]	**Average zeta potential [mV]**				
40.7	-49.2	-54.70	-49.60	-32.00	-37.60
33.5	-41.3	-54.20	-49.50	-30.00	-26.00
22.7	-44.4	-33.30	-35.40	-29.50	-14.30
Oxidation [%]	**Standard deviation [mV]**				
40.7	3.80	2.68	3.03	1.43	5.54
33.5	2.03	1.89	2.20	2.81	4.14
22.7	2.81	4.59	1.76	6.92	1.37

Table E.6 Results on hydrodynamic size at 0 days after sonication (phase I)

0-day results					
Concentration [wt%]	0.0005	0.001	0.005	0.02	0.05
Oxidation [%]	**Average HDS [nm]**				
40.7	2468	2404	3300	784	2140
33.5	2021	2216	1730	2312	3081
22.7	4712	4325	4245	2159	5664
Oxidation [%]	**Standard deviation [nm]**				
40.7	162.6	152.8	172.3	19.5	77.5
33.5	88.0	114.4	111.1	129.5	268.7
22.7	923.7	1163.0	207.9	120.2	335.8

Table E.7 Results on hydrodynamic size at 7 days after sonication (phase I)

7-day results					
Concentration [wt%]	0.0005	0.001	0.005	0.02	0.05
Oxidation [%]	**Average HDS [nm]**				
40.7	2830	2371	1751	4100	3422
33.5	2532	2148	4960	4716	3111
22.7	5391	4004	3378	6374	5421
Oxidation [%]	**Standard deviation [nm]**				
40.7	372.8	142.5	81.9	386.6	394.5
33.5	255.9	215.4	291.9	211.4	595.9
22.7	1166.0	946.1	96.2	1236.3	341.1

Table E.8 Results on hydrodynamic size at 14 days after sonication (phase I)

Concentration [wt%]	0.0005	0.001	0.005	0.02	0.05
Oxidation [%]	**Average HDS [nm]**				
40.7	2276	2218	2169	3930	3754
33.5	2474	1837	3588	2037	5420
22.7	2636	3113	5039	6361	6363
Oxidation [%]	**Standard deviation [nm]**				
40.7	468.3	176.7	232.8	288.6	261.7
33.5	108.1	133.4	183.5	112.4	1178.0
22.7	612.7	387.7	173.5	359.2	1724.0

Table E.9 Results on hydrodynamic size at 21 days after sonication (phase I)

Concentration [wt%]	0.0005	0.001	0.005	0.02	0.05
Oxidation [%]	**Average HDS [nm]**				
40.7	1276	1048	1194	1391	1729
33.5	1411	1362	1532	1326	1001
22.7	3561	3859	1958	1177	2538
Oxidation [%]	**Standard deviation [nm]**				
40.7	216.6	130.8	10.4	139.1	53.0
33.5	121.8	97.6	106.8	167.6	12.8
22.7	365.6	890.3	241.2	81.1	183.2

Table E.10 Results on hydrodynamic size at 28 days after sonication (phase I)

Concentration [wt%]	0.0005	0.001	0.005	0.02	0.05
Oxidation [%]	**Average HDS [nm]**				
40.7	1838	1804	2669	3645	2756
33.5	2500	2322	3569	2841	3490
22.7	5280	5013	2809	7565	4173
Oxidation [%]	**Standard deviation [nm]**				
40.7	625.4	383.7	111.1	274.9	199.9
33.5	538.1	310.9	512.8	281.8	245.1
22.7	2041.0	1533.0	530.3	720.2	464.0

Table E.11 Results on zeta potential at 0 days after sonication (phase II)

Concentration [wt%]	0.0005	0.005	0.05
Oxidation [%]	**Average zeta potential [mV]**		
41.3	-58.1	-45	-37.1
32.3	-44.5	-51.6	-41
Oxidation [%]	**Standard deviation [mV]**		
41.3	3.21	1.78	1.41
32.3	4.86	1.99	0.989

Table E.12 Results on zeta potential at 7 days after sonication (phase II)

Concentration [wt%]	0.0005	0.005	0.05
Oxidation [%]	**Average zeta potential [mV]**		
41.3	-44.3	-43.6	-35.9
32.3	-64.6	-47.7	-43.3
Oxidation [%]	**Standard deviation [mV]**		
41.3	3.39	1.81	1.09
32.3	1.66	1.28	1.17

Table E.13 Results on hydrodynamic size at 0 days after sonication (phase II)

Concentration [wt%]	0.0005	0.005	0.05
Oxidation [%]	**Average HDS [nm]**		
41.3	2166	1117	2708
32.3	3479	1434	3692
Oxidation [%]	**Standard deviation [nm]**		
41.3	175.7	209.9	460
32.3	119.2	139.7	583.1

Table E.14 Results on hydrodynamic size at 7 days after sonication (phase II)

Concentration [wt%]	0.0005	0.005	0.05
Oxidation [%]	**Average HDS [nm]**		
41.3	1907	948.8	1738
32.3	1535	1764	3394
Oxidation [%]	**Standard deviation [nm]**		
41.3	79	121.5	245.1
32.3	201.5	199.4	1153

Table E.15 Ordinary Portland cement concrete mixes

GONR [mg]	GONR concentration [wt%]	GONR/water [g/L]	Aqueous solution [g]	Cement [g]	Sand [g]	Crushed stone [g]
0.00	0	0	430	1075	1745	1513
5.38	0.0005	0.0125	430	1075	1745	1513
53.75	0.005	0.125	430	1075	1745	1513
537.5	0.05	1.25	430	1075	1745	1513

Table E.16 Properties of crushed stone (Vulcan Materials Company, Columbia, SC)

Dry rodded unit weight [kg/m^3]	Specific gravity	Absorption capacity [%]	Moisture content [%]
1510	2.60	0.8	0.5

Table E.17 Compressive strength of control and GONRs-amended cement concrete samples after 7 days of curing

Compressive strength [MPa]				
Concentration	**0 wt%**	**0.0005 wt%**	**0.005 wt%**	**0.05 wt%**
Sample ID	**7 days**	**7 days**	**7 days**	**7 days**
1	26.00	31.90	32.47	36.10
2	22.07	33.48	30.65	34.58
3	22.12	31.45	35.82	35.67
4	32.50	28.78	29.54	29.09
Average [MPa]	25.67	31.40	32.12	33.86
Standard deviation [MPa]	4.91	1.95	2.75	3.24

E.2.FIGURES

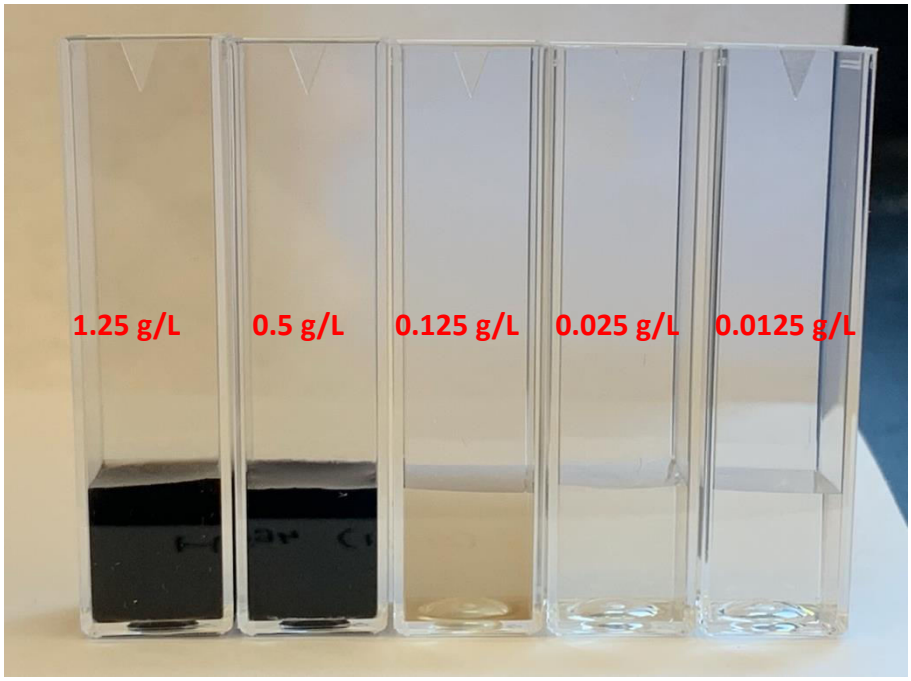

Figure E.1 Visual inspection of 40.7 wt% oxidized GONR-suspensions at 7 days after sonication

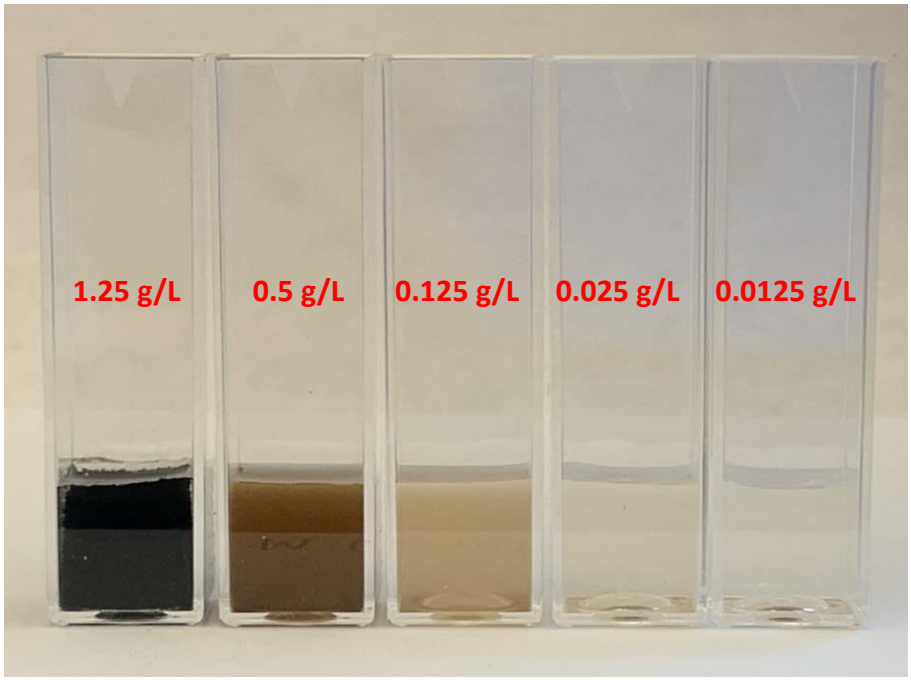

Figure E.2 Visual inspection of 33.5 wt% oxidized GONR-suspensions at 7 days after sonication

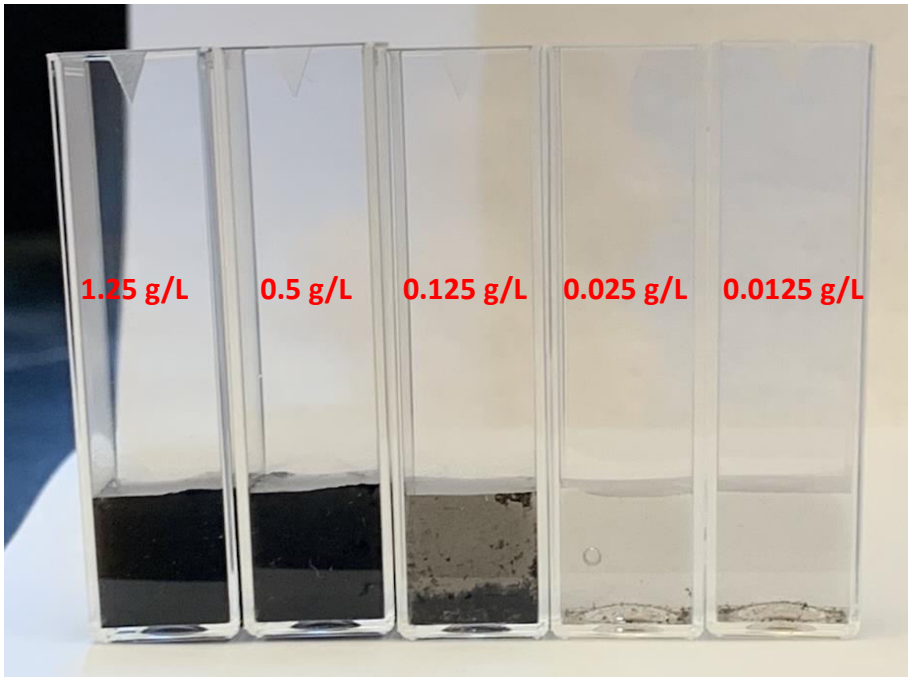

Figure E.3 Visual inspection of 22.7 wt% oxidized GONR-suspensions at 7 days after sonication

(a) 

(b)

(c)

Figure E.4 Casting cement concrete cylinders (a) DI water, OPC, sand, and crushed stone (b) GONR-suspension (0.0125 g/L, equivalent to 0.0005 wt%), OPC, sand, and crushed stone (c) GONR-suspension (0.125 g/L, equivalent to 0.005 wt%), OPC, sand, and crushed stone

(a) 

(b) 

(c) 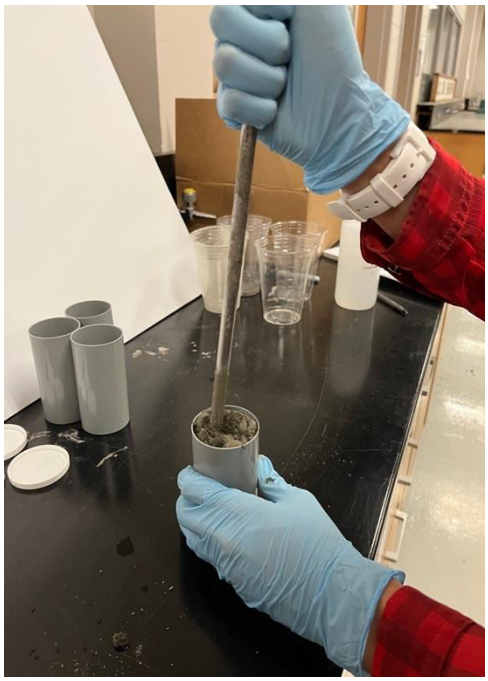

(d) 

Figure E.5 Casting cement concrete cylinders (a) mixing (b) concrete after mixing (c) compaction (d) the cylinders in plastic molds

(a) 

(b) 

(c) 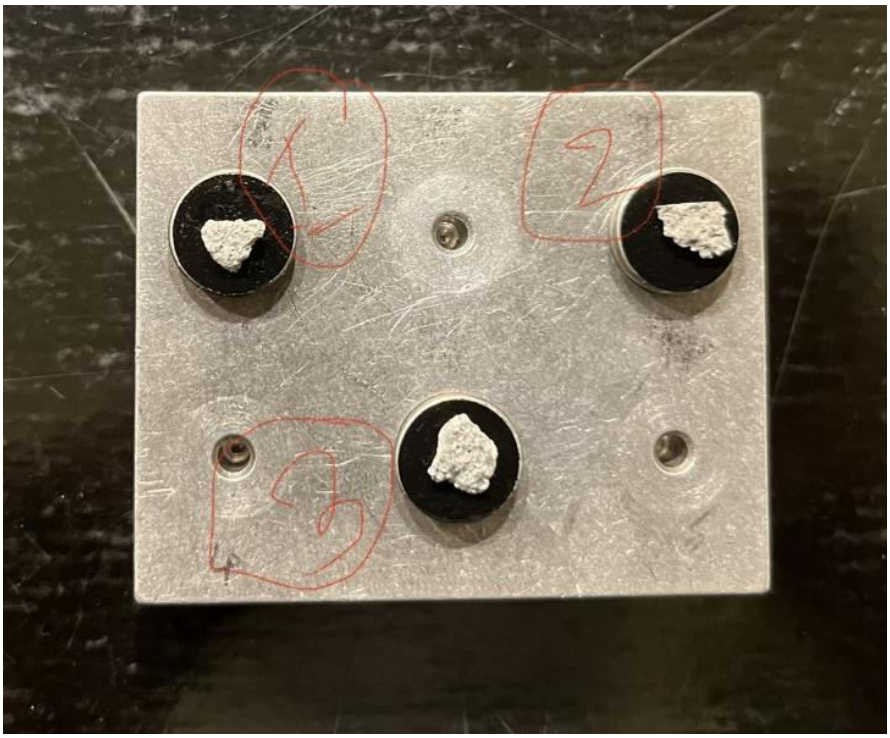

Figure E.6 Preparation for SEM imaging (a) broken cylinders after compression testing (b) air drying (c) samples in stubs

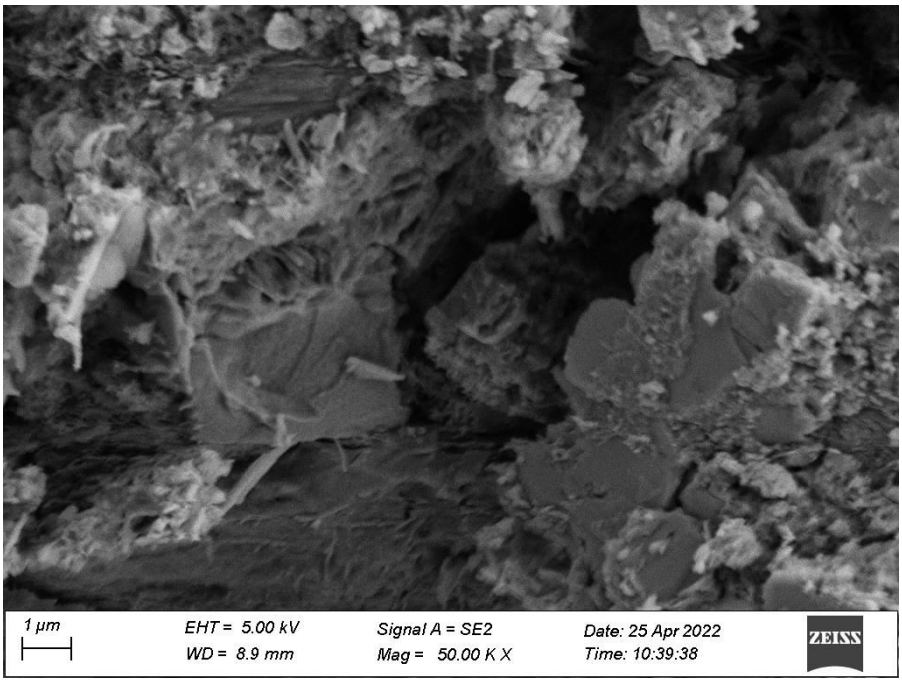

Figure E.7 Nano- and micro-structure of control cement concrete (0 wt%) after 7 days of curing

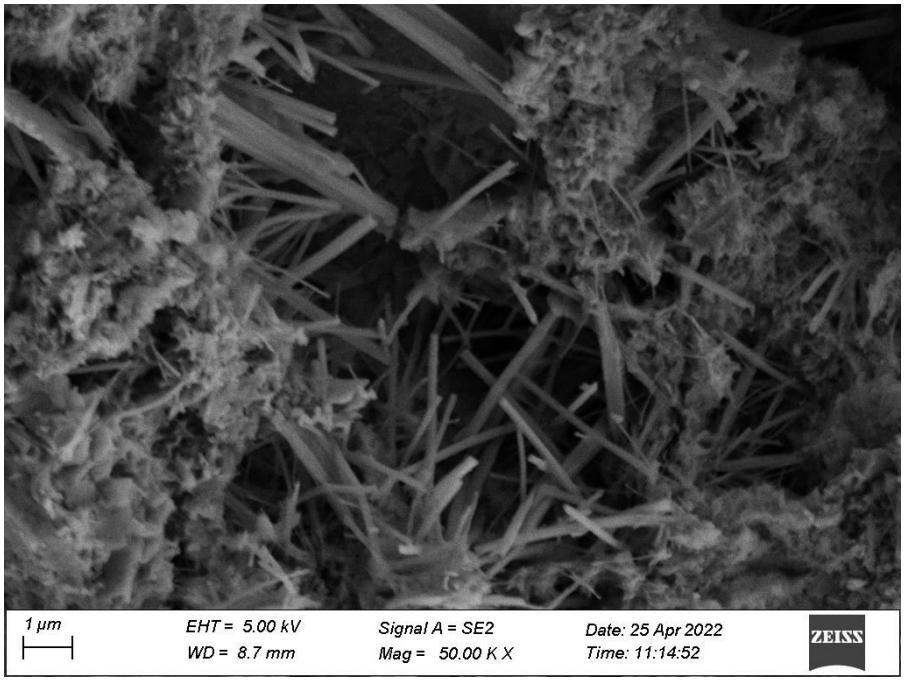

Figure E.8 Nano- and micro-structure of cement concrete for 0.0005 wt% GONR (32.3 wt% oxygen content) concentration after 7 days of curing

(a)

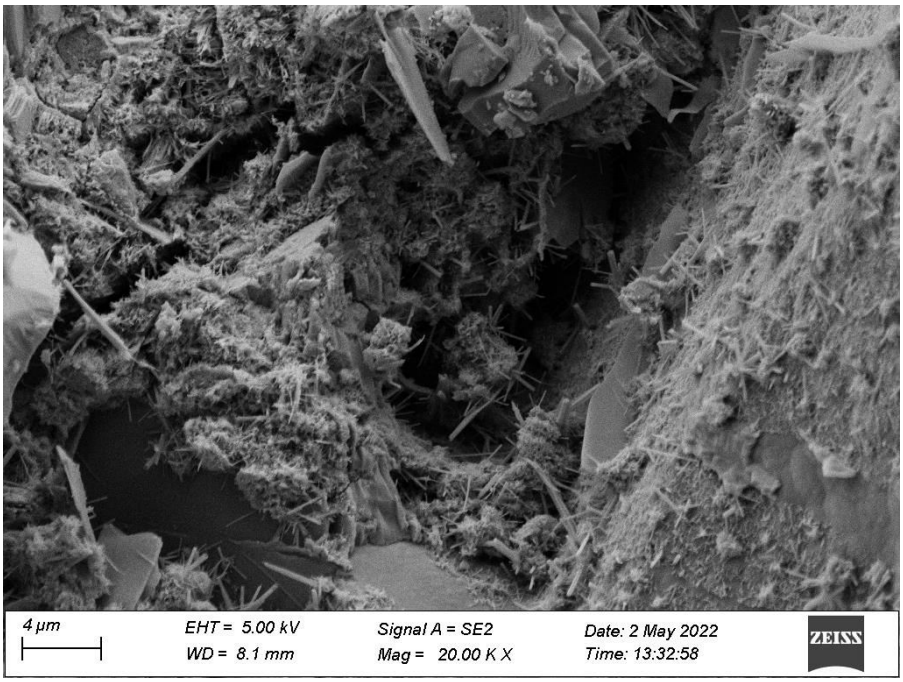

(b)

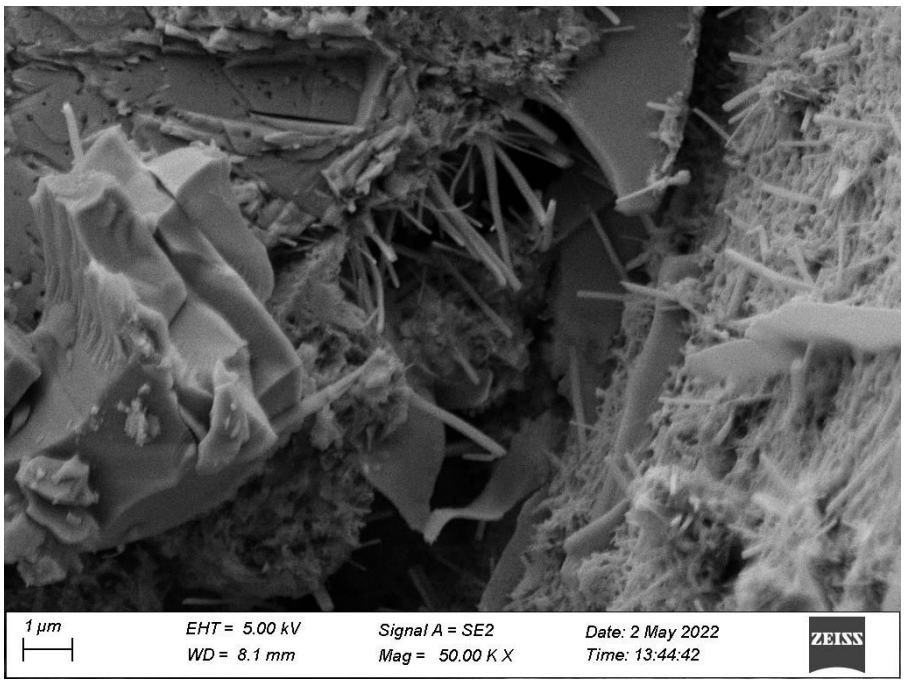

Figure E.9 Nano- and micro-structure of cement concrete for 0.005 wt% GONR (41.3 wt% oxygen content) concentration after 7 days of curing

(a)

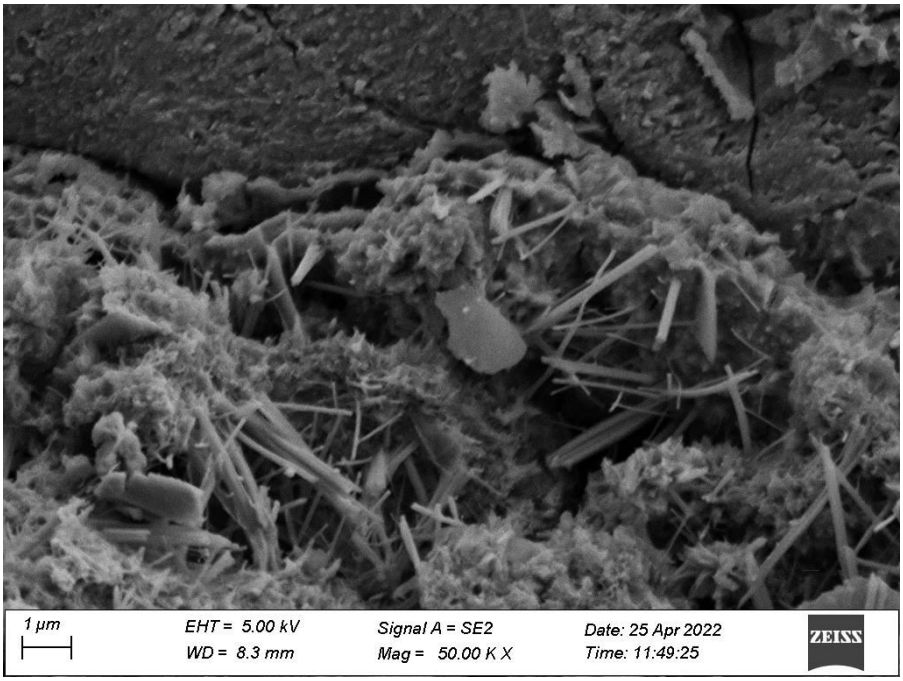

(b)

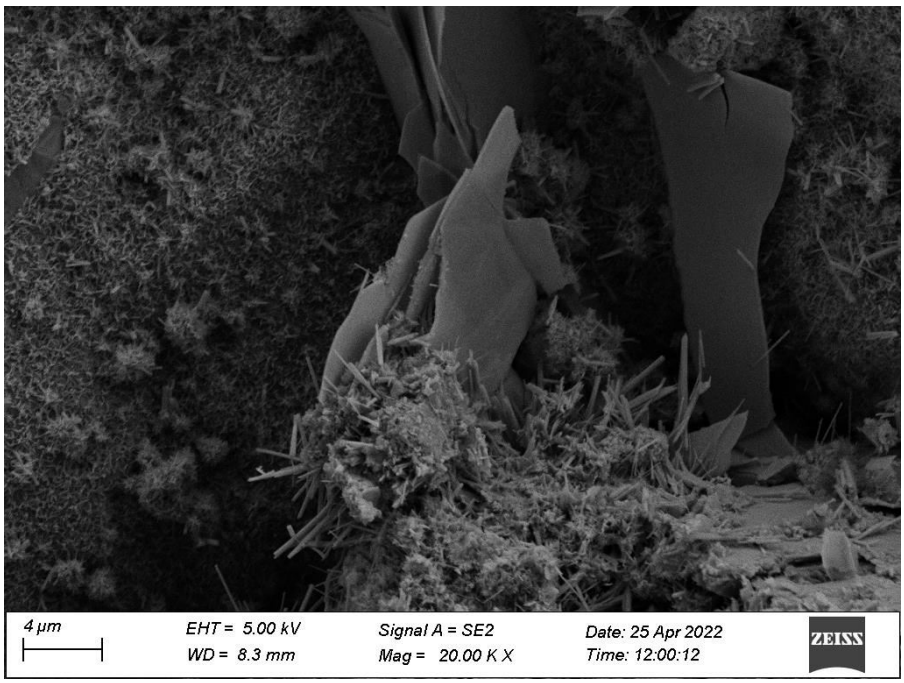

(c)

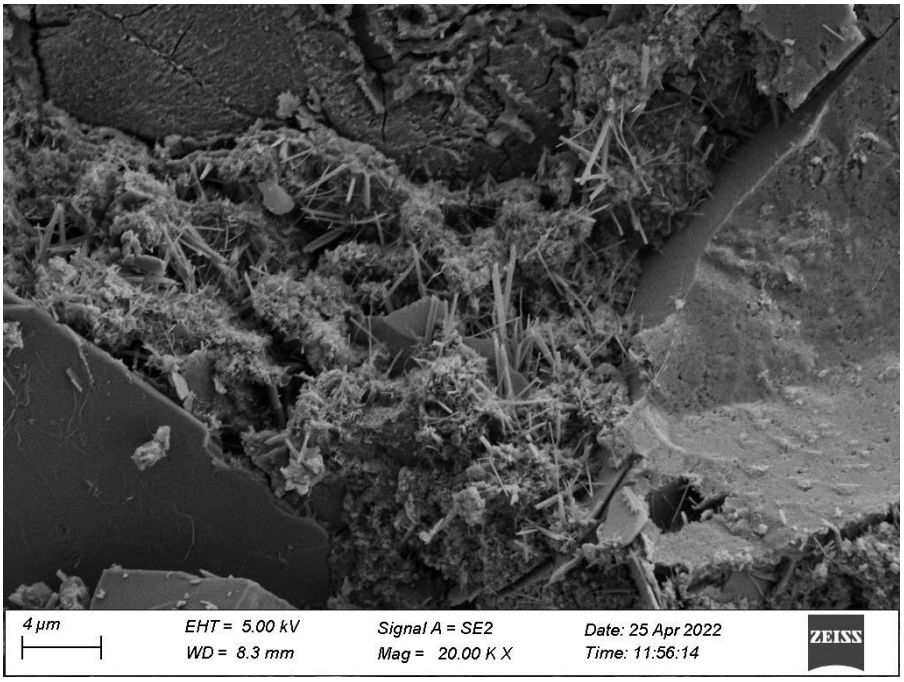

Figure E.10 Nano- and micro-structure of cement concrete for 0.05 wt% GONR (41.3 wt% oxygen content) concentration after 7 days of curing